AERODYNAMIC STABILITY AND CONTROL/WIND TUNNEL DATA CORRELATION

G. R. CASTEEL

NORTH AMERICAN ROCKWELL CORPORATION

FOREWORD

This report was prepared by the Aerodynamic Group of the Aerospace and Systems Group, Los Angeles Division of North American Rockwell Corporation of Los Angeles, California under USAF Contract No. AF33(615)-5323. The Contract was initiated under Technical Development Plan 698BT, Vertical Integrated Flight Control System (VIFCS) Program. The contract was administered by the Air Force Flight Dynamics Laboratory, Wright-Patterson Air Force Base, Ohio, under the technical direction of Mr. W. F. Brown (AFFDL/FGS). Mr. A. G. Jones (AFFDL/FGC) was the project engineer on Task II under this contract, Stability, Control and Aerodynamic Data Correlation. Only Task II is covered by this report.

This Final Technical Report covers the work performed from 15 October 1966 to 31 August 1970. It was released by the author in August 1970. Four preliminary aerodynamic analysis reports and two wind tunnel data reports were issued at different stages of the project (references 1 through 6).

Significant and valuable contributions to the technical efforts described in this volume were made by Mr. J. F. Hardesty, Mr. P. L. Lemoine, and Mr. C. R. Leef, Members of the Technical Staff. Their enthusiastic support was greatly appreciated. The contractor's report number is NA-70-327-2.

This technical report has been reviewed and is approved.

C. B. WESTBROOK
Chief, Control Criteria Branch
Aeronautical Systems Division
Air Force Flight Dynamics Laboratory

ABSTRACT

This report presents the results of work performed under Task II (Aerodynamic Stability and Control) of the VTOL Integrated Flight Control System Program (VIFCS). The general objective of Task II was to collect and analyze aerodynamic stability and control data for the XV-4B, XV-5A and P-1127 VTOL configurations. Correlation and analysis of existing model data were made to investigate hover and transition characteristics. Particular emphasis was placed on the aerodynamic power effects, sometimes referred to as interference effects. Other areas of investigation were nondimensional coefficients used to present VTOL data and wind tunnel test techniques. Wind tunnel tests were conducted using an inlet only model and a jet only model to investigate special test and analysis problems for these components.

The agreement between different sets of XV-4B model data was, in general, found to be poor. However, the nondimensional coefficients used by Lockheed to reduce to XV-4B model data appear to be valid parameters for this category of VTOL airplane. The jet entrainment flow was shown by experiment to be the primary cause of the XV-4B power effects, and the XV-4B jet path was experimentally and theoretically determined.

TABLE OF CONTENTS

v

INDEX OF FIGURES

NOMENCLATURE

A_F, A_{FAN}	Total area of fans based on fan diameter, ft.^{2}
A_j, A_{JET}	Total area of jet exits, ft.^{2}
A_R	Total maximum nozzle exit area for reaction control about any one airplane axis, ft.^{2}
b, b_w	Reference wing span
$\bar{c}$, $\bar{c}_w$	Reference wing aerodynamic chord
C_D	Drag coefficient, D/qS
C_ℓ	Rolling moment coefficient, $\mathcal{L}/qSb$
$C_{\ell \delta_A}$	Aileron effectiveness parameter, $\partial C_\ell / \partial \delta_A$
$C_{\ell p}$	Damping-in-roll parameter, $\partial C_\ell / \partial (pb/2v)$
$C_{\ell \beta}$	Lateral stability parameter, $\partial C_\ell / \partial \beta$
C_L	Lift coefficient, L/qS
$C_{L\alpha}$	Lift curve slope, $\partial C_L / \partial \alpha$
$C_{L\delta_e}$	Elevator effectiveness parameter, $\partial C_L / \partial \delta_e$
C_m	Pitching moment coefficient, $M/qS\bar{c}$
$C_{m\alpha}$	Pitching moment curve slope, $\partial C_m / \partial \alpha$
$C_{m\delta_e}$	Elevator effectiveness parameter, $\partial C_m / \partial \delta_e$
$C_{m\delta_f}$	Flap effectiveness parameter, $\partial C_m / \partial \delta_f$
C_{m_o}	Pitching moment coefficient at $C_L = 0$
C_{m_q}	Damping-in-pitch parameter, $\partial C_m / \partial (q\bar{c}/2V_o)$
C_N	Normal force coefficient, F_N/qS
C_n	Yawing moment coefficient, N/qSb
$C_{n\beta}$	Directional stability parameter, $\partial C_n / \partial \beta$
$C_{n\delta_r}$	Rudder effectiveness parameter, $\partial C_n / \partial \delta_r$
C_T	Thrust coefficient, T/qS
C_Y	Side force coefficient, F_Y/qS

$C_{Y_{\delta_T}}$	Rudder effectiveness parameter, $\partial C_Y / \partial \delta_T$
C_{Y_β}	Side force slope, $\partial C_Y / \partial \beta$
d	Exit nozzle diameter, ft.
D	Jet exit diameter, in.; drag force, lb.
D_e	Effective diameter, diameter of a circle equivalent in area to total jet-exit area of a given configuration, in.
D_{eff}	Effective jet exit diameter, $\sqrt{4 A_{ex}/\pi}$
D_F, D_{FAN}	Diameter of fan, ft.
F_c	Chord force, lb.
F_N	Normal force, lb.
FRL	Fuselage reference line in the plane of symmetry
F_Y	Side force, lb.
g	Acceleration due to gravity, 32.2 ft./sec.^{2}
h, H	Height above ground or distance between bottom of fuselage at exit nozzles and ground plane, ft.
h'	Vertical distance, in the plane of the jet path, from the jet exit to the tunnel floor.
I	Moment of inertia, slug-ft.^{2}
L	Lift force, lb.
ℓ	Rolling moment, ft.-lb.
m	Mass, slugs
M	Pitching moment, ft.-lb.
N	Yawing moment, ft.-lb.
p	Roll rate, rad./sec.
$\dot{p}$	Roll acceleration, rad/sec.^{2}
q	Dynamic pressure, lb./ft.^{2}; pitch rate, rad./sec.
$\dot{q}$	Pitch acceleration, rad./sec.^{2}
r	Yaw rate, rad./sec.

$\dot{r}$	Yaw acceleration, rad./sec.^{2}
RN	Reynolds number based on $\bar{c}$
S	Reference wing area, ft.^{2}
T	Total engine thrust, lb.
T_R	Total reaction control thrust, lb.
u	Linear motion along x axis, ft./sec.
v	Linear motion along y axis, ft./sec.
V	Velocity
w	Linear motion along Z axis
$\dot{\omega}_A$	Airflow rate, lb./sec.
X	Airplane body axis in the plane of symmetry parallel to the fuselage reference line; distance along this axis
X'	Longitudinal distance from the jet exit to a point along the jet path, positive aft.
Y	Airplane body axis perpendicular to the plane of symmetry; distance along this axis
Z	Airplane body axis in the plane of symmetry perpendicular to the fuselage reference line; distance along this axis
Z'	Vertical distance from the jet exit to a point along the jet path, positive downward

GREEK SYMBOLS

α	Angle of attack of the FRL, deg.
$\Delta\alpha_S$	Local flow angularity: for experimental data, due to power; for theoretical data, due to splash
β	Angle of sideslip, deg.
Δ , δ	Increment
ϵ	Downwash angle, deg.
η_{TAIL}	Horizontal tail efficiency factor, q_{TAIL} / q_{∞}
θ	Pitch angle, deg.
θ_{j_0}	Initial inclination of the jet axis to the vertical, positive rearward

ρ	Mass air density, slugs/ft.^{3}
σ	Sidewash angle, deg.
ϕ	Bank angle, deg.
ψ	Yaw angle, deg.

Subscripts

a	Aileron
A	Air, ambient, area
AERO	Basic power-off aerodynamic force or moment
e	Elevator
EX., EXIT	Jet exit
F, FAN	Wing lift fan
GYRO	Gyroscopic
H, H.TAIL	Horizontal tail
i	Point of maximum rate of change of decay parameter
IN, INLET	Inlet flow
INT.	Interference
j, JET	Jet exit, jet exhaust
L, LS	Large test section
LOUVERS	Fan-in-wing louvers
MAX.	Maximum
n	At nozzle exit
o, ∞	Freestream
ooo	Condition of zero forward velocity, zero jet thrust vector angle, Zero jet thrust stagger angle
P	Fan power effect
PE	Power effect
r	Rudder

xvi

R	Reaction control nozzle exit
RC	Reaction control
S , SS	Small test section
T, THRUST	Thrust
TAIL	Horizontal tail
V	Thrust vector
V.TAIL	Vertical tail
W	Wing
X	At location X distance downstream from jet exit; with respect to X axis
Y	With respect to Y axis
Z	With respect to Z axis
XZ	With respect to X and Z axes

Section I

INTRODUCTION

VTOL technology is in a rapid evolutionary stage at the present time, and a general consensus concerning basic aerodynamic test and analysis techniques has not yet emerged. The wide variety in airframe-propulsion variables has made the task of developing general analysis techniques particularly challenging. In recognition of the need to improve test and analysis techniques for VTOL airplanes, the USAF has for many years sponsored research work in this area. NR became an important partner in this general research effort when it was selected by the USAF to carry out the VTOL Integrated Flight Control Program (VIFCS).

The objectives of the VIFCS program with regard to aerodynamic stability and control data collection, correlation, and support were as follows:

a. Determine by analysis of model and flight test data the stability and control characteristics of certain VTOL vehicles, particularly in the hover and transition flight regime.

b. Provide these data as required to other parts of the total Integrated Flight Control System Program.

c. Investigate the correlation of flight and wind tunnel tests in different facilities to determine the degree of correlation.

d. Develop improved correction techniques and testing techniques that will enable confident prediction of actual vehicle characteristics from model tests.

e. Develop a consistent approach to representing VTOL aircraft stability and control parameters.

Three VTOL configurations were to have been investigated as part of the program, the XV-4B, XV-5A and P-1127. Early in the program NR was notified of the unavailability of wind tunnel models for the XV-5A and P-1127. As a consequence, the detailed requirements for the study vehicles were revised in accordance with USAF desires. The revised program called for a larger portion of the total effort to be expended on the XV-4B, and efforts expended on the XV-5A and P-1127 were to be used to verify the results of the XV-4B effort. Also, two additional XV-4B wind tunnel tests, exit model and inlet model tests, were substituted for XV-5A and P-1127 model tests which were originally planned.

The loss of the XV-4B airplane during flight test activities on 14 March 1969 led to the USAF decision to terminate the program. The termination effort calls for documenting all efforts expended prior to the loss of the aircraft. In addition, the USAF requested that the originally planned XV-4B inlet model test be conducted.

1

This report describes the efforts expended on aerodynamic stability and control data collection, correlation, and support. Obviously, the early termination of the program meant that the objectives of the VIFCS program could not be fully met. However, to the extent possible the comments are directed toward the initially stated objectives. At the time the program was terminated, numerous individual tasks were in various stages of completion. All applicable flight test and wind tunnel data for the designated airplanes had been collected. Considerable analysis of the XV-4B model data had been completed, and a small amount of analysis of the XV-5A had been completed. No analysis of the P-1127 data had yet been performed, and no effort had been expended analyzing flight test data. It is worth noting that some of the test and analysis work completed can be considered as basic VTOL research having general usefulness in addition to a specific VIFCS application.

A discussion of aerodynamic data requirements for future VTOL developments was prepared. This work has been included in Section VI.

2

Section II

SUMMARY

This report describes the efforts expended by the aerodynamic group in support of the VTOL Integrated Flight Control System program, referred to herein as the VIFCS program. The general purpose of this effort was to collect and analyze aerodynamic stability and control data for the XV-4B, XV-5A, and P-1127 airplanes. The aerodynamic data for these VTOL airplanes was provided, as required, to other parts of the VIFCS program and was used to investigate the adequacy of present test and analysis techniques for this category of VTOL airplanes. Because of the early termination of the program much of the detailed work could not be carried through to completion. As a consequence, it was difficult to draw many firm conclusions.

Eight trips by NR representatives to various facilities were required in support of aerodynamic data collection efforts. Five trips were made to Langley Research Center in connection with model test activities for the XV-4B and P-1127. One trip was made to Lockheed, Georgia, for a conference on XV-4B model tests. One trip was made to the Ryan Aeronautical Company to discuss the XV-5A program, and one trip was made to Ames Research Center to discuss their plans for testing of the XV-5A aircraft.

Support to other parts of the VIFCS program consisted mainly of coordination with the flight controls and flight simulation groups with reference to aerodynamic input data for the equations of motion of study vehicles. Some effort was expended in support of planned XV-4B flight test activities.

The primary configuration for aerodynamic data collection and analysis was the XV-4B airplane. Analysis effort was concentrated on the power effects which result from the engine inlet and exit flows inducing aerodynamic interference forces on the airplane. Comparisons between sets of XV-4B model data were made to determine the degree of correlation. Approximately 900 hours of XV-4B model testing was completed. The wind tunnel test techniques and data correlation methods which were used in connection with the XV-4B model data were investigated to determine if they were adequate.

As a result of the analysis work performed on the XV-4B model data for the transition flight mode the following conclusions were drawn.

1. The power effect data for Langley Test 178 and LTV Test 195 did not correlate well in many instances. Attempts to explain observed discrepancies in terms of model differences, data fairing or tunnel wall interference were not successful. The Langley data is judged to be the more accurate and should be used to define the XV-4B characteristics. The LTV data is judged to be somehow in error and should be used only to observe data trends.

2. The Lockheed nondimensional power effect coefficients appear to be valid correlating parameters for the XV-4B. These parameters were effective in reducing the test data for different thrust and speed conditions to a single curve.

3. The XV-4B longitudinal power effects are approximately independent of angle of attack which results in the longitudinal static stability being approximately independent of the power effects. The primary longitudinal influence of power is to change the aircraft trim control requirement with change in speed or power.

4. The XV-4B lateral directional power effects are a function of angle of sideslip. As a consequence, the lateral and directional static stability are significantly different power-on compared to power-off. Increasing speed or power results in an increase in lateral and directional static stability.

5. The experimental evidence indicates the entrainment action of the exhaust flow produces a significant change in the wing spanwise load distribution. As a consequence, the wing stall angle of attack and the wing downwash are altered by changes in speed or power.

The effects of thrust, ground height, attitude change, and very large angles of sideslip were investigated for the XV-4B in the hover mode. Also, correlation and analysis of existing experimental data were made to study the nondimensional coefficients being used, hover test techniques, and model differences. These efforts indicated the following:

1. To correlate hover lift loss, out of ground effect, NASA has been using a complicated jet decay parameter. It was found that the NASA jet decay parameter is proportional to jet exit circumference. It may be that a simpler correlation parameter utilizing exit circumference can be developed.

2. The results of Langley wind tunnel tests and Lockheed outdoor hover rig tests were found to correlate poorly. Both sets of data have question-able aspects. The Langley data may have been influenced by the wind tunnel walls, and the Lockheed data may have had unintended interaction between the ground and the test rig. It was not established which, if any, of the XV-4B hover data is representative of the airplane.

3. Slight motions or winds can result in sideslip angles of zero to ±180 degrees during hover operation. The data indicates a complicated vari-ation of forces and moments over this large range of sideslip angles. Because of the complex nature of hover motion characteristics the over-all importance of these terms was investigated. Comparisons of hover motion effects with available control power were made for a velocity of 30 knots and a thrust of 10,560 pounds. It was found that the control required to handle hover motion effects is not large relative to the available control power. Thus, a rigorous representation of the hover motion effects may not be required.

The results of low speed wind tunnel tests for XV-4B type inlet and exit models indicated the following conclusions:

1. The flow disturbance caused by the inlet flow is highly localized and rapidly becomes negligible moving away from the inlet. The incremental downwash angle due to inlet flow at the horizontal tail was less than one degree in all cases. The inlet flow had no effect on the local angles measured at the nose boom location.

2. The flow disturbance caused by the exit flow was powerful and can influence the local angles of attack over the entire airplane. Examples of the incremental angles of attack due to jet power are 0.5 to 1.8 degrees at the nose, zero to -15 degrees at the wing M.A.C., and -0.2 to -8.0 degrees at the tail (actual values depend upon specific speed and thrust).

3. The jet entrainment flow is the primary cause of the power effects measured in the XV-4B model tests. The jet entrainment effects the model data by changing the wing load distribution which then changes the wing downwash field. The jet entrainment flow can be suppressed by as much as 25 percent when the model is operated in a small wind tunnel.

4. The jet path was visualized by introducing water vapor into the exhaust flow. Theoretical expressions for the jet path developed by Ivanov were compared with the observed jet paths. General agreement between the observed path and Ivanov's equation was obtained. However, in certain respects the Ivanov equation did not adequately match the present test data, and a proposed modification or adaptation of Ivanov's equation is advanced to improve the degree of correlation.

Model and flight test data for the XV-5A and P-1127 were collected, and a small amount of analysis was completed for the XV-5A. Certain impressions were formed as a result of the limited XV-5A effort. It appears that the XV-5A data could be successfully correlated using the Lockheed speed-power parameter $(1/C_T)^{\frac{1}{2}}$. Also, it appears that a common analysis technique could be developed which would be valid for both fan-in-wing and lift jet configurations.

5

Section III

AERODYNAMIC TEST AND ANALYSIS TECHNIQUES

A brief discussion of some VTOL technology subjects related to the VIFCS program is presented in this section. Many of the test and analysis techniques applied to VTOL aircraft are unique, and a concensus concerning many practices has not yet emerged. Since this report is concerned mainly with the XV-4B airplane, the discussion will center on problems associated with this category of VTOL aircraft. Also, the power-off characteristics are fairly well understood by the current state of the art, and no attempt will be made in this section to analyze them.

AERODYNAMIC ANALYSIS TECHNIQUES

One objective of the VIFCS program was to develop a consistent approach to representing VTOL aircraft stability and control parameters. The main problem in representing VTOL parameters is how to best provide for the aerodynamic power effects in hover and transition flight. These aerodynamic power effects are the result of propulsion-airframe interference and are functions of different variables than the conventional power-off aerodynamic parameters. A discussion of the current techniques used to represent VTOL stability and control parameters is now presented using the XV-4B as a prime example.

BASIC FEATURES OF THE XV-4B AIRPLANE

The Lockheed XV-4B "Hummingbird" is a representative lift engine VTOL aircraft. A brief description of the important features of this aircraft is given here in order to familiarize the reader with basic operating features. The general arrangement of the XV-4B is shown in figure 1.

The main propulsion system consists of the six J-85 engines with a total take-off thrust of about 16,000 pounds on a sea level standard day. Four of the engines are installed vertically with inlets on the upper fuselage. Two of the engines are installed horizontally with a tail pipe arrangement that permits the exhaust to be diverted down or aft. All of the nozzles are arranged such that the resultant thrust vector is inclined at an angle of approximately 10 degrees forward of the vertical and located as close as possible to the airplane center of gravity. The exhaust nozzles can be vectored ±10 degrees from a neutral point. Acceleration is accomplished by means of changing aircraft attitude and can be modified by exit nozzle vector angle. There are many combinations of angle of attack, lift nozzle deflection angle, and engine thrust which will satisfy the steady-state conditions during transition flight.

A typical take-off transition is accomplished by accelerating to a speed at which the available wing lift is equal to or greater than the thrust lift provided by the two lift/cruise engines. The airplane is then rotated to an angle of attack to develop the required wing lift and the two lift/cruise engines are diverted to the conventional thrust mode simultaneously. Acceleration is continued to a speed at which wing borne flight is achieved. Finally, the four lift engines are shut down and the exit doors are closed and the airplane is in conventional flight. A typical landing transition is essentially the reverse of the above described procedure.

Control is obtained by means of the combined effect of aerodynamic control and reaction control. The controls are electrically and mechanically connected to power actuators which drive the aerodynamic surfaces and reaction control valves. The reaction control is operated by compressor bleed air. A system of interconnecting ducts allows the air to flow to any reaction control nozzle. The pitch control nozzles are located at the forward and aft extremities of the fuselage and direct the air downward. The yaw control nozzles are located at the aft end of the fuselage and direct the air to the right or left. The roll control nozzles are located at the wing tips. The air can be directed either upward or downward. The nozzles are rigged so that the upward nozzle on one wing tip and the downward nozzle on the other wing tip open simultaneously to produce the rolling moment. Hover height control is obtained by thrust modulation of all six engines.

DEFINITION OF AERODYNAMIC POWER EFFECTS

Initial efforts to represent VTOL forces and moments were directed toward establishing simple nondimensional parameters which would be similar to the conventional aerodynamic coefficients. To date, no simple overall parameters have come into general use. At present, the external force and moment effects are regarded as a number of individual effects superimposed upon each other and functions of different variables. In the equations of motion the aerodynamic forces and moment contribution are best represented by two terms; the conventional power-off aerodynamic effects and the aerodynamic power effects. The aerodynamic power effects are the result of propulsion-airframe interaction. The equations of motion used by Lockheed for the XV-4B are presented in general form in figure 2.

The complete model power effect terms are defined by the equations in figure 3. Complete model power effect values are calculated from wind tunnel data by subtracting from the total power-on values the power-off contribution and the thrust contribution.

A broad objective of the VIFCS program was to develop a consistent approach to representing VTOL parameters. The possibility of expressing the complete model power effects by means of an airplane build-up technique was investigated. It would be useful to know if the power effects can be built up from individual contributing factors which can be expressed in a common form for a variety of dissimilar VTOL aircraft. In the case of the XV-4B aircraft, the primary sources of complete model power effects are inlet effects, jet exit effects, and tail effects (refer to figure 3). The inlet effects consist of negative pressures induced on the upper surface of the

7

wing-body due to the acceleration of free air into the inlet and a ram drag force which is associated with turning the inlet flow. The exit effects consist of incremental pressures being induced on the wing-body by the free-stream air going around the jet and from entrainment action of the jet. The tail effects consist of changes in downwash and sidewash at the tail due to power.

Transition Power Effects

The general influence of power on the aerodynamic characteristics during transition flight is indicated in figure 4. In general, the power effects produce a shift in the longitudinal data which is independent of angle of attack. Thus, the primary longitudinal influence of power is a change in the aircraft trim control requirements. The power effect has an approximately neutral effect upon the longitudinal static stability. Jet powered config-urations tend to show a loss in lift and a nose up pitching moment due to power. Fan-in-wing configurations tend to show a lift increase and a nose up pitching moment due to power.

The power effects are a function of angle of sideslip for the lateral directional data. Thus, the lateral or directional static stability are significantly different power-on compared to power-off. Jet powered and fan-in-wing configurations investigated by NR have both indicated a larger lateral or directional static stability power-on than power-off.

Hover Power Effects

An important consideration in hover analysis is the complicated inter-action between the airframe-propulsion system and the ground. Because of ground interference it is necessary to analyze the hover interference effects as a function of airplane height above the ground. For purposes of discussion the hover interference effects have been grouped into four flight modes, (1) hover out of ground effect, (2) hover in ground effect, (3) attitude change in ground effect and (4) hover motions. Each of these flight modes will be discussed separately.

The phrase, out of ground effect, means that there is no interaction between the airframe-propulsion system and the ground. When hovering out of ground effect aerodynamic forces induced by the propulsion system inlet and exit flows are present. The aerodynamic forces induced by the inlet flow are restricted to the bellmouth area and are fairly well understood. On the other hand, the aerodynamic forces induced by the exit flow can be distributed over the entire planform area and are not completely understood at the present time. The propulsion exhaust flow mixes with the surrounding air inducing a cross flow toward the exhaust from all directions, figure 5. Air is drawn across the bottom surfaces resulting in a negative pressure distribution on the aircraft bottom. The normal force, chord force, and pitching moment can be affected by the exhaust interference pressure field.

The factors having an influence upon the power induced lift loss out of ground effect were investigated in reference 7. Based on small model tests the power effect lift due to jet entrainment action was shown to be a function of thrust, the ratio of total planform area to jet exit area, and a jet decay parameter. Some of the test results are shown in figure 6. The jet decay parameter is based on the maximum rate of decay of jet dynamic pressure and the point downstream of the jet exit where the maximum decay rate occurs. While analyzing these data the thought occurred that the jet decay which depends on mixing between the jet and surrounding air should be a function of the surface area of the jet. In turn the jet surface area should be a function of the jet exit circumference. This idea was tested by plotting jet exit circumference versus jet decay. It can be seen in figure 6 that the jet exit circumference is proportional to the jet decay. Obviously jet exit circumference is a much simpler parameter to determine than jet decay. It may be that the data in reference 7 can be correlated in a simpler form. Unfortunately, time did not permit investigating this approach any further than indicated.

When hovering in ground effect the jet exhaust flow contacts the ground and spreads in all directions. A result of this spreading is to bring a greater portion of the airplane planform area closer to the jet thereby increasing the power effect. In the case of a single centerline jet there is usually a larger negative lift force near the ground. In the case of spaced multiple jets some of the flow spreading along the ground interact with each other resulting in an upward flow between the jets. The upward flow causes positive forces to be generated on a portion of the airplane. In some instances the positive pressure forces due to multiple jet interaction is greater than the negative pressure forces due to jet entrainment action, and the net power effect lift is less in ground effect than out of ground effect, figure 5.

Figure 7 presents pictures of oil flow studies made to visualize the jet exhaust flow, in ground effect, for a NR fighter model which was similar to the XV-4B configuration. These pictures indicate the complex nature of the exhaust flow near the ground. It can be seen that the exhaust does not spread uniformly along the ground. Also, the vertical movement of the exhaust between the jets is clearly visible. It can also be seen that the vertically rising exhaust spreads along the entire underside of the fuselage.

The factors having an influence upon the hover interference lift in ground effect have been investigated by means of small model tests. However, attempts to generalize on the results of these tests and correlate them have had limited success to date. Results for single jets have been more successful than for multiple jets. Unfortunately, most actual VTOL airplanes are multiple jet configurations.

If the airplane is pitched or rolled while in ground effect, the interference forces and moments can be altered, figure 8. A change in attitude moves some parts of the airplane closer to the spreading jet and moves other parts farther away from it. Also, the jet does not spread equally in all directions when contacting the ground at an angle. Preliminary indications are that the interference effects due to attitude change while in ground effect are relatively small in most instances.

9

While hovering the aircraft may move about slightly in a three dimensional manner for one reason or another. These slight movements, here called hover motions, are characterized by very low values of velocity (0 to 30 knots) and unusual values of angle-of-sideslip (0 to ±180 degrees). Some distinct types of hover motion are indicated in figure 9. The forces and moments caused by vertical movement during hover are predominately due to the airplane power-off aerodynamic characteristics and are not analyzed in this report. Motion resulting in very large sideslip angles, such as side movement and rear movement, produces the same type of power effects as those experienced in transition flight. However, the direction and location of power effect forces will vary as a function of angle of sideslip. Power effects for very large angles of sideslip are analyzed in this report.

NONDIMENSIONAL COEFFICIENTS

A matter of concern for the VTOL designer is the selection of nondimensional coefficients for expressing aerodynamic power effects. A variety of nondimensional coefficients have been tried. Each agency has tended to develop coefficients for their own particular airframe-propulsion application, and the variety of coefficient forms in use hinders attempts to compare the data for different VTOL aircraft. This situation is likely to continue unless a satisfactory approach to representing VTOL forces and moments can be identified which will be valid for a wide variety of airframe-propulsion combinations. It is essential that a valid nondimensional coefficient be used. Data is normally available only for a limited number of speed and power conditions. The accuracy with which this limited data can be extrapolated or interpolated is related to the validity of the coefficient used.

A sample of coefficients in use to correlate test data taken at fixed values of thrust, velocity, and density conditions is presented in figure 10. Conventional airplane coefficients are based on the fact that the aerodynamic forces are proportional to the freestream dynamic pressure. In the case of VTOL aircraft the power effects are not proportional to freestream dynamic pressure. Even at zero forward velocity a finite aerodynamic power effect force is present. Thus, early attempts to present VTOL data in conventional aircraft form resulted in such difficulties as the coefficients approaching infinity as the speed approached zero. The present thinking is that a VTOL coefficient for power effects should be related to the freestream dynamic pressure and the dynamic pressure of the propulsion exit flow.

A nondimensional speed-power parameter found in NASA reports to correlate jet model data is shown in figure 10. Power effects are plotted versus the square root of the ratio of freestream density times freestream velocity squared to jet density times jet velocity squared.

$$\sqrt{\frac{\rho_\infty V_\infty^2}{\rho_{JET} V_{JET}^2}} = \sqrt{\frac{q_\infty}{\frac{T}{2 A_{JET}}}}$$

10

This parameter is basically similar to the simple speed ratio V_∞/V_{JET} which is also found in use. However, the newer form has generally come to be preferred because it accounts for any jet temperature effects which may exist between cold model jets and hot airplane jets.

The nondimensional coefficient form adopted by Lockheed to correlate XV-4B data is shown in figure 10. Power effects are plotted versus the square root of the ratio of freestream dynamic pressure times wing area to thrust.

$$\sqrt{\frac{q_\infty S}{T}} = \sqrt{\frac{1}{C_T}}$$

The Lockheed parameter is basically the same as the one used by NASA, and data generated by the Lockheed parameter would be proportional to data generated by the NASA parameter.

Coefficient forms selected for the Ryan XV-5A fan-in-wing airplane are also shown in figure 10. In this instance it was assumed that the total force acting on the aircraft was proportional to the sum of the freestream dynamic pressure plus the fan slipstream dynamic pressure $(q + T/A_{JET})$. This was an attempt to account for all effects by a single coefficient. This coefficient form has been used by NASA for tilt-wing propeller models. Conventional propeller model data is normally plotted using a thrust coefficient. There is some question whether the characteristics of a fan-in-wing aircraft like the XV-5A are closer to those of a propeller configuration or are closer to those of a lift jet configuration.

MODEL TEST TECHNIQUES

Model test techniques developed for conventional airplane testing are often not adequate when utilized for VTOL models. It is not uncommon to find significant differences between two sets of model data obtained in different facilities and between model and airplane characteristics. Some unique problems have been encountered in testing VTOL models for which workable solutions are not presently available. One objective of the VIFCS program was to develop improved test techniques that would enable confident prediction of airplane characteristics from model tests. A discussion of current test techniques will now be presented.

TEST FACILITIES

Two primary types of installations have been employed, to date, for testing VTOL models. Conventional wind tunnels have been used to obtain transition flight data, and special outdoor rigs have been used to obtain hover flight data. In some instances, combined hover and transition tests have been conducted in the wind tunnel where proper model support could be provided. In general, a VTOL model requires a more sophisticated facility

than a conventional model. Special provision to power the model are required, and the support system must be capable of positioning the model in a large number of unusual attitudes. Also, some method must be found to minimize or eliminate interference between the model propulsion system and the test apparatus.

Transition tests have, until recently, been conducted in existing wind tunnel facilities which were designed prior to the arrival of VTOL testing. It was inevitable that problems of incompatibility between model requirements and tunnel capability would arise. It quickly became apparent that conventional size models experienced excessive interference between the propulsion wake and the tunnel walls, and adequate theoretical techniques for correcting the model data for this interference were not available. Thus, the trend in recent VTOL testing has been to test the model in a larger test section to reduce or minimize jet wake distortion. However, suitable large test sections are just becoming available. In an attempt to utilize available facilities, VTOL models are often tested in the larger tunnel area just forward of the conventional test section. The maximum velocity available in forward sections is considerably less than that available in the conventional test section. The lower test velocities result in very low Reynolds numbers and make questionable those values which are functions of Reynolds number. Also, the low test velocities require that the data be extrapolated, sometimes extensively, in order to cover the entire transition speed range. In recognition of these problems many agencies are building new wind tunnels specifically designed for VTOL testing. The newer facilities tend to provide much larger test sections than existing tunnels in combination with adequate tunnel velocities.

In the case of the XV-4B airplane, Lockheed used two powered models of different size which were tested in different size tunnels to obtain transition flight data. An 0.18 scale XV-4B powered model was tested in the Ling-Temco-Vought 7 x 10 foot conventional low speed tunnel, and an 0.16 scale XV-4B powered model was tested in the Langley 17 foot section which is just forward of their conventional low speed test section. The different test section arrangements for these two tests is indicated in figure 11, and a detailed comparison of the test data for these two tests is presented in Section IV.

One approach to VTOL wind tunnel problems is to test a full scale airplane with actual propulsion units in a very large tunnel, like the Ames 40 x 80 facility. A considerable amount of this type of testing has been done. Full scale models of the XV-5A, XV-4A, XV-22, etc., have been tested. This approach provides good data but is expensive and slow.

Hover tests are a unique requirement for VTOL aircraft, and hover test techniques and facilities are still in a developing state. Hover simulation of a VTOL airplane must include very low velocities from any direction to the vehicle as well as static conditions. Static hover tests have been conducted using transition models tested in the wind tunnel and simplified models tested on special outdoor hover rigs. The primary difference between these test installations is the walls surrounding the model when it is tested in a wind tunnel. At the present time, not enough is known about the probable effect of tunnel walls on hover tests to determine if outdoor tests are absolutely necessary. Obviously, using one model in one test facility for both hover

12

and transition testing is a desirable arrangement. Since hover simulation involving low velocity movement in any direction must be conducted in a wind tunnel, why not strive to develop adequate test techniques for obtaining all hover data in a wind tunnel?

During the development of the XV-4B airplane, hover tests were conducted in the Langley 17 foot test section and on a Lockheed outdoor hover rig. These two test arrangements are illustrated in figure 11, and a detailed comparison of the test data for these two installations is presented in Section IV.

MODELS

Accurate simulation of the aircraft propulsion system by the model appears to be important. The ideal situation would be to match the inlet conditions, the exit conditions, and the freestream conditions for any flight condition. However, existing models seldom provide this degree of versatility. Some models match the exit conditions but may not provide an inlet flow. In some instances, the exit conditions cannot be exactly simulated by the model because of an inadequate power supply or limitations of the model propulsion units. For instance, the maximum model thrust for the Ryan XV-5A model was 30 percent of the equivalent full scale thrust, and the maximum model thrust for the 0.16 scale XV-4B model was 60 percent of the equivalent full scale thrust. In some instances the inlet conditions cannot be exactly simulated because of limitations of the model units. Inlet flow is often provided by means of suction lines or the entrainment action of jet pumps. Neither of these techniques has much flexibility to match inlet conditions for a variety of thrust conditions. In the long run, more versatile propulsion units for models having characteristics closer to the full scale propulsion units will probably need to be developed. For the present, the VTOL engineer must be very careful of the basis upon which data for different tests and models is correlated.

For practical reasons, VTOL models normally employ cold air jets to simulate the hot exhaust flow of full scale engines. The ability of a cold jet to simulate hot exhaust flow is investigated in reference 8. Small models powered with cold jets were correlated with similar full scale models powered with a J-85 engine. It was concluded that the small-scale, cold-jet model test results correlated reasonably well with the full scale turbojet powered models.

Indeterminate interferences in wind tunnel data can be caused by model mounting systems. The proper formation of the jet wake may be circumvented by wing and tail strut mounts, such as those used in the LTV tests of the XV-4B model. The wake may be distorted by wing struts and impinge on the tail strut in close proximity to the model. These distortions will interfere with proper simulation requirements and cause extraneous distortion of the free air over the model. It is therefore suggested that future model mounting supports should be placed above or well behind the model so that they will not obstruct the lifting system wake and result in indeterminate errors.

13

Extracting power effects from total force measurements requires very careful and precise work to avoid errors. The direct thrust is the predominate force acting, and small errors in the thrust terms can result in large errors in power effect terms. Errors in determining the thrust terms could result from many things. The thrust moment is normally determined by assuming that the thrust acts along the geometric centerline of the exit nozzle. A non-uniform exit flow or a distorted wake due to tunnel wall interference would result in an actual thrust line different from the apparent geometric one. During Langley Test 178 an incorrect distance between the nozzle exit and the center of gravity was inadvertently used in the data reduction program. As a consequence, all of the power effect pitching moment data was in error by a significant amount.

One way to ensure greater accuracy in the determination of power effect terms would be to measure the aerodynamic forces separately. Models should be built as a shell, separate from the inlet and exhaust plumbing, and supported to the plumbing by a force balance which can be sized for the aerodynamic forces. The total force including propulsion forces would be measured by an additional force balance.

These modeling techniques have been used by NR for a company sponsored V/STOL fighter program (model built as shell and mounted independent of propulsion piping). Also, NR, NASA, and the industry has recently put this modeling method to use to obtain installed propulsion nozzle and afterbody force data on more recent air vehicle designs (F-111, F-14, F-15, etc.).

STRAKE
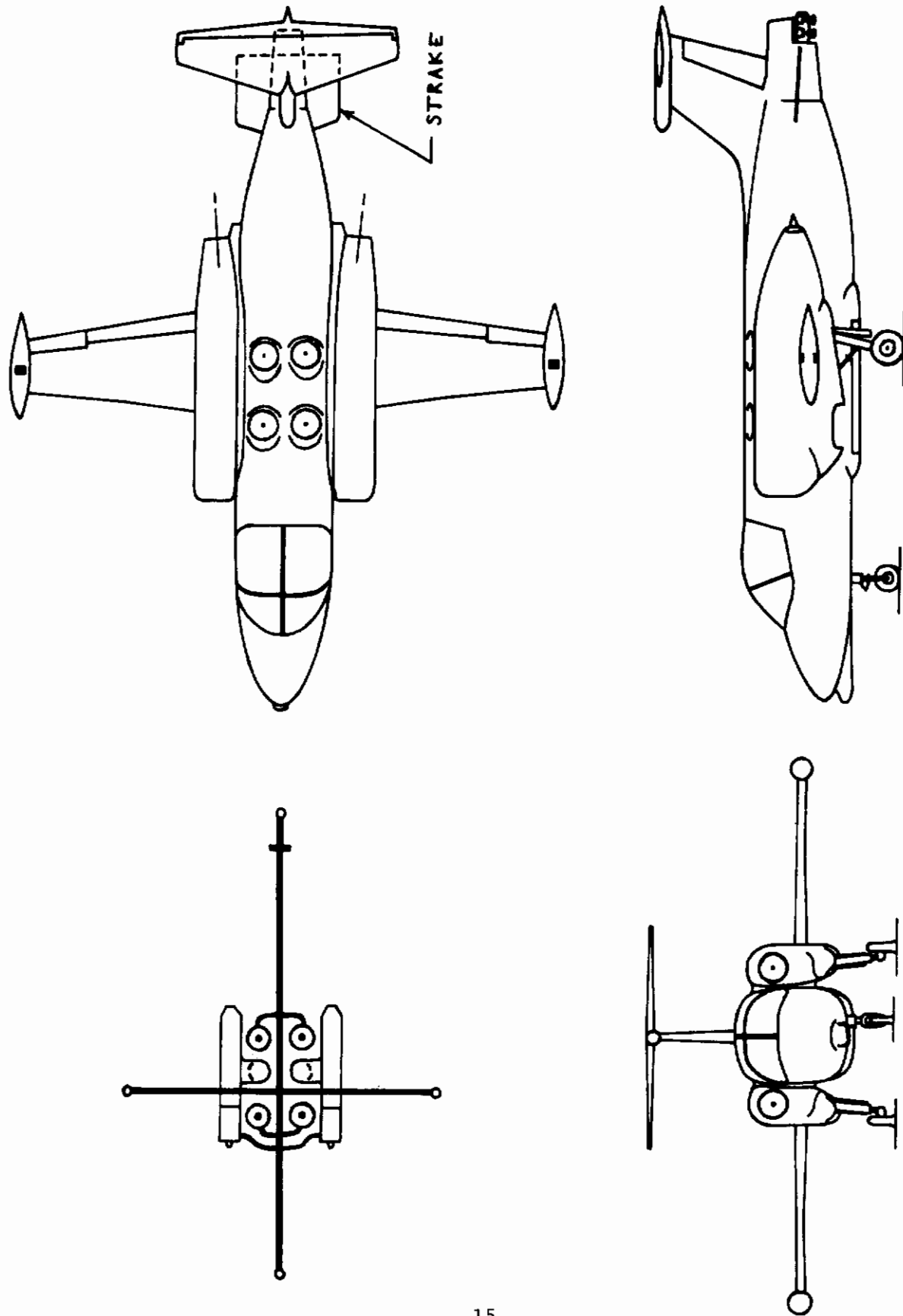
Fig. 1. General Arrangement of XV-4B
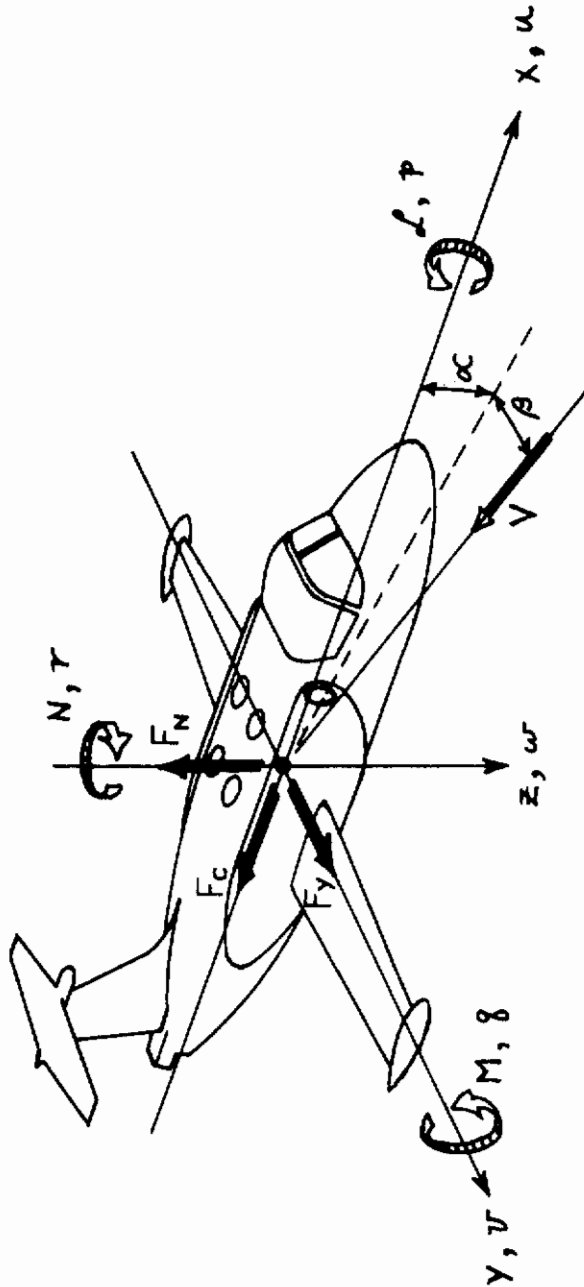
	AERO. POWER-OFF	POWER EFFECT	ENGINE THRUST	REACTION CONTROL	ENGINE GYROSCOPIC
$I_y \dot{q} - I_{xz}(r^2 - p^2) - pr(I_z - I_x) =$	$+M_{AERO}$	$+M_{PE}$	$+M_T$	$+M_{RC}$	$+M_{GYRO}$
$I_x \dot{p} - I_{xz}(\dot{r} + pq) - qr(I_y - I_z) =$	$+\mathcal{L}_{AERO}$	$+\mathcal{L}_{PE}$	$+\mathcal{L}_T$	$+\mathcal{L}_{RC}$	$+\mathcal{L}_{GYRO}$
$I_z \dot{r} - I_{xz}(\dot{p} - qr) - pq(I_x - I_y) =$	$+N_{AERO}$	$+N_{PE}$	$+N_T$	$+N_{RC}$	$+N_{GYRO}$
$m(\dot{u} - rv + qw + g\sin\theta\cos\phi) =$	$-F_{C_{AERO}}$	$-F_{C_{PE}}$	$+F_{X_T}$	$\cdots$	
$m(\dot{v} - pw + ru - g\cos\theta\sin\phi) =$	$+F_{Y_{AERO}}$	$+F_{Y_{PE}}$	$\cdots$	$+F_{Y_{RC}}$	
$m(\dot{w} - qu + pv - g\cos\theta\cos\phi) =$	$-F_{N_{AERO}}$	$-F_{N_{PE}}$	$-F_{N_T}$	$-F_{N_{RC}}$	

MOMENTS | FORCES

Fig. 2.   XV-4B Equations of Motion

16

$$F_{N_{PE}} = F_{N_{POWER \atop ON}} - \left[F_{N_{POWER \atop OFF}} + F_{N_{THRUST}} \right] = F_{N_{INLET}} + F_{N_{EXIT}} + F_{N_{H.TAIL}}$$

$$F_{C_{PE}} = F_{C_{POWER \atop ON}} - \left[F_{C_{POWER \atop OFF}} + F_{C_{THRUST}} \right] = F_{C_{INLET}} + F_{C_{EXIT}}$$

$$M_{PE} = M_{POWER \atop ON} - \left[M_{POWER \atop OFF} + M_{THRUST} \right] = M_{INLET} + M_{EXIT} + M_{H.TAIL}$$

$$F_{Y_{PE}} = F_{Y_{POWER \atop ON}} - \left[F_{Y_{POWER \atop OFF}} + F_{Y_{THRUST}} \right] = F_{Y_{INLET}} + F_{Y_{EXIT}} + F_{Y_{V.TAIL}}$$

$$N_{PE} = N_{POWER \atop ON} - \left[N_{POWER \atop OFF} + N_{THRUST} \right] = N_{INLET} + N_{EXIT} + N_{V.TAIL}$$

$$\mathcal{L}_{PE} = \mathcal{L}_{POWER \atop ON} - \left[\mathcal{L}_{POWER \atop OFF} + \mathcal{L}_{THRUST} \right] = \mathcal{L}_{INLET} + \mathcal{L}_{EXIT} + \mathcal{L}_{V.TAIL}$$

COMPLETE MODEL POWER EFFECT SOURCE OF POWER EFFECT

Fig. 3. Definition of Power Effect Terms

17
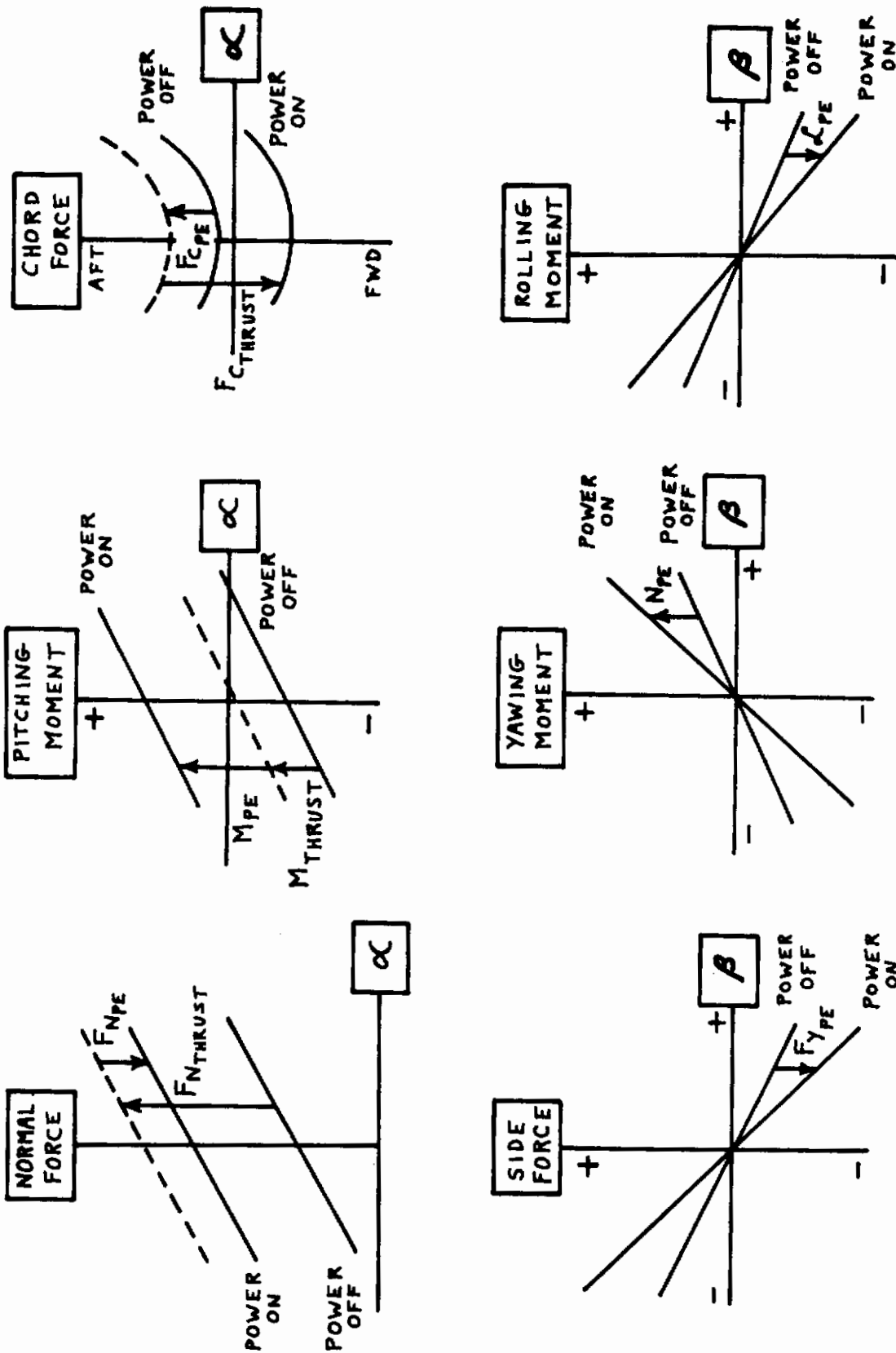
Fig. 4. Results of Power Effects on Aerodynamic Characteristics during Transition Flight

18
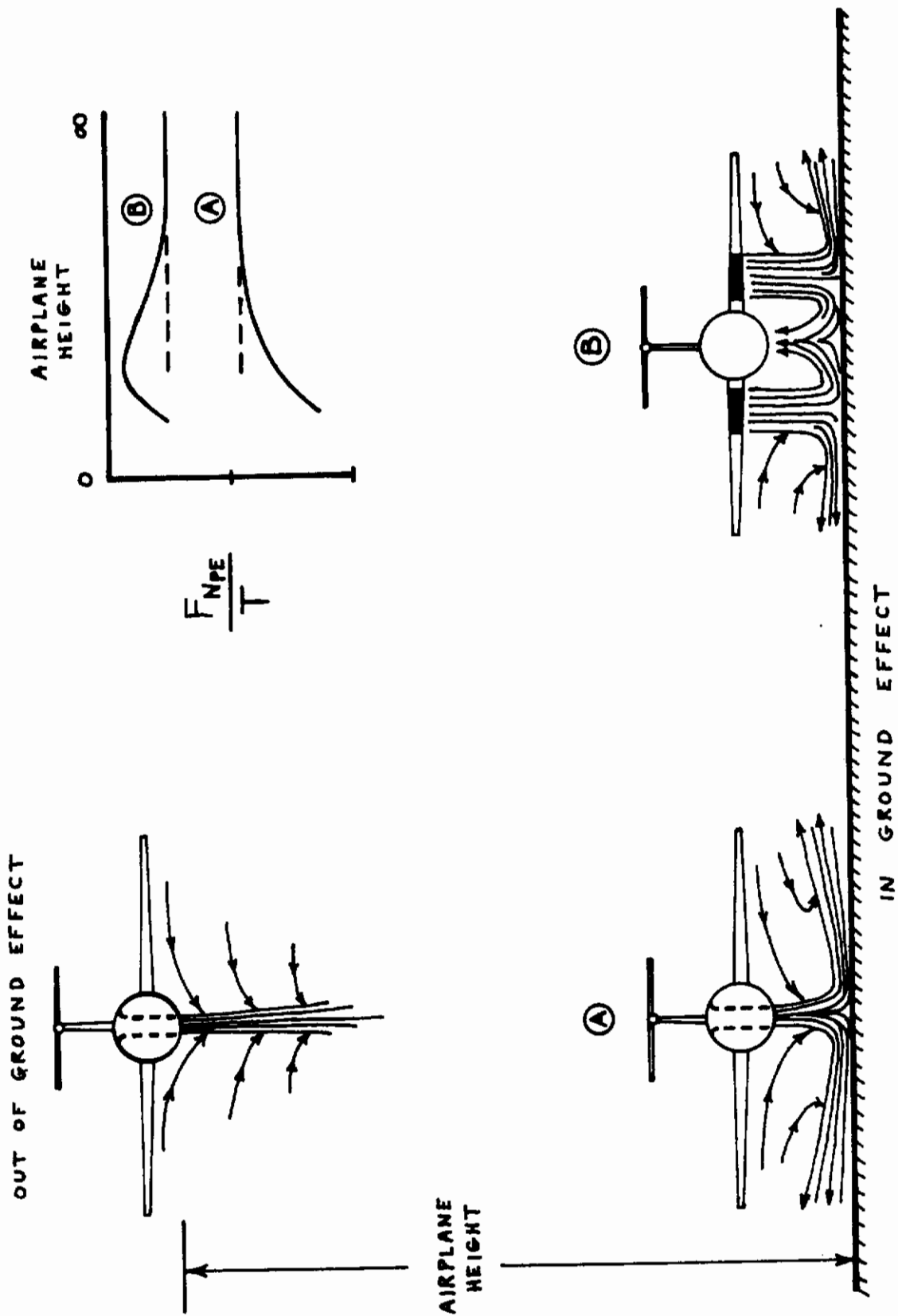
Fig. 5.   Exhaust Flow Fields in Hover

19
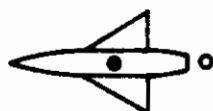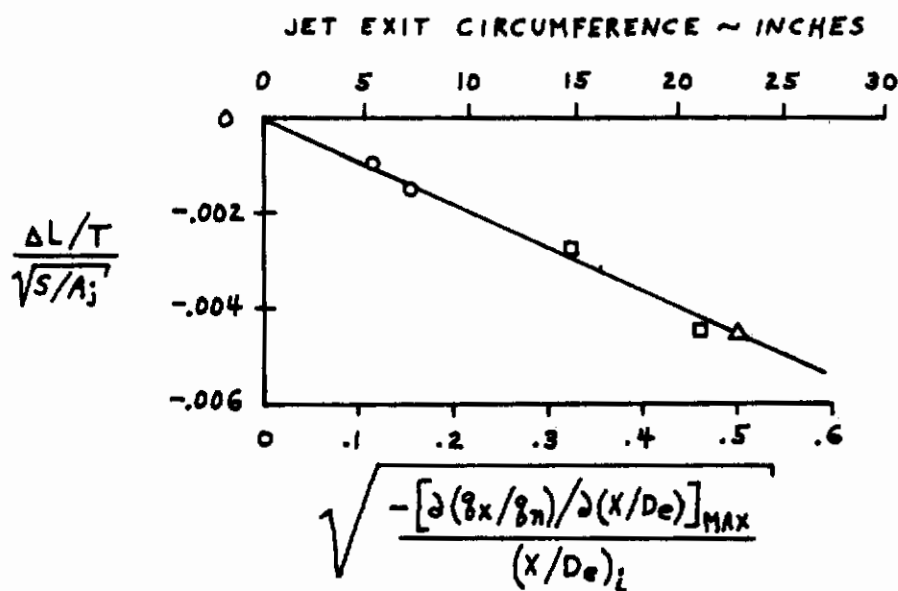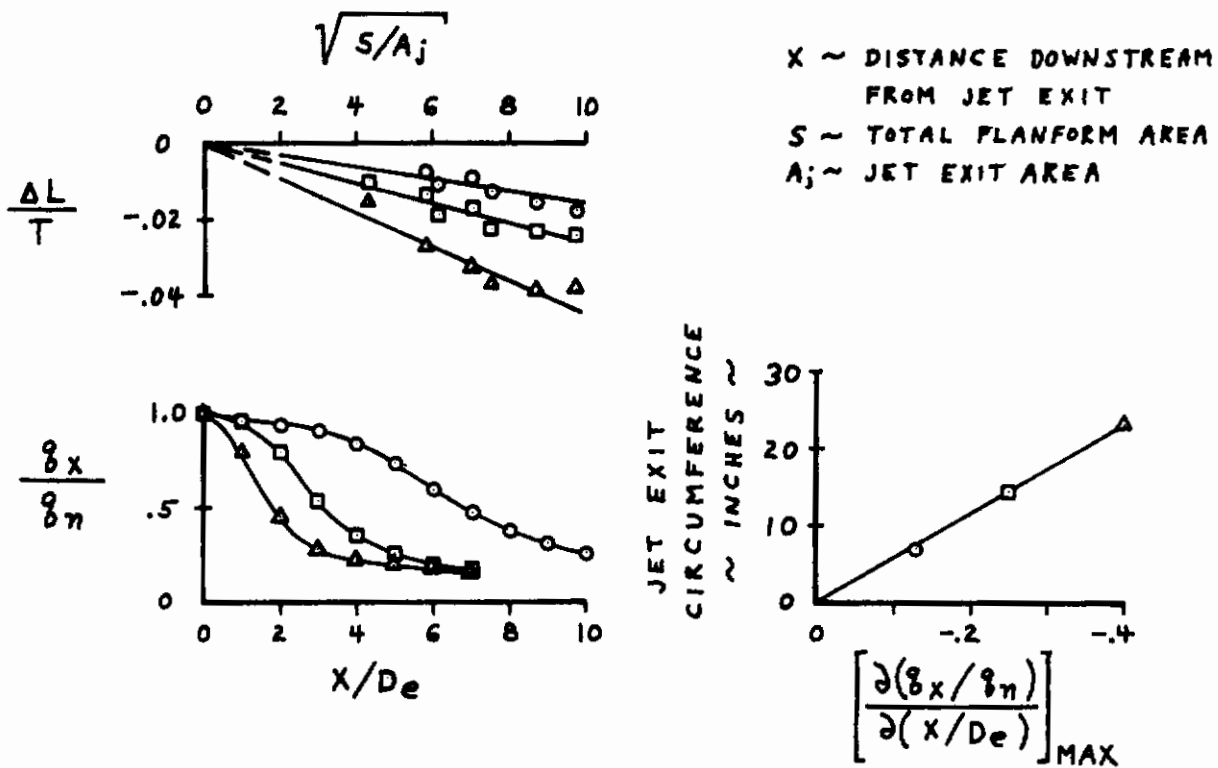
Fig. 6. Effect of Jet Exit Geometry and Jet Decay on
Power Effect Lift out of Ground Effect

20
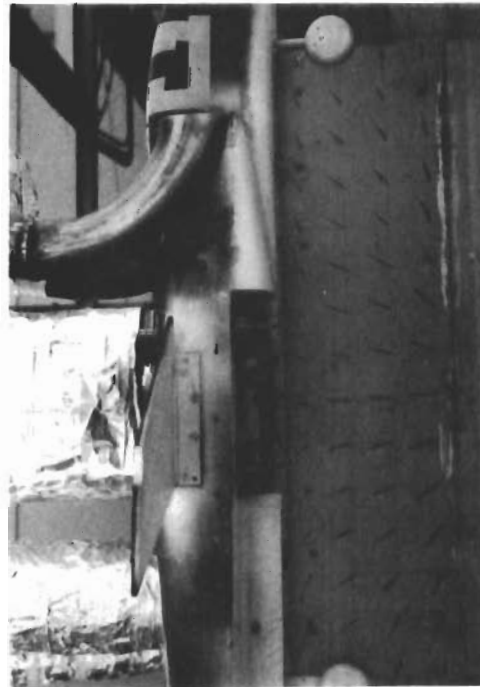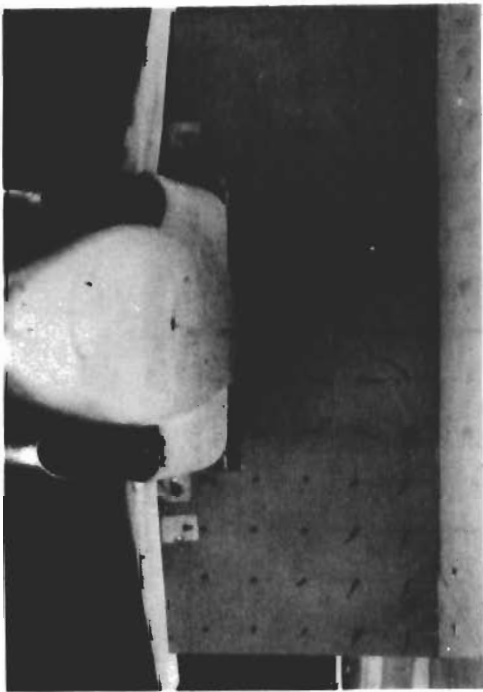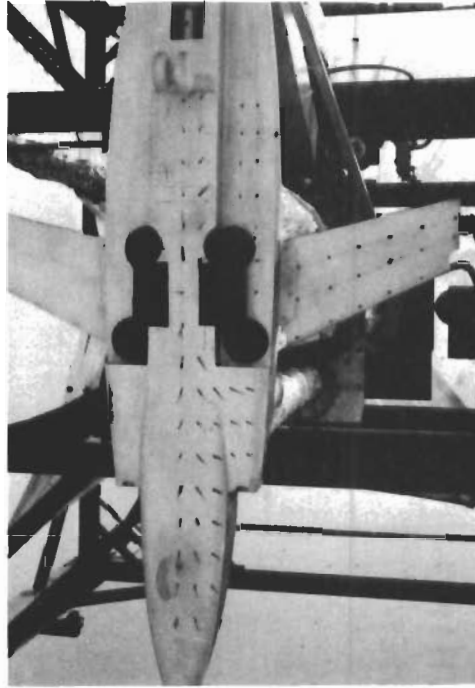
Fig. 7. Oil Flow Visualization in Hover

21

PITCHING MOMENT

ROLLING MOMENT

IN GROUND EFFECT
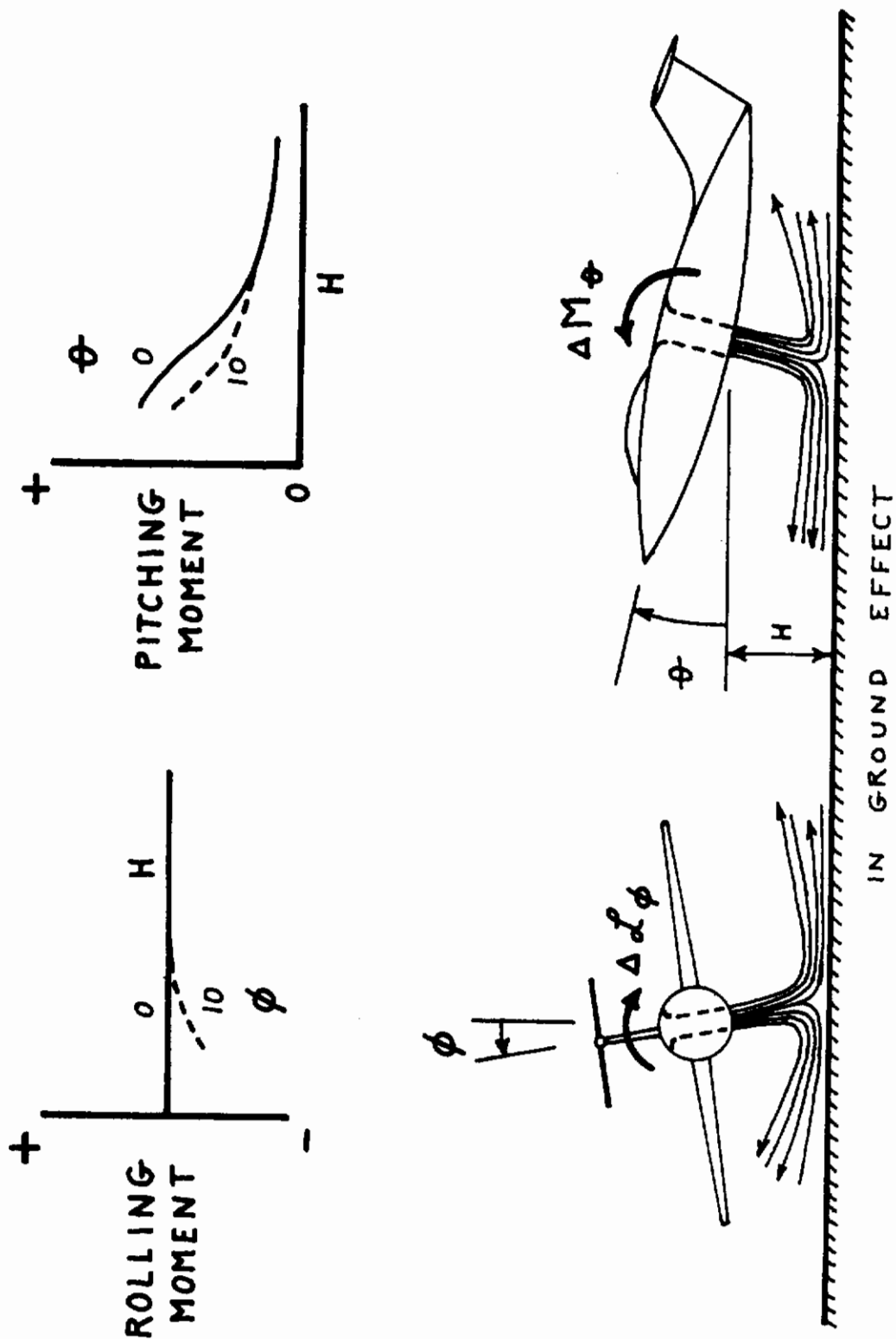
Fig. 8.   Effect of Changing Attitude while Hovering near the Ground

22

VERTICAL
MOVEMENT
$(\alpha = 90°\quad \beta = 0)$

V

$F_{N_{AERO}}$

SIDE
MOVEMENT
$(\alpha = 0 \quad \beta = 90°)$

Fy_{AERO} Fy_{PE}

V

$F_{N_{PE}}$
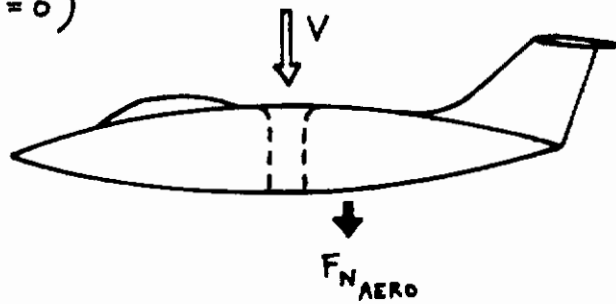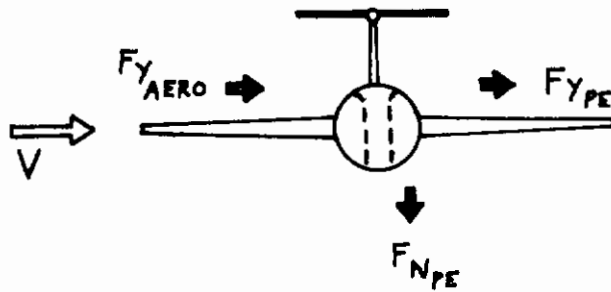
REAR
MOVEMENT
$(\alpha = 180°\quad \beta = 180°)$

$F_{N_{AERO}}$

$F_{C_{PE}}$

V

$F_{N_{PE}}$

Fig. 9. Hover Motion Effects

23

$$L = L_{AERO} + T + L_{PE}$$

TOTAL LIFT = POWER-OFF LIFT + THRUST + POWER EFFECT

L_{AERO} L_{PE} T

8;V

EVENTUAL VTOL SPEED-POWER PARAMETER

NASA JET MODELS

$$\left[\frac{L_{PE}}{T}\right] \text{ vs } \sqrt{\frac{\rho_\infty V_\infty^2}{\rho_{JET} V_{JET}^2}}$$

XV-4B MODEL

$$\left[\frac{L_{PE}}{T}\right] \text{ vs } \sqrt{\frac{gS}{T}}$$

XV-5A MODEL

$$\left[\frac{L}{\left(g + T/A_{JET}\right)A_{JET}}\right] \text{ vs } \left[\frac{T}{\left(g + T/A_{JET}\right)A_{JET}}\right]$$

PROPELLER MODELS

$$\left[\frac{L}{gS}\right] \text{ vs } \left[\frac{T}{gS}\right]$$

$\dfrac{L_{PE}}{T}$

+   −

XV-5A   XV-X   XV-4B

?
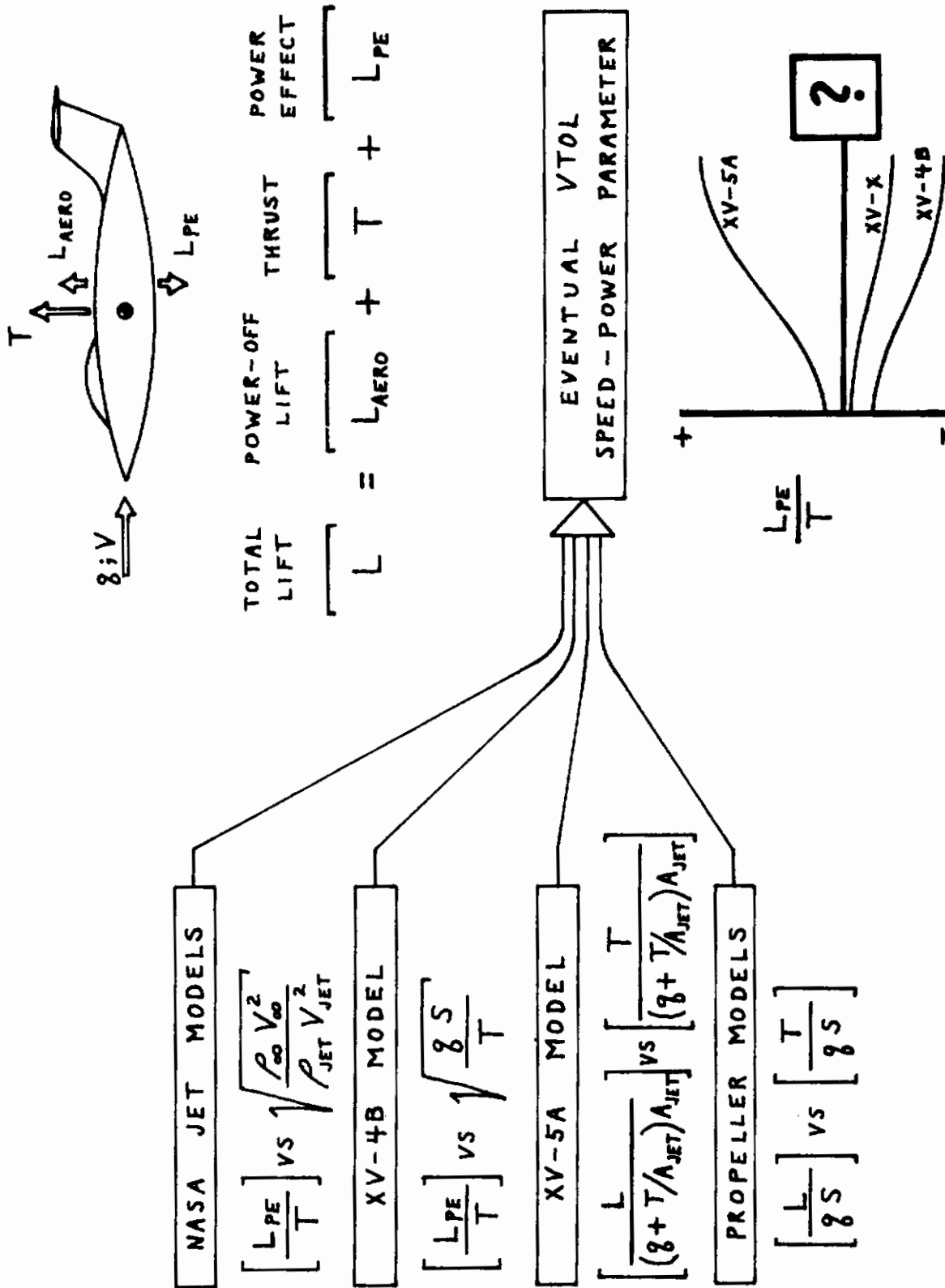
Fig. 10. VTOL Nondimensional Coefficients

24
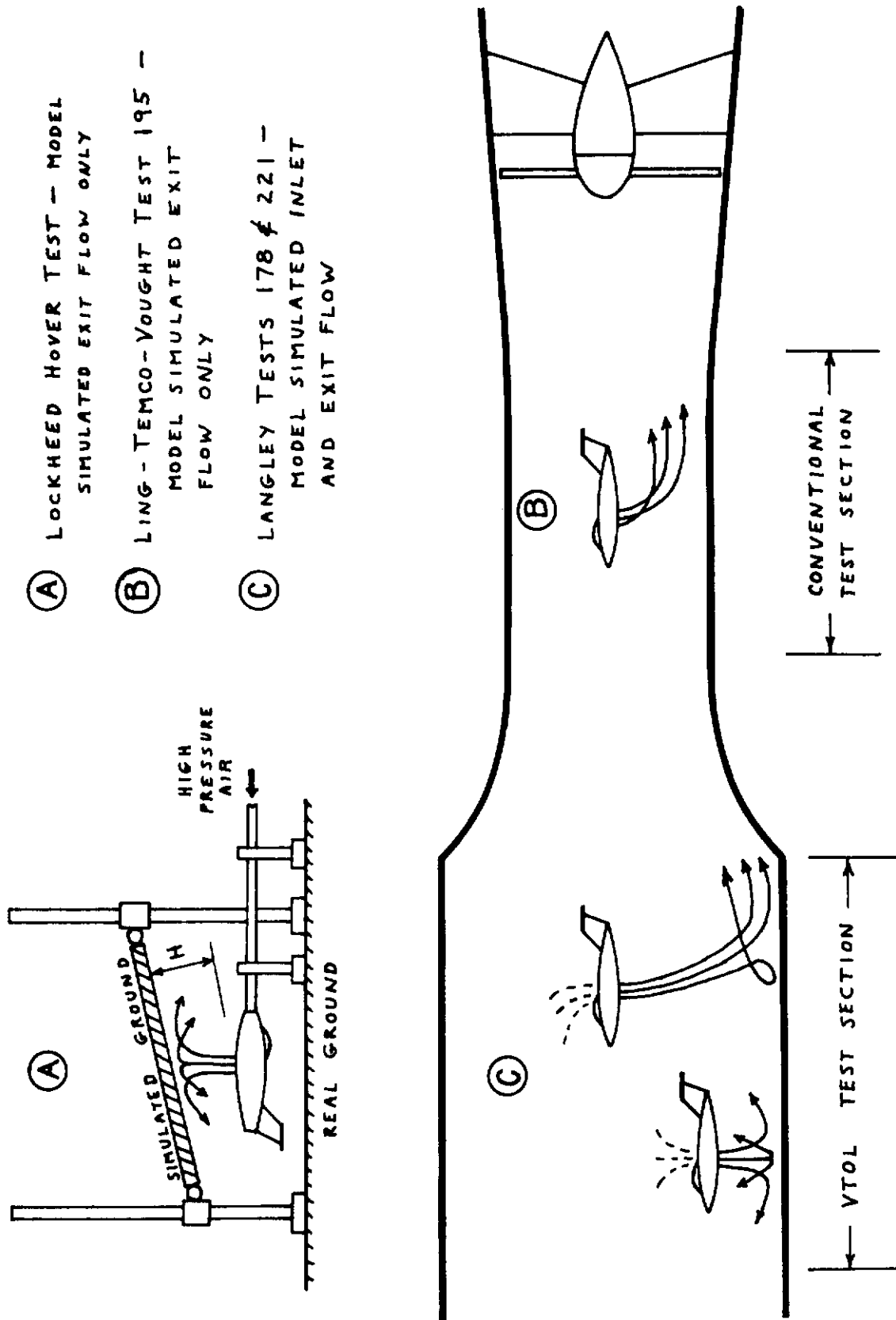
(A) LOCKHEED HOVER TEST — MODEL SIMULATED EXIT FLOW ONLY

(B) LING-TEMCO-VOUGHT TEST 195 — MODEL SIMULATED EXIT FLOW ONLY

(C) LANGLEY TESTS 178 & 221 — MODEL SIMULATED INLET AND EXIT FLOW

Fig. 11. Types of XV-4B Powered Model Tests conducted as Part of VIFCS Program

25

Section IV

ANALYSIS AND CORRELATION OF AERODYNAMIC DATA

This section describes analysis and correlation work carried out as part of the VIFCS program. The analysis work presented was directed toward the following objectives: (1) estimate from model data the power effects in hover and transition, (2) show the degree of correlation that exists between different model tests, (3) investigate the influence of wind tunnel wall interference and test techniques upon the experimental data, and (4) investigate nondimensional coefficients for defining VTOL characteristics.

The primary configuration for which analysis was performed was the XV-4B. Other configurations for which some effort was expended were the XV-5A and the P-1127.

LIST OF XV-4B MODEL TESTS

A series of powered and unpowered XV-4B model tests were conducted as part of the VIFCS program. A variety of different models and different test facilities were employed to obtain this data. Details of these tests are contained in Section V. A list of tests which were considered to some degree in carrying out the analysis work in this section follows:

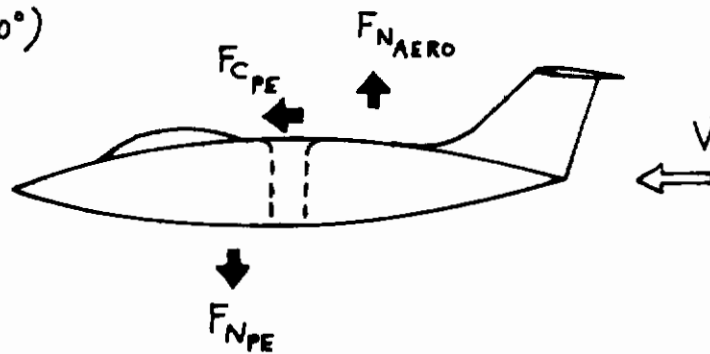| LOCATION	TEST NO.	REF. NO.	TYPE OF DATA
Lockheed, Ga.		25	Outdoor hover rig
Ling-Temco-Vought	195	26	Transition power effects
Langley, Va.	178	11 & 27	Powered and unpowered phases of conventional, hover and transition flight
University of Maryland	488 & 493	28 & 29	Power-off characteristics
Langley, Va.	221	12	Additional powered tests for hover and transition flight
Langley, Va.	226	30	Additional unpowered tests
NR, Los Angeles	592	5	Jet exhaust flow studies
NR, Los Angeles	622	6	Inlet flow studies

ANALYSIS OF XV-4B POWER EFFECTS IN TRANSITION FLIGHT

ANALYSIS GUIDELINES

The model configuration was Phase I (six engines in lifting mode), without ground plane, and with wing flaps down 40 degrees. Except where noted otherwise, the data are for the basic nozzle vector angle of zero degrees. It should be noted that the data analyzed herein are for models which did not have strakes on the aft fuselage. The strakes shown in figure 1 were not originally part of the configuration but were added later in the program. Power-on tests to evaluate the effect of the strakes were conducted, but the results had not yet become available at the time this analysis was completed.

All data was first plotted in dimensional form, force in pounds, moment in foot pounds, for the full-scale airplane and sea level standard conditions. Using dimensional data for analysis purposes is possible for a VTOL airplane because they tend to operate in a narrow speed and altitude range. It is felt that some of the data trends are more apparent in dimensional form than in coefficient form. Also, a better appreciation for the magnitude of the effects is possible. After analyzing the data in dimensional form the results were converted into the Lockheed nondimensional coefficient form.

All analysis work is based on a body axis system. This is felt to have several advantages. Flight simulation work is based on a body axis system, and it is customary to supply input data in a body axis form. Also, indications are that many VTOL power effects may be relatively independent of angle of attack and should correlate better in the body axis system.

In presenting the data the power-on values are plotted and the sum of the power-off values plus the thrust contribution is plotted. The difference between the two plots is by definition the power effect.

LONGITUDINAL DATA

Normal Force

The effect of angle of attack upon the complete model power effect was investigated first. Typical normal force versus angle of attack data for several combinations of thrust and tunnel dynamic pressure are presented in figure 12. This data was obtained from Langley Test 178 and LTV Test 195.

The data shows that the power effect normal force is approximately independent of angle of attack below the wing stall point. Above the wing stall point the data indicates that the power effect changes abruptly. This abrupt change in power effect is a result of the stall angle of attack being a function of thrust and dynamic pressure. The change in wing angle of attack at stall due to power is plotted in figure 13. The power-off load distribution at a given angle of attack is reduced by the jet induced load. This results in the wing stall occurring at a higher angle of attack with power-on than with power-off. Thus, the power effect is not the difference between

27

the two plots in figure 12 for angles beyond the stall. To indicate the true power effect beyond the stall the power-off data should be adjusted to have the same stall angle as the power-on data. When this is done the power effect normal force is approximately constant over the entire angle of attack range.

The effect of thrust upon the power effect normal force was investigated at zero angle of attack. A plot of power effect normal force versus thrust for various dynamic pressures is presented in figure 14. The Langley data indicates that the power effect normal force is linear with thrust, and the LTV data indicates that the power effect normal force is slightly nonlinear with thrust. The Langley data includes a lot more test points than the LTV data, but the LTV data covers a wider range of thrust and dynamic pressure values. It is felt that the power effect normal force is linear with thrust, but the data is not conclusive on this point.

An area of possible disagreement between the two sets of test data is model differences. The Langley test used a model which simulated engine inlet flow, and the model used for the LTV test did not simulate the engine inlet flow. To investigate the effect of inlet flow the Langley model was tested with the inlet open and with the inlet blocked. The results are plotted in figure 15. The data indicates that the power effect normal force with inlet open is approximately 125 percent of the power effect normal force with inlet closed.

Based on the preceding analysis, it was felt that two adjustments should be made to the data at this point. The LTV data was refaired to be linear with thrust, and the effect of inlet flow was removed from the Langley data. These adjustments were applied to the power effect normal force data shown in figure 14 and the results are presented in figure 16.

The power effect normal force versus thrust data shown in figures 14 and 16 is shown cross plotted versus dynamic pressure for constant thrust values (6,100; 10,560; 14,920) in figure 17. The results indicate that the power effect normal force is a nonlinear function of dynamic pressure. Also, the data plotted in this form clearly indicates the degree of agreement between the Langley and LTV test results.

A final plot was prepared which nondimensionalizes the cross plotted data in the Lockheed coefficient form, figure 18. The Lockheed parameter did a good job of correlating the normal force data. Also, the final adjusted data indicates good agreement between the Langley and LTV data. However, no adjustment for tunnel wall effects has been applied to the data at this point.

Pitching Moment

Typical pitching moment versus angle of attack data is presented in figure 19 for several combinations of thrust and dynamic pressure. This data is from Langley Test 178 and LTV Test 195. The power effect pitching moment is not constant with angle of attack as was the power effect normal force. The power effect pitching moment increases slightly with increasing angle of attack. The nonlinear nature of the power effect pitching moment is due to the nature of the downwash acting on the tail. With the tail-off the power effect pitching moment is constant with angle of attack.

28

The effect of thrust upon the power effect pitching moment was investigated at zero angle of attack. A plot of power effect pitching moment versus thrust for various dynamic pressures is shown in figure 20. This data is taken directly from Langley Test 178 and LTV Test 195.

The measured pitching moment due to inlet momentum based on Langley Test 178 is shown in figure 21. The effect was determined by testing the model with the inlet open and with the inlet blocked. The inlet momentum causes a nose up pitching moment which increases with increasing thrust or increasing dynamic pressure. The total moment results from incremental normal forces and chord forces acting on the lift engine bellmouths and the cruise engine. The moment can be expressed in a simplified form by multiplying the ram drag by an effective lever arm, refer to figure 21.

Adjustments which were applied to the normal force data were also applied to the pitching moment data. The LTV data was refaired versus thrust, and the effect of inlet flow was removed from the Langley data. The power effect pitching moment versus thrust with these adjustments is presented in figure 22.

The power effect pitching moment versus thrust data in figures 20 and 22 is cross plotted versus dynamic pressure for constant thrust values in figure 23. The results indicate that the inlet momentum has a large influence on the power effect pitching moment. Also, the adjusted test data shows a large disagreement between the Langley and LTV test results. The good agreement shown between the Langley and LTV unadjusted data is felt to be only a coincidence.

In figure 24 the power effect pitching moment data is nondimensionalized in the Lockheed coefficient form. Neglecting the mismatch between sets of data, the Lockheed parameter appears to do a good job of correlating the pitching moment data for each of the tests taken separately. No adjustment for tunnel wall effects has been applied to the data at this point.

Chord Force

Typical chord force versus angle of attack data is shown in figure 25 for several combinations of thrust and dynamic pressure. The data is from Langley Test 178 and LTV Test 195. The data shows that the power effect chord force is approximately independent of angle of attack below the wing stall point. Above the wing stall point the data indicates that the power effect changes abruptly. This abrupt change in power effect is a result of the stall angle of attack being a function of thrust and dynamic pressure. For a more detailed description of the effect of power on stall angle of attack, refer to the preceding analysis of the normal force. If the chord force data is adjusted to have the same stall angle of attack power on or off the power effect chord force is approximately independent of angle of attack over the entire angle of attack range.

The effect of thrust on the power effect chord force at zero angle of attack for different values of dynamic pressure is indicated in figure 26. The two sets of test data compared are in very poor agreement. The Langley Test 178 results indicate a positive chord force, but the LTV Test 195 results indicate a negative chord force.

29

The measured chord force due to inlet momentum based on Langley Test 178 is shown in figure 27. The incremental chord force was measured by testing the model with the inlet open and with the inlet blocked. The inlet momentum causes a significant drag force which increases with increasing thrust or increasing dynamic pressure.

Adjustments which were applied to the normal force and pitching moment data were also applied to the chord force data. The LTV data was refaired versus thrust, and the effect of inlet flow was removed from the Langley data. The power effect chord force versus thrust with these adjustments is presented in figure 28. It can be seen that substantial differences between the two sets of data still exist. This problem was investigated but no satisfactory reason for the discrepancy can be given at this time. However, it can be observed that the Langley data is orderly whereas the LTV data exhibits large data scatter and lack of order. As a result it is felt that the Langley data probably represents the airplane and the LTV data is somehow in error.

The power effect chord force versus thrust data in figures 26 and 28 was cross plotted versus dynamic pressure for constant thrust values, figure 29. The large discrepancy in the two sets of test data is also clearly evident in these plots.

In figure 30 the power effect chord force data is nondimensionalized in the Lockheed coefficient form. The Lockheed parameter does a good job of correlating the Langley data but cannot correlate the LTV data. This is further evidence that the LTV chord force data is probably in error, since the Lockheed parameter worked well for both sets of data in the case of normal force and pitching moment. No adjustments for tunnel wall effects has been applied to the data at this point.

Downwash

Downwash with and without power was determined using horizontal stabilizer effectiveness runs obtained during Langley Test 178. The downwash is plotted versus angle of attack in figure 31. The downwash is substantially larger with power-on than with power-off, and the rate of change of downwash with angle of attack is larger power-on than power-off.

The increment in downwash due to power at zero angle of attack indicated in figure 32 was used to investigate the probable effect of thrust and dynamic pressure. Because of the small number of test points, an empirical expression was used to extrapolate the power effect of downwash data with thrust and dynamic pressure. It was assumed that the power effect downwash is proportional to the square root of the ratio of thrust divided by the dynamic pressure, figure 32. Utilizing this simple relationship the **power effect downwash could** be represented as a single curve when plotted versus the Lockheed nondimensional speed-power parameter.

An NR correlation of fan-in-wing model data was also replotted versus the Lockheed speed-power parameter. The results are shown in figure 32 along with the XV-4B data. Both sets of data show a similar trend. Although the limited evidence presented here is far from conclusive, it appears probable

30

that the power effect downwash can be correlated using the Lockheed speed-power parameter.

An attempt was made to determine the relative contribution of the inlet and exit flow to the total power effect downwash. The downwash produced by an XV-4B type inlet only and an XV-4B type exit only were experimentally determined. Detailed descriptions of these tests are given in section V. In figure 33 the downwash produced by an inlet only and an exit only are compared with the Langley complete model data. The component tests indicate a downwash only about 40 percent as large as that measured for the complete model. The following explanation for this result is offered. The inlet and exit models did not include a wing. The jet entrainment flow significantly alters the wing spanwise load and wing downwash. This explanation logically leads to the conclusion that the effect of the exit flow on the wing downwash is the primary mechanism for the XV-4B power effect downwash. Less than 10 percent of the XV-4B power effect downwash can be attributed to the inlet flow.

Wind Tunnel Wall Effect

The influence of the wind tunnel walls on the XV-4B jet powered model data was experimentally investigated by testing an XV-4B type jet only. A detailed description of this test is given in Section V, subsection 1 and will not be repeated here. This test was conducted in such a way that jet flow, tunnel size and speed ranges for Langley Test 178 and LTV Test 195 could be represented at a smaller scale. Angle of attack changes at wing and tail locations due to jet power and tunnel speed were measured in the two tunnel sizes. The incremental changes in angle of attack due to tunnel size only were estimated using this data.

A tunnel wall adjustment to the LTV Test 195 longitudinal data was estimated to indicate the nature and magnitude of the effect. The data is not corrected to free air conditions but rather to a larger tunnel size. The adjusted data would be what you might expect if the LTV model had been tested in the larger test section used for Langley Test 178.

The LTV data normal force and pitching moment were adjusted for the influence of the wind tunnel walls using the following equations.

$$\Delta F_{N_{WALLS}} \approx \left(\frac{\partial F_N}{\partial \alpha}\right)_{\substack{TAIL \\ OFF}} \left(\Delta \alpha_L - \Delta \alpha_s\right)_{WING} + \left(\frac{\partial F_N}{\partial \alpha}\right)_{TAIL} \left(\Delta \alpha_L - \Delta \alpha_s\right)_{TAIL}$$

$$\Delta M_{WALLS} \approx \Delta F_{N_{\substack{TAIL \\ OFF}}} X_{\substack{TAIL \\ OFF}} + \Delta F_{N_{TAIL}} X_{TAIL}$$

31

The equations provide for a separate increment in normal force for the wing-body and tail. The change in normal force is based on multiplying the change in angle of attack due to tunnel size by the power-off slope of the normal force versus angle of attack curve. The values used for change in angle of attack at the wing-body and tail are experimentally determined values given in figures 126 and 127. The change in pitching moment was obtained by multiplying the increment in normal force by the distance from the c.g. to the normal force center of pressure.

The estimated effect of the wind tunnel walls on the data for LTV Test 195 is presented in figure 34. The experimental evidence indicates the model is operating in a strong power induced downwash field. When confined in a wind tunnel this power induced downwash field is reduced somewhat. Logically the effect of increasing the tunnel size for the LTV model would be to increase the jet entrained downwash somewhat with a resulting increase in the power effect values. This can be seen in figure 34 to be the case. It can also be seen in figure 34 that adjusting the LTV data for wall effect resulted in a larger disagreement between the Langley and LTV data.

LATERAL DIRECTIONAL DATA

Side Force

Typical wind tunnel side force data at zero angle of attack (α) are shown in figure 35 as a function of sideslip angle (β) for power-on and for power-off plus direct thrust force. Good linearity is seen for β values between ±10 degrees. The difference between the two sets of data is called power effect side force ($F_{Y_{PE}}$) and includes inlet flow as well as exhaust flow effects for the Langley data, and exhaust flow effects only for the LTV data. As mentioned previously, the LTV model had no provision for simulating the airplane inlet flow.

The variation of side force and power effect side force with α for β = 0° and 5° based on Langley Test 221 is given in figure 36. The tunnel data show some side force at zero β. As discussed in reference 3, this shift is attributed to a small amount of rotational flow in the Langley tunnel, because runs made at β = 0° and 180° ruled out model and thrust asymmetry as being the cause of the forces and moments at zero sideslip. The power effect side forces are presented both without the correction for tunnel flow and with the correction at zero sideslip applied to data at β = 0° and 5°. Increasing α makes the power effect side force more negative at α's up to about 17 degrees.

The slope of power effect side force vs. β is plotted as a function of thrust in figure 37 for the Langley and LTV data. Here, the Langley data include effects of inlet flow, but show fair correlation with the LTV data. Figure 38 has Langley data with inlet effects removed plotted with LTV data; a small improvement in correlation is noted. At thrust values above 4000 lb. power effect side force increases linearly with thrust.

32

The variation of side force power effect slope with dynamic pressure (q) is given in figure 39. The result of removing the Langley model inlet effect was to reduce the power effect a small amount with little if any improvement in correlation with the LTV data.

The Lockheed speed-power parameter, $(1/C_T)^{\frac{1}{2}}$, described previously is used in figure 40 to correlate nondimensionalized side force power effects ($F_{y_{PE}}/\beta T$) for Langley and LTV tests with fair success. Removing the Langley inlet effect did not improve the correlation.

Yawing Moment

Langley and LTV yawing moment data are plotted vs. β in figure 41 for power-on and power-off plus direct thrust moment. The effect of power is to increase directional stability. Angle of attack variations of yawing moment and power effect yawing moment are shown in figure 42 and display the effects of the correction for tunnel rotational flow discussed previously. Increasing α makes the power effect yawing moment more positive at α's up to about 17 degrees.

Figure 43 presents power effect yawing moment slope as a function of thrust from Langley and LTV data. Correlation between the two sets of test data is only fair, and putting both sets of data on the same basis of no inlet flow effects deteriorates the correlation somewhat (figure 44).

The variation of power effect yawing moment slope with q is nearly linear (figure 45). However, correlation between Langley and LTV tests is not improved by removing the inlet effect from the Langley data.

Nondimensionalized power effect yawing moment slope ($N_{PE}/\beta T b$) data correlate well with the speed-power parameter, $(1/C_T)^{\frac{1}{2}}$, for both the Langley and LTV data(figure 46) except for the highest q, lowest thrust, Langley data points, which fell below the curve of the LTV data.

Rolling Moment

Typical rolling moment data from Langley and LTV tests are plotted against β in figure 47. Power effects increase the positive dihedral effect.

In figure 48, angle of attack is seen to have only a small influence on rolling moment and power effect rolling moment within airplane α's of -4° to +8°. The power effect rolling moment is given also with the residual moment at β = 0° removed to more closely simulate free air characteristics.

Figures 49 and 50 show power effect rolling moment slope vs. thrust for Langley and LTV data with and without Langley inlet flow, respectively. Removing the inlet effects lowered the Langley power effect rolling moment so as to degrade the correlation between the tests.

33

The LTV power effect rolling moment slopes vary linearly with dynamic pressure over the test q range, whereas the Langley data (taken at low q only) are nonlinear. Correlation between the Langley data with inlet effects and the LTV data is fairly good, but deteriorates when the inlet effect is removed (figure 51). A similar degradation in correlation between Langley and LTV data is observed in figure 52, where nondimensionalized power effect rolling moment slope is plotted vs. the Lockheed speed-power parameter, $(1/c_T)^{\frac{1}{2}}$. This parameter enables all the data points of each test to fall on a single curve, however.

For convenience, the inlet effects that were removed from some of the preceding Langley data are plotted in figure 53 for all three lateral directional parameters.

Sidewash

The lift-engine inlets pull in air and change the local angle of cross flow on the fuselage and tail surfaces. The lift-engine exit flow probably has an effect on the local flow, but the inlet and exit effects cannot be separated in the Langley data because tail-off Phase I powered yaw runs without secondary flow were not made. Although quantitative comparisons are not advisable due to model differences, reference to the sidewash angle increment due to inlet flow alone (figure 139), shows the power-induced sidewash angle changes negatively when sideslip angle increases negatively, the same as the Langley data of figure 54. It will be noted that this sidewash angle increment due to power is favorable up to $\beta = 12°$ (increases directional stability) and that the increment due to inlet flow alone is small compared with the total sidewash angle increment shown in the Langley data for both inlet and exit flows.

CONTROL EFFECTS

The roll control jets located at the wing tips will experience aerodynamic power effects which are similar in nature to the fuselage lift engine power effects. As a consequence, the net roll control effectiveness is the sum of the jet thrust roll control plus an incremental power effect. The power effect rolling moment associated with the wing tip jets was estimated from NASA test data in reference 9. The estimated power effect rolling moment is presented in figure 55 in the same nondimensional parameter form used for the lift engine power effects. The following example indicates the relative importance of the roll control power effect. For an engine thrust of 10,000 pounds at sea level the maximum rolling moment computed for the thrust of the wing jets is 7850 foot-pounds. At 100 knots forward velocity the power effect reduces this static rolling moment to 7120 foot-pounds, refer to figure 55.

The effect of thrust vectoring on the power effect pitching moment was investigated for Langley Test 178. Three exhaust nozzle angles were tested $(\delta_v = -10°, 0°, +10°)$, and the power effect pitching moment for these vector angles is compared in figure 56. In general, deflecting the nozzle 10 degrees forward of the zero position caused a small negative change in moment, and

34

deflecting the nozzle 10 degrees aft of the zero position resulted in a large negative change in moment.

The effect of power upon the elevator effectiveness was investigated. Power-off elevator effectiveness data from the University of Maryland Test 493 and power-on elevator effectiveness data from Langley Test 178 are presented in figure 57. The same model was used in both tests. The data indicates that the elevator effectiveness is approximately the same power-on or power-off when the tail is operating in its unstalled angle of attack range. With power-on the aircraft can operate to higher angles of attack before the tail effectiveness falls off due to tail stall.

Sufficient data was not obtained to extract the separate influence of power on the aileron and rudder effectiveness. However, the effect of power on the effectiveness of these control surfaces is probably of minor importance.

Reynolds Number Effects

No XV-4B wind tunnel tests were made to establish the effect of Reynolds number on power effects at constant dynamic pressure. Although the Reynolds number of the XV-4B tests varied from 0.25×10^6/ft. to 1.45×10^6/ft. because of varying dynamic pressure in the atmospheric wind tunnels used, a true effect of Reynolds number on power effects cannot be determined because of the influence that changing freestream dynamic pressure has on power effects.

However, Reynolds number effects on power-off data can be extracted from the XV-4B wind tunnel data; figure 58 is a sample of such data. Flaps-down maximum lift coefficients are approximately the same for the Langley low RN tests as the data from the LTV and Univ. of Maryland tests at higher Reynolds number, while flaps-up maximum lift coefficients show a less than normal increase with Reynolds number. The reason for this may be the relatively small size of the XV-4B wing in comparison with the fuselage plus nacelles, thereby reducing the influence of the wing-flow Reynolds number effects that are normally predominant. The full-scale XV-4A wind tunnel data (reference 10) are included because that airplane was almost identical to the XV-4B from an aerodynamic lift standpoint.

ANALYSIS OF XV-4B POWER EFFECTS IN HOVER

Analysis and review of XV-4B hover data in this section is directed toward the following objectives; (1) to identify from model data the important aerodynamic parameters, (2) to determine the influence of test facilities and test techniques upon the experimental data, and (3) to investigate the non-dimensional coefficients used to define indirect power effects.

WINGS LEVEL EFFECTS

Figure 59 presents a comparison between hover data obtained in a wind tunnel, Langley Tests 178 and 221, and hover data obtained on a Lockheed outdoor test rig. All data are out of ground effect. The various sets of data in figure 59 show poor correlation. The pitching moment correlation is particularly bad and indicates there is something more fundamental than data scatter responsible.

One possible cause of the differences between the indoor and outdoor test results is model differences with regard to simulated inlet flow. The outdoor model did not have an inlet, but the wind tunnel model did. A limited amount of hover data were obtained in Langley Test 178 with the inlet closed, and the effects of inlet flow were studied in the NR inlet test (see Section V). The inlet effects do not appear to be able to account for the large differences in test results indicated in figure 59.

Another possible cause of the difference between the indoor and outdoor test results is wind tunnel wall effects. During Langley Test 221 the model was positioned in three different attitudes relative to the tunnel walls; (1) model pitched 90 degrees with the jet directed down the tunnel, (2) model yawed 90 degrees with the jet directed toward the floor, (3) model in conventional position. The results are presented in figure 60. It can be seen that the results with the model pitched or yawed 90 degrees are approximately the same, but the results with the model in the conventional position are substantially different than the other two positions. This is strong circumstantial evidence that the tunnel walls may in fact influence the results. Because of the in-line nozzle arrangement of the XV-4B, it is probable that the exhaust flow spreads predominately sideward. This was the case for a NR model similar in configuration to the XV-4B (see figure 7). Assuming this to be the case, then the largest tunnel wall effect should result when the model is placed in the tunnel in a conventional position. In this position the jet moves to the floor, spreads sideward, and then is impeded by the tunnel sidewall. With the model yawed 90 degrees the jet would spread predominately up and down the tunnel, and with the model pitched 90 degrees the jet simply moves down the tunnel. The limited data presented in figure 60 suggests that a wall effect may be present in the Langley hover test data.

Figure 61 presents longitudinal interference data in ground effect obtained in the Langley 17 foot tunnel at zero tunnel velocity during Test 178. Power effect normal force ($F_{N_{PE}}$) initially increases negatively with increasing height, then generally decreases. Interference pitching moment (M_{PE}) initially increases negatively with increasing height, then decreases at about five feet above the ground. M_{PE} increases again as the height increases from eight feet to about twenty feet, where it reaches an approximately constant value.

Shown in figure 62 are $F_{N_{PE}}$ and M_{PE} data obtained from a model in the Lockheed hover rig. Poor agreement is noted between these data and those from the Langley Test 178. Pitching moment has a positive sign rather than the negative sign of Langley 178 and 221. Lockheed disclosed that some exhaust flow appeared to bounce from the ground plane (above the inverted model) to the ground and back onto the model, and for that reason Lockheed discounted the value of the data. Lockheed hover rig data are shown herein despite their questionable nature, but should be viewed accordingly.

36

The same data shown in figures 61 and 62 are given in nondimensionalized form in figure 63. The correlation for each set is poor and indicates that the interference effects were not a linear function of thrust in ground effect.

Figure 64 shows that the Langley 178 power effect normal forces increase with thrust up to about 7000 lbs. of thrust at two ground plane heights, then decrease with thrust. A similar effect is noted in power effect pitching moment for Langley 178 data, but the Lockheed hover rig data show a steady increase with thrust and have pitching moment signs opposite from the Langley data. This decrease at 7000 lbs. of thrust might be caused by wind tunnel wall interference.

EFFECTS OF ATTITUDE CHANGE

Power effect rolling moment ($\mathscr{L}_{PE}$) obtained on the Lockheed hover rig at two bank angles and thrust levels are presented in figure 65. The $\mathscr{L}_{PE}$ values act to restore the airplane to a horizontal position if banked. Levels of $\mathscr{L}_{PE}$ are low relative to the available roll reaction control power when the airplane is higher than 10 feet above the ground. However, when hovering at heights lower than 10 feet the model data indicate much larger levels of interference with reversals in sign versus bank angle. The interference data are also presented in nondimensional form and show poor correlation with thrust.

HOVER MOTION EFFECTS

Any sideslip angle between zero and ±180 degrees is within the operational envelope of a hovering VTOL airplane. These sideslip angles can result from either aircraft motion or winds. The aerodynamic effects at these very large angles of sideslip were estimated for the XV-4B based on data from references 11 and 12. The power-off characteristics are presented in figures 66 and 67 for angles of sideslip between zero and -180 degrees. Also, the effect of a 20 degree bank angle during side movement is indicated. It can be seen that there is a large variation in all the airplane power-off characteristics versus angle of sideslip. Also, the bank angle has a large effect on normal force, pitching moment and rolling moment and a small effect on side force and yawing moment. The power effect characteristics are presented in figures 68 and 69 for angles of sideslip between zero and -180 degrees. Conditions for the power effect data are a thrust of 7200 lbs, zero thrust vector angle, a dynamic pressure of 11.2 lbs. per square foot, zero angle of attack, and zero bank angle. It can be seen that the power effect forces and moments have a complicated variation with angle of sideslip.

Attempts to nondimensionalize the hover motion power effects using the Lockheed parameter $(1/C_T)^{1/2}$ were inconclusive. Almost all of the data was taken at one thrust (7200 lbs.) and one dynamic pressure ($q = 11.2$ lb/ft.^{2}). As a consequence, only one value of $(1/C_T)^{1/2}$ was available for all but one large sideslip angle. The one exception was a -90 degree sideslip case for which dynamic pressure was varied. It was found that the power effect could not be nondimensionalized with a single curve, as in the case of forward transition flight. Instead, it appears that each value of sideslip angle has it's own nondimensional variation with speed and power.

37

The effect of dynamic pressure upon the power effects was investigated for side movement (β = -90 degrees). The results are shown in figure 70. In general, the power effects increase with increasing dynamic pressure, as would be expected.

The effects of bank angle and height above ground on pitching moment and rolling moment are indicated in figure 71. The total power-on pitching and rolling moment were plotted versus dynamic pressure for bank angles of -7, 0, 7, and 20 degrees. In all instances the moments were approximately linear functions of bank angle. In order to determine if the interference effects were functions of bank angle an analysis of the +7 degree and -7 degree bank angle data was made. Both the pitching and rolling moment interference increments were about the same for these two bank angles. This result was expected and indicates that the relationship between the jet and airframe are not altered by attitude change when out of ground effect. At this point it was fairly clear that the power-off characteristics were responsible for the pitching moment and rolling moment being a function of bank angle. To complete this phase of the analysis, the effect of height above ground upon pitching and rolling moment during side movement was investigated. It can be seen in figure 71 that the moments, in general, decrease with decreasing height above ground.

Because of the complexity of power-off and power effect characteristics versus large sideslip angles, it was though desirable to establish the overall importance of these terms. After some consideration it was decided to compare the control power available and required versus angle of sideslip for a particular set of conditions. The conditions selected were a thrust of 10,560 lbs., a velocity of 30 knots, and standard sea level atmosphere. The control power about a given axis was assumed to be 100 percent in combination with 50 percent control about the other two axis. The control power available was estimated from reference 13 and is presented in figure 72. The comparisons between available control power and aerodynamic requirements are shown in figures 73 and 74. It can be seen that the aerodynamic requirements are not large relative to the available control power. However, one factor needs to be noted. The control power for the XV-4B is relatively large because of its research mission. An operational airplane might have much less control power. Even so, it seems that a rigorous representation of the hover motion aerodynamic effects may not be required.

SUMMARY OF XV-4B AERODYNAMIC CHARACTERISTICS

This subsection contains a summary of those XV-4B aerodynamic stability and control derivatives that had been investigated prior to the time the program was terminated. The derivatives presented are not complete or adequate enough for analysis of vehicle performance. The usefulness of this data is limited to comparisons between initial and final estimates for individual aerodynamic coefficients.

POWER-OFF CHARACTERISTICS

The power-off data presented here was obtained directly from two Lockheed reports; XV-4B, "Hummingbird Aerodynamic Analysis Report, ER-9052,"and the (rough draft)"XV-4B Equations of Motion"(references 13 and 14). The data presented here is for a configuration with tail-on, strakes on, flaps down 40 degrees and a center of gravity located at .10$\bar{c}_w$.

The slope-intercept method of presentation was used wherever possible and the data are presented in tabulated form. When the data were reasonably linear through the unstalled angle of attack range, slopes and intercepts were used for convenience and simplicity. Nonlinear data are presented in curve form and are primarily drag data and incremental inputs of landing gear and exit doors.

The data are presented for Mach numbers of 0.20, 0.30 and 0.40 which covers the transition flight mode, and are an attempt to apply the data to Lockheed's coefficients and equations as presented in reference 14.

Figure 75 presents a tabulation of aerodynamic derivatives for the power-off, untrimmed configuration with strakes and tail on and the flaps deflected down 40 degrees. All data which were essentially linear for the angle of attack range of 0° to 8° are presented here in slope form with corresponding intercepts for longitudinal and lateral directional airplane characteristics, control effectiveness and damping parameters.

Figure 76 shows airplane drag coefficient versus angle of attack for the low speed range with flaps deflected down 40 degrees. The drag is assumed to be constant for the Mach range covered during the transition stage. This data was not tabulated in slope form due to its nonlinearity.

The tail efficiency factor is shown in figure 77 as a function of angle of attack for the flaps down case. This parameter is required to complete the equations of motion in reference 14. The variation with angle of attack is typical. The dynamic pressure ratio is 1.0 at low angles of attack and drops off as the tail is immersed in the wing wake.

Figure 78 gives the effect of sideslip angle on airplane pitching moment. These data are required for the equations of motion of reference 14 and are presented here in curve form because of the nonlinearity with both angle of attack and angle of sideslip.

Figure 79 presents roll due to rudder deflection versus angle of attack and drag due to rudder deflection. Rudder effectiveness in yaw is given in slope form in figure 75 for Mach numbers .20, .30 and .40. For these parameters ($C_{n_{\delta_r}}$ and $C_{y_{\delta_r}}$) the values are reasonably constant with angle of attack over the range of α's for typical flight conditions. However, $C_{l_{\delta_r}}$ decreases rapidly with angle of attack so it is represented here in curve form. Drag coefficient versus rudder deflection is in incremental form and nonlinear with deflection.

The incremental effects of the landing gear and the lift engine exit doors are presented in figures 80 and 81, respectively.

The damping parameters for pitch and roll (C_{m_q} and C_{l_p}) are given in tabulated form in figure 75. However, damping in yaw and the cross derivative of damping in yaw due to rate of roll are shown in figure 82 as a function of lift coefficient.

TRANSITION POWER EFFECTS

The primary power effects at zero angle of attack were estimated from Langley Test 178 and LTV Test 195 and are presented in summary form in figures 83 and 84. Based upon the completed analysis of these sets of data, the Langley data was judged to be more representative of the airplane. The summary curves presented here are based on the Langley test results. Factors which weighed in favor of the Langley data were a larger tunnel test section, a more accurate model, a cleaner model support system and the greater knowledge and experience of the NASA agency in VTOL testing. The LTV data was judged to be somehow in error, and this data was used only as trend data to help extrapolate the Langley data to higher speed and power ranges.

Figure 83 presents the primary longitudinal power effects at zero angle of attack. The normal force and chord force data can be assumed to be independent of angle of attack. However, the pitching moment data is somewhat dependent on angle of attack (refer to figure 19), and a complete definition would require some provision for the effect of angle of attack.

The primary lateral directional power effects are given in figure 84. The side force and rolling moment data can be assumed to be independent of angle of attack, but the yawing moment data is a function of angle of attack (refer to figure 42). A good definition of the power effect yawing moment data must include some provision for the influence of angle of attack.

DISCUSSION OF XV-4B FLIGHT TEST DATA

Reference 15 gives some of the data recorded during the flight tests. Only one flight, number 23, shows data taken in flight mode VTOL Phase I, which is the condition used for the NR power effect studies of the XV-4B wind tunnel data. The data given for flight 23 are in the form of a long time-history run, and the gross weight and c.g. values given are an average over the run. There is no means of calculating a more exact c.g. and gross weight than these average values. Therefore, calculating power effect pitching moment from the flight test data would give questionable results because of possible errors in thrust moment arms.

For flight 23, at one point approximately midway in Phase I slowdown run, the power effect normal force was calculated and it agreed closely with the value obtained from the LTV wind tunnel test 195, as corrected for secondary airflow in reference 2. Power effect pitching moment calculated at this point did not give a comparable check.

40

Some of the other flights give more exact gross weights and c.g. positions, apparently, as they are not presented as time histories, but angle of attack and engine speed or thrust are not given. Consequently, checks against wind tunnel data are of limited utility.

In summation, the flight data given in reference 15 are insufficient to allow more than rough checks of aerodynamic power effects in transition flight.

Some unpublished Lockheed test data for the flight test airplane on the inverted telescope hover rig was transmitted to NR by the USAF on 18 November 1969. This data was very meager and was limited to only one height above the ground (eleven feet). With just one ground height, correlation of the full scale hover data with the model hover data would be of limited value.

XV-5A AND P-1127 ANALYSIS

The VIFCS program called for most of the analysis and correlation effort to be expended on the XV-4B configuration. However, the results of the XV-4B studies were to have been verified by comparison with available XV-5A and P-1127 data. At the time the program was terminated only a very limited effort had been expended on the XV-5A and P-1127 configurations. A discussion of the limited effort for these configurations follows.

P-1127 EFFORTS

P-1127 reports and data upon which analysis work was to be performed were assembled, but no analysis was performed. A powered model of the P-1127 was tested by Langley (Test 228). A set of tabulated data for this test was obtained. Flight test data for the P-1127 was obtained through the USAF. The data is contained in Technical Report No. 68-10, Volumes I through VI, entitled "P-1127 (XV-6A) Technology Test".

XV-5A EFFORTS

Basic Features of XV-5A Airplane

The general arrangement of the XV-5A airplane is shown in figure 85. The main propulsion system consists of two J-85 engines driving two wing mounted lift fans and one nose mounted lift fan. The basic engine thrust of 5300 lbs. is increased almost 300 percent by the fans. The engine tailpipe is equipped with a diverter valve which directs the engine exhaust to the fans in the lift mode or out the tailpipe in the conventional flight mode.

A typical take-off transition is accomplished by accelerating, normally at zero angle of attack, to a speed at which wing borne flight is possible. The acceleration is provided by vectoring the wing thrust by means of exit louvers. When flying speed is reached the engine thrust is diverted to the tailpipe, the airplane is rotated to the proper angle of attack, the fan inlet and exit holes are closed, and the airplane is in conventional flight.

Control is obtained by means of the combined effect of aerodynamic control and fan louver control. The pitch control is obtained by means of a nose fan thrust reverser door. By opening or closing the doors from an intermediate position the required pitching moment is obtained. The yaw control is obtained by an opposite louver deflection of each wing fan. Roll control is obtained by an opposite thrust modulation of the wing fans by means of louver stagger deflection. Stagger deflection is alternately deflecting the louvers in such a way as to increase or decrease the fan exit area. Hover height control is obtained by a similar stagger deflection of the louvers of both wing fans. The pilot has a hand operated lift stick for height control.

Analysis Guidelines

The results of the analysis and correlation of the aerodynamic data from the model tests of references 16 through 20 are presented herein. The principle effort was to determine the interference or power effects of the wing mounted lift fans. The same analysis techniques are used in this analysis of the XV-5A data as in the XV-4B analysis.

The fan thrust was determined by integrating the fan total pressure rake data found in reference 16. This rake data was taken for only one fan RPM value. The fan thrust through the entire RPM range was assumed to be a constant percent of the net thrust measured at zero velocity and zero fan louver deflection (T_{ooo}). The estimated fan thrust versus motor RPM for the model is shown in figure 86. The maximum net thrust which could be developed by the model fans was 117 pounds which is equivalent to 4200 pounds full scale. The maximum model thrust was about 30 percent of the maximum airplane thrust.

The inlet ram drag effects were removed from the XV-5A power effect data to be consistent with the XV-4B analysis work. The fan inlet ram drag effects were calculated from the following equations and are shown plotted versus thrust in figure 87.

$$\Delta F_{C_{INLET}} = V_{\infty} \sqrt{\rho_{\infty} A_{FAN} T_{FAN}}$$

$$\Delta M_{INLET} = -.585 \, \Delta F_{C_{INLET}}$$

XV-5A Power Effects

Typical power effect normal force data versus angle of attack are shown in figure 88 for two combinations of thrust and dynamic pressure. The power effects are favorable due to the negative pressure on the wing upper surface created by the fan inlet airflow. The power effects are essentially independent of angle of attack.

42

Figure 89 shows a summary of the power effect normal force data at zero angle of attack. A plot of the power effect ratio $(F_{N_{PE}}/T)$ versus the Lockheed speed-power parameter $(1/C_T)^{1/2}$ is presented. There is good correlation using these parameters for all values of thrust and dynamic pressure tested.

Typical power effect chord force data versus angle of attack are shown in figure 90 for two combinations of thrust and dynamic pressure. The power effects cause a large increase in chord force. This chord force increment remains constant with angle of attack at $q = 0.5$ lb./ft.^{2} and decreases slightly with α at $q = 9.3$ lb./ft.^{2}.

Figure 91 presents a summary of the power effect chord force data at zero angle of attack. A plot of the power effect ratio $(F_{C_{PE}}/T)$ versus the Lockheed speed-power parameter $(1/C_T)^{1/2}$ is presented. There is good correlation using these parameters for all values of thrust and dynamic pressure tested.

Typical power effect pitching moment data versus angle of attack are presented in figure 92 for two combinations of thrust and dynamic pressure. The power effect causes a nose up pitching moment which is approximately independent of angle of attack. The power effect moment increases with increasing speed or thrust.

Figure 93 presents a summary of the power effect pitching moment data at zero angle of attack. A plot of the power effect ratio (M_{PE}/T) versus the Lockheed speed-power parameter $(1/C_T)^{1/2}$ is presented. There is good correlation using these parameters for all values of thrust and dynamic pressure tested.

Figure 94 compares power effect normal force and pitching moment versus thrust at $q = 9.3$ lb./ft^2 as determined by using the Ryan nondimensional data of reference 18 in one instance and the nondimensional data of this report based on the Lockheed parameter. These data show different trends versus thrust. Since these values were not correlated against flight test results, it cannot be stated which coefficient form gave the more accurate results.

A comparison of full scale XV-5A model data from reference 20 and 1/6 model scale data is shown in figure 95. The data is presented in coefficient form, $(M_{PE}/T\bar{c})$ vs $(1/C_T)^{1/2}$ for the increment of pitching moment due to power effects. The correlation shows that the speed-power parameter, $(1/C_T)^{1/2}$ is a good correlation parameter for the power effects and is influenced only slightly by the scale factor.

Downwash data versus angle of attack for three different values of the speed-power parameter $(1/C_T)^{1/2}$ available from reference 16 is shown in figure 96. The data have the same general trend and indicate the parameter, $(1/C_T)^{1/2}$ is a good correlation term showing a maximum deviation of about two degrees. The increment in downwash angle due to fan power at zero angle of attack vs. the Lockheed speed-power parameter, $(1/C_T)^{1/2}$ is also shown. The power induced downwash for the XV-5A shows the same general trend indicated for the XV-4B.

43

Lateral directional power effects are shown in figure 97, and are based on the Ryan data in reference 18. The data indicate that the power effects due to fan thrust increase the lateral directional stability. Also, the data appears orderly when plotted versus the Lockheed speed-power parameter $(1/c_T)^{1/2}$.

Concluding Remarks

Because of the brief nature of the XV-5A investigation it is difficult to draw any firm conclusions. However, certain impressions were formed. It appears that the analysis techniques which were applied to the XV-4B are also applicable in the case of the XV-5A. The XV-5A data could be correlated using the Lockheed speed-power parameter. Ryan and Lockheed coefficient forms give slightly different values at full scale thrust, but it cannot be stated which is the more accurate without analyzing the flight test results.
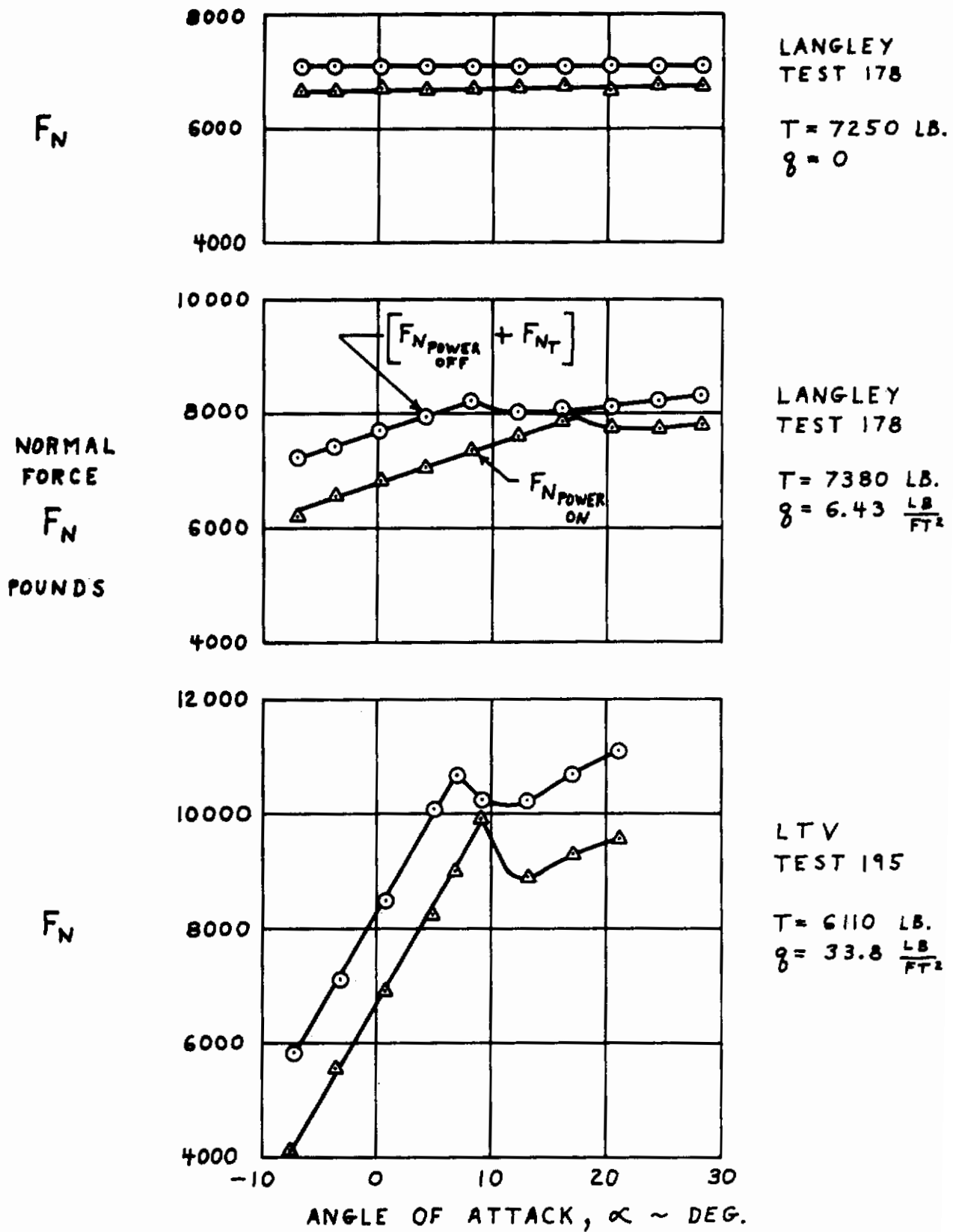
Fig. 12. Typical Normal Force versus Angle of
Attack Data (Basic Unadjusted Data)

45
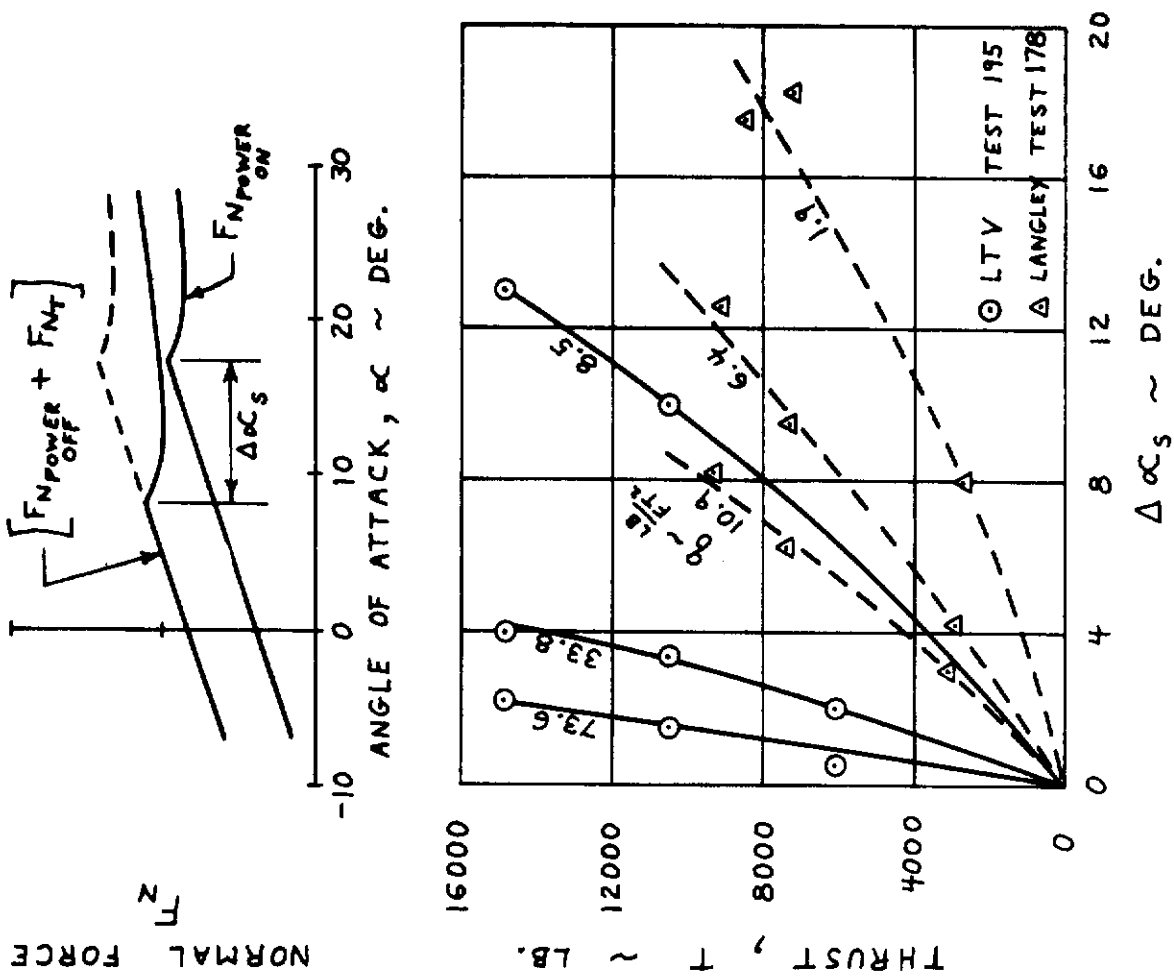
Fig. 13. Change in Wing Angle of Attack at Stall due to Power
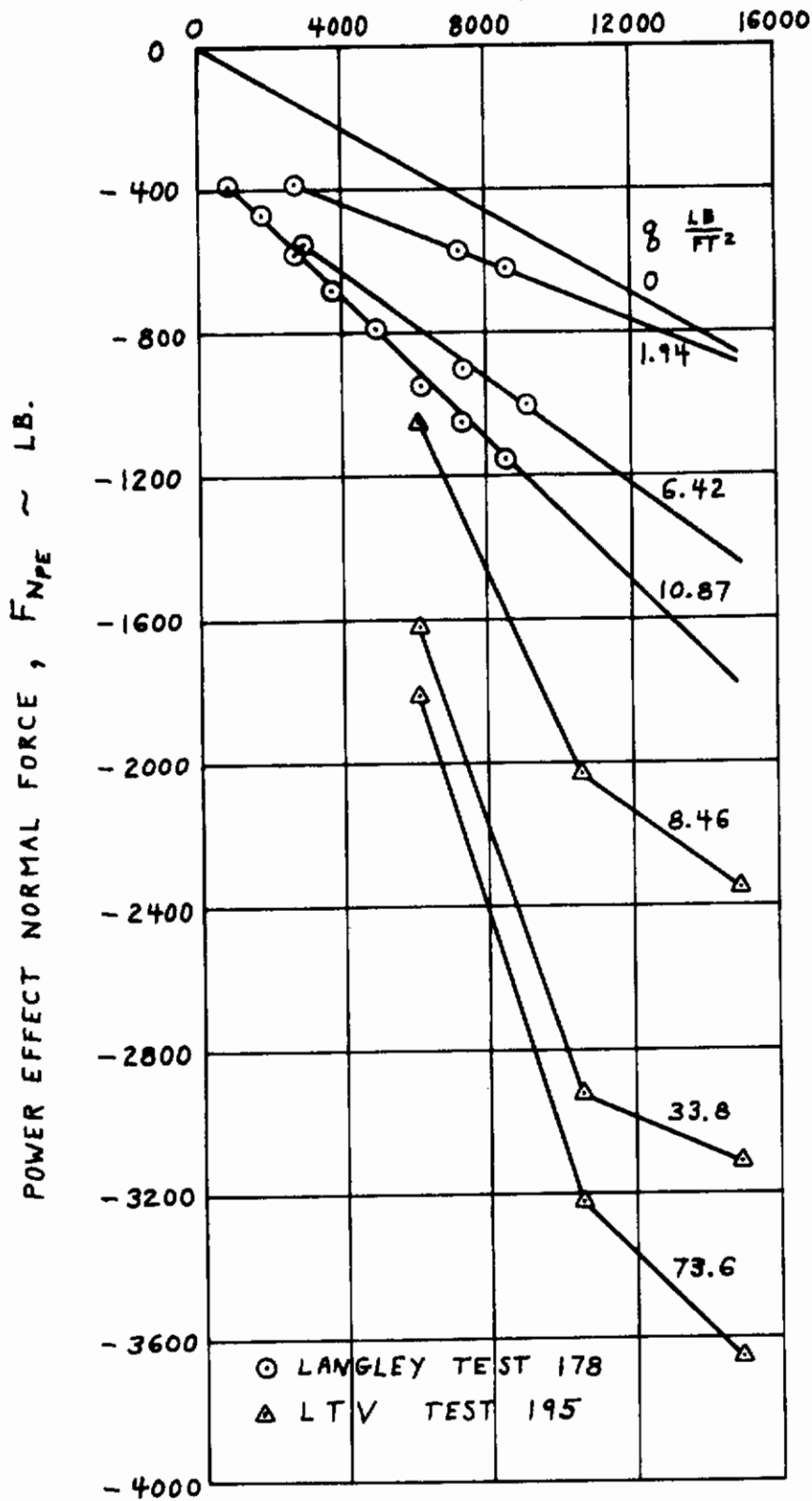
Fig. 14. Power Effect Normal Force versus Thrust for
Different Values of Dynamic Pressure (Basic Unadjusted Data; $\alpha=0$)

47
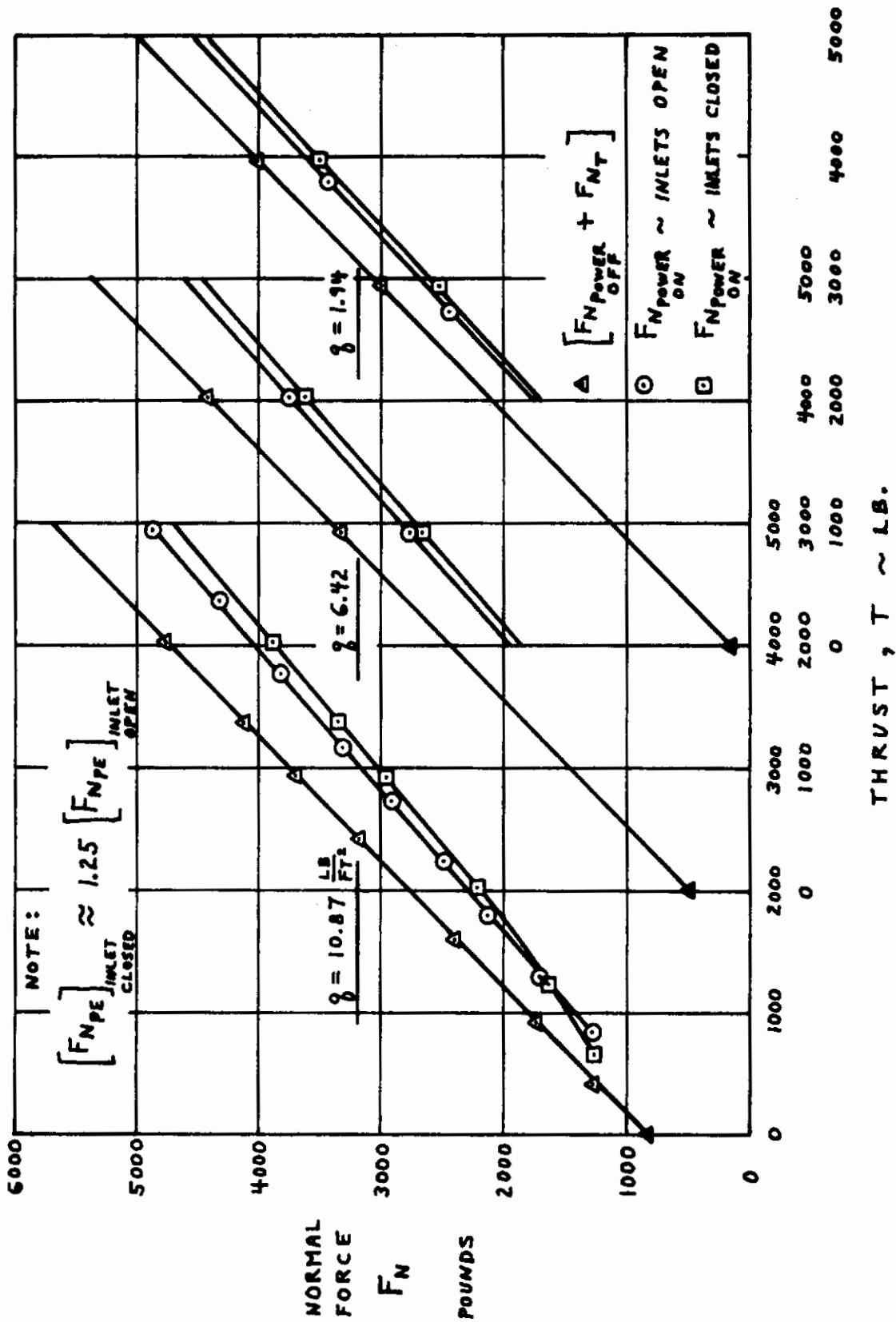
Fig. 15. Effect of Inlet Flow on Normal Force for Langley Test 178 (α=0)
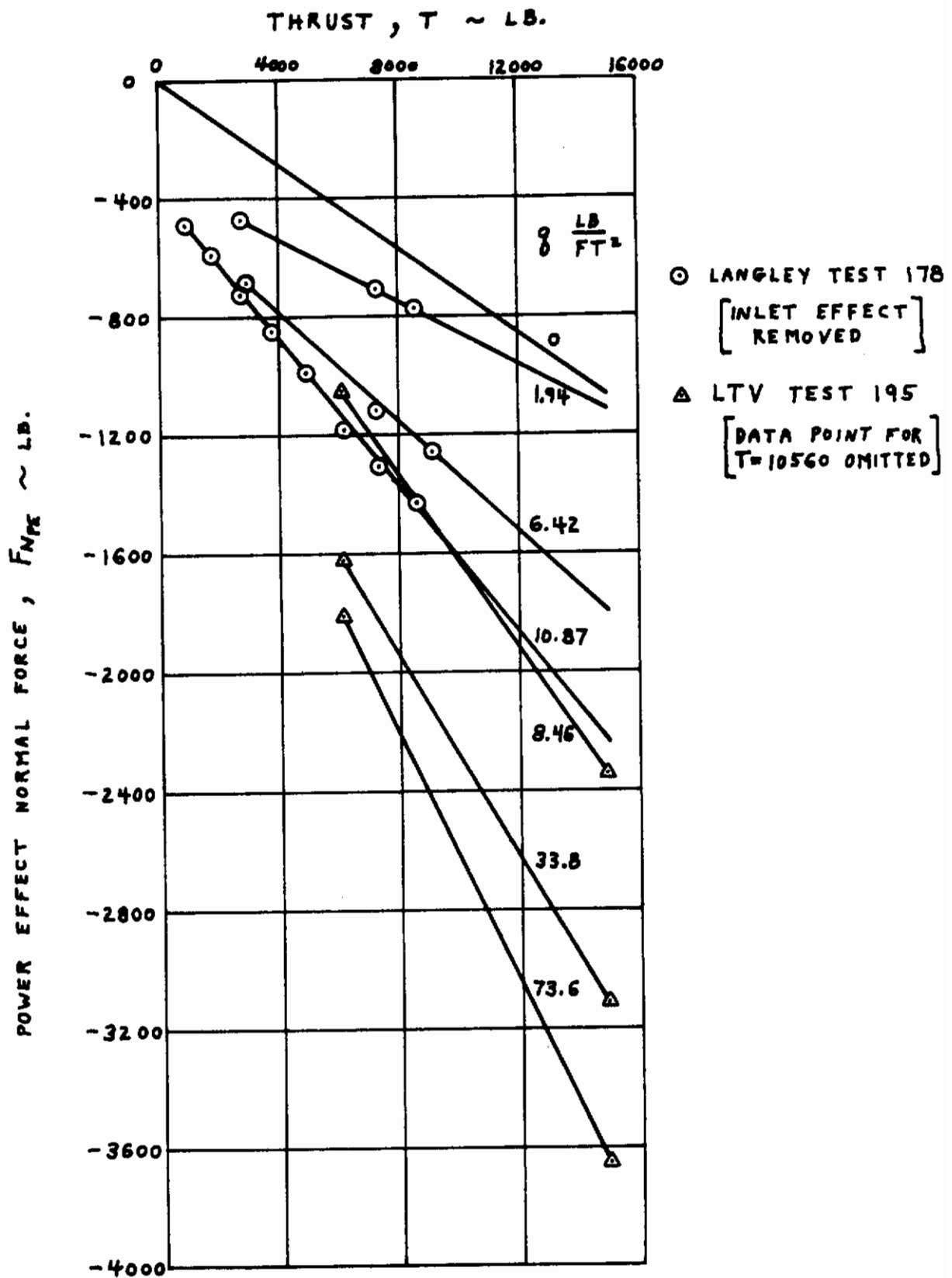
Fig. 16. Power Effect Normal Force versus Thrust for Different
Values of Dynamic Pressure (Adjusted Data; α=0)
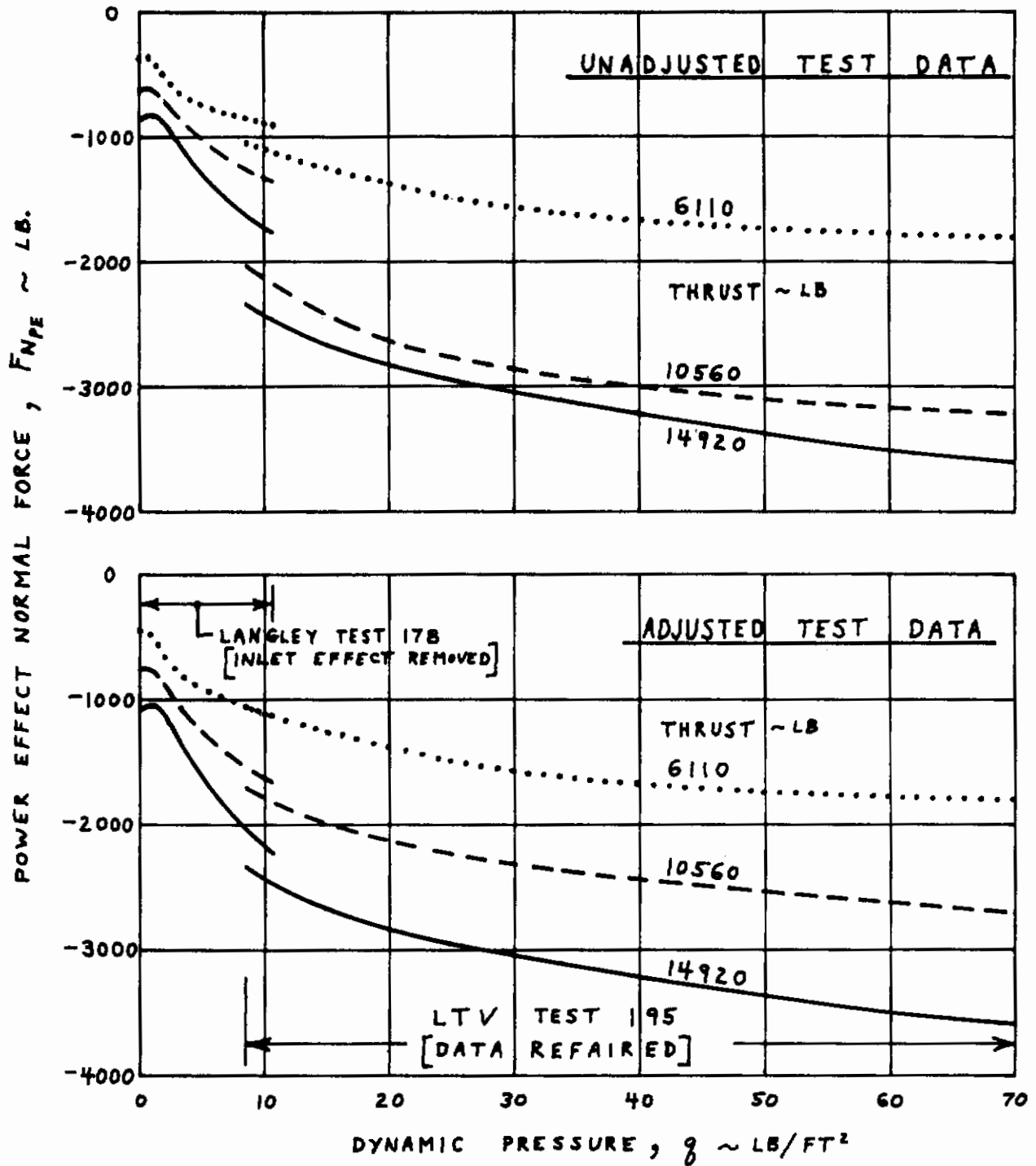
FIGURE 17. POWER EFFECT NORMAL FORCE VERSUS DYNAMIC
PRESSURE FOR DIFFERENT VALUES OF THRUST $(\alpha = 0)$

50
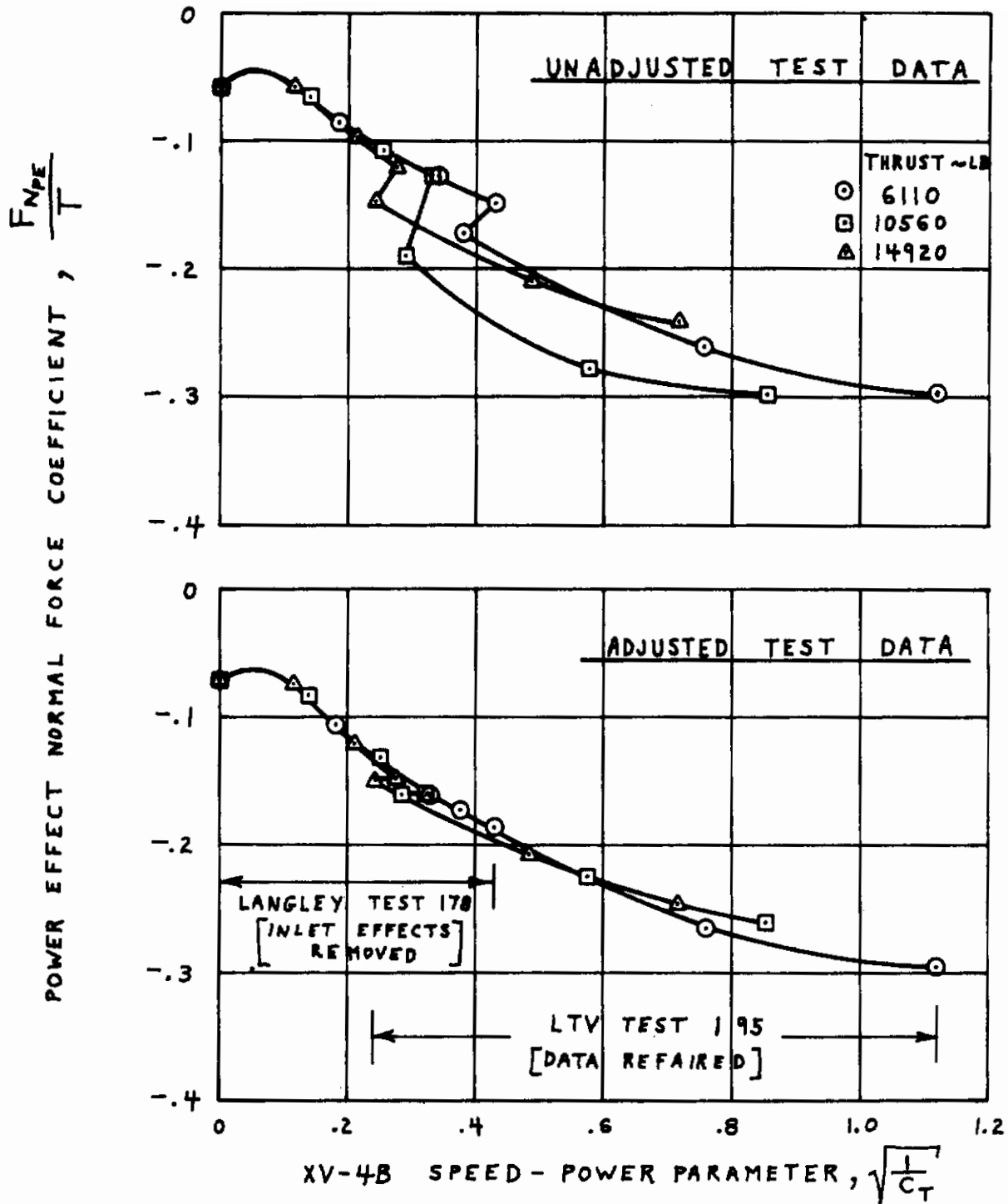
FIGURE 18. POWER EFFECT NORMAL FORCE COEFFICIENT VERSUS
XV-4B SPEED-POWER PARAMETER AT $\alpha = 0$

51
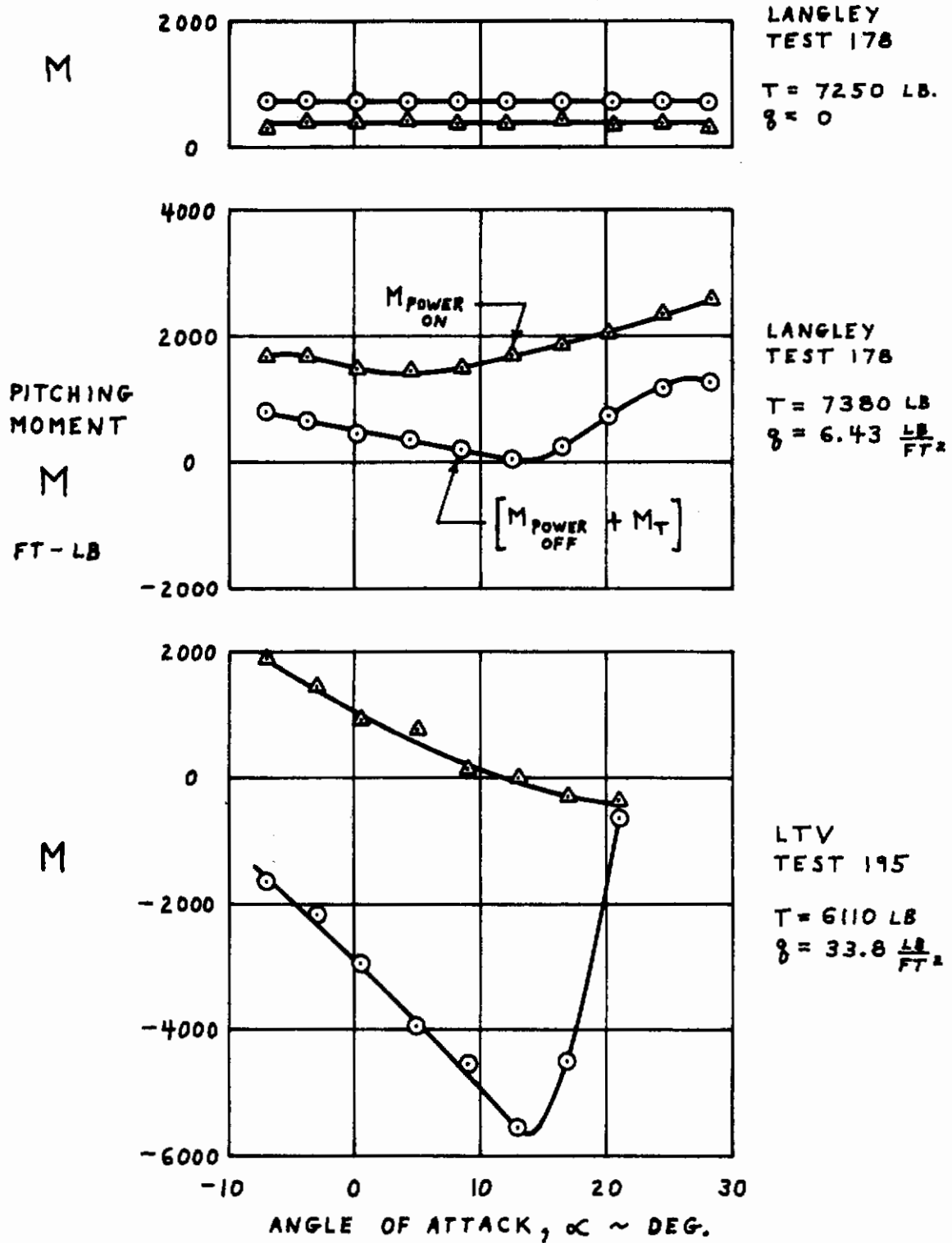
FIGURE 19. TYPICAL PITCHING MOMENT VERSUS ANGLE OF
ATTACK DATA (UNADJUSTED TEST DATA)

52
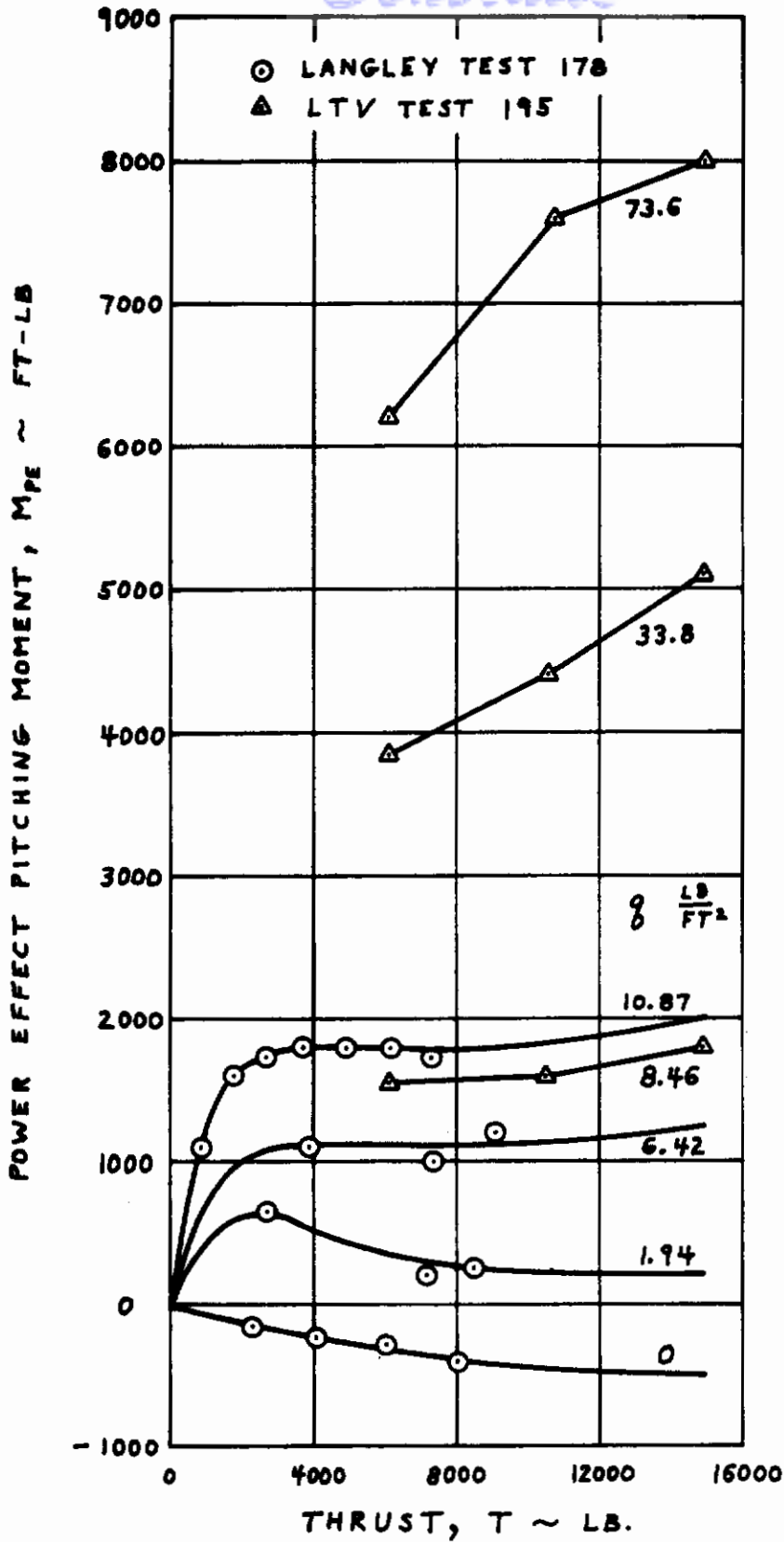
FIGURE 20. POWER EFFECT PITCHING MOMENT VERSUS THRUST
FOR DIFFERENT VALUES OF DYNAMIC PRESSURE
(UNADJUSTED TEST DATA)

53

$$\sum (\Delta F_c)_{IN} \, Z + \sum (\Delta F_N)_{IN} \, X = M_{INLET} = Z_M \, F_{C_{INLET}}$$
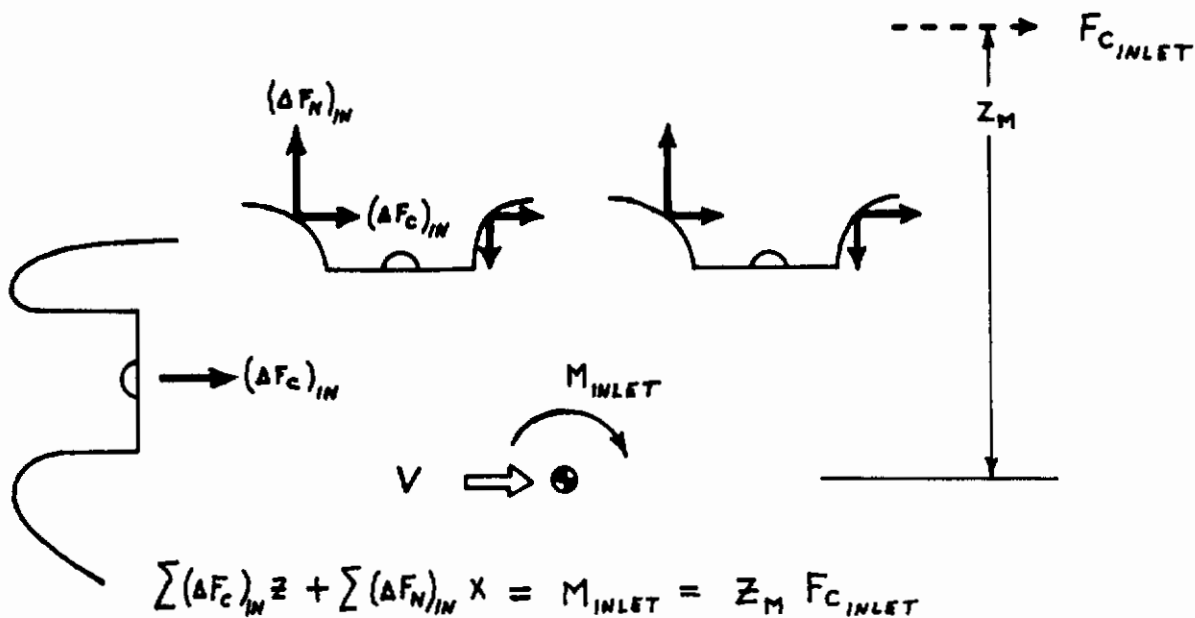
NOTE: Z_M IS POINT AT WHICH RAM DRAG MUST BE APPLIED TO PRODUCE INLET MOMENT
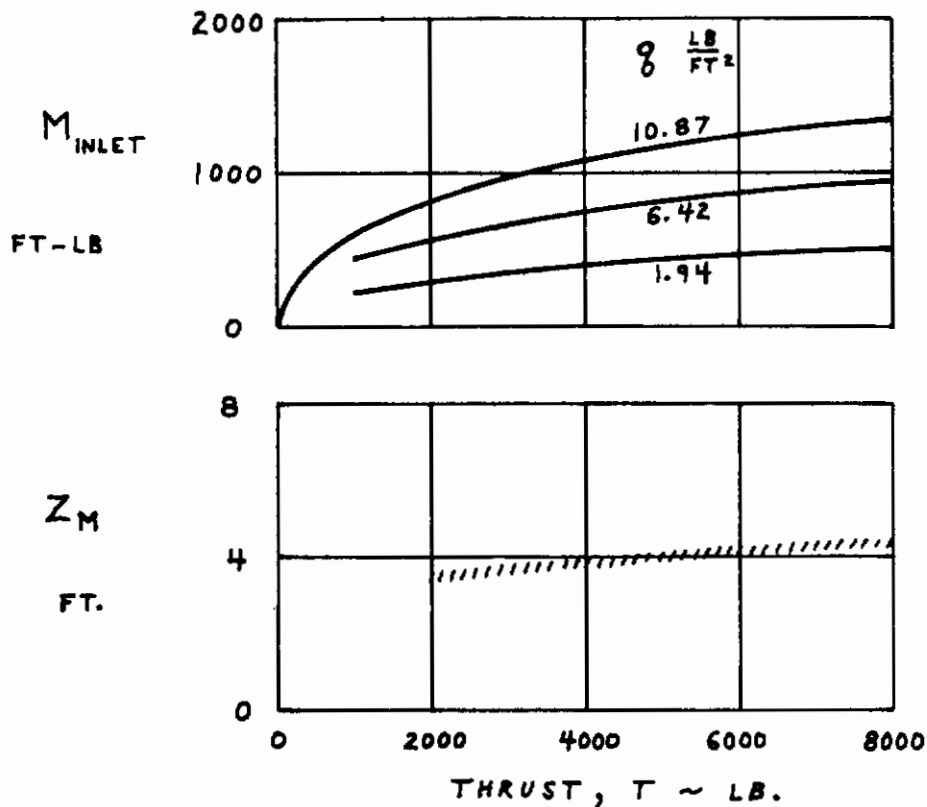
FIGURE 21. MEASURED PITCHING MOMENT DUE TO INLET MOMENTUM (LANGLEY TEST 178 ; $\alpha = 0$)
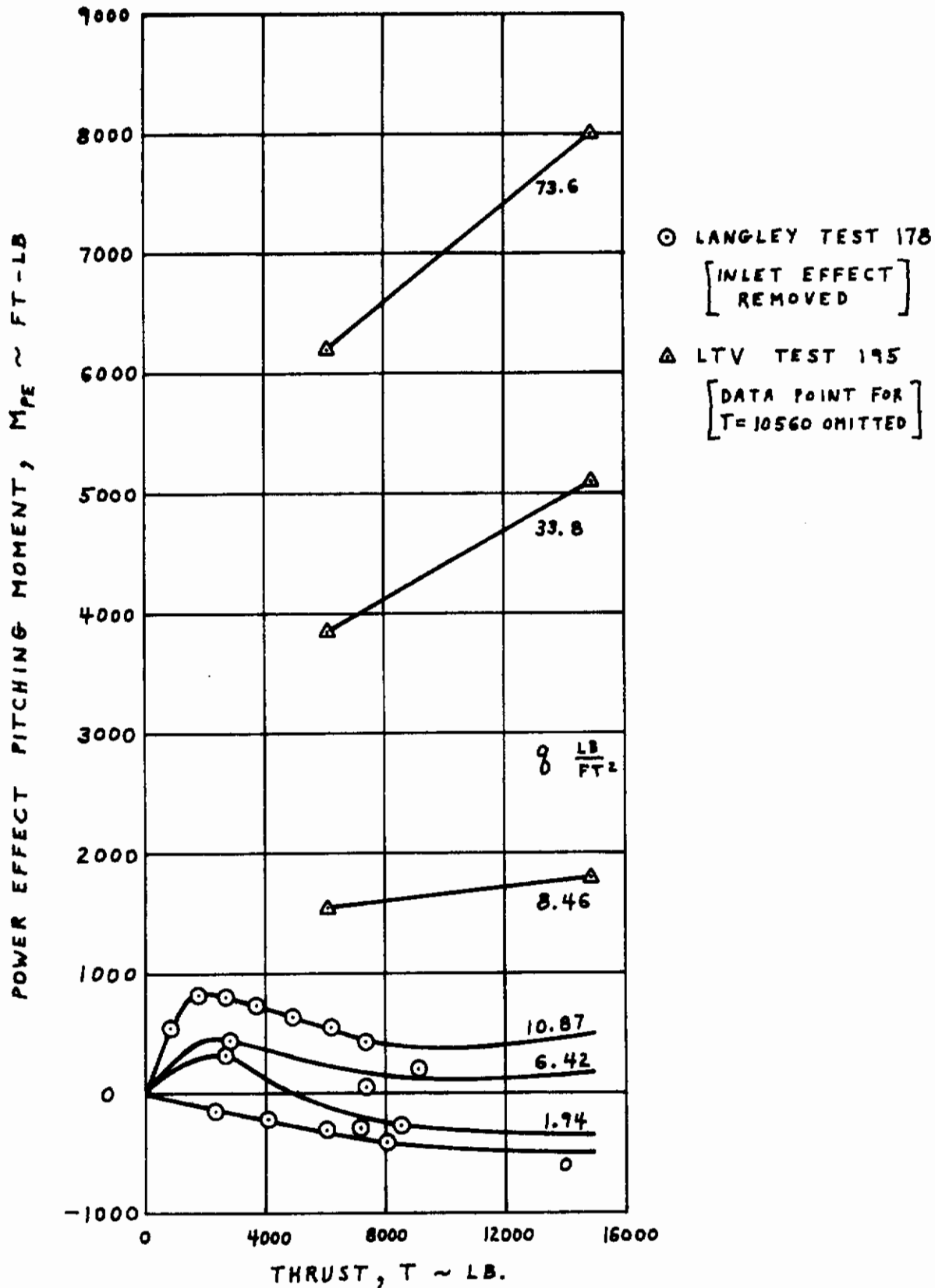
FIGURE 22. POWER EFFECT PITCHING MOMENT VERSUS THRUST FOR
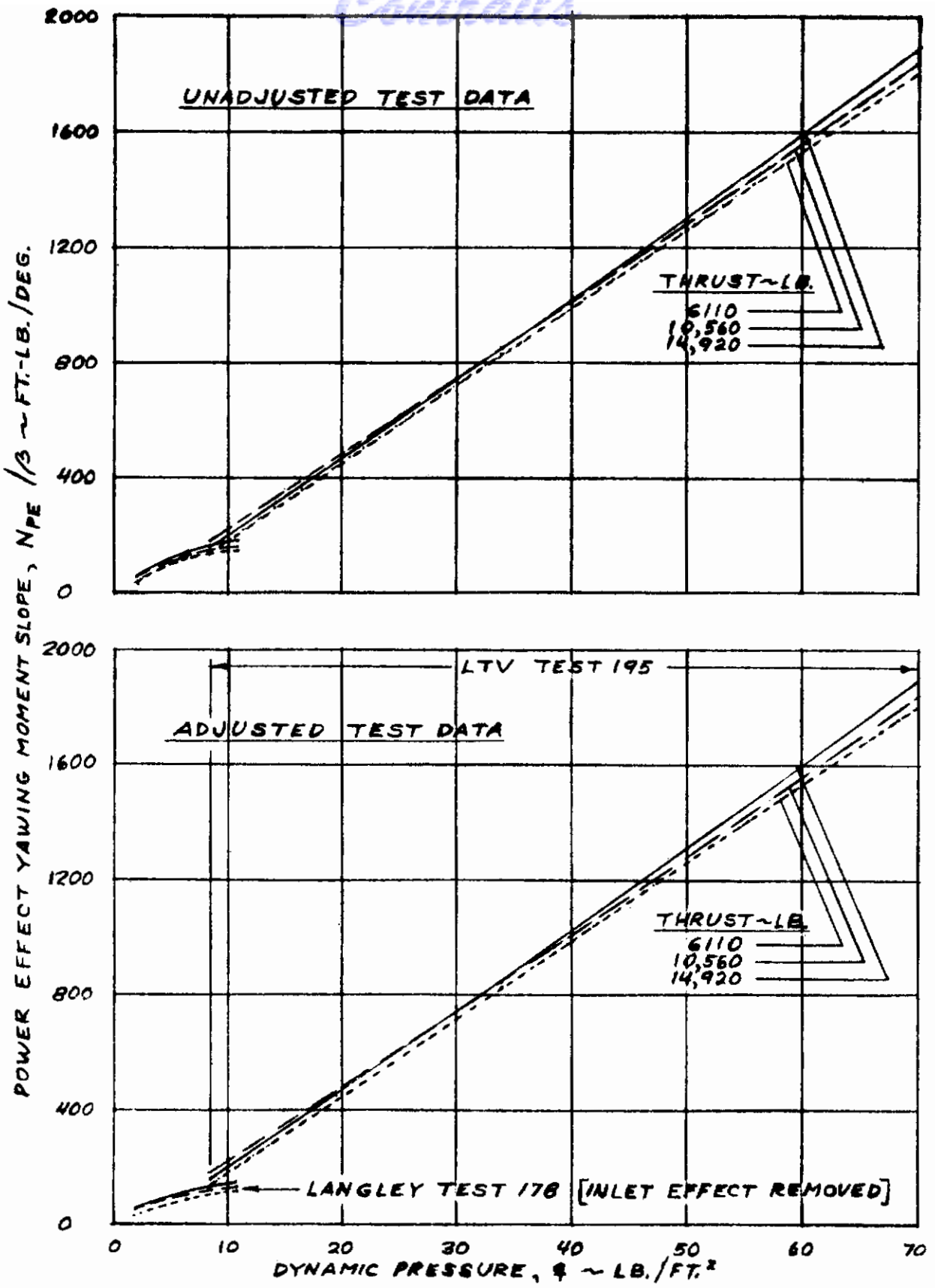DIFFERENT VALUES OF DYNAMIC PRESSURE
(ADJUSTED TEST DATA)

55
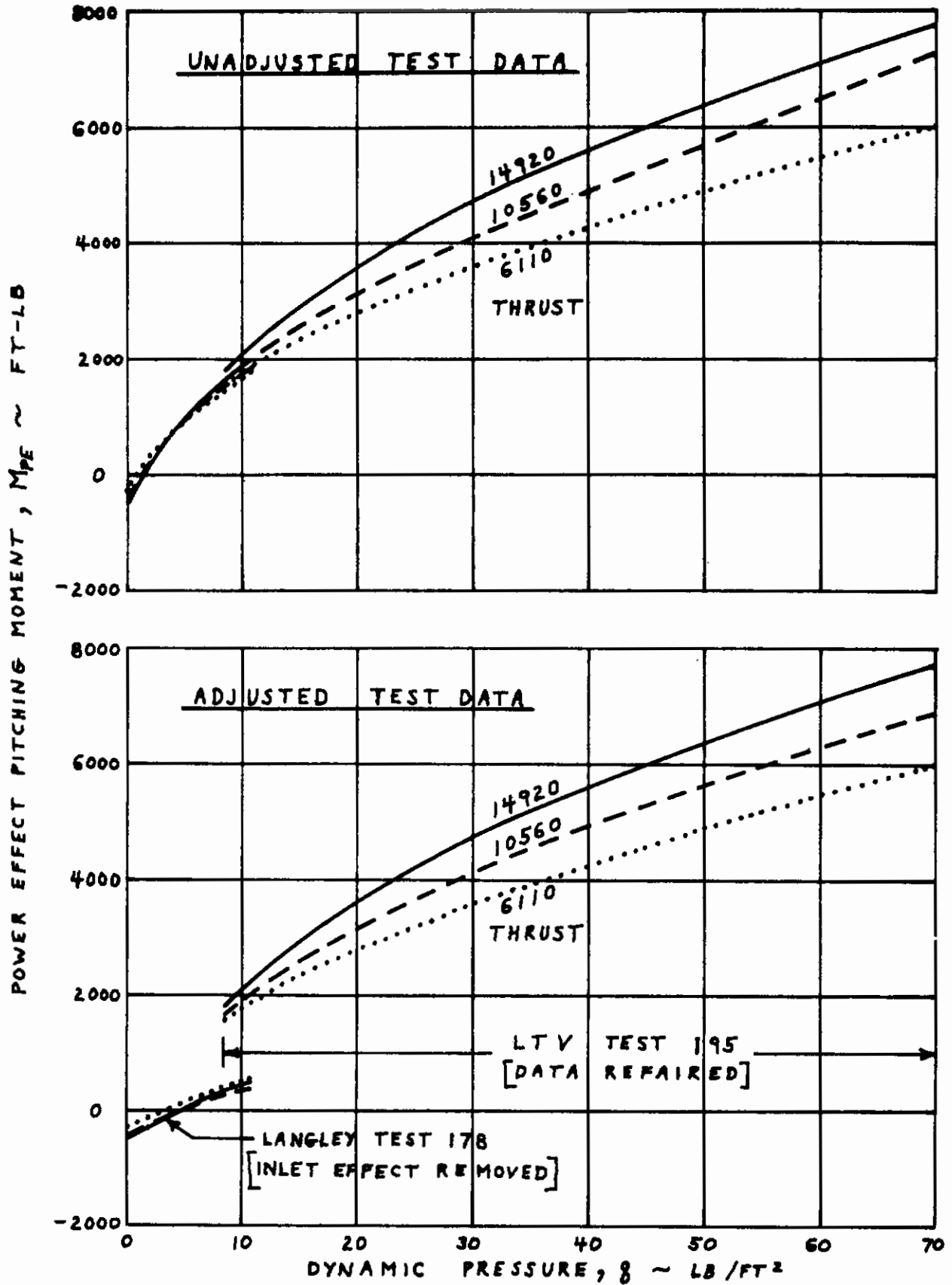
FIGURE 23. POWER EFFECT PITCHING MOMENT VERSUS DYNAMIC
PRESSURE FOR DIFFERENT VALUES OF THRUST ($\alpha = 0$)

56
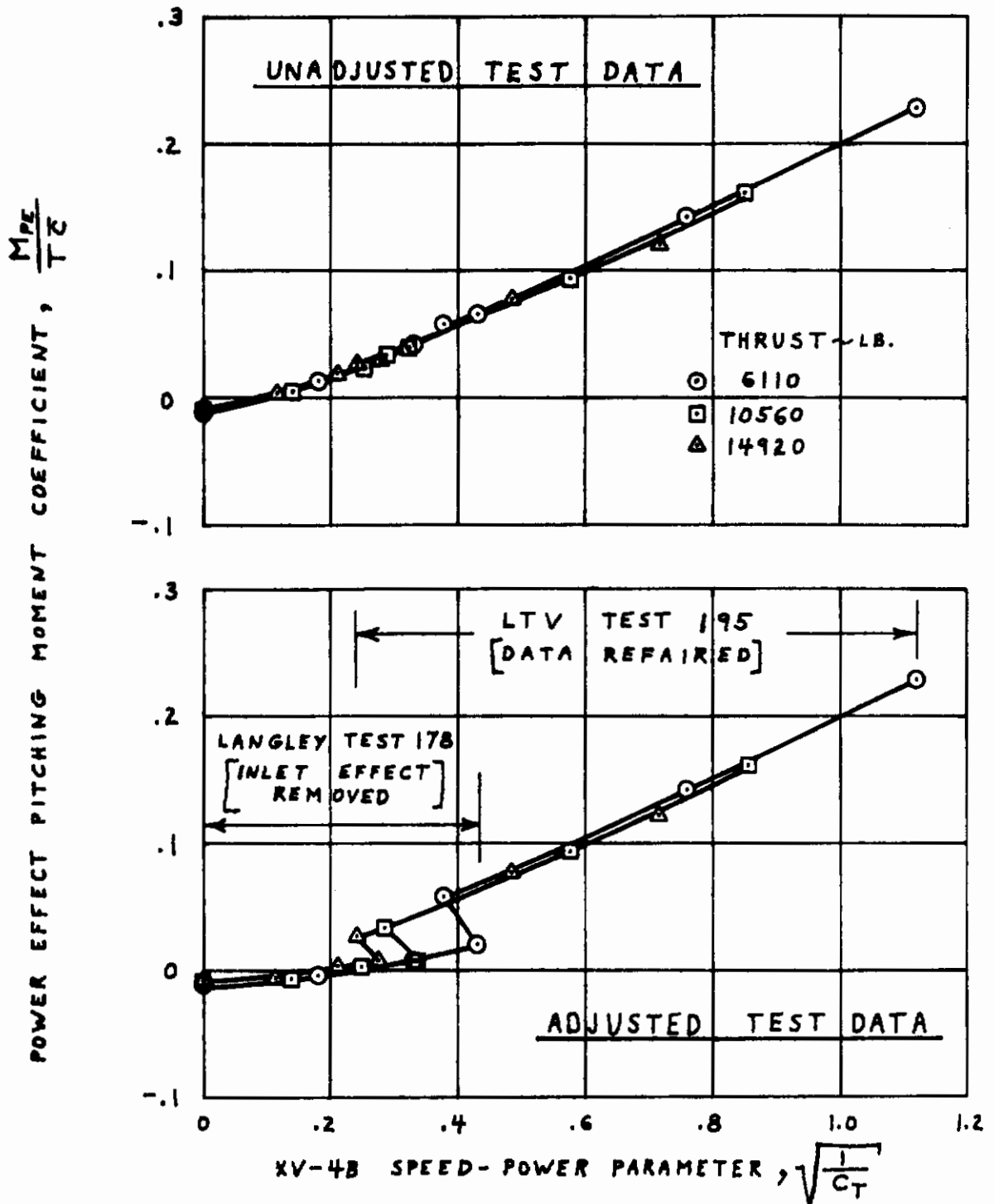
FIGURE 24. POWER EFFECT PITCHING MOMENT COEFFICIENT VERSUS
XV-4B SPEED-POWER PARAMETER ($\alpha = 0$)

57
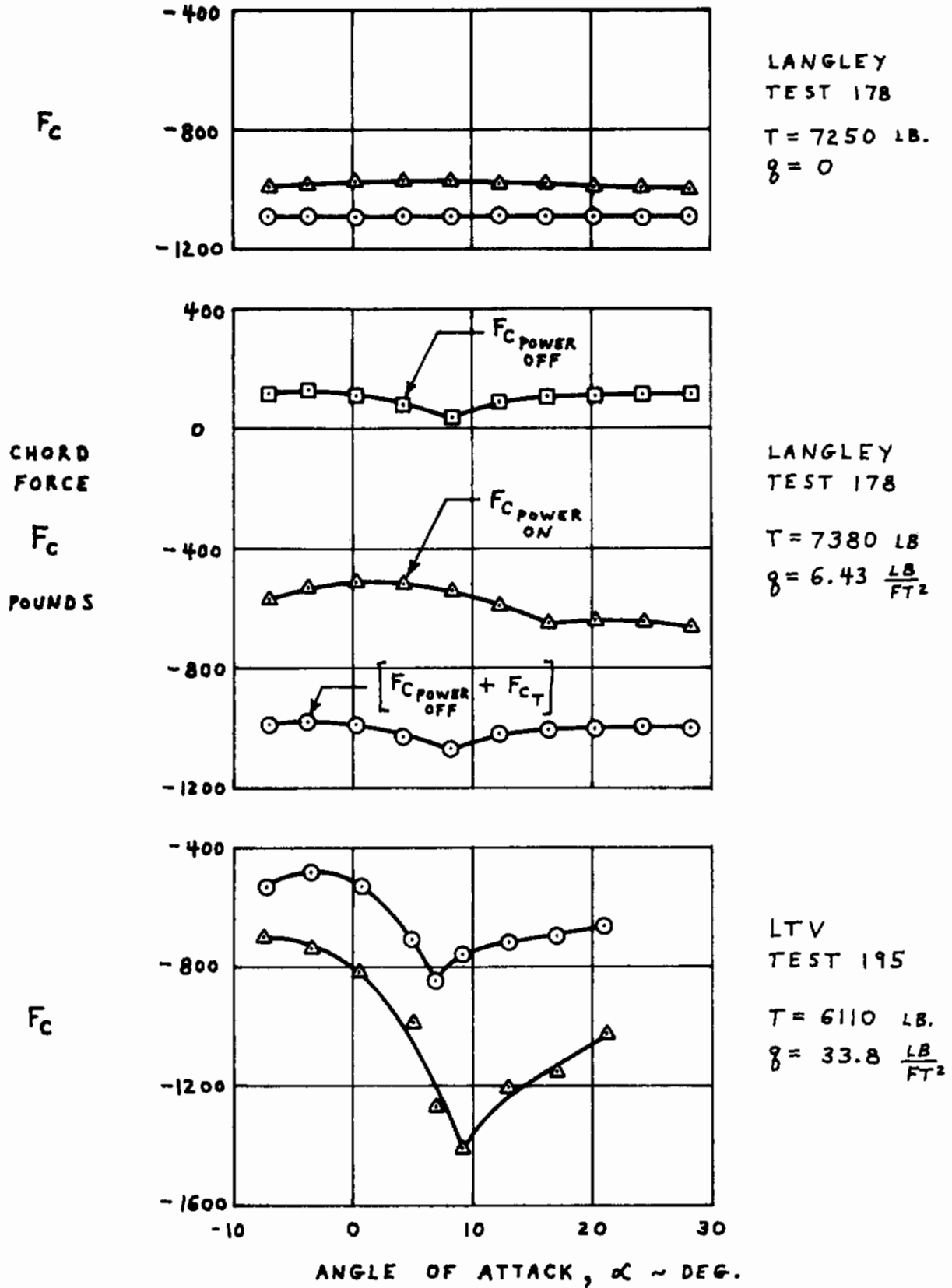
FIGURE 25. TYPICAL CHORD FORCE VERSUS ANGLE OF ATTACK DATA (UNADJUSTED TEST DATA)
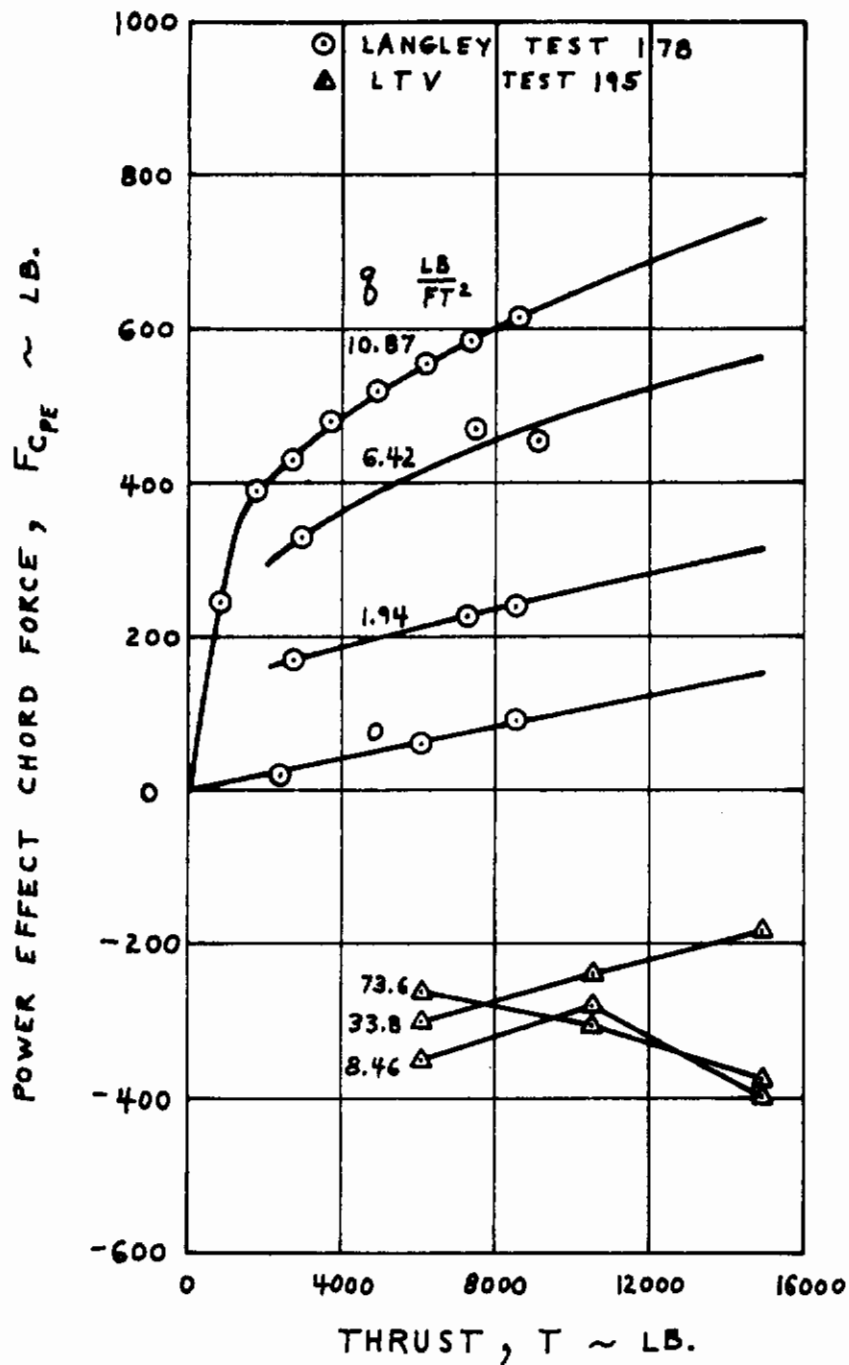
FIGURE 26. POWER EFFECT CHORD FORCE VERSUS THRUST FOR
DIFFERENT VALUES OF DYNAMIC PRESSURE
(UNADJUSTED TEST DATA)

59
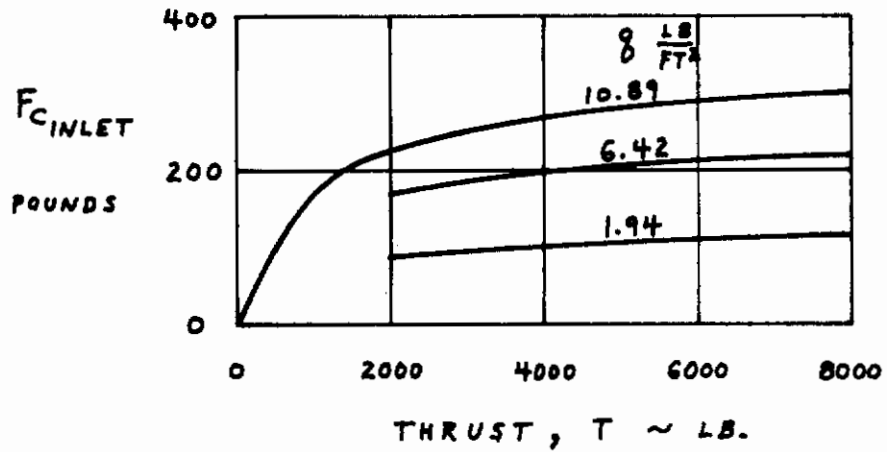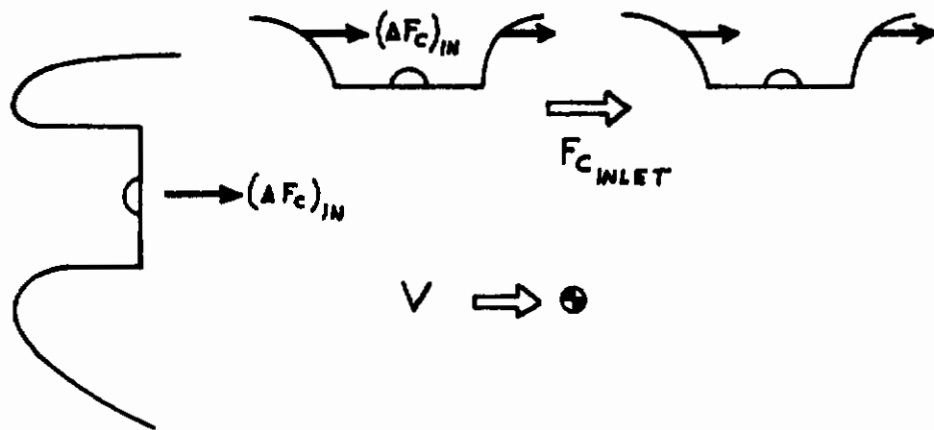
FIGURE 27. MEASURED CHORD FORCE DUE TO INLET
MOMENTUM (LANGLEY TEST 178 ; $\alpha = 0$)

60

FIGURE 28. POWER EFFECT CHORD FORCE VERSUS THRUST FOR
DIFFERENT VALUES OF DYNAMIC PRESSURE
(ADJUSTED TEST DATA; $\alpha = 0$)

61
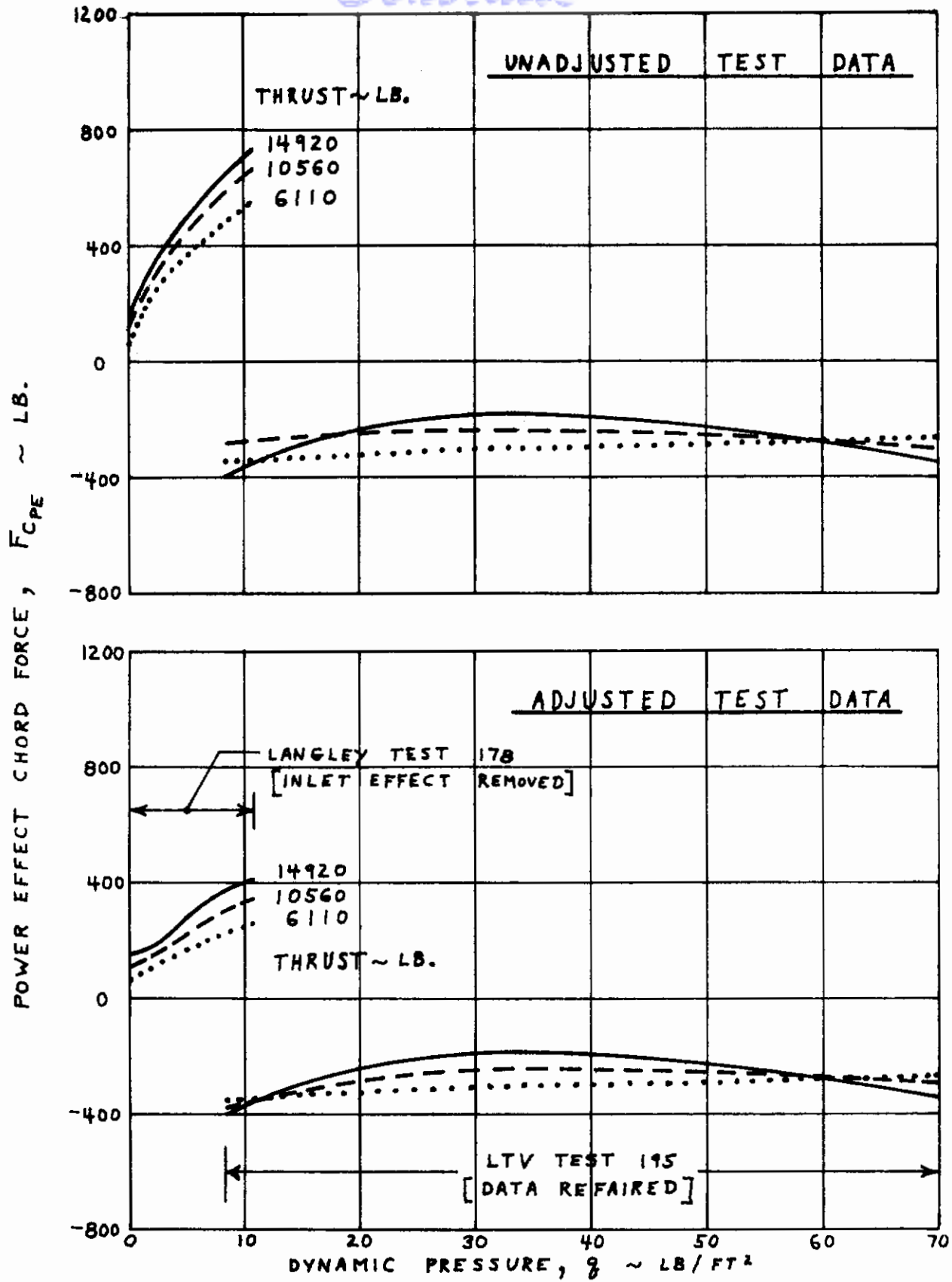
FIGURE 29. POWER EFFECT CHORD FORCE VERSUS DYNAMIC
PRESSURE FOR DIFFERENT VALUES OF THRUST ($\alpha = 0$)

62
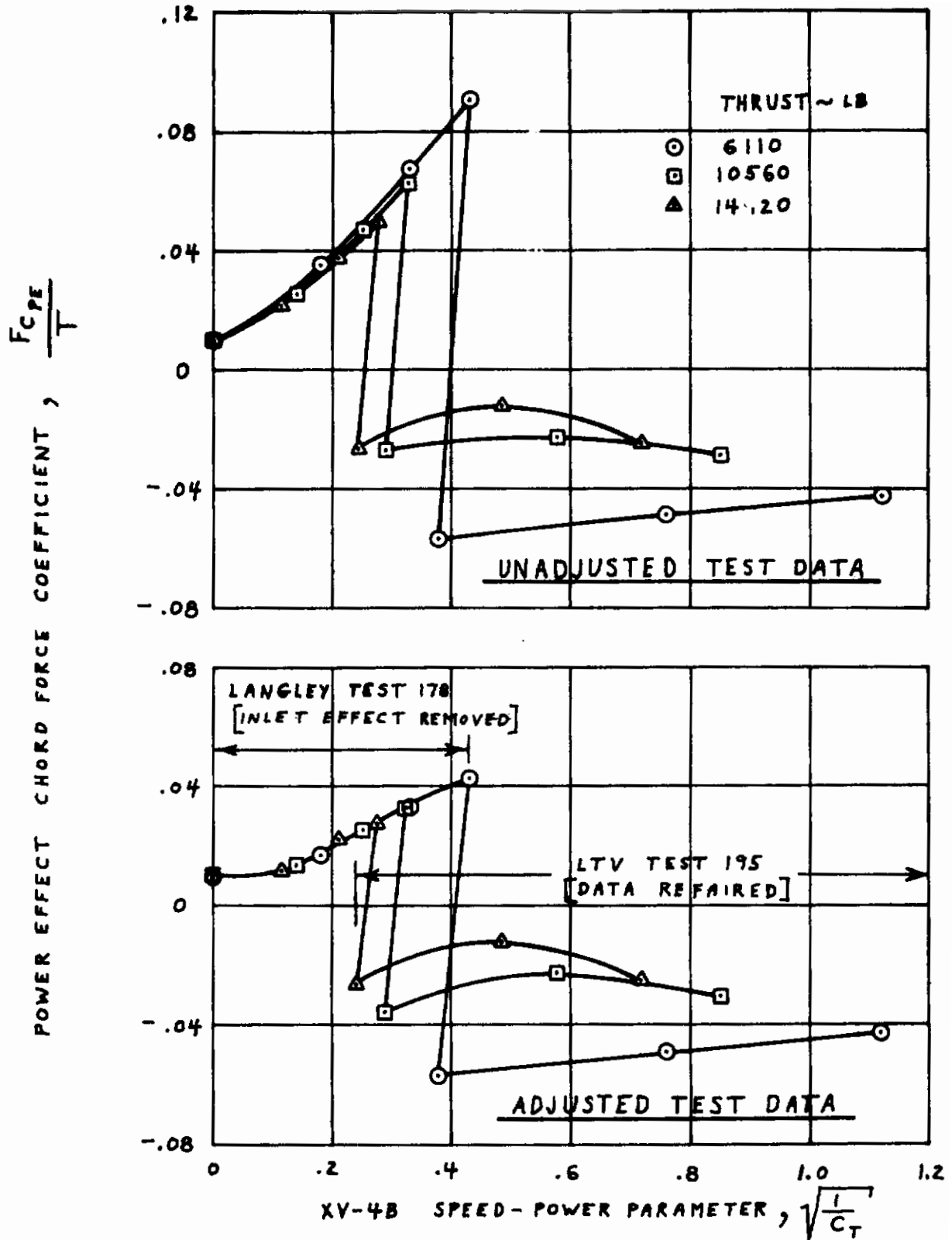
FIGURE 30. POWER EFFECT CHORD FORCE COEFFICIENT VERSUS
XV-4B SPEED - POWER PARAMETER ($\alpha = 0$)

63
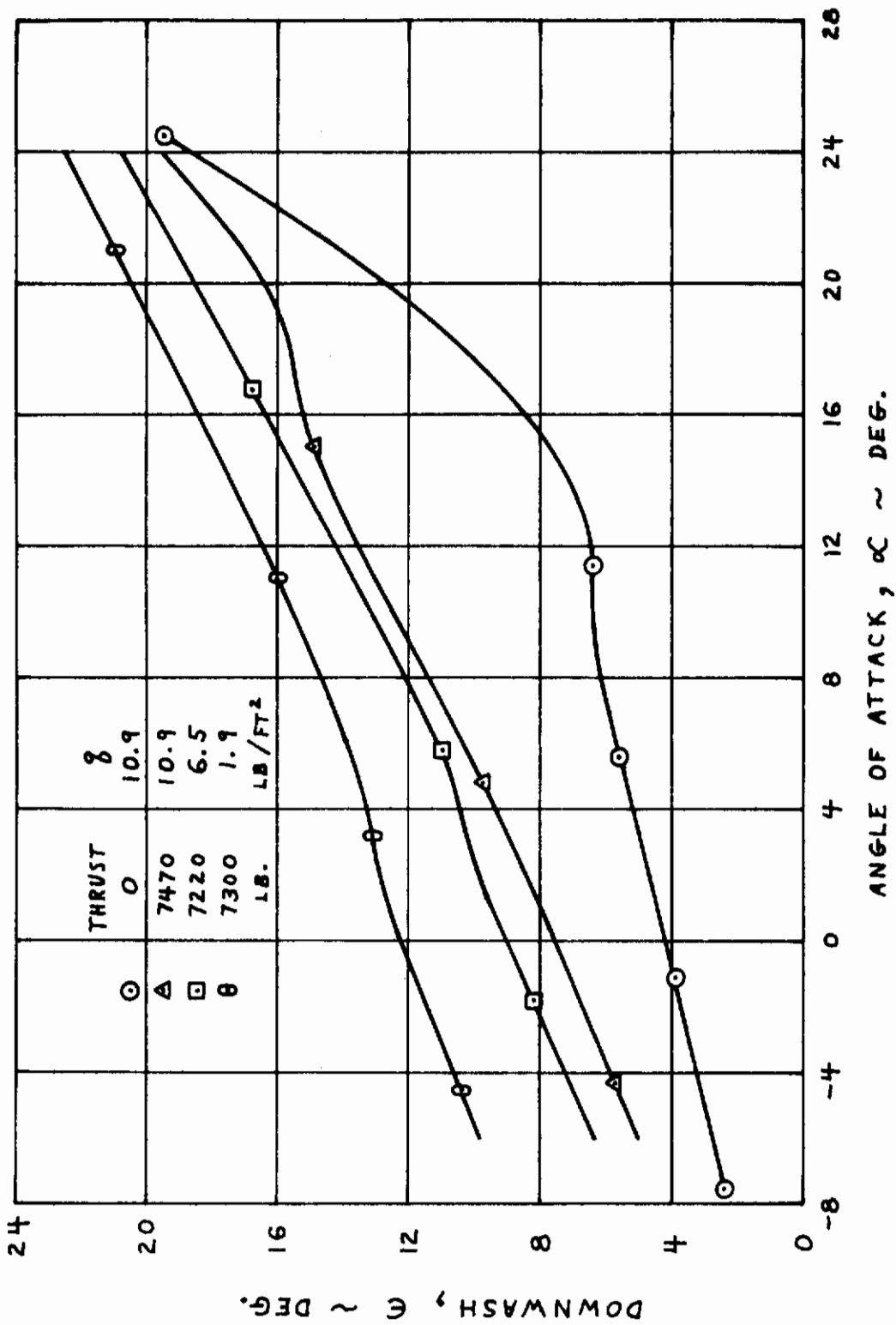
FIGURE 31. DOWNWASH AT HORIZONTAL TAIL VERSUS ANGLE
OF ATTACK BASED ON LANGLEY TEST 178

64

$$\Delta \epsilon = .13 \sqrt{\frac{T}{g}}$$
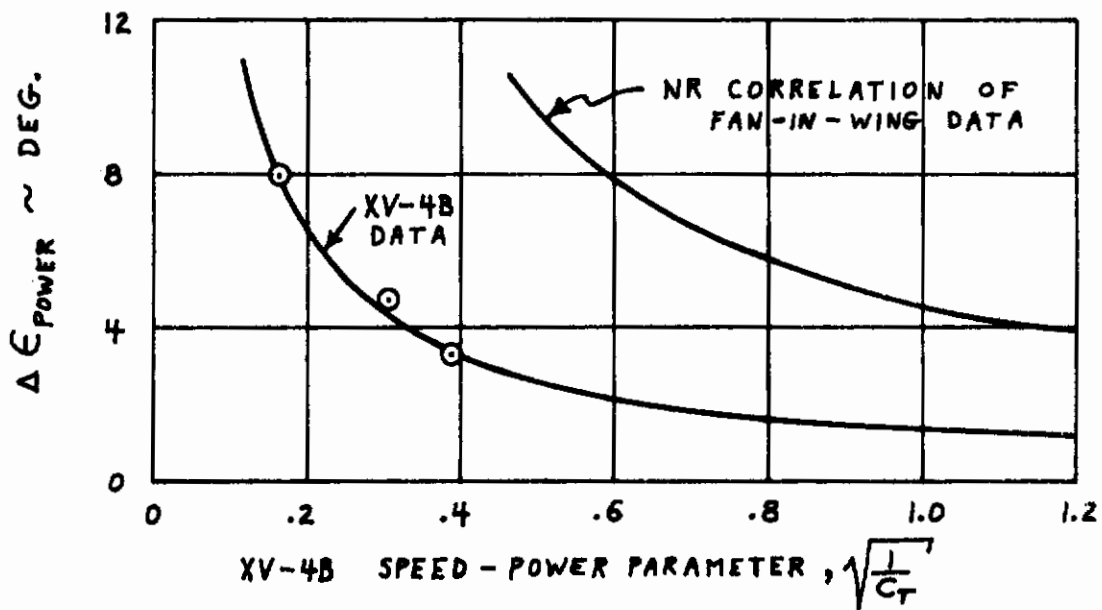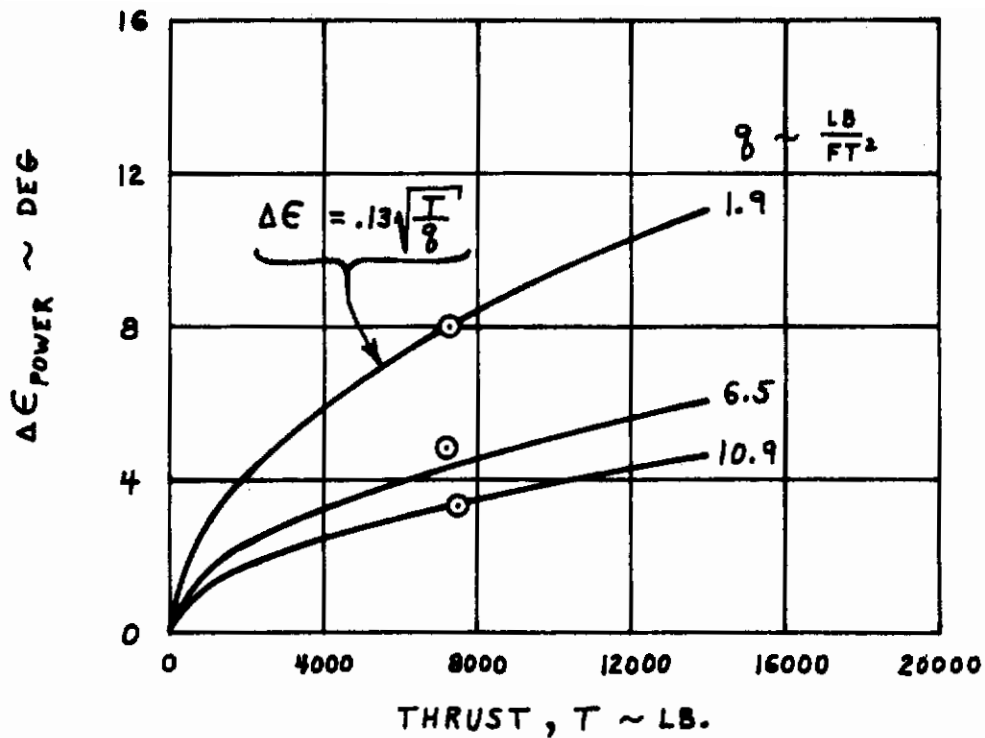
FIGURE 32. INCREMENT IN DOWNWASH DUE TO POWER AT ZERO ANGLE OF ATTACK BASED ON LANGLEY TEST 178
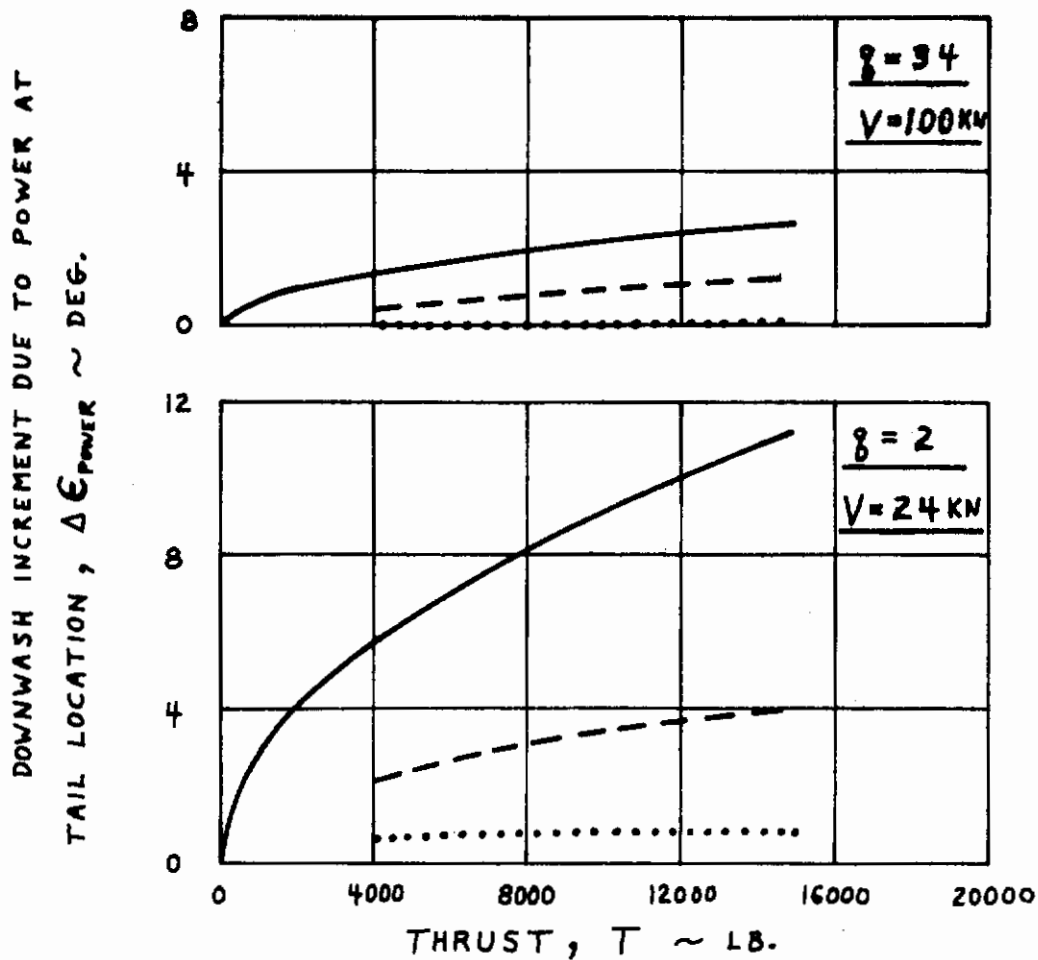
65
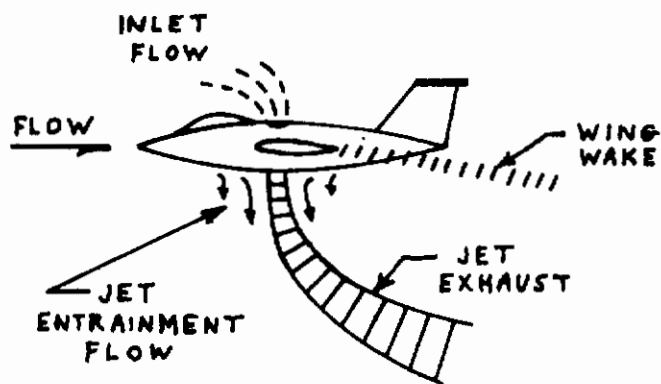
FIGURE 33. INFLUENCE OF INLET AND EXIT FLOW ON DOWNWASH DUE TO POWER
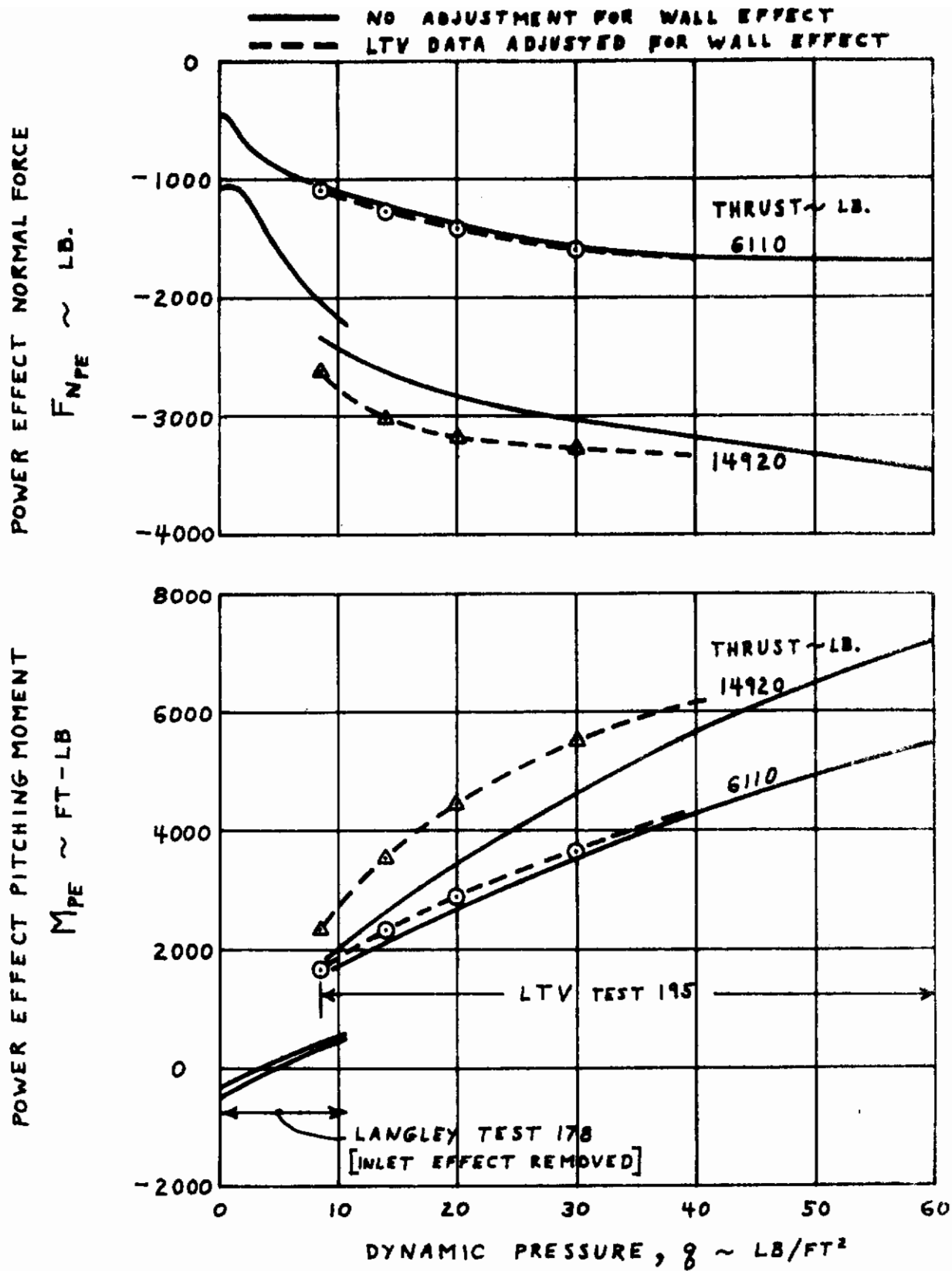
FIGURE 34. EFFECT OF WIND TUNNEL WALLS ON THE
DATA FOR LTV TEST 195
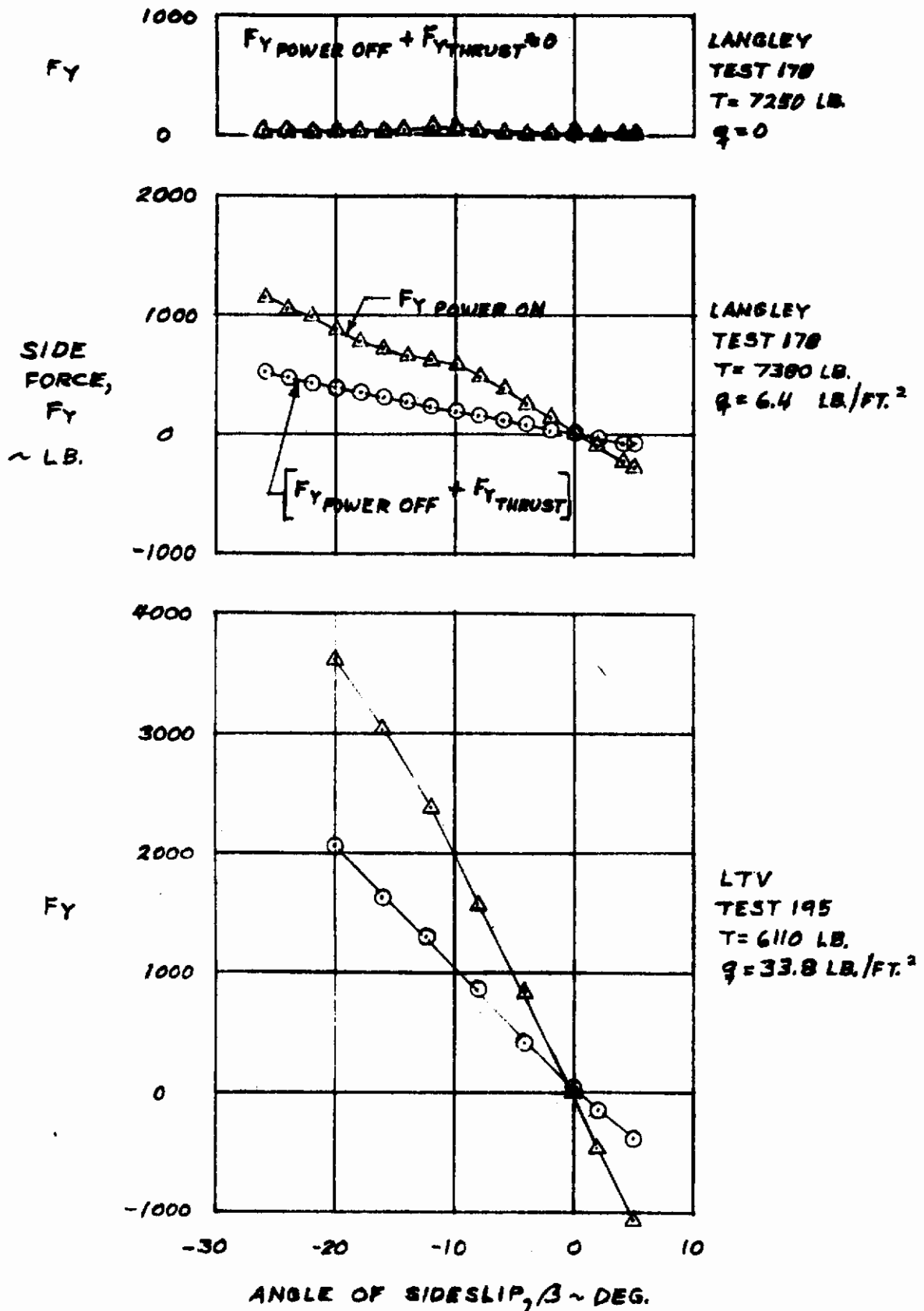
FIGURE 35. TYPICAL SIDEFORCE VERSUS ANGLE OF SIDESLIP
DATA (UNADJUSTED TEST DATA ; $\alpha = 0$)

○ β=0, POWER OFF + DIRECT THRUST EFFECTS   △ β=0, THRUST=7600 LB
◻ β=5°,   "   "   +   "   "   "   "   ▽ β=5°,   "   ＝   "

SIDE FORCE, F_Y ~ LB.

POWER EFFECT SIDE FORCE, $F_{Y_{PE}}$ ~ LB.
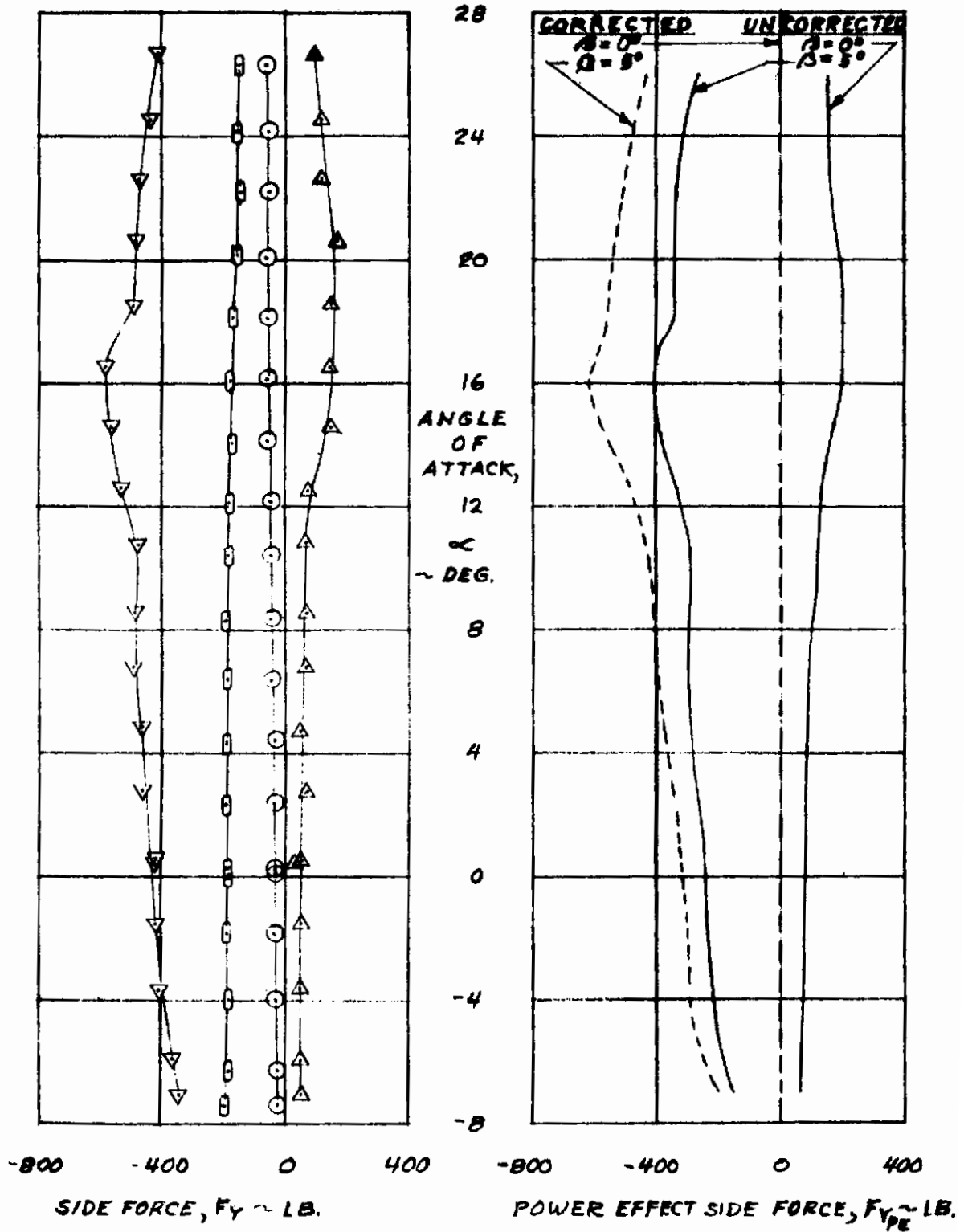
FIGURE 36. VARIATION OF SIDEFORCE AND POWER EFFECT SIDEFORCE
WITH ANGLE OF ATTACK (q = 11 PSF)

○ LANGLEY TEST 178
△ LTV TEST 195
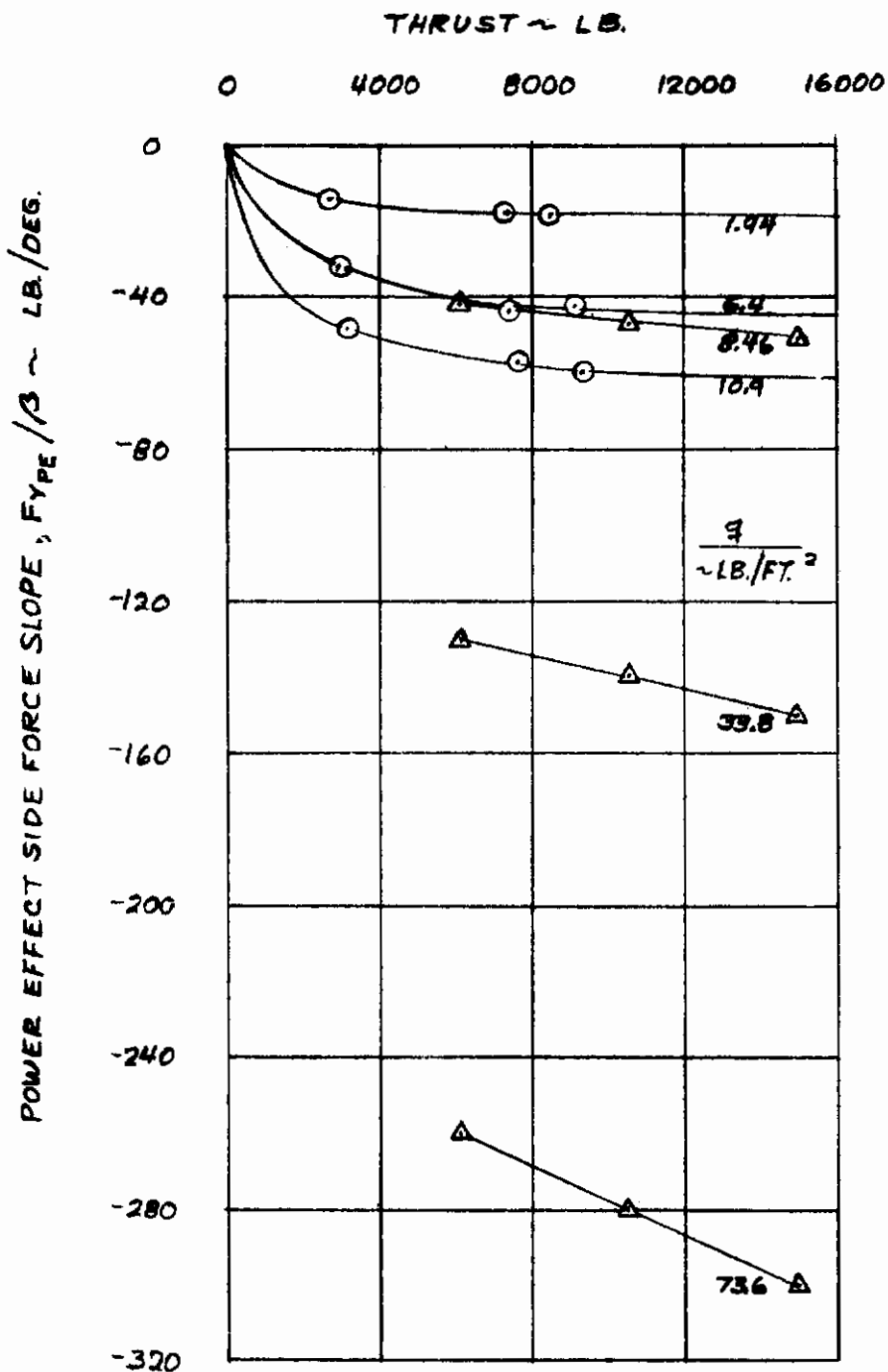
FIGURE 37. POWER EFFECT SIDE FORCE SLOPE VERSUS THRUST FOR
DIFFERENT VALUES OF DYNAMIC PRESSURE
(UNADJUSTED TEST DATA ; $\alpha = 0$)

70

○ LANGLEY TEST 178 (INLET EFFECTS REMOVED)
△ LTV TEST 195
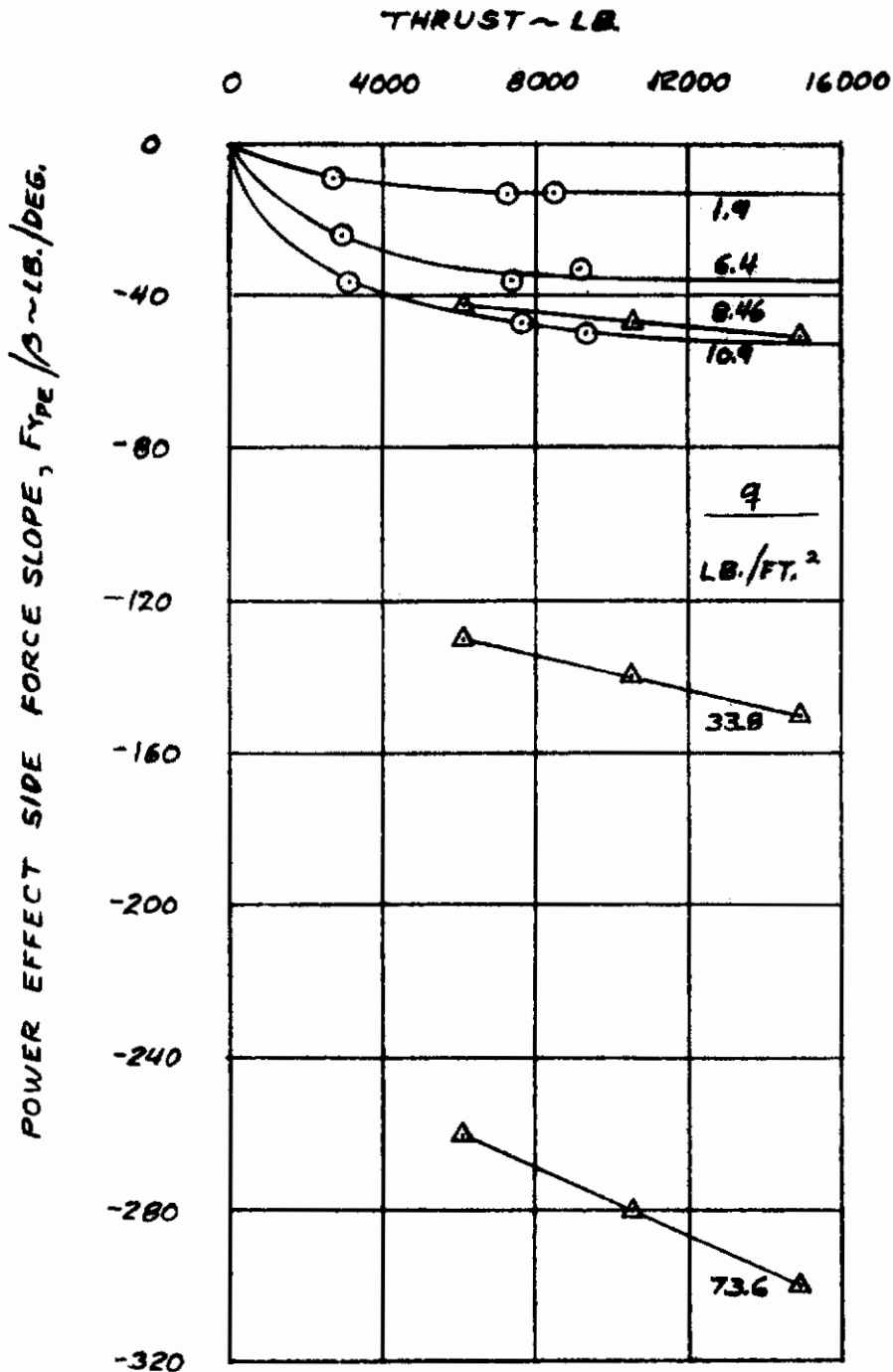
FIGURE 38. POWER EFFECT SIDE FORCE SLOPE VERSUS THRUST FOR
DIFFERENT VALUES OF DYNAMIC PRESSURE
(ADJUSTED TEST DATA ; ∝ = 0)

71

DYNAMIC PRESSURE, q ~ LB./FT.²

UNADJUSTED TEST DATA

THRUST ~ LB.
6110
10,560
14,920

DYNAMIC PRESSURE, q ~ LB./FT.²

LANGLEY TEST 178
[INLET EFFECT REMOVED]

ADJUSTED TEST DATA

THRUST ~ LB.
6110
10,560
14,920

LTV TEST 195

POWER EFFECT SIDE FORCE SLOPE, Fy_{PE}/β ~ LB./DEG.
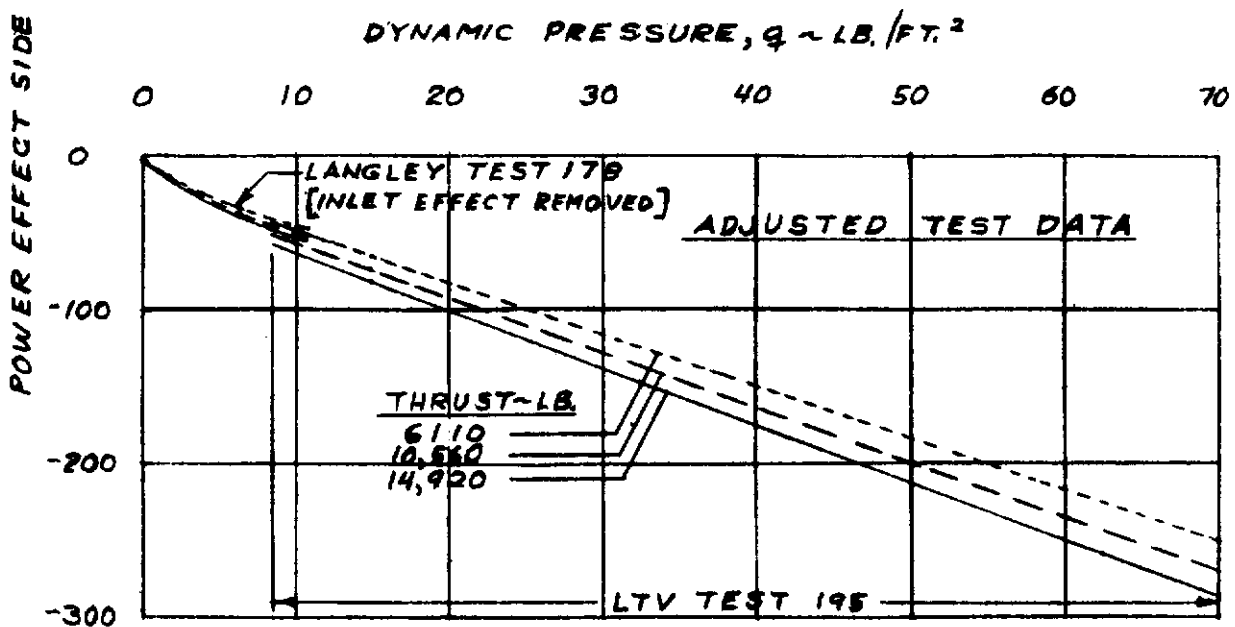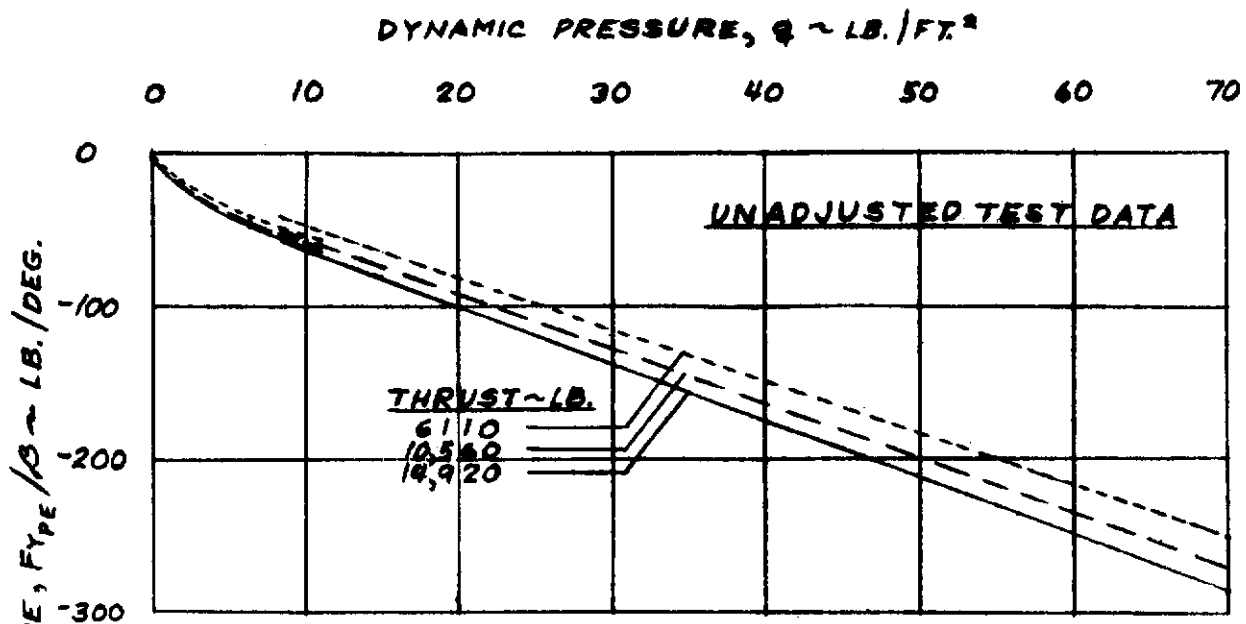
FIGURE 39. POWER EFFECT SIDE FORCE SLOPE VERSUS DYNAMIC PRESSURE FOR DIFFERENT VALUES OF THRUST ($\alpha = 0$)

72
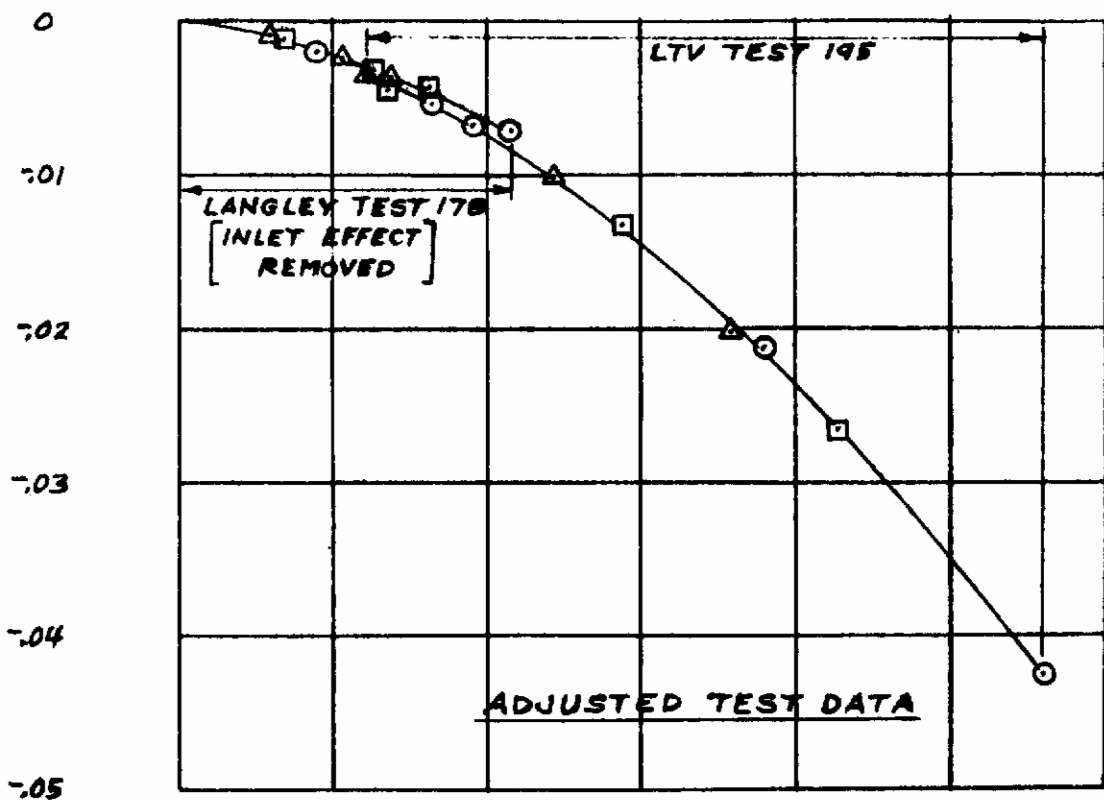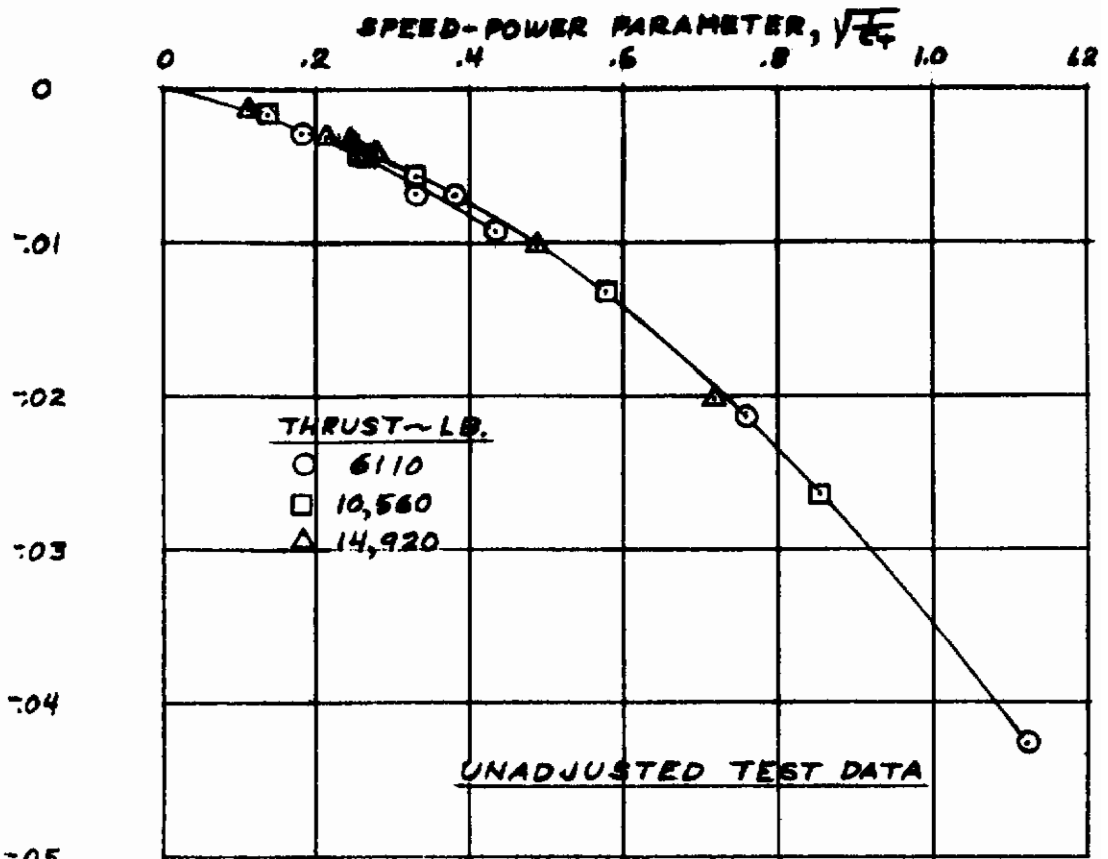
FIGURE 40. POWER EFFECT SIDE FORCE SLOPE VERSUS LOCKHEED
SPEED-POWER PARAMETER (α = 0)
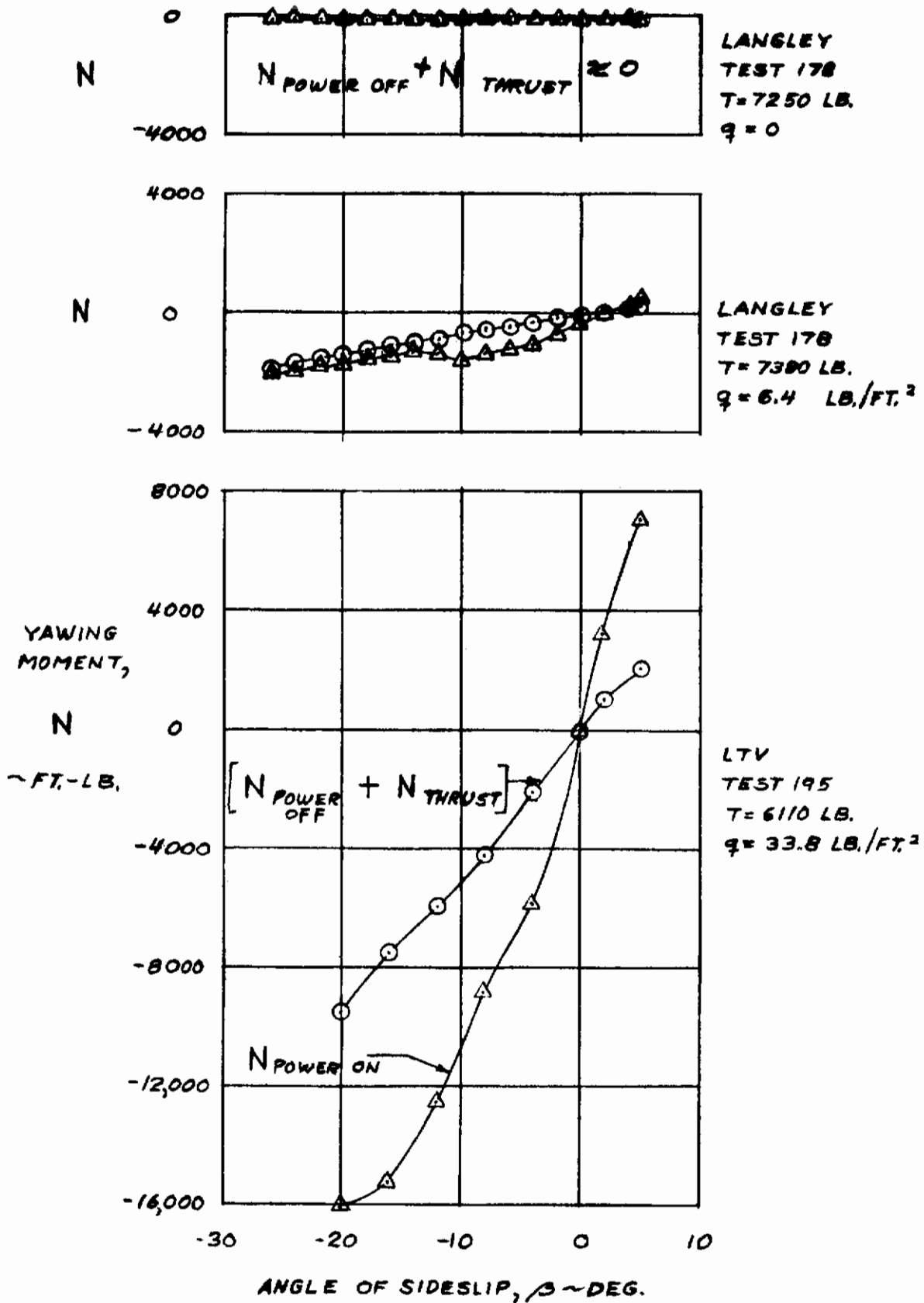
FIGURE 41. TYPICAL YAWING MOMENT VERSUS ANGLE OF SIDESLIP
DATA (UNADJUSTED TEST DATA ; α = 0)

74

○ β=0, POWER OFF + DIRECT THRUST EFFECTS   △ β=0, THRUST=7600 LB.
◻ β=5°,   "   "   +   "   "   "   ▽ β=5°,   "   =   "

UNCORRECTED   CORRECTED
β=0°   β=0°
β=5°   β=5°

ANGLE OF ATTACK, ∝ ~ DEG.

YAWING MOMENT, N ~ FT.-LB.

POWER EFFECT YAWING MOMENT, N_{PE} ~ FT.LB.
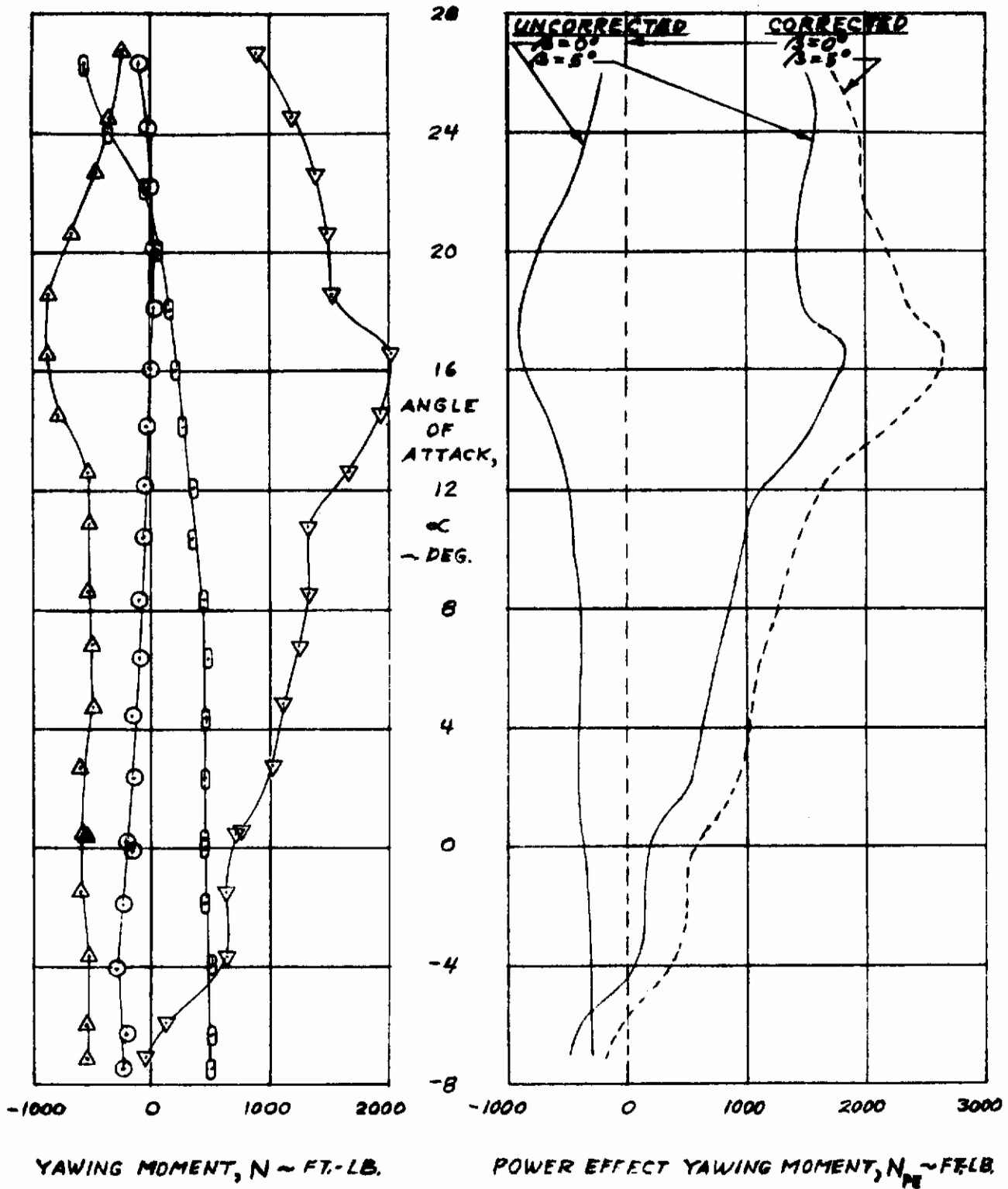
FIGURE 42. VARIATION OF YAWING MOMENT AND POWER EFFECT YAWING MOMENT WITH ANGLE OF ATTACK (q = 11 PSF)

75
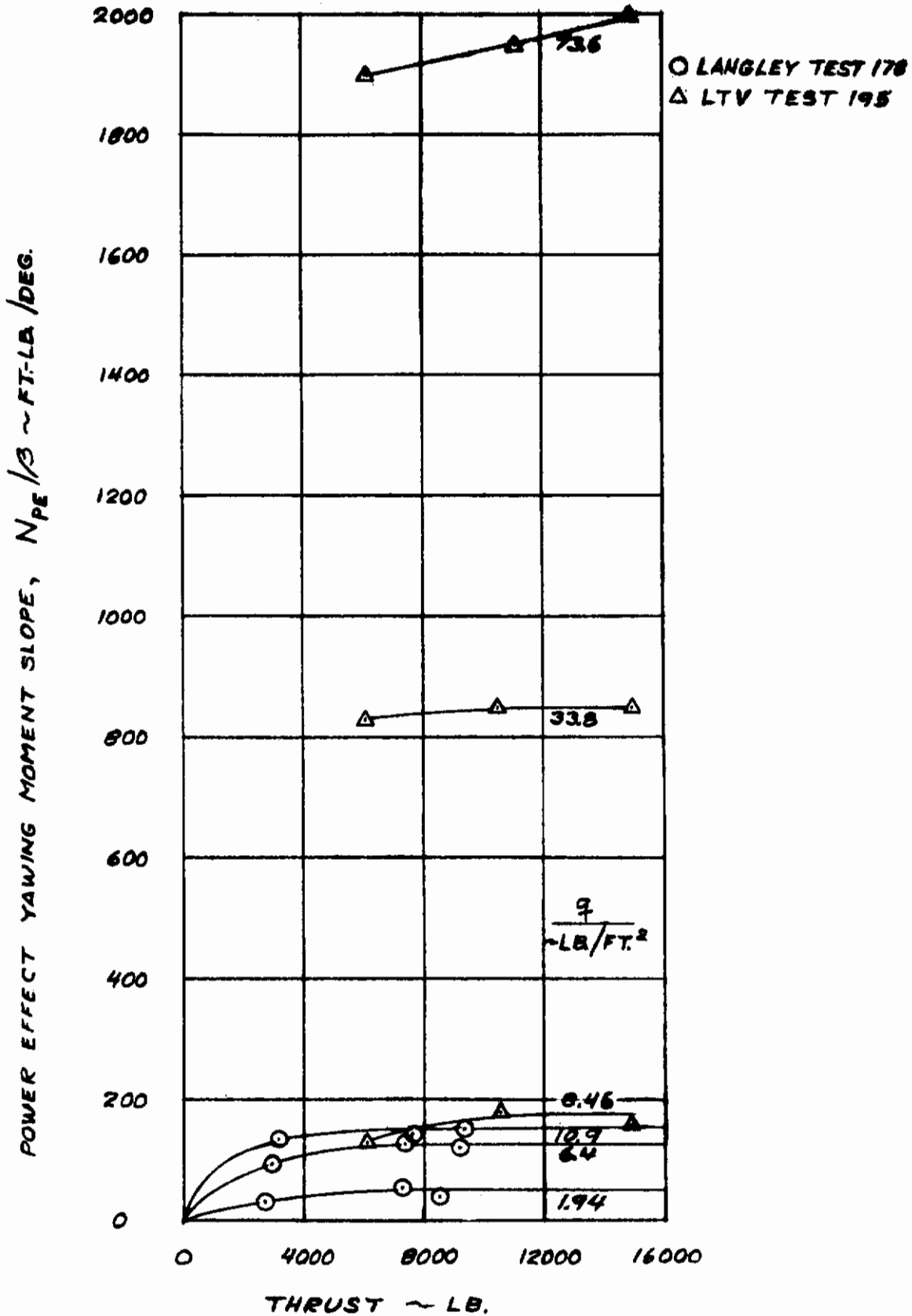
FIGURE 43. POWER EFFECT YAWING MOMENT SLOPE VERSUS THRUST
FOR DIFFERENT VALUES OF DYNAMIC PRESSURE
(UNADJUSTED TEST DATA ; $\alpha = 0$)

76
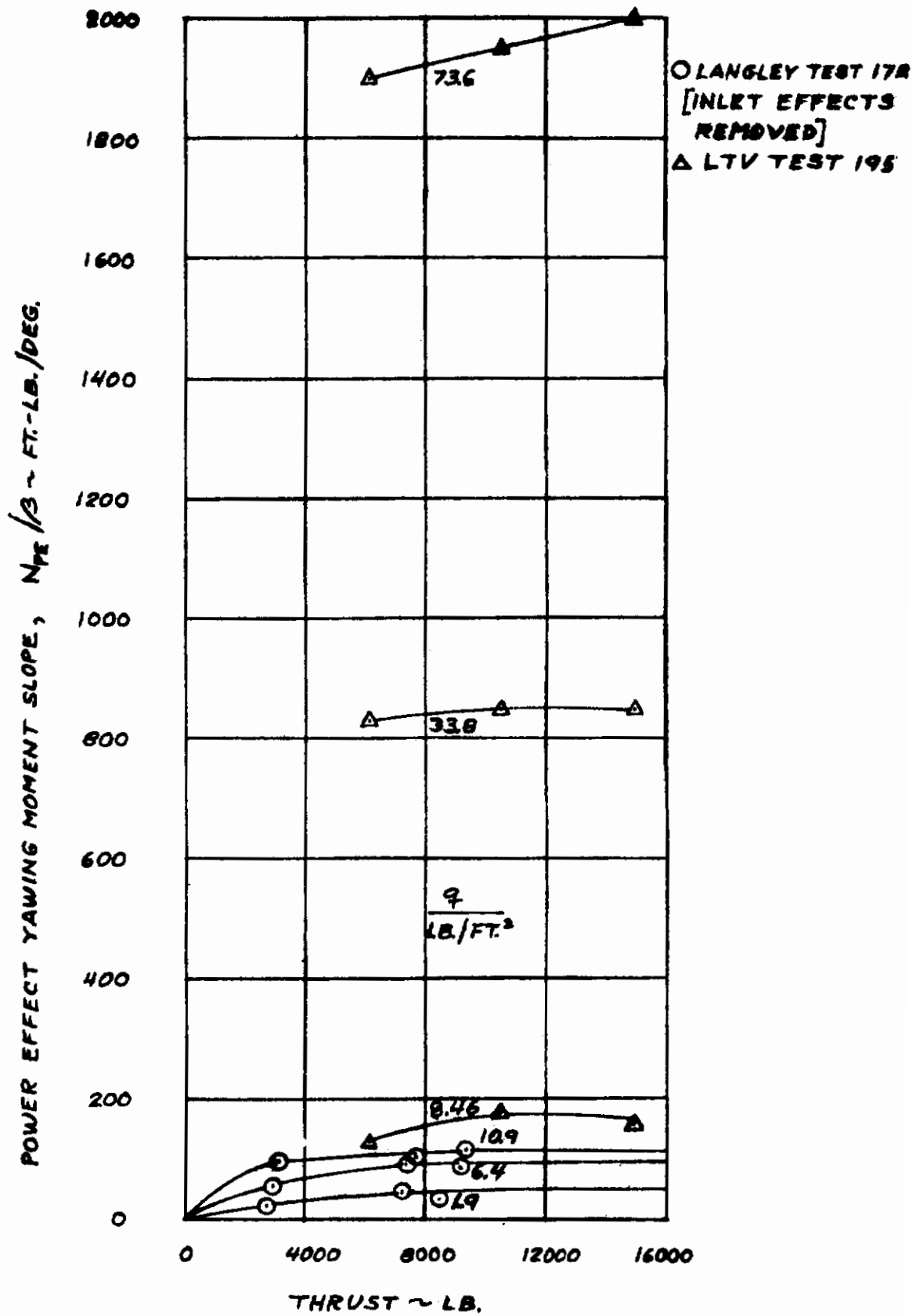
FIGURE 44. POWER EFFECT YAWING MOMENT SLOPE VERSUS THRUST
FOR DIFFERENT VALUES OF DYNAMIC PRESSURE
(ADJUSTED TEST DATA ; $\alpha = 0$)

FIGURE 45. POWER EFFECT YAWING MOMENT SLOPE VERSUS
DYNAMIC PRESSURE FOR DIFFERENT VALUES OF THRUST
$(\alpha = 0)$

78
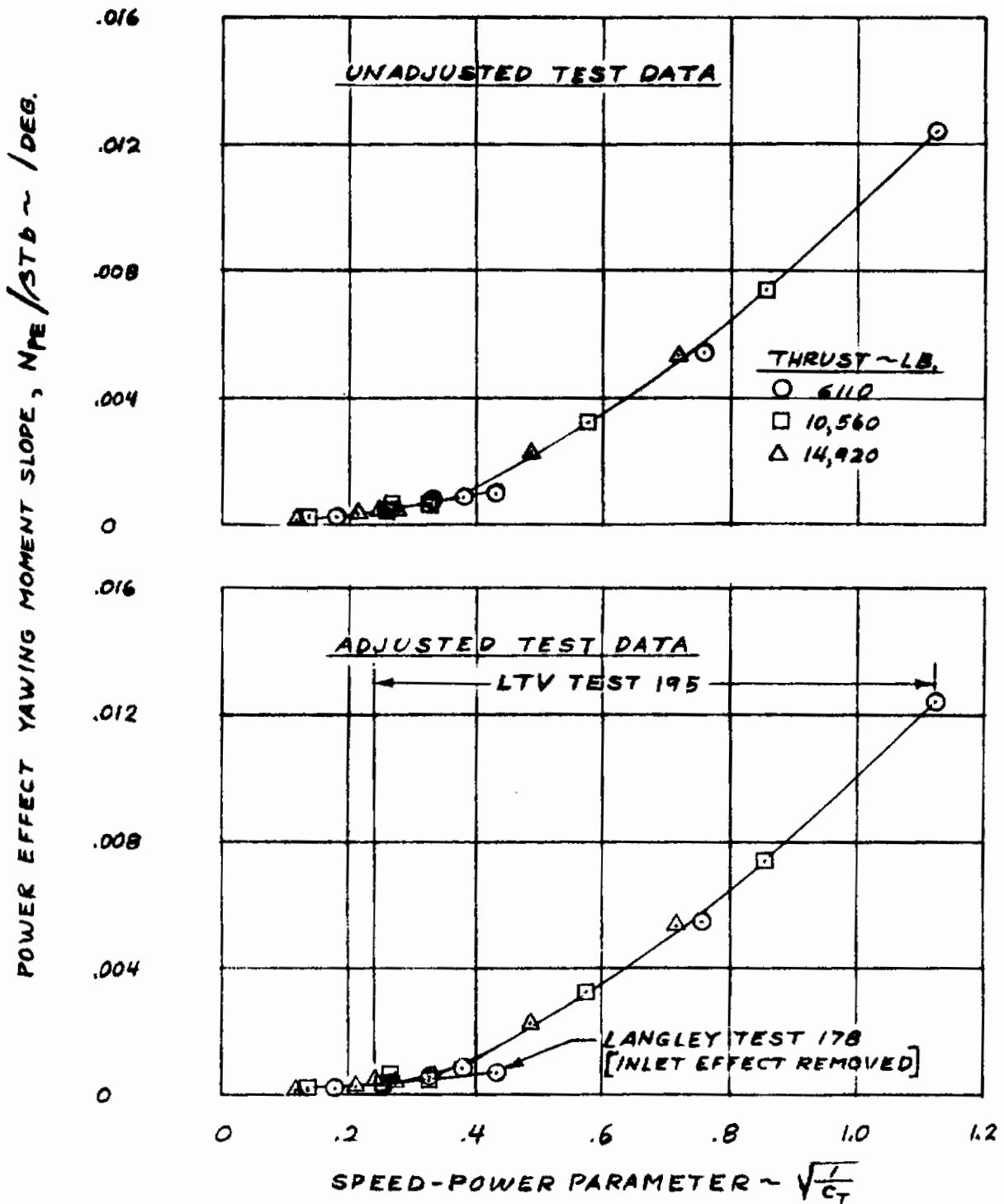
FIGURE 46. POWER EFFECT YAWING MOMENT SLOPE VERSUS LOCKHEED SPEED-POWER PARAMETER ($\alpha = 0$)

79
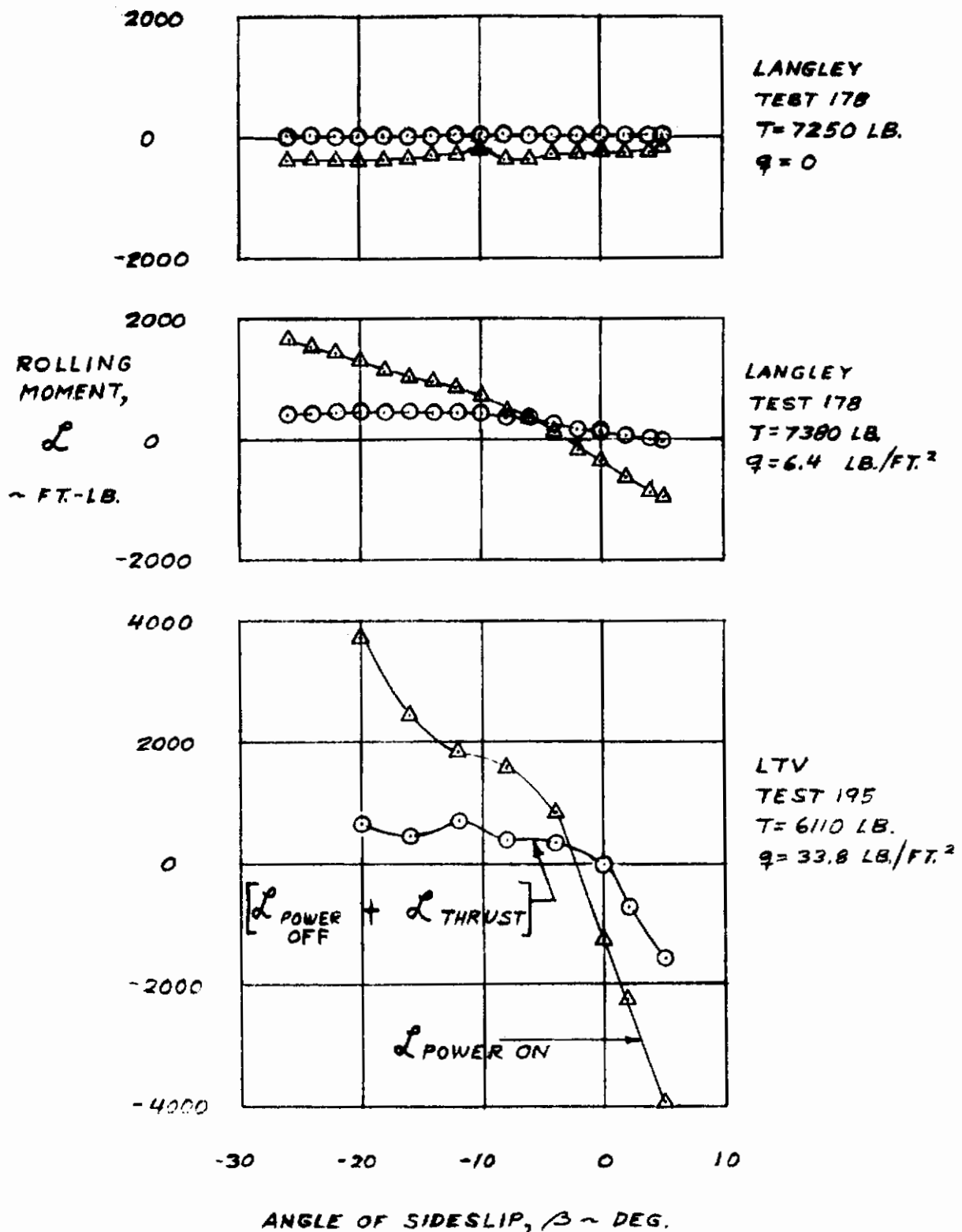
FIGURE 47. TYPICAL ROLLING MOMENT VERSUS ANGLE OF
SIDESLIP DATA (UNADJUSTED TEST DATA ; $\alpha = 0$)

80

○ β=0, POWER OFF + DIRECT THRUST EFFECTS   △ β=0, THRUST = 7500 LB.
◻ β=5°, " " + " " "   ▽ β=5°, " " "

ROLLING MOMENT, $\mathcal{L}$ ~ FT.-LB.   POWER EFFECT ROLLING MOMENT, $\mathcal{L}_{PS}$ ~ FT-LB.
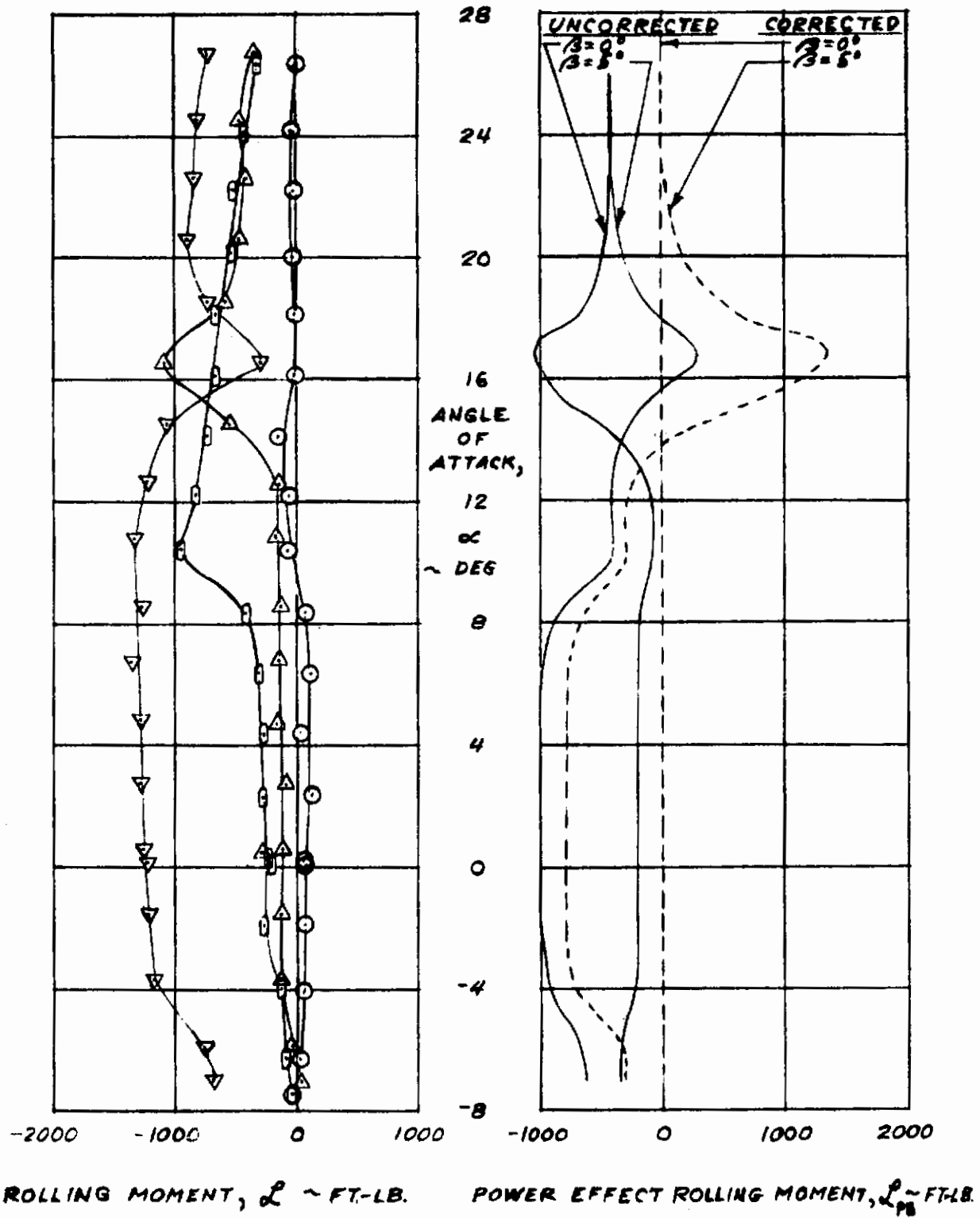
FIGURE 48. VARIATION OF ROLLING MOMENT AND POWER EFFECT ROLLING
MOMENT WITH ANGLE OF ATTACK (q = 11 PSF)

81

○ LANGLEY TEST 178
△ LTV TEST 195

FIGURE 49. POWER EFFECT ROLLING MOMENT SLOPE VERSUS
THRUST FOR DIFFERENT VALUES OF DYNAMIC
PRESSURE (UNADJUSTED TEST DATA ; $\alpha = 0$)

82

FIGURE 50. POWER EFFECT ROLLING MOMENT SLOPE VERSUS
THRUST FOR DIFFERENT VALUES OF DYNAMIC
PRESSURE (ADJUSTED TEST DATA ; $\alpha = 0$)

83
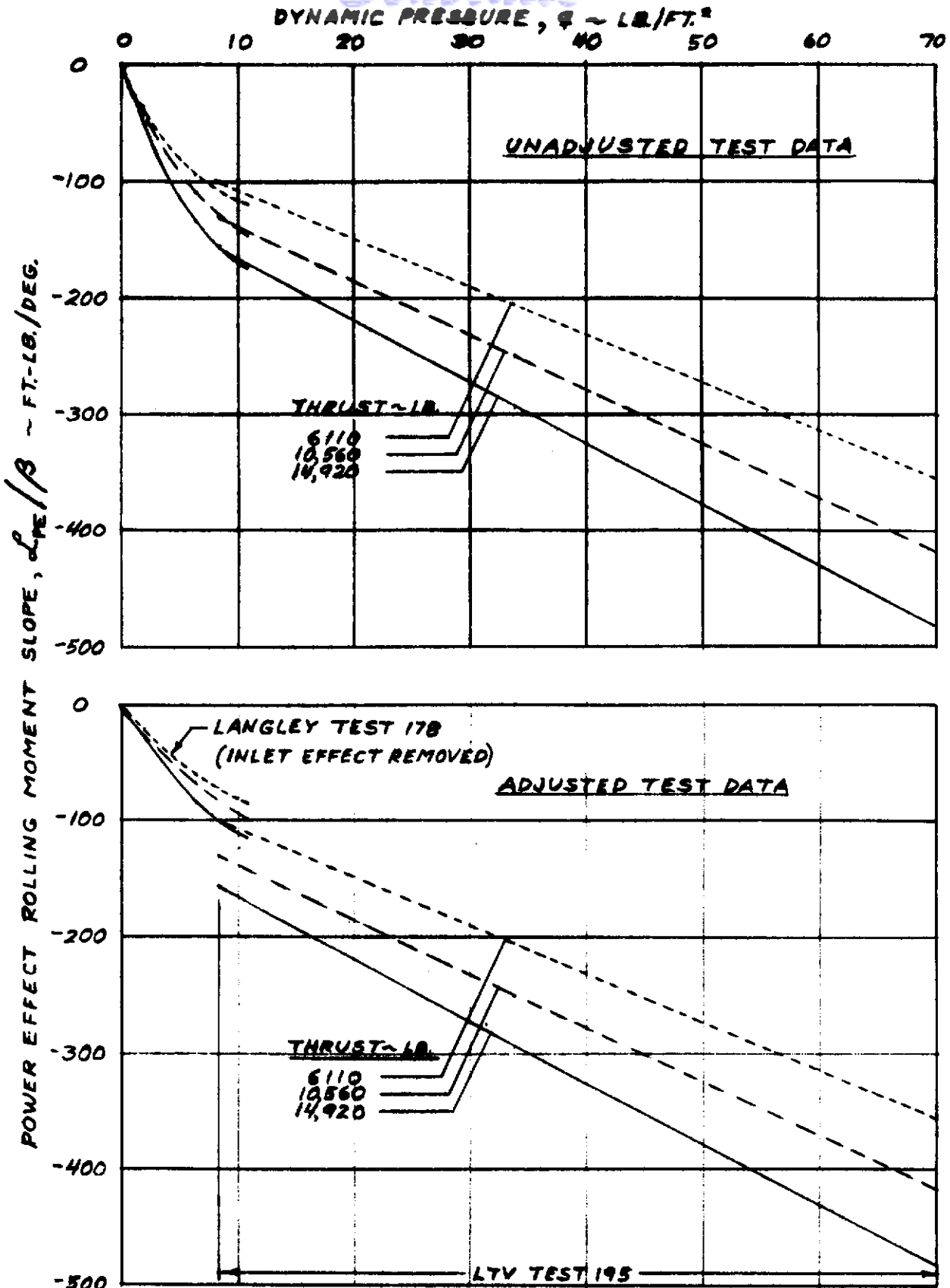
FIGURE 51. POWER EFFECT ROLLING MOMENT SLOPE VERSUS
DYNAMIC PRESSURE FOR DIFFERENT VALUES
OF THRUST ($\alpha = 0$)

84

FIGURE 52. POWER EFFECT ROLLING MOMENT SLOPE
VERSUS LOCKHEED SPEED-POWER PARAMETER $(\alpha=0)$

85

THRUST ~ LB.
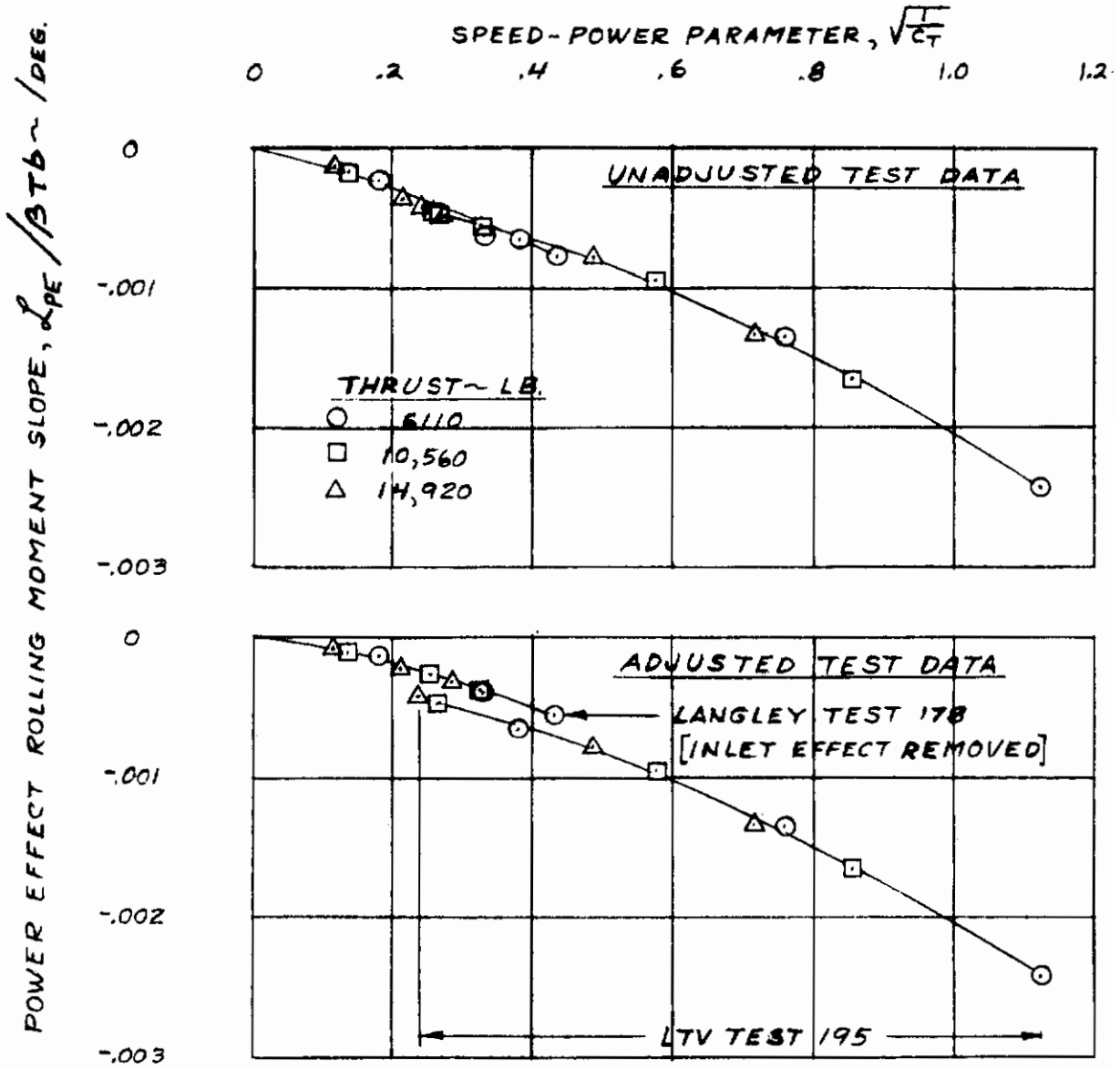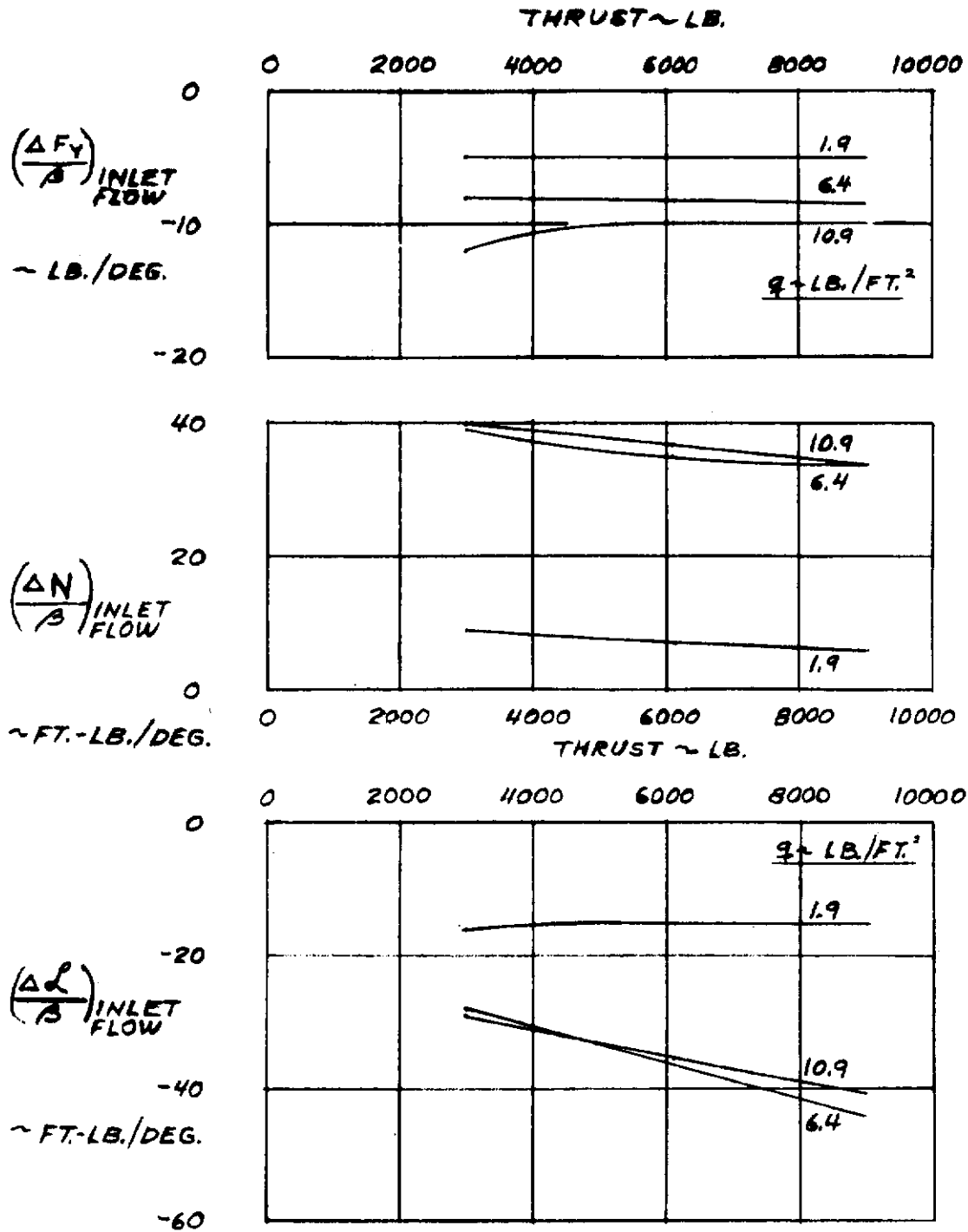
FIGURE 53. EFFECT OF INLET FLOW ON LATERAL-DIRECTIONAL
POWER EFFECT SLOPES (∝ = 0)

86

LANGLEY TEST 178 $q = 10.9$ LB./FT.^{2}

$\alpha = 0$ $\sqrt{\frac{T}{C_T}} = .386$

SIDEWASH
ANGLE,
$\sigma \sim$ DEG.

THRUST = 0

THRUST = 76 40 LB.
(INLET AND EXIT FLOW
EFFECTS INCLUDED)

ANGLE OF SIDESLIP, $\beta \sim$ DEG.

POWER-
INDUCED
SIDEWASH
ANGLE,
$(\Delta\sigma)_{POWER}$
$\sim$ DEG.

ANGLE OF SIDESLIP, $\beta \sim$ DEG.
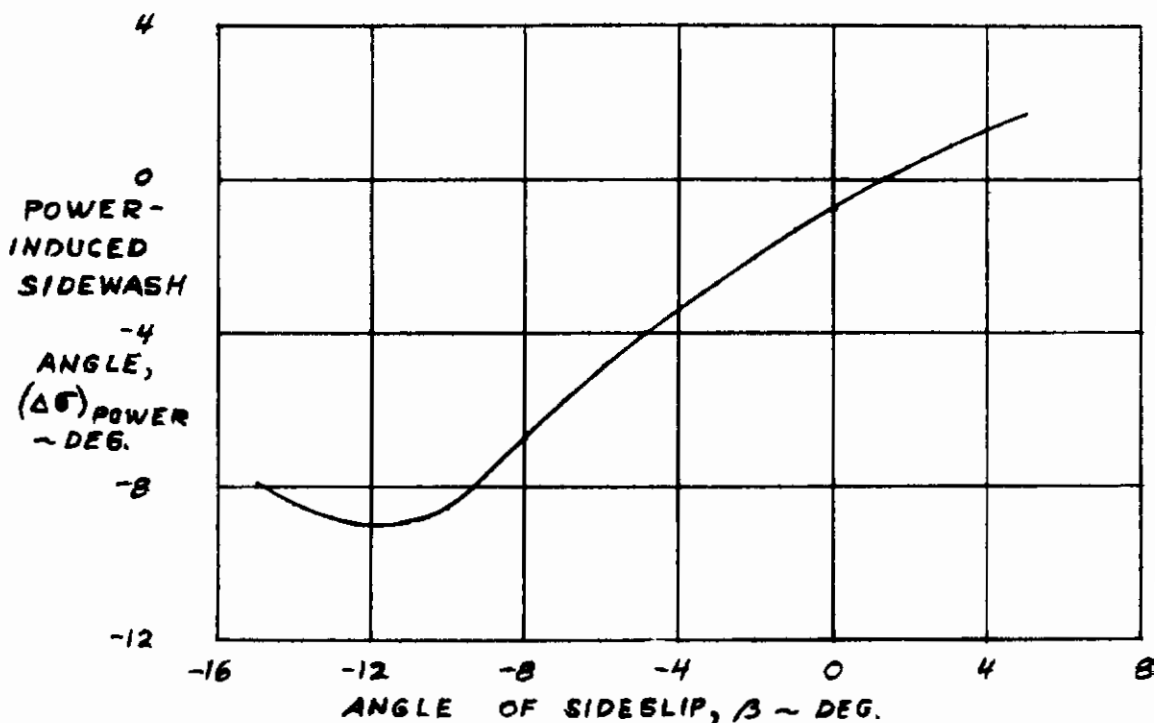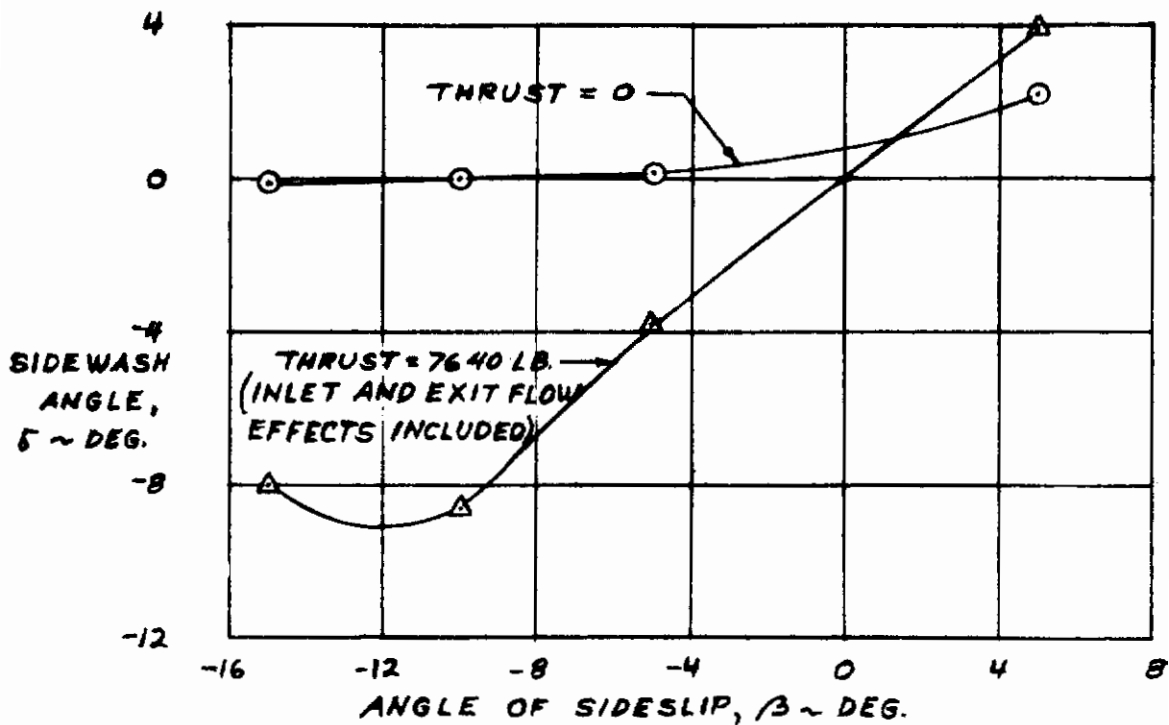
FIGURE 54. EFFECT OF POWER ON SIDEWASH ANGLE $(\alpha = 0)$
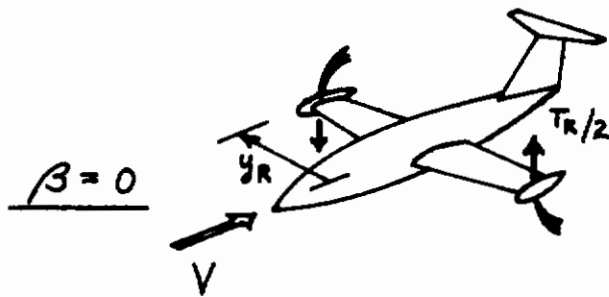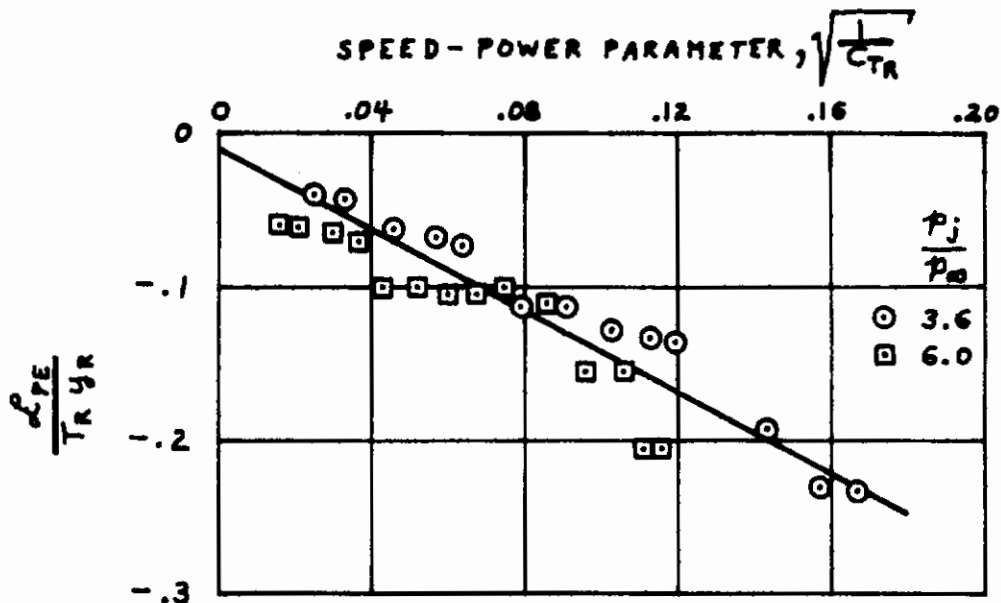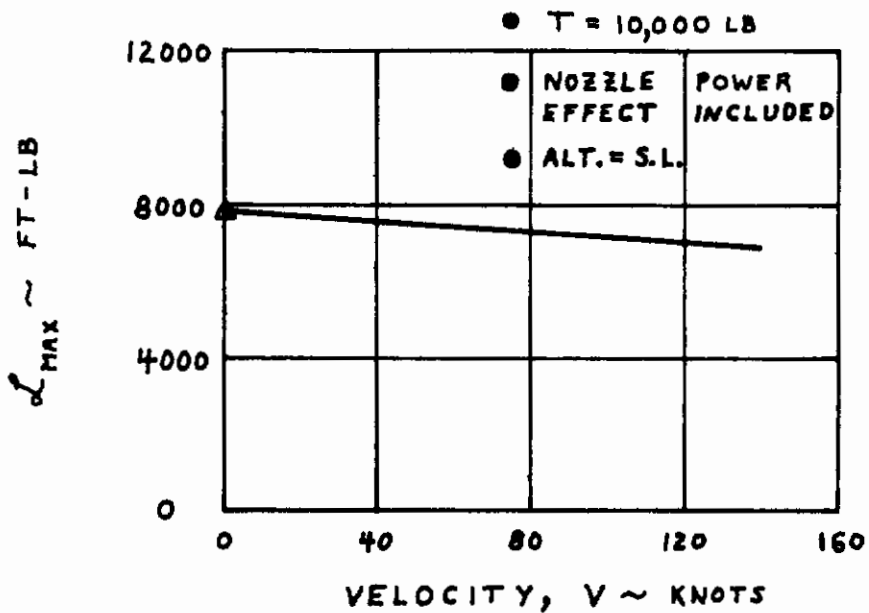
FIGURE 55. ESTIMATED POWER EFFECT FOR WING
TIP ROLL CONTROL JETS

88

$T \approx 7400$ LB.

$\frac{q}{\delta} = 10.91 \ \frac{LB}{FT^2}$
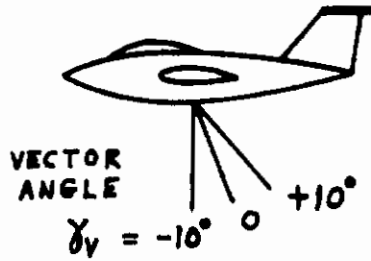
$\frac{q}{\delta} = 6.41 \ \frac{LB}{FT^2}$

$\frac{q}{\delta} = 1.96 \ \frac{LB}{FT^2}$

POWER EFFECT PITCHING MOMENT, $M_{PE} \sim$ FT-LB
(INCLUDES INLET MOMENTUM)

ANGLE OF ATTACK, $\alpha \sim$ DEG.
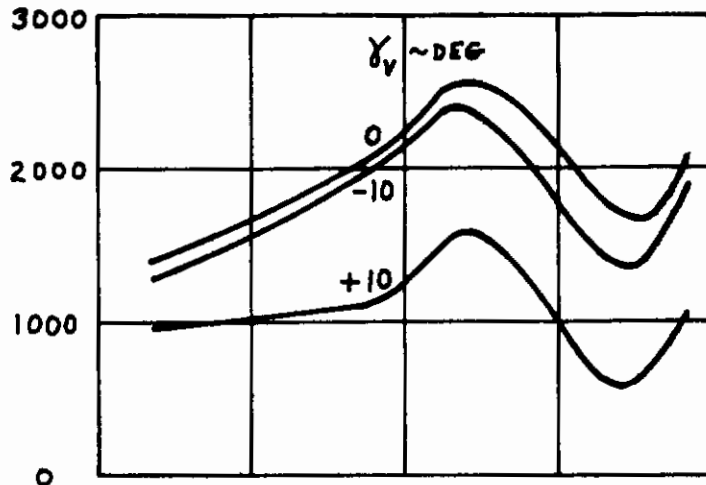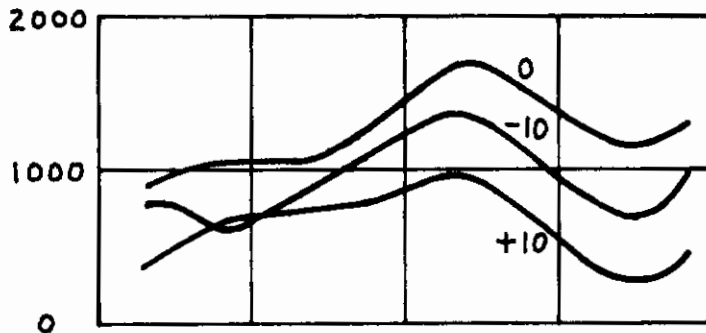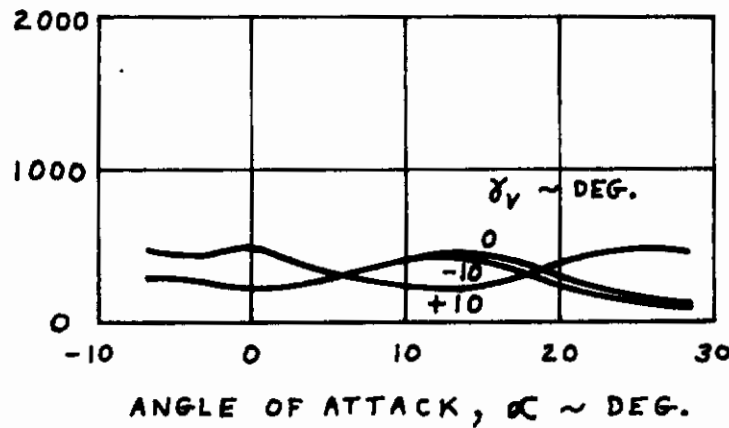
FIGURE 56. EFFECT OF EXHAUST NOZZLE VECTOR ANGLE ON THE POWER EFFECT PITCHING MOMENT (LANGLEY TEST 178)

89
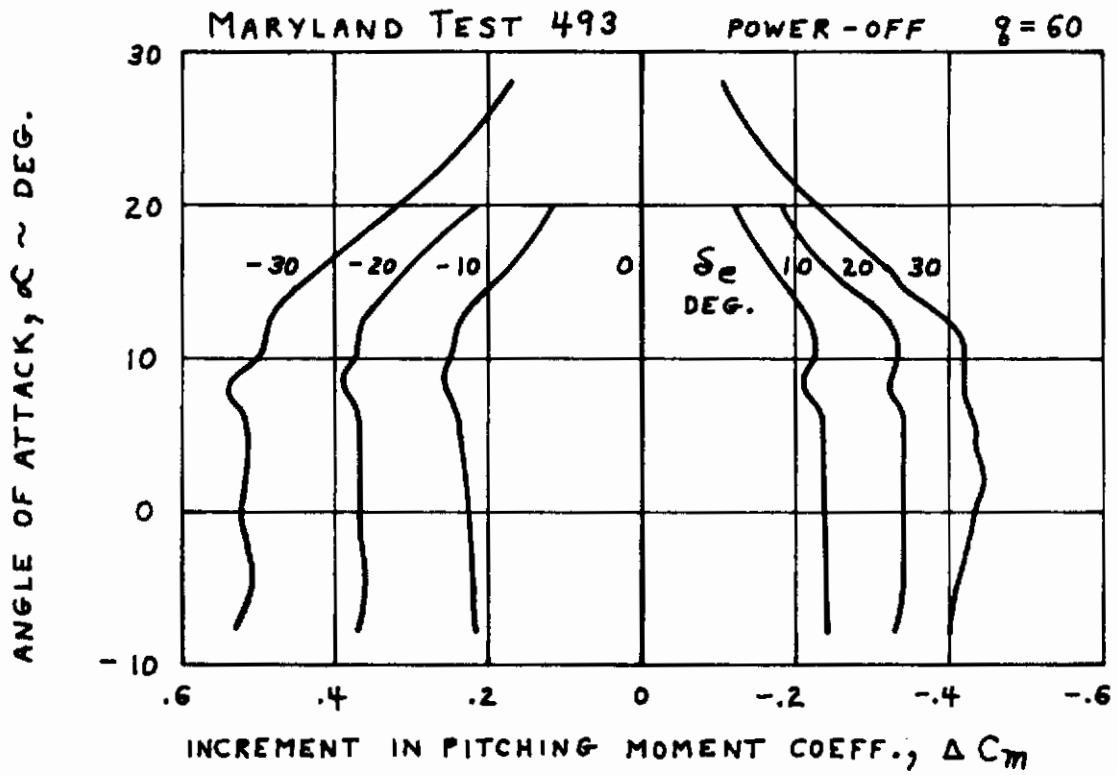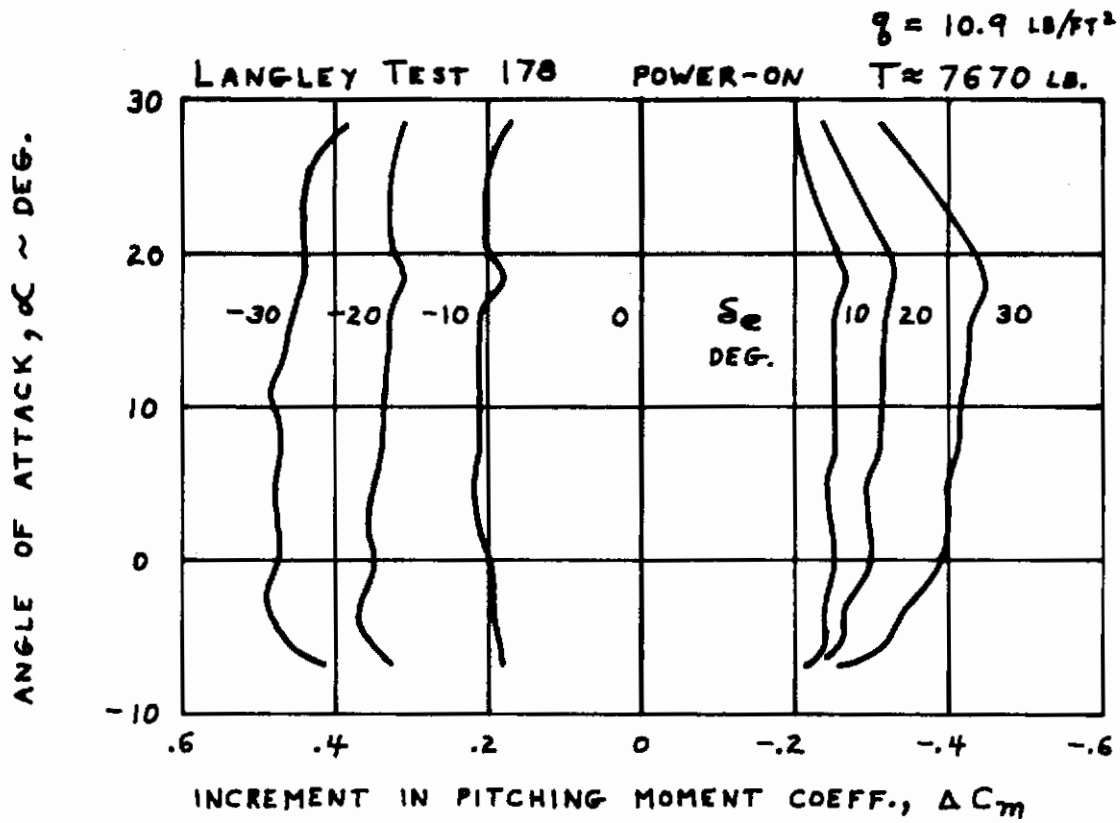
FIGURE 57. THE EFFECT OF POWER ON THE ELEVATOR EFFECTIVENESS
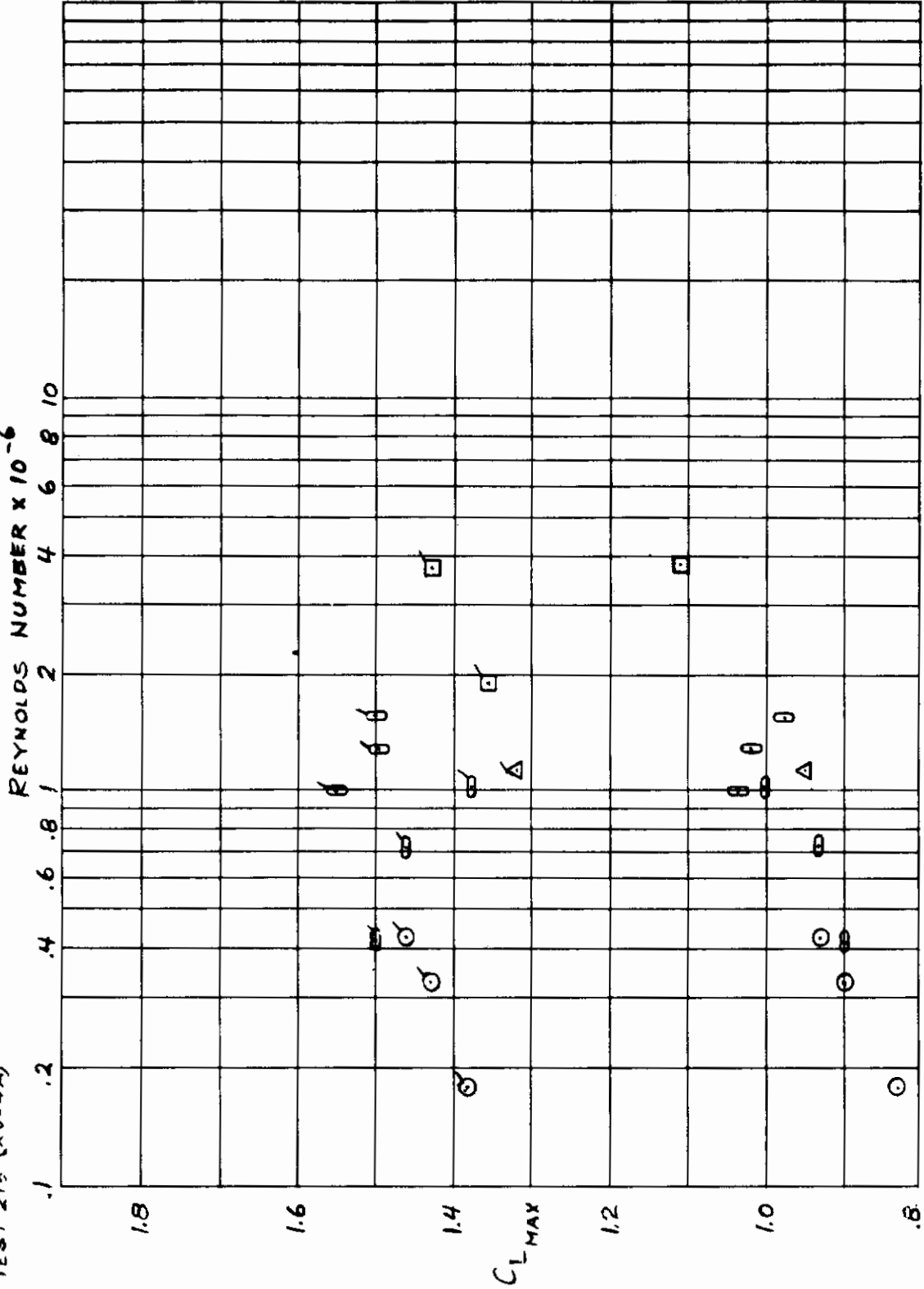
FIGURE 58. MAXIMUM LIFT COEFFICIENT
VERSUS REYNOLDS NUMBER

91

⊙ LANGLEY TUNNEL TEST 221
□ LANGLEY TUNNEL TEST 178
▲ LOCKHEED OUTDOOR TEST RIG

$H = 41.5$ FT. ; $q = 0$; $\gamma_V = 0$; STRAKES OFF
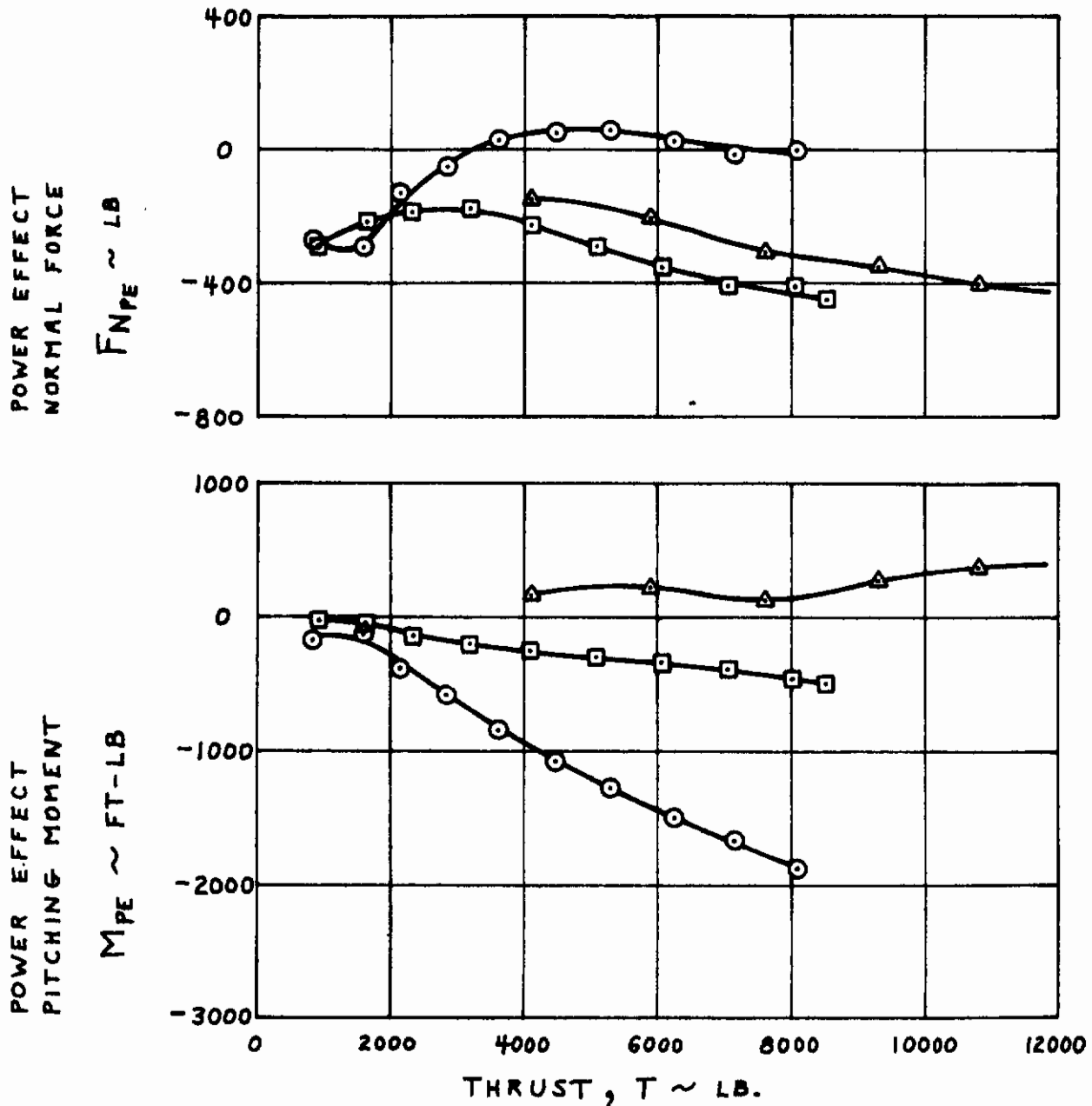
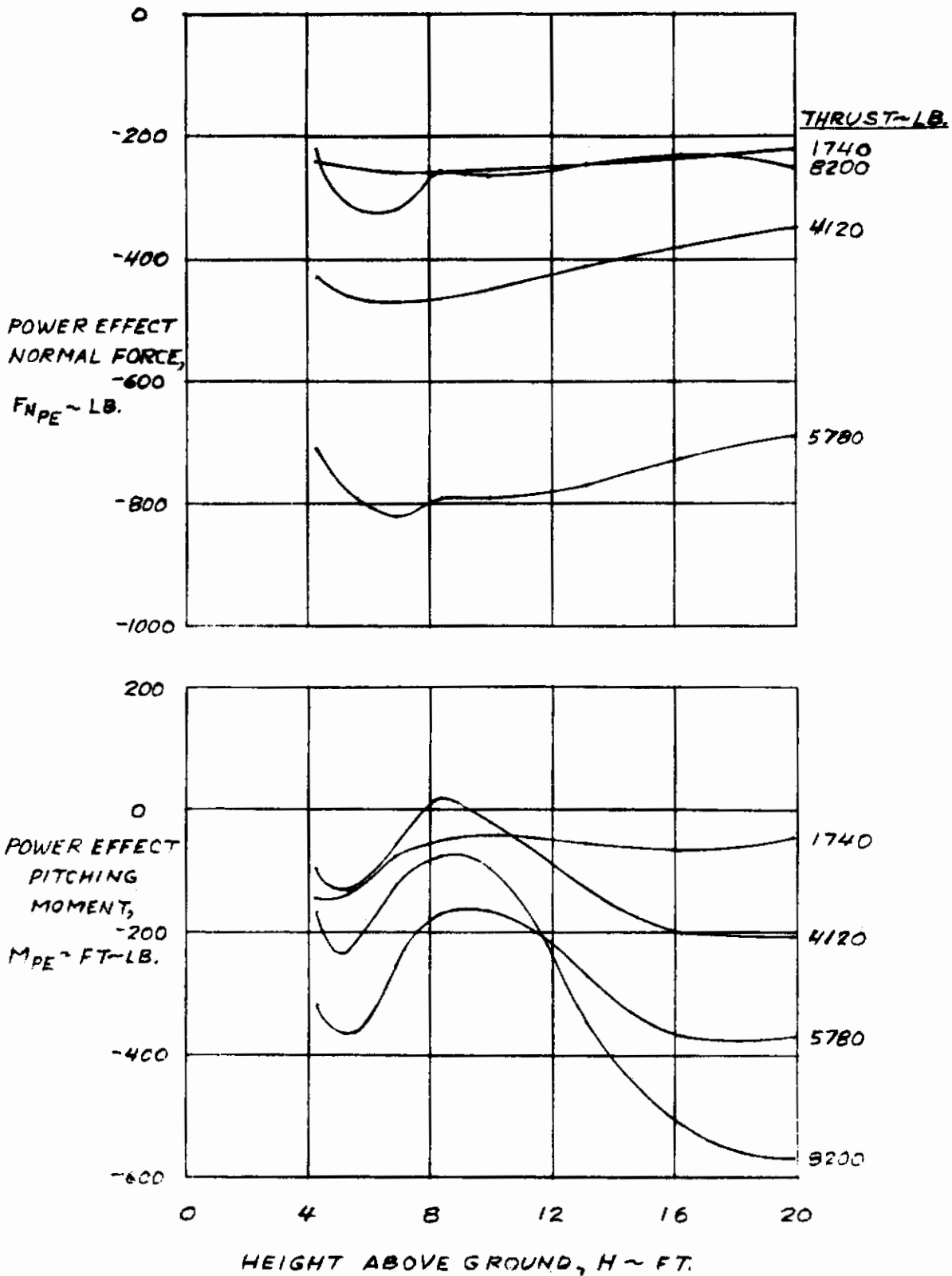FIGURE 59. COMPARISON OF TUNNEL AND OUTDOOR HOVER
DATA OUT OF GROUND EFFECT

92

WIND TUNNEL CEILING

$q = 0$

$\square$ $\theta = 90°$ $\psi = 0$
STRAKES ON

$\odot$ $\theta = 0$ $\psi = 0$
STRAKES OFF

$\triangle$ $\theta = 0$ $\psi = 90°$
STRAKES ON

WIND TUNNEL FLOOR

POWER EFFECT
NORMAL FORCE

$F_{N_{PE}} \sim LB.$

POWER EFFECT
PITCHING
MOMENT

$M_{PE} \sim FT\text{-}LB$

THRUST, $T \sim LB.$
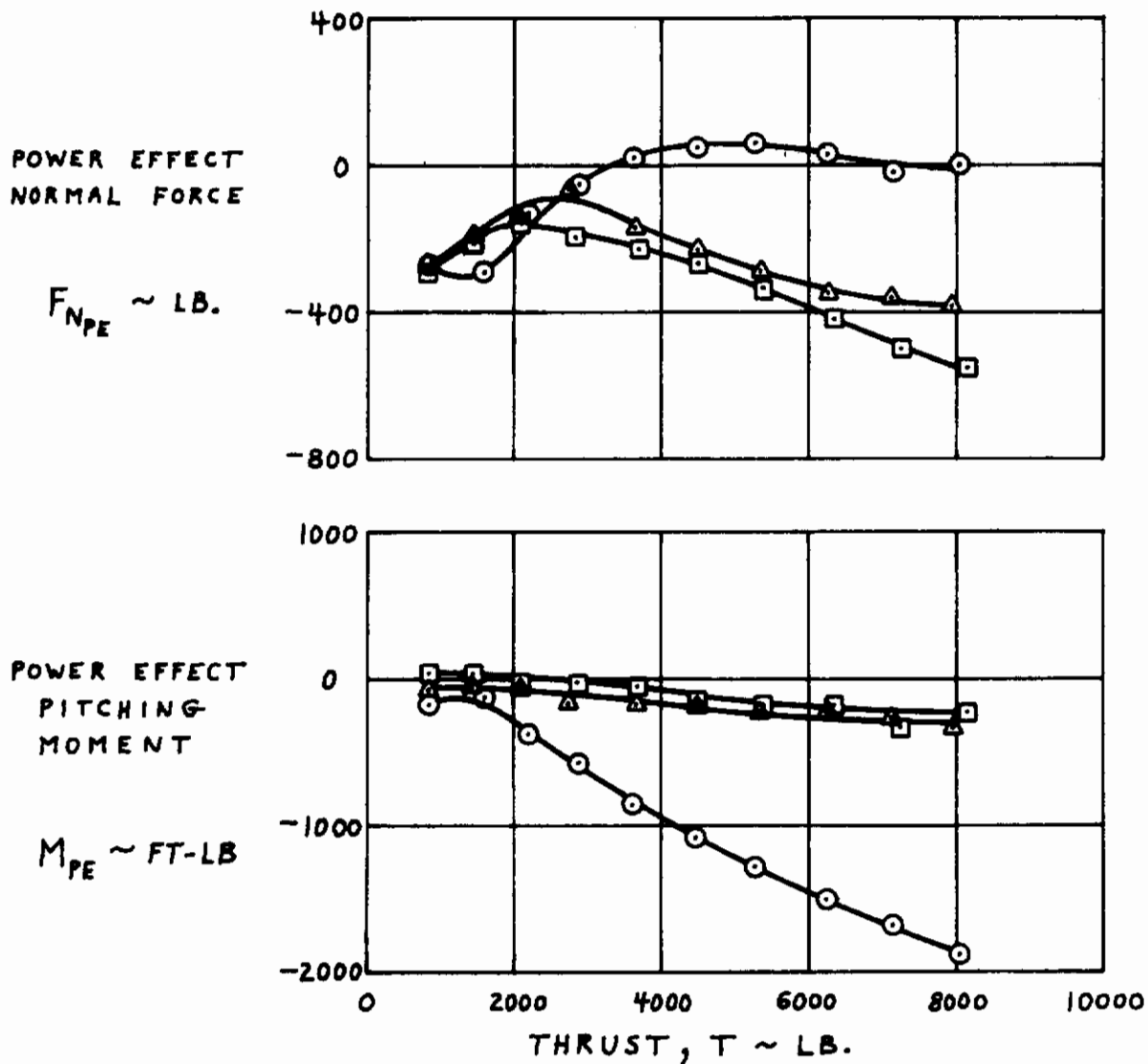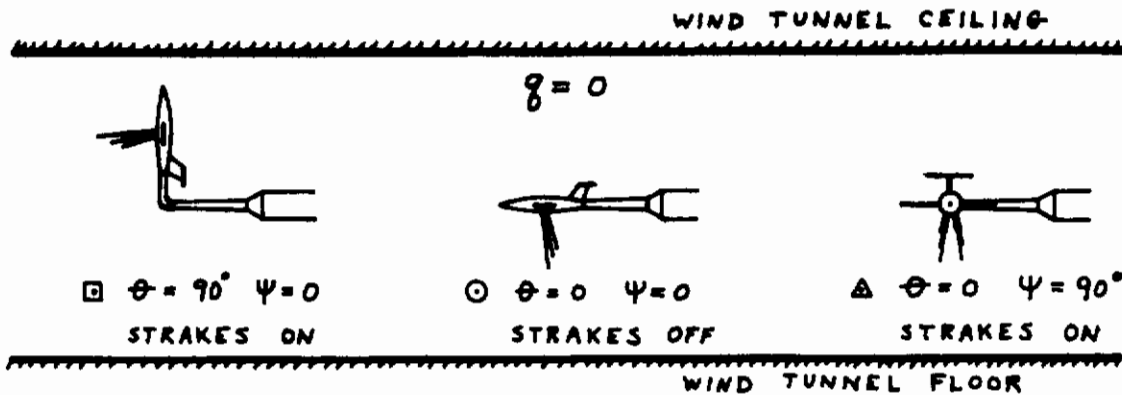
FIGURE 60. EFFECT OF MODEL ATTITUDE IN TUNNEL ON
HOVER DATA OUT OF GROUND EFFECT
(LANGLEY   TEST 221 ; $\gamma_V = 0$)

93

$q = 0$ $\gamma_v = 0$ $\theta = 0$

FIGURE 61. EFFECT OF HEIGHT ABOVE GROUND ON
LONGITUDINAL DATA (LANGLEY TEST 17B)

94
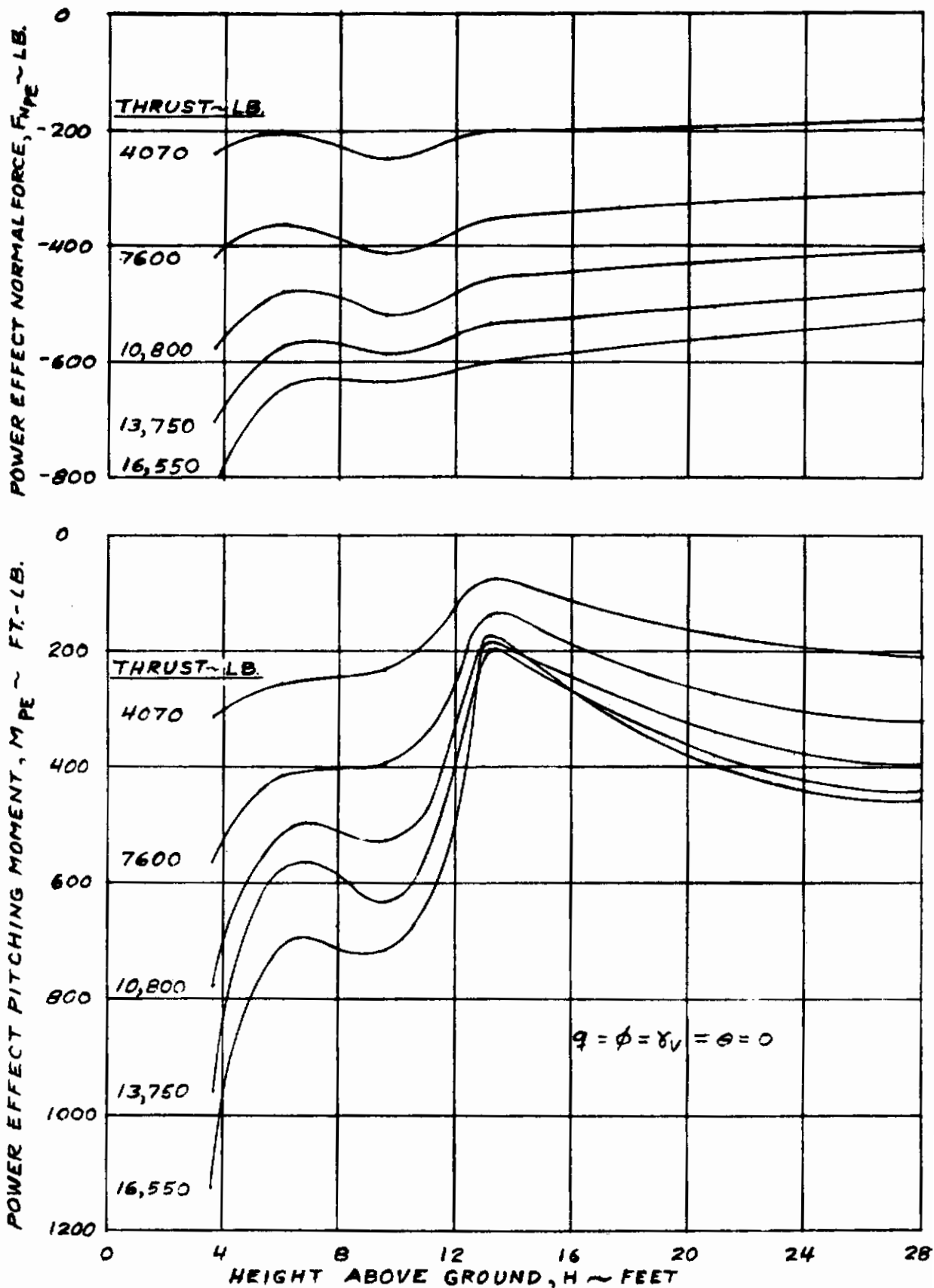
FIGURE 62. EFFECT OF HEIGHT ABOVE GROUND ON LONGITUDINAL HOVER DATA (LOCKHEED HOVER RIG)

95
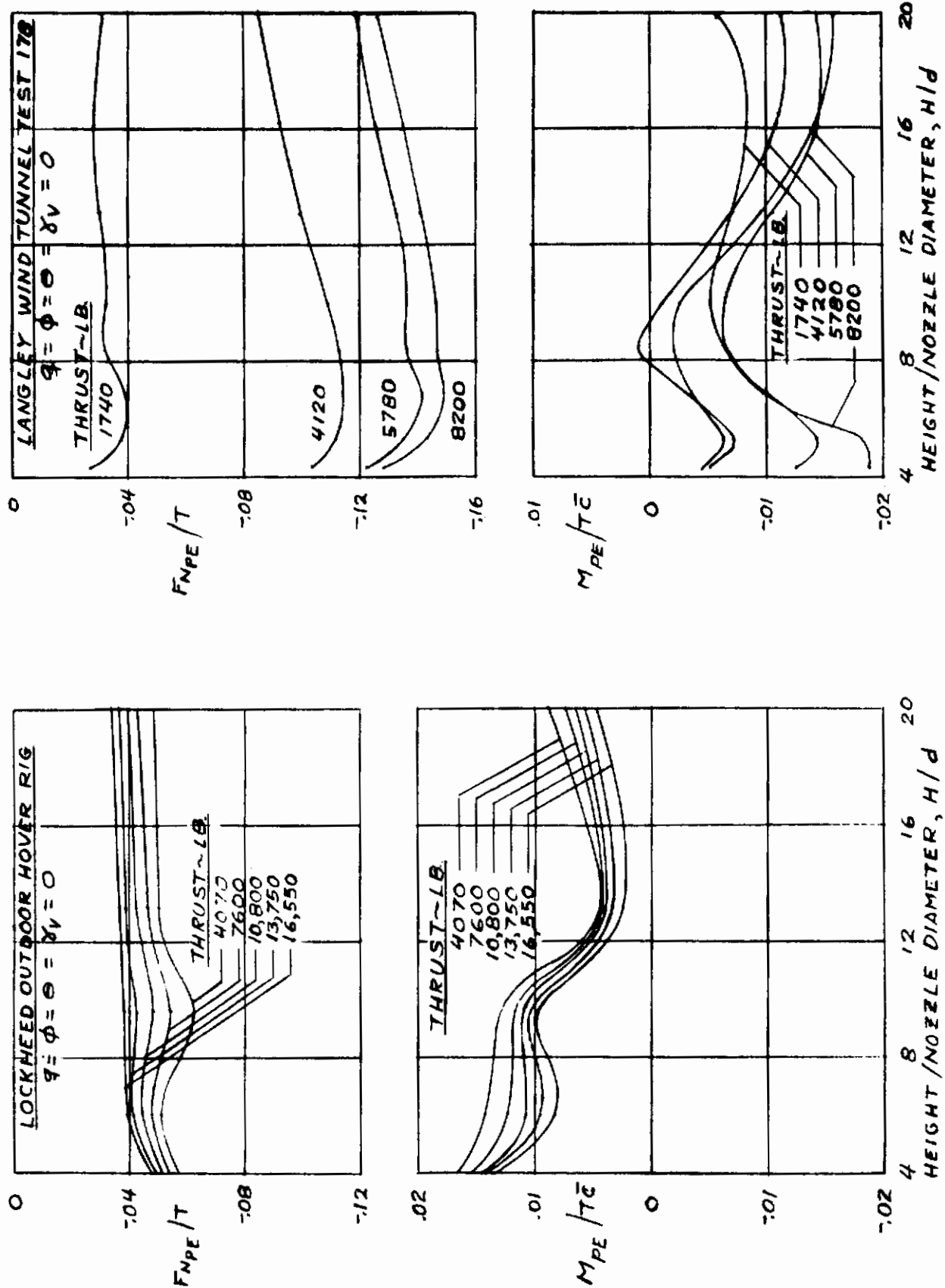
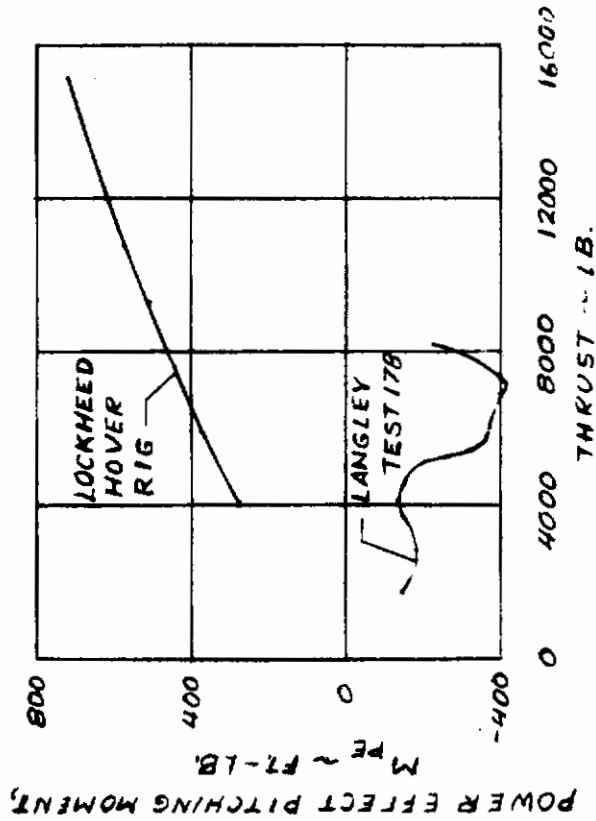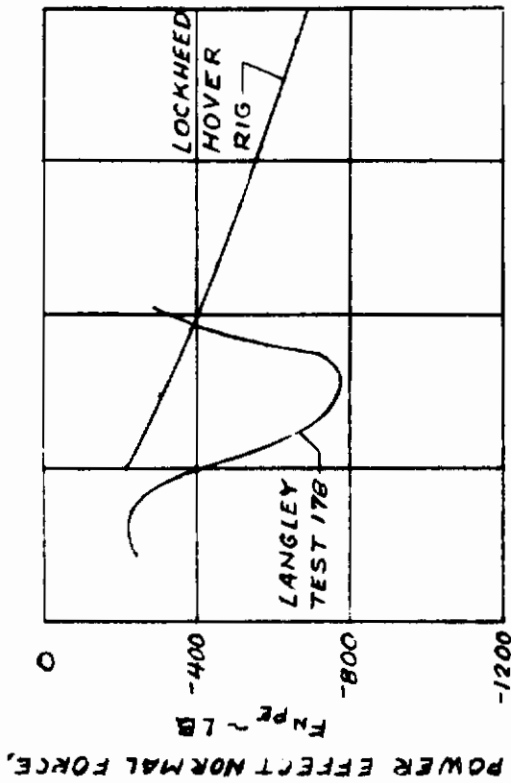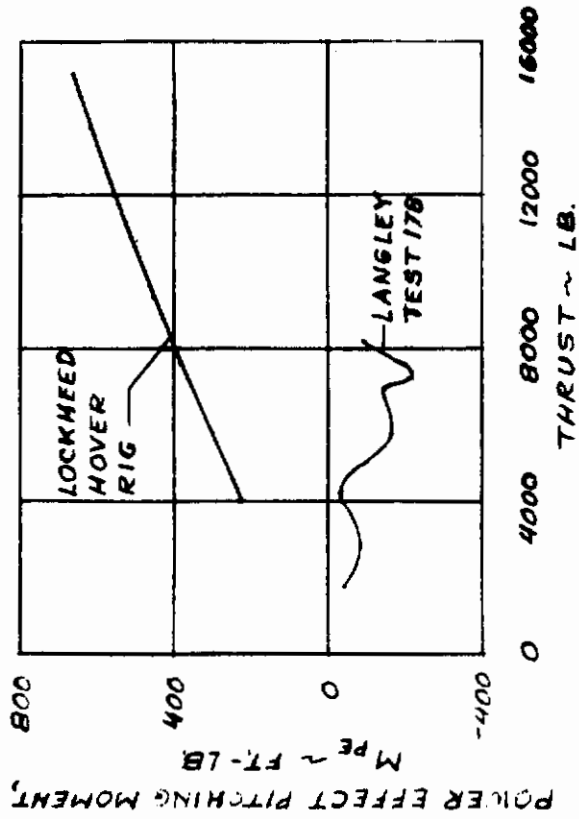FIGURE 63. EFFECT OF HEIGHT ABOVE GROUND ON NONDIMENSIONAL HOVER DATA (LOCKHEED HOVER RIG)

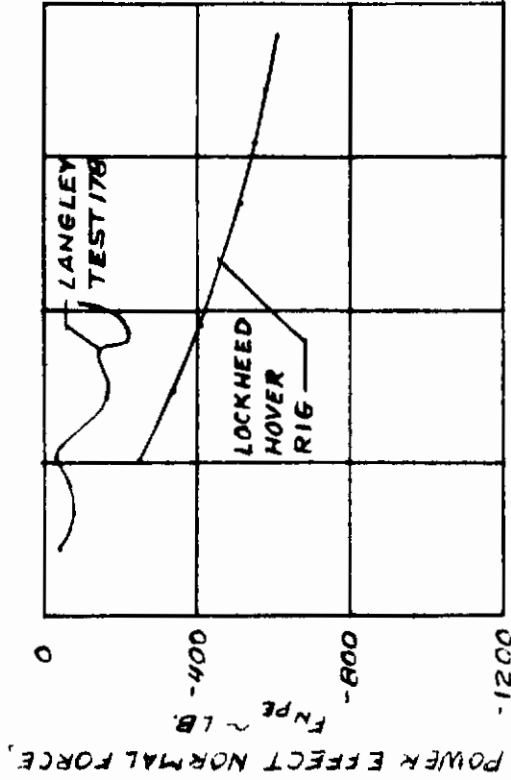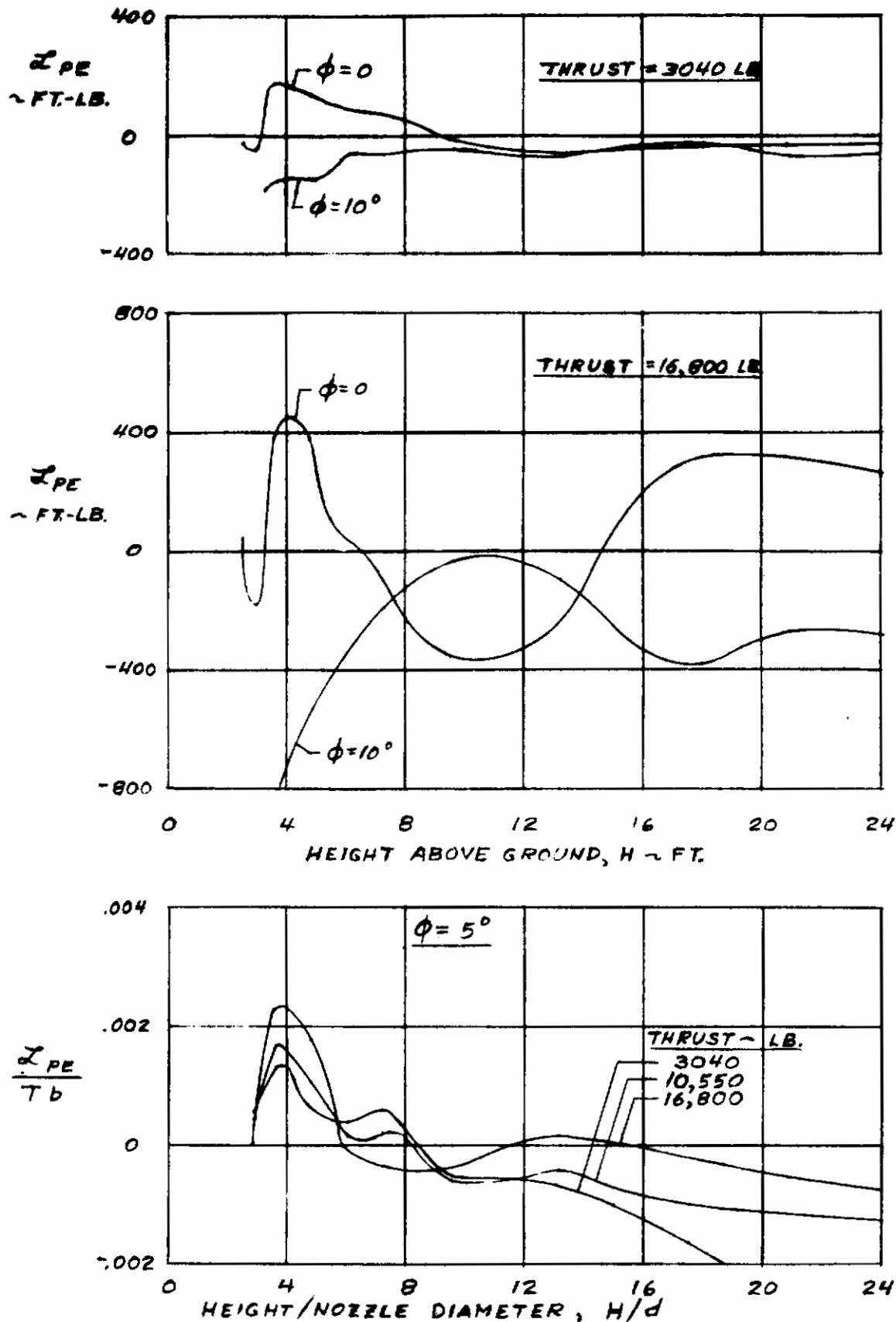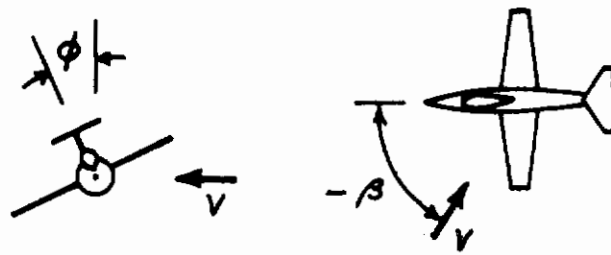FIGURE 64. EFFECT OF THRUST IN GROUND EFFECT ON POWER EFFECT NORMAL FORCE AND PITCHING MOMENT

97

FIGURE 65. EFFECT OF BANK ANGLE AND GROUND HEIGHT ON POWER EFFECT ROLLING MOMENT ($\theta = 8.9°$; $\gamma_V = 0$; LOCKHEED HOVER RIG)

98

$T = 0$
$\alpha = 0$

NORMAL
FORCE
COEFF.

C_N

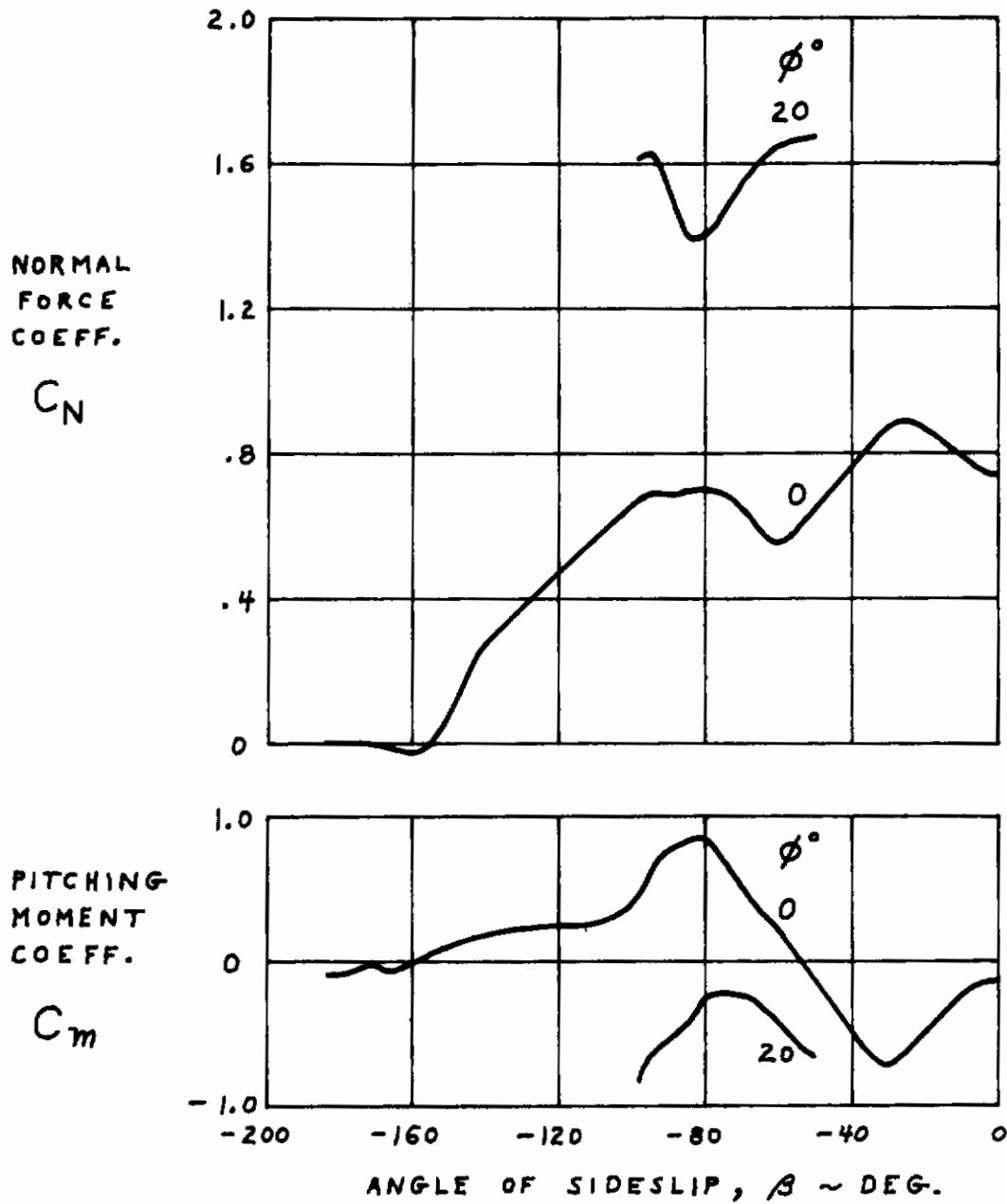PITCHING
MOMENT
COEFF.

C_m

ANGLE OF SIDESLIP, $\beta \sim$ DEG.

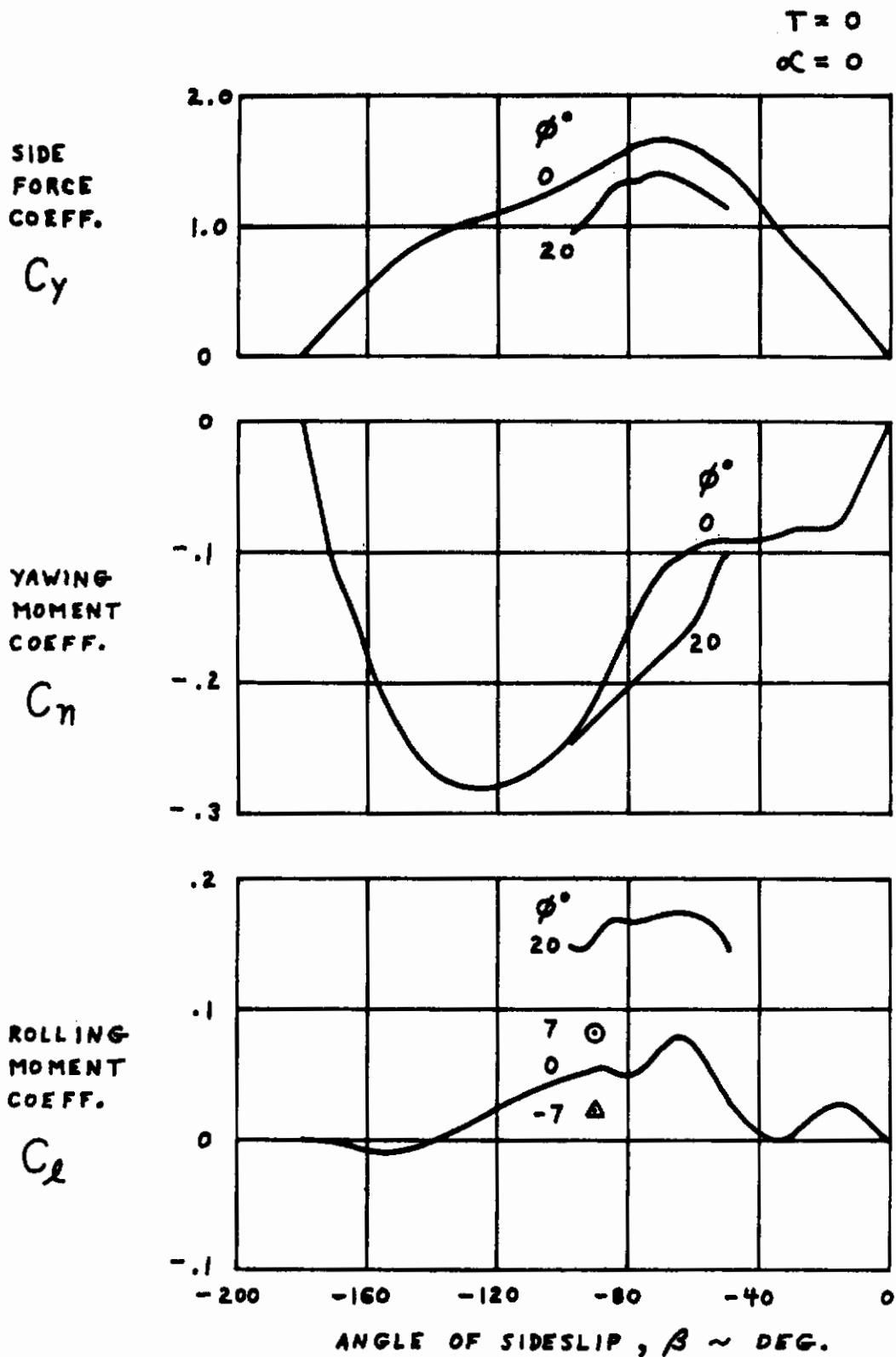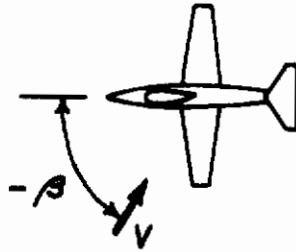FIGURE 66. EFFECT OF VERY LARGE ANGLE OF SIDESLIP ON
POWER-OFF LONGITUDINAL DATA

99

FIGURE 67. EFFECT OF VERY LARGE ANGLE OF SIDESLIP ON
POWER-OFF LATERAL-DIRECTIONAL DATA

100

$T = 7200 \text{ LB.}$

$g = 11.2 \text{ LB}/FT^2$

$\alpha = 0$

$\phi = 0$

$\gamma_v = 0$

NORMAL FORCE

F_N

LB.

$\left[F_{N_{POWER\ OFF}} + F_{N_T}\right]$

$F_{N_{POWER\ ON}}$

PITCHING MOMENT

M

FT-LB

$M_{POWER\ ON}$

$\left[M_{POWER\ OFF} + M_T\right]$

ANGLE OF SIDESLIP, $\beta \sim$ DEG.
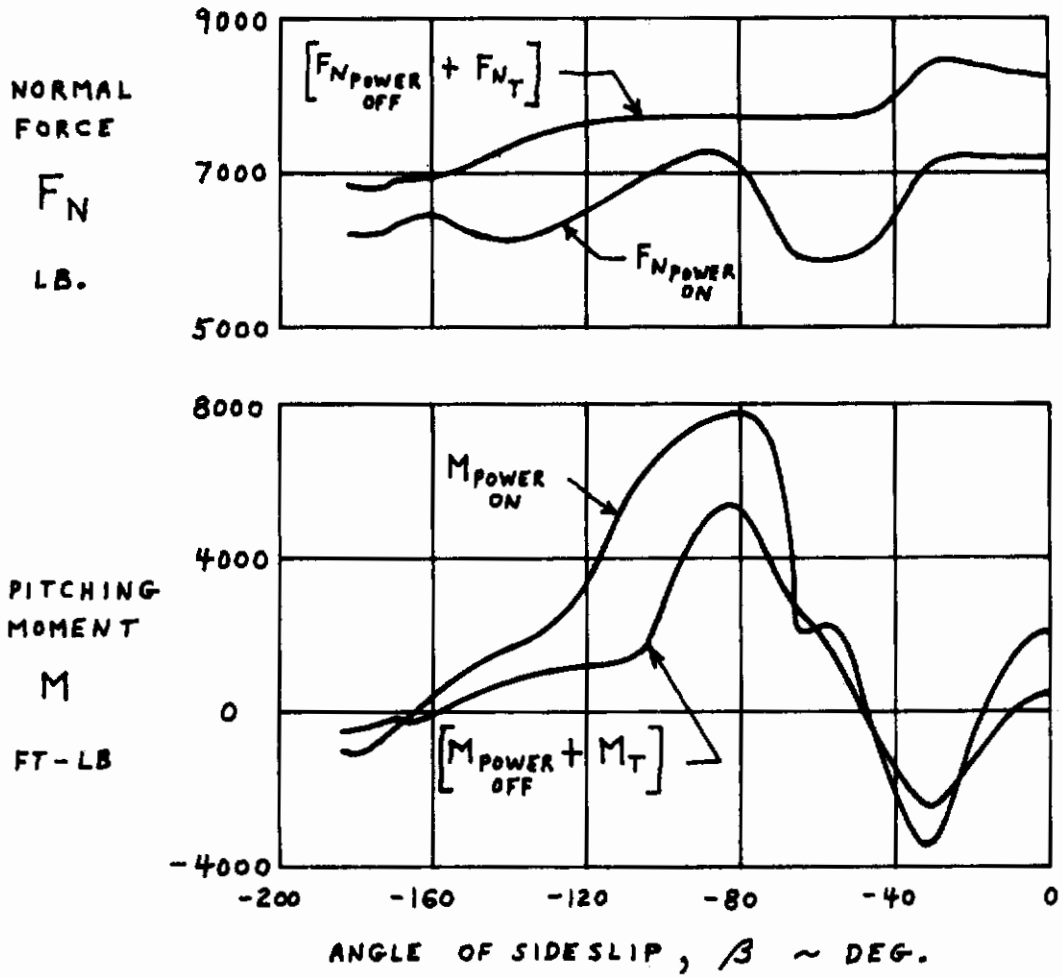
FIGURE 68. EFFECT OF VERY LARGE ANGLES OF SIDESLIP ON LONGITUDINAL POWER EFFECT DATA

101

SIDE FORCE

F_Y

LB.

$F_{Y_{POWER\ ON}}$

$\left[F_{Y_{POWER\ OFF}} + F_{Y_T}\right]$

YAWING MOMENT

N

FT - LB

$N_{POWER\ ON}$

$\left[N_{POWER\ OFF} + N_T\right]$

ROLLING MOMENT

$\mathcal{L}$

FT - LB

$T = 7200$ LB.
$q = 11.2$ LB/FT^2
$\alpha = 0$
$\phi = 0$
$\gamma_V = 0$

$\mathcal{L}_{POWER\ ON}$

$\left[\mathcal{L}_{POWER\ OFF} + \mathcal{L}_T\right]$

ANGLE OF SIDESLIP, $\beta \sim$ DEG.
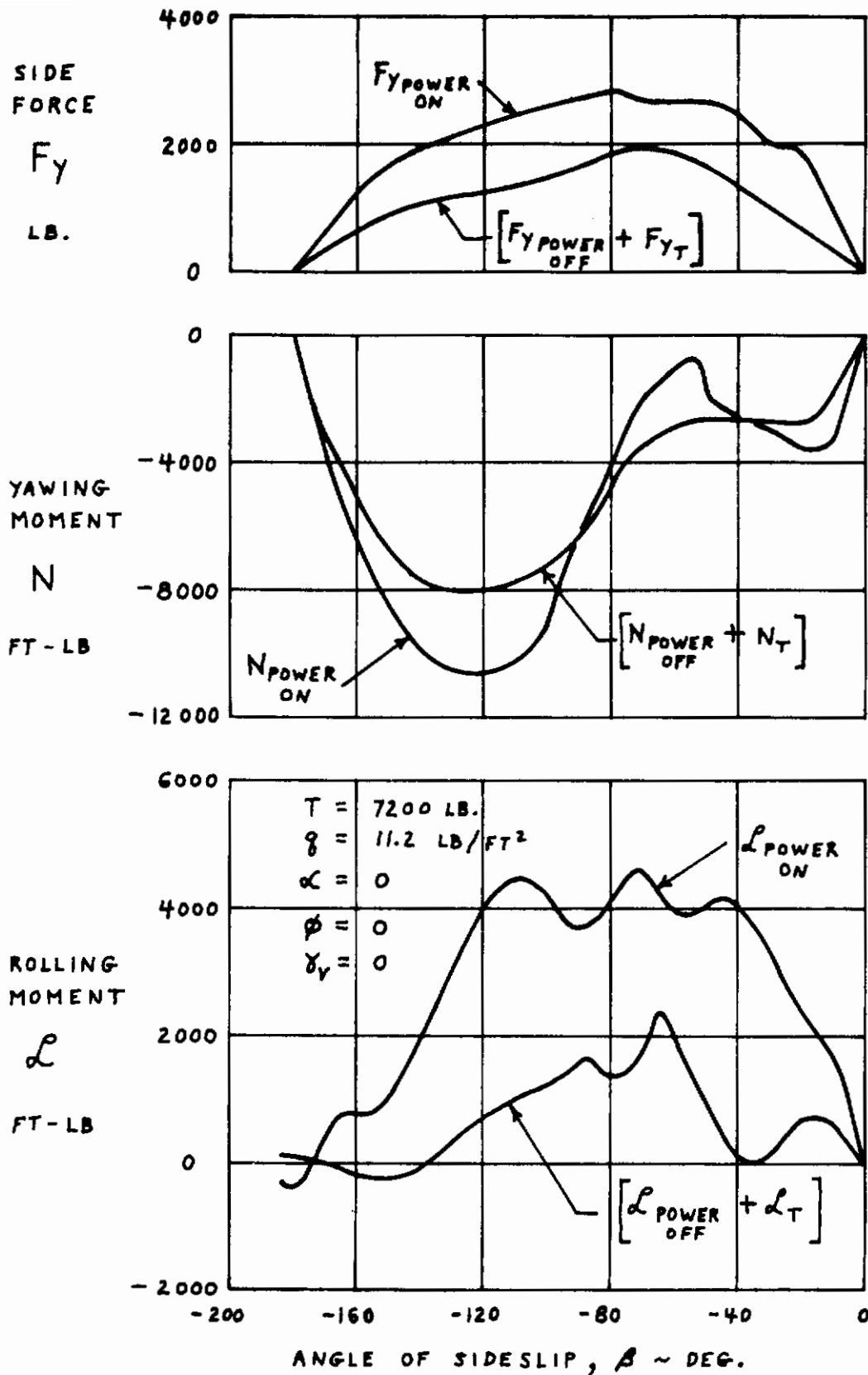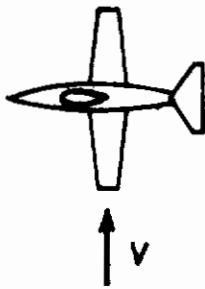
FIGURE 69. EFFECTS OF VERY LARGE ANGLES OF SIDESLIP ON LATERAL - DIRECTIONAL POWER EFFECT DATA

$\beta = -90°$

$T = 7200$ LB.

$\phi = 0$

$\alpha = 0$

V

POWER ON DATA

$\left[\begin{array}{c} \text{POWER} \\ \text{OFF} \end{array} + \begin{array}{c} \text{THRUST} \\ \text{EFFECT} \end{array} \right]$
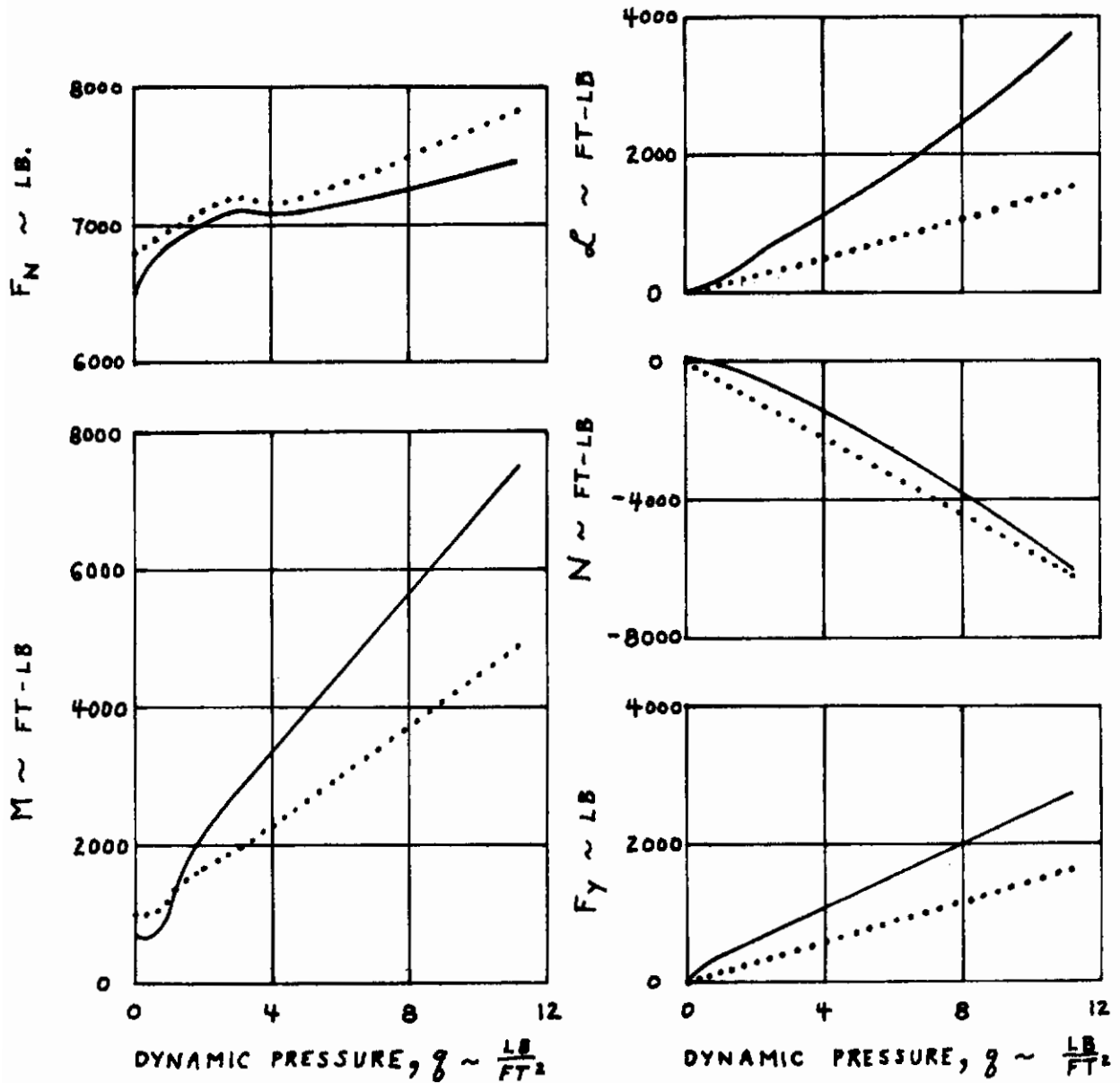
FIGURE 70. EFFECT OF DYNAMIC PRESSURE AT
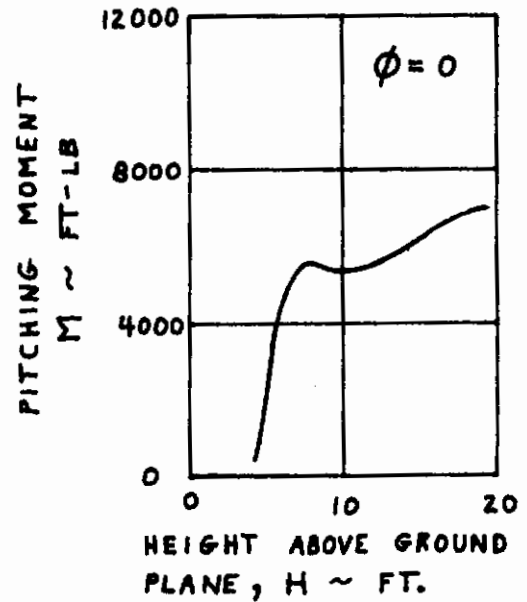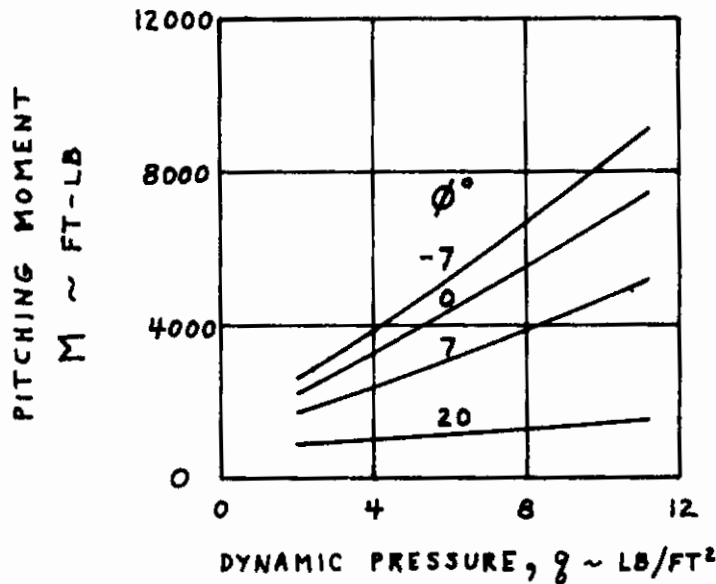90 DEGREES ANGLE OF SIDESLIP

103
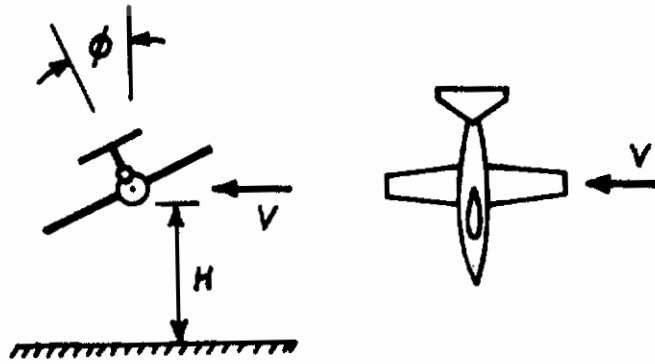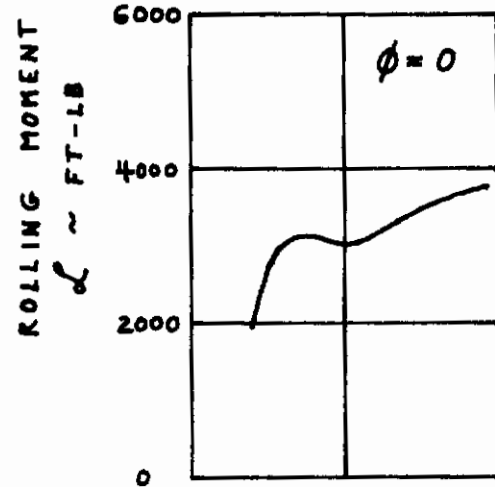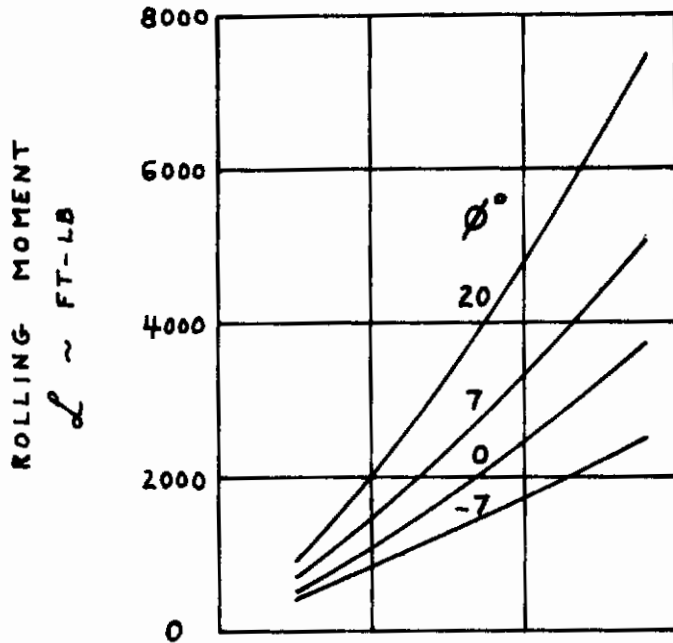
FIGURE 71. EFFECT OF BANK ANGLE AND GROUND HEIGHT ON
PITCHING MOMENT DURING SIDE MOVEMENT

104

LOCKHEED DATA (ref. 13)
SEA LEVEL, STD. DAY

NOTE: MAXIMUM PITCHING MOMENT
VALUES ARE THE SAME AS
THOSE SHOWN FOR THE
YAW NOZZLES.

FIGURE 72. HOVER REACTION CONTROL POWER

MAXIMUM YAWING MOMENT FOR AFT FUSELAGE
REACTION NOZZLES, $(N_{Rc})_{MAX} \sim$ FT-LB

THRUST, T $\sim$ LB.

MAXIMUM ROLLING MOMENT FOR WING TIP
REACTION NOZZLES, $(\mathcal{L}_{Rc})_{MAX} \sim$ FT-LB

THRUST, T $\sim$ LB.

105
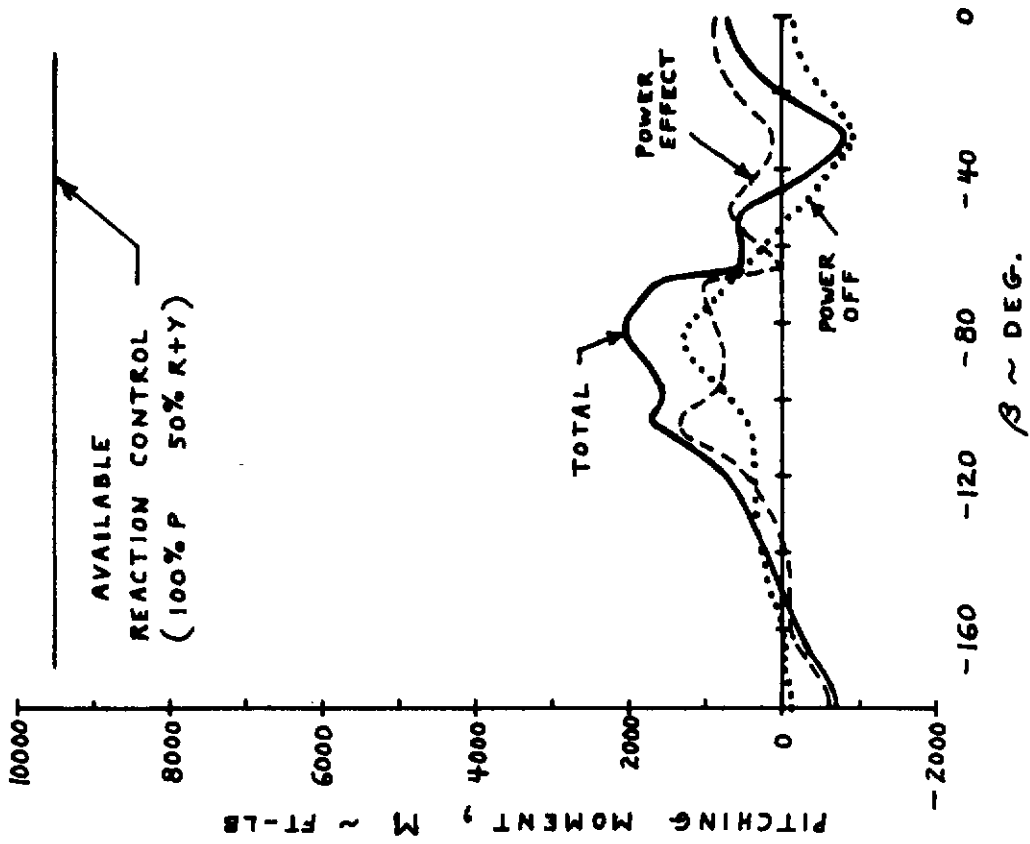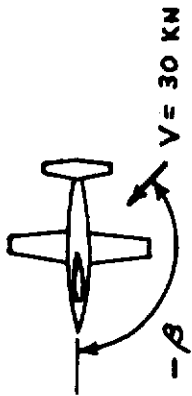
FIGURE 73. EFFECT OF LARGE β VALUES ON TOTAL ROLLING AND PITCHING MOMENT
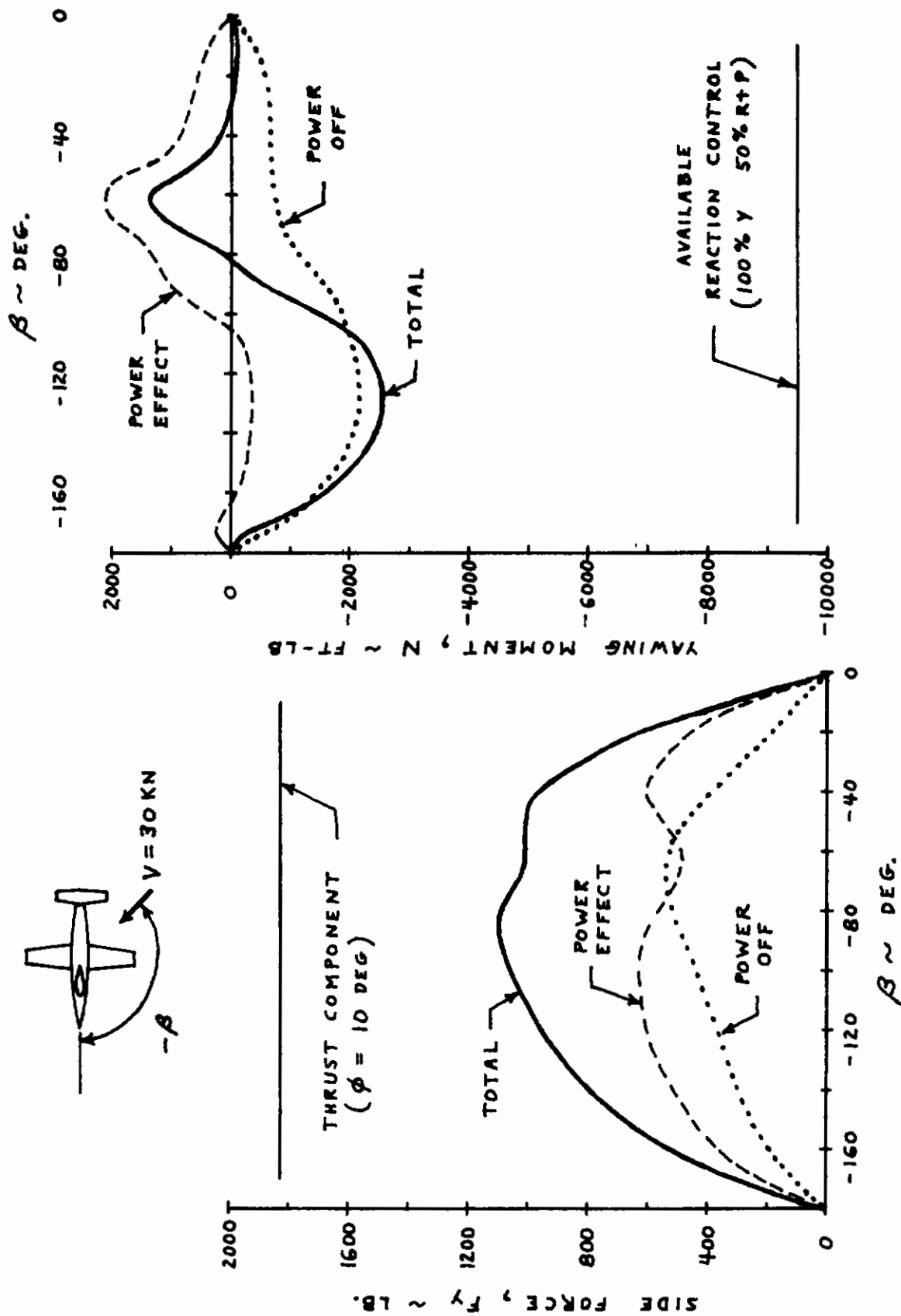
FIGURE 74. EFFECT OF LARGE β VALUES ON TOTAL SIDE FORCE AND YAWING MOMENT

UNTRIMMED , TAIL-ON
GEAR UP, FLAPS DOWN 40°
STRAKES ON
C.G @ .10 $\bar{c}_w$

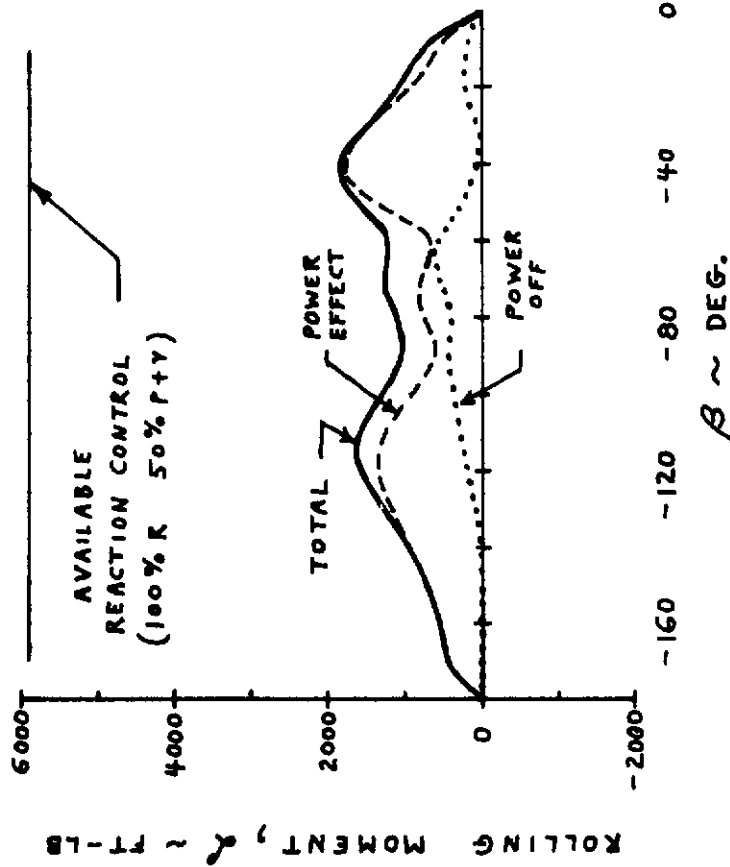| MACH NUMBER	0.20	0.30	0.40
$C_{L\alpha}$	0.1035	0.1051	0.1074
$\alpha_{ZERO\ LIFT}$	−6.38	−6.39	−6.39
$C_{L\ @\ \alpha=0°}$	0.660	0.672	0.686
dC_M/dC_L	−0.1585	−0.1522	−0.1546
C_{M_0}	−0.0444	−0.0508	−0.0569
$C_{M\alpha}$	−0.0164	−0.0160	−0.0166
$C_{M\ @\ \alpha=0°}$	−0.149	−0.153	−0.163
$C_{L\delta_e}$	.0062	.0062	.0062
$C_{m\delta_e}$	−.0223	−.0223	−.0223
$C_{m\delta_F}$	−.0050	−.0050	−.0050
C_{m_q} /P.D.	−20.9	−21.1	−21.6
$C_{Y\beta}$	−.0231	−.0234	−.0237
$C_{n\beta}$	.00355	.00360	.00365
$C_{\ell\beta}$	−.00165	−.00167	−.00170
$C_{Y\delta_r}$ (β=0°)	.00475	.00480	.00485
$C_{n\delta_r}$ (β=0°)	−.00278	−.00281	−.00285
$C_{\ell\delta_a}$	.00097	.00097	.00097
$C_{\ell p}$ /RAD.	−.389	−.391	−.3945

FIGURE 75. XV-4B POWER-OFF AERODYNAMIC DERIVATIVES
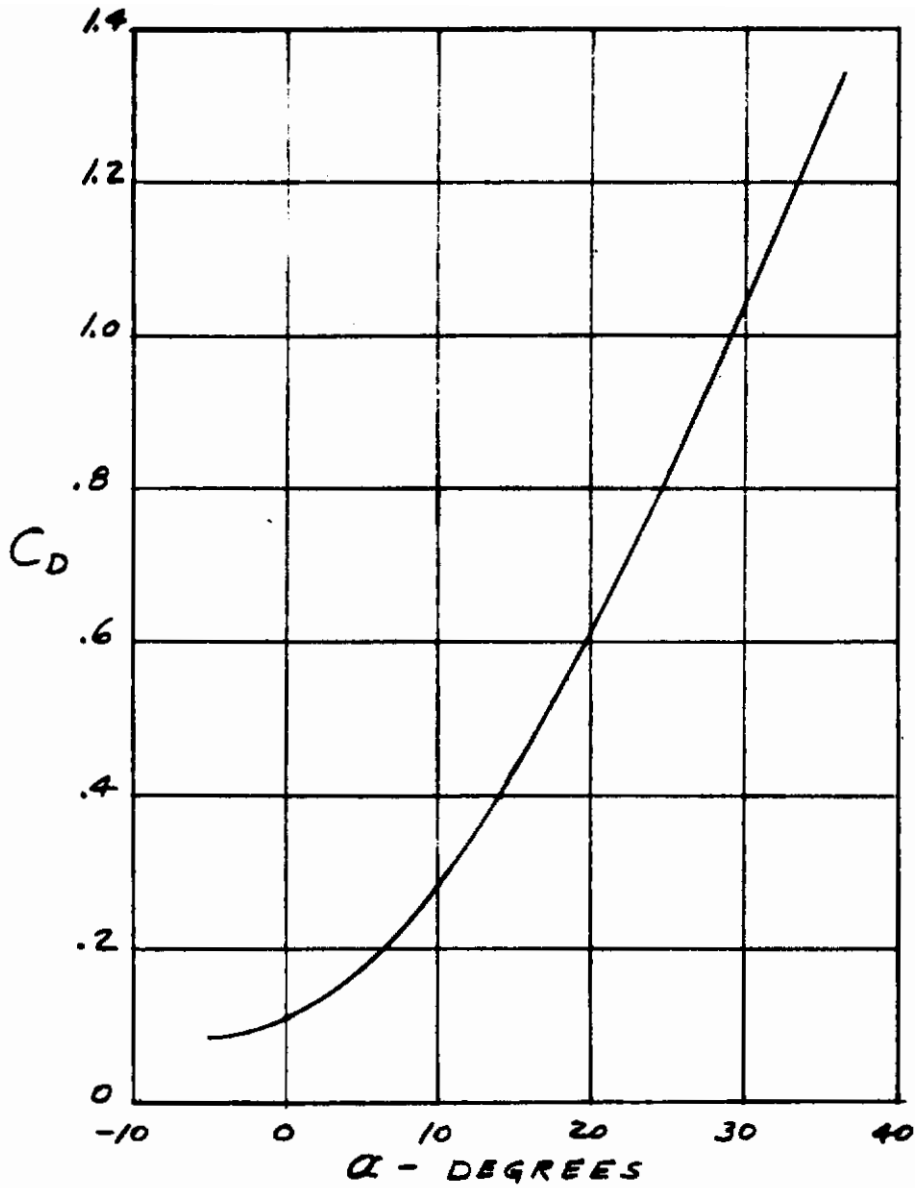
FIGURE 76. XV-4B POWER-OFF DRAG COEFFICIENT VERSUS
ANGLE OF ATTACK (FLAPS DOWN 40°; M=.2 TO.4)

109

η_{TAIL}

α - DEG.
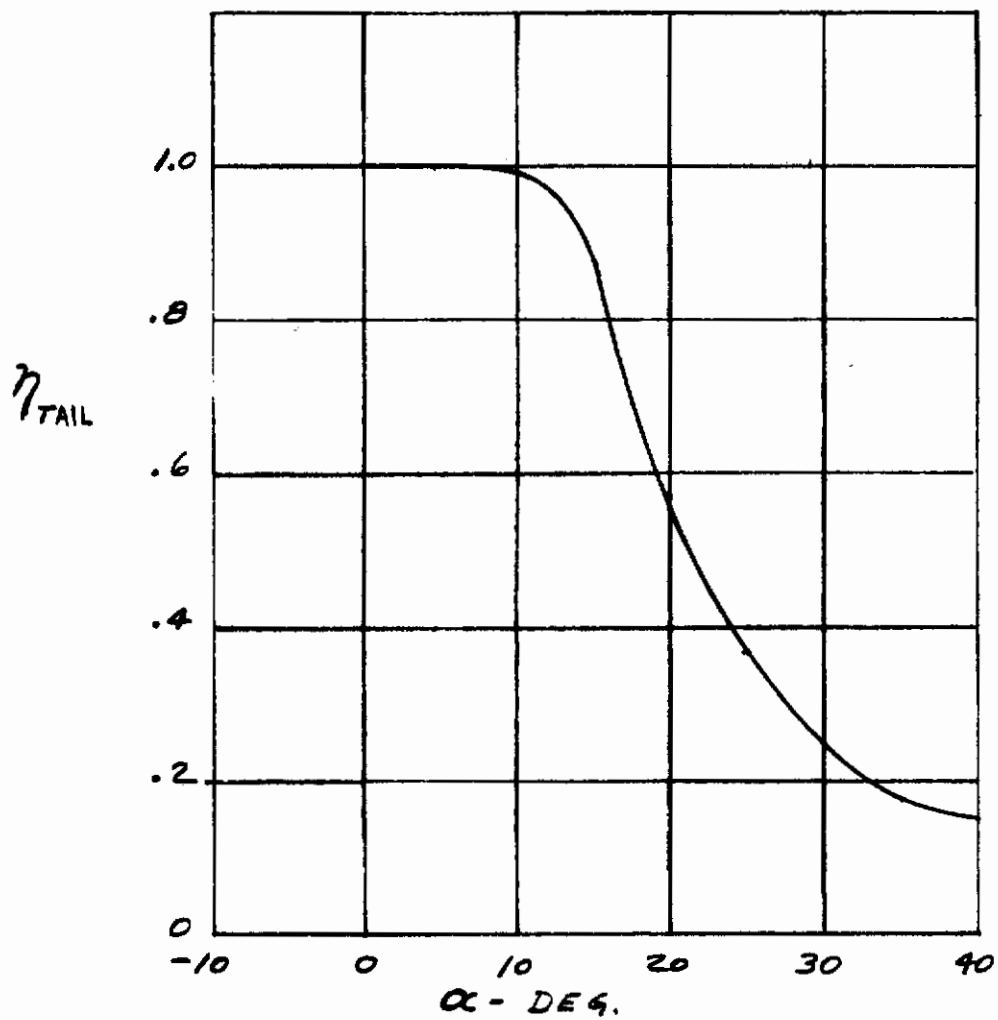
FURE 77. TAIL EFFICIENCY VERSUS ANGLE OF ATTACK
(FLAPS DOWN 40° ; LOW SPEED)

110
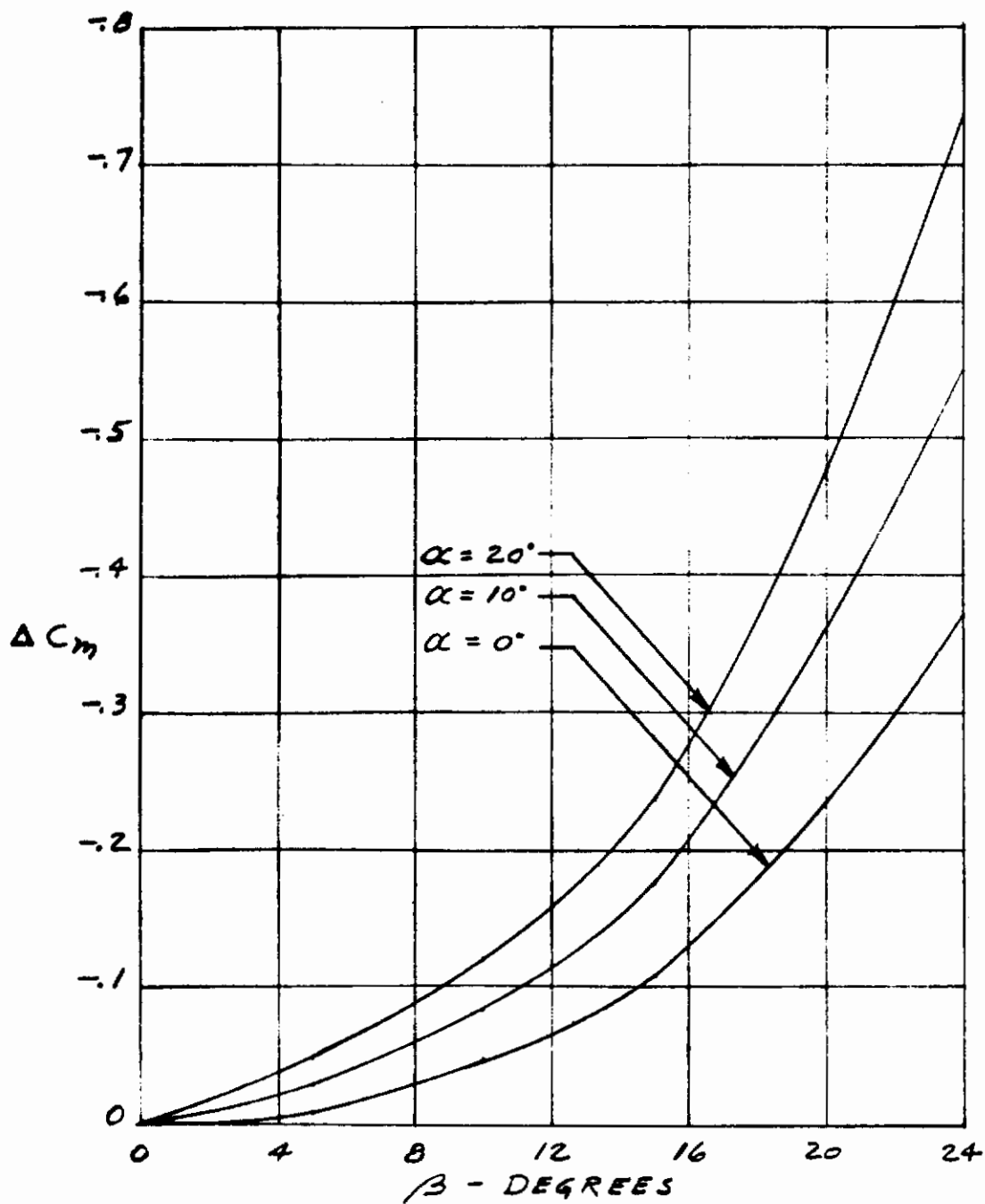
FIGURE 78. INCREMENTAL PITCHING MOMENT DUE TO SIDESLIP
(POWER - OFF ; FLAPS DOWN 40° ; M = .2 TO .4)

111
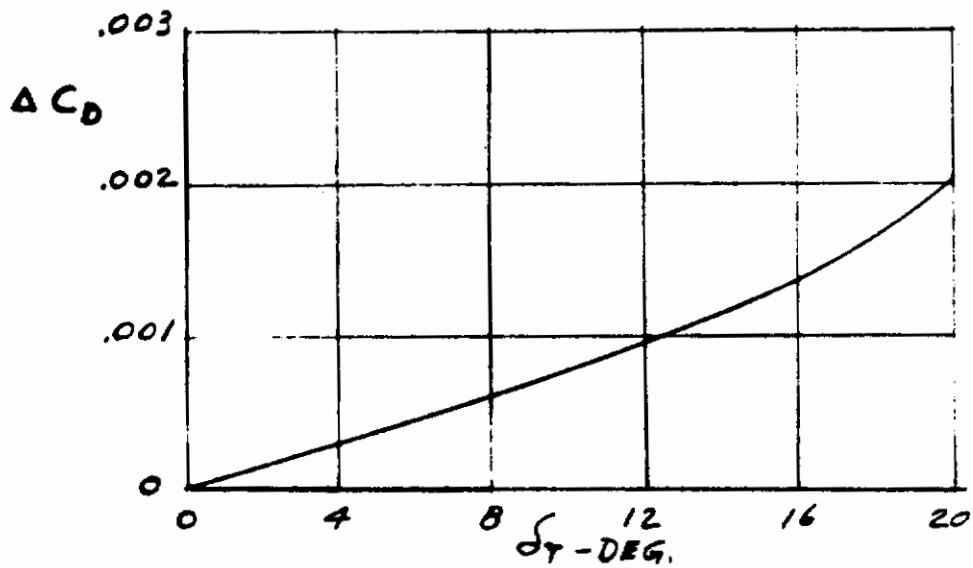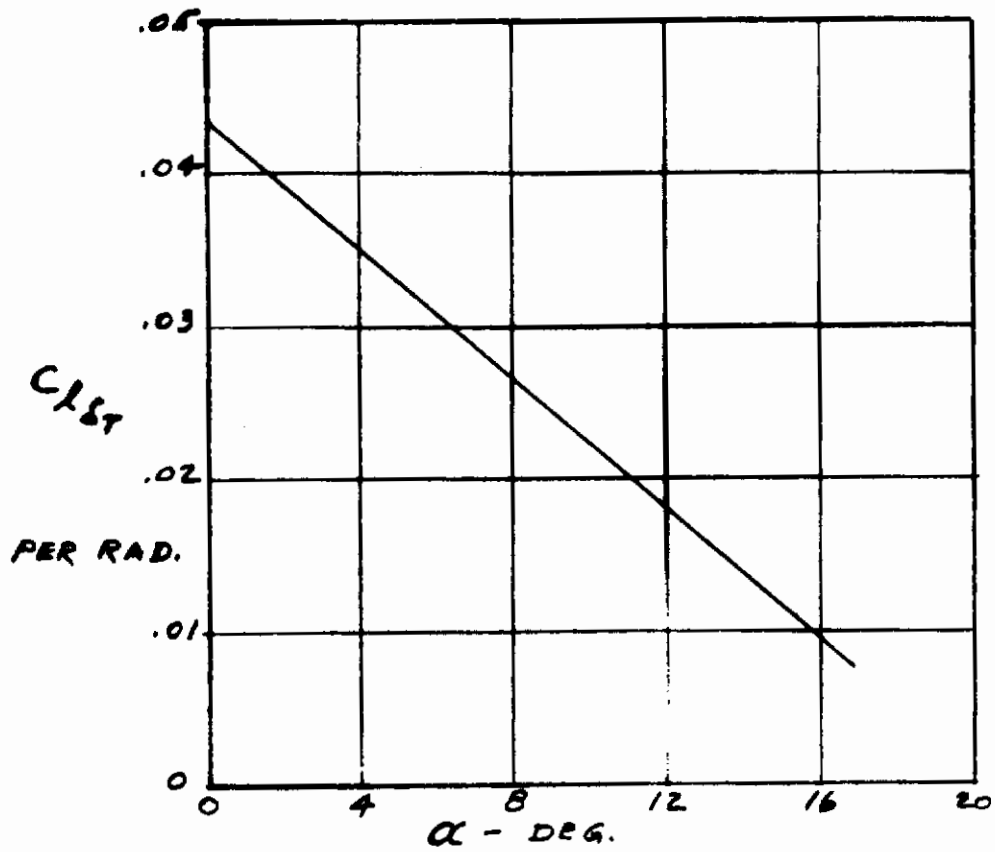
FIGURE 79. ROLLING MOMENT AND DRAG DUE TO RUDDER DEFLECTION (POWER-OFF)

112

NOTE: ΔC_Y, ΔC_m, ΔC_ℓ CURVES ARE SYMMETRICAL WITH RESPECT TO THE ORIGIN
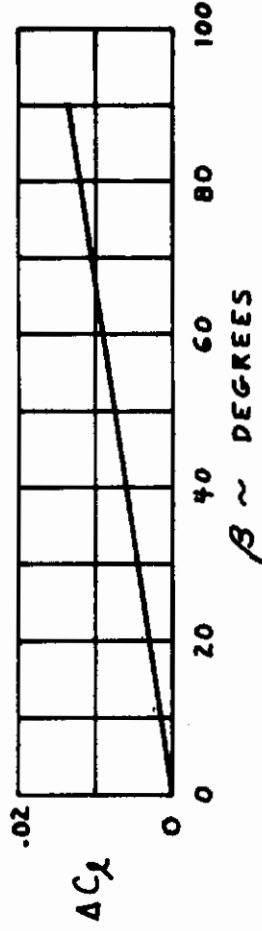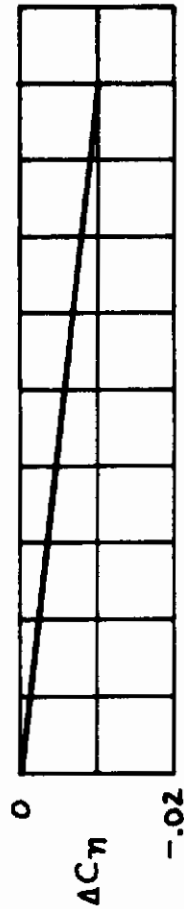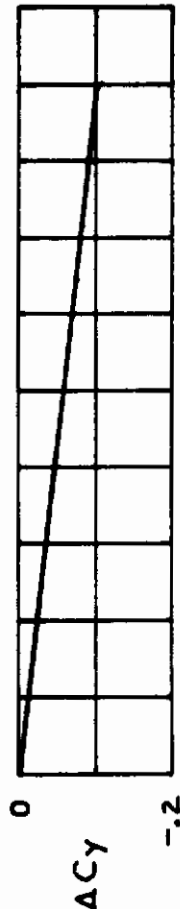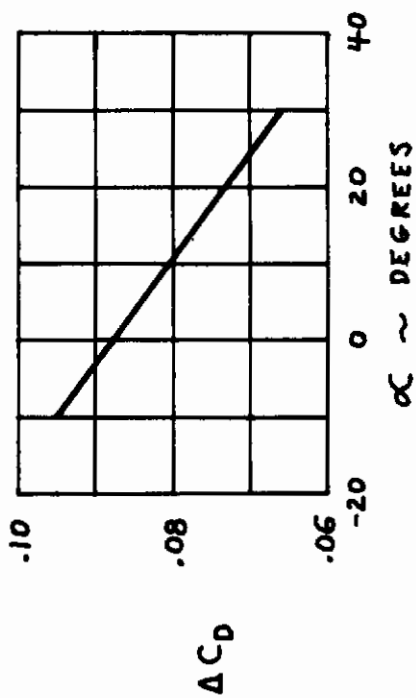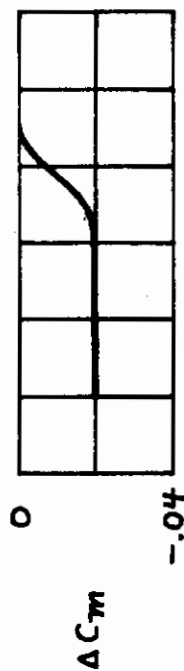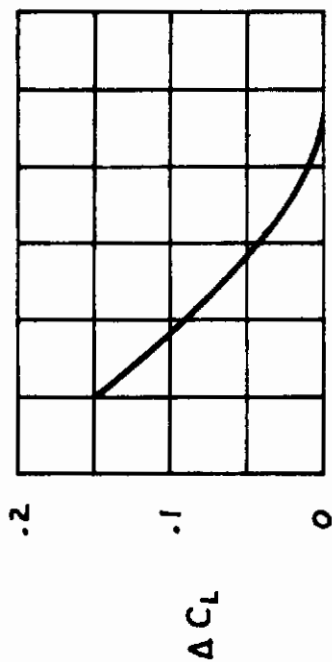
FIGURE 80. AERODYNAMIC INCREMENTS DUE TO GEAR

113
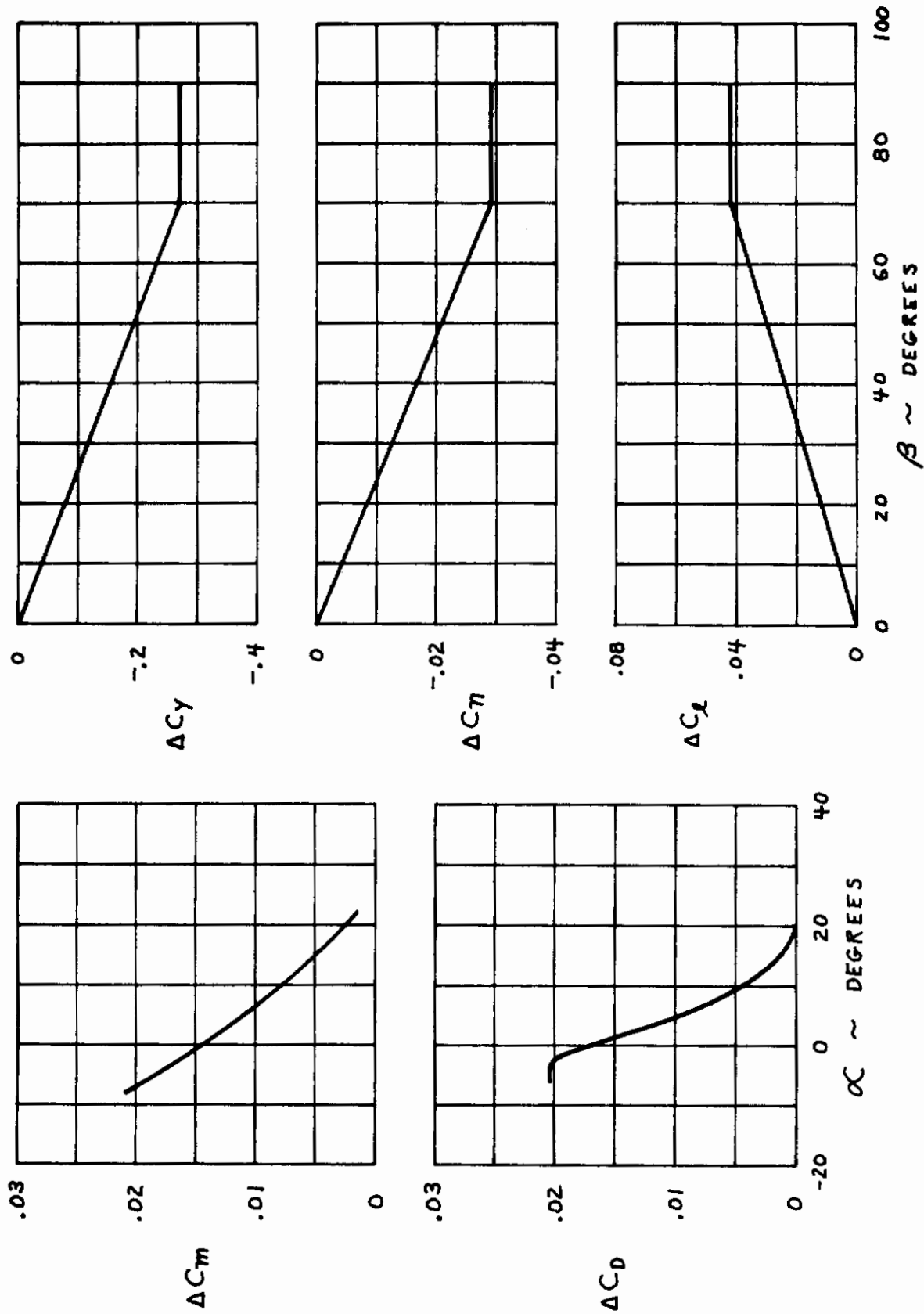
FIGURE 81. AERODYNAMIC INCREMENTS DUE TO LIFT ENGINE EXIT DOORS
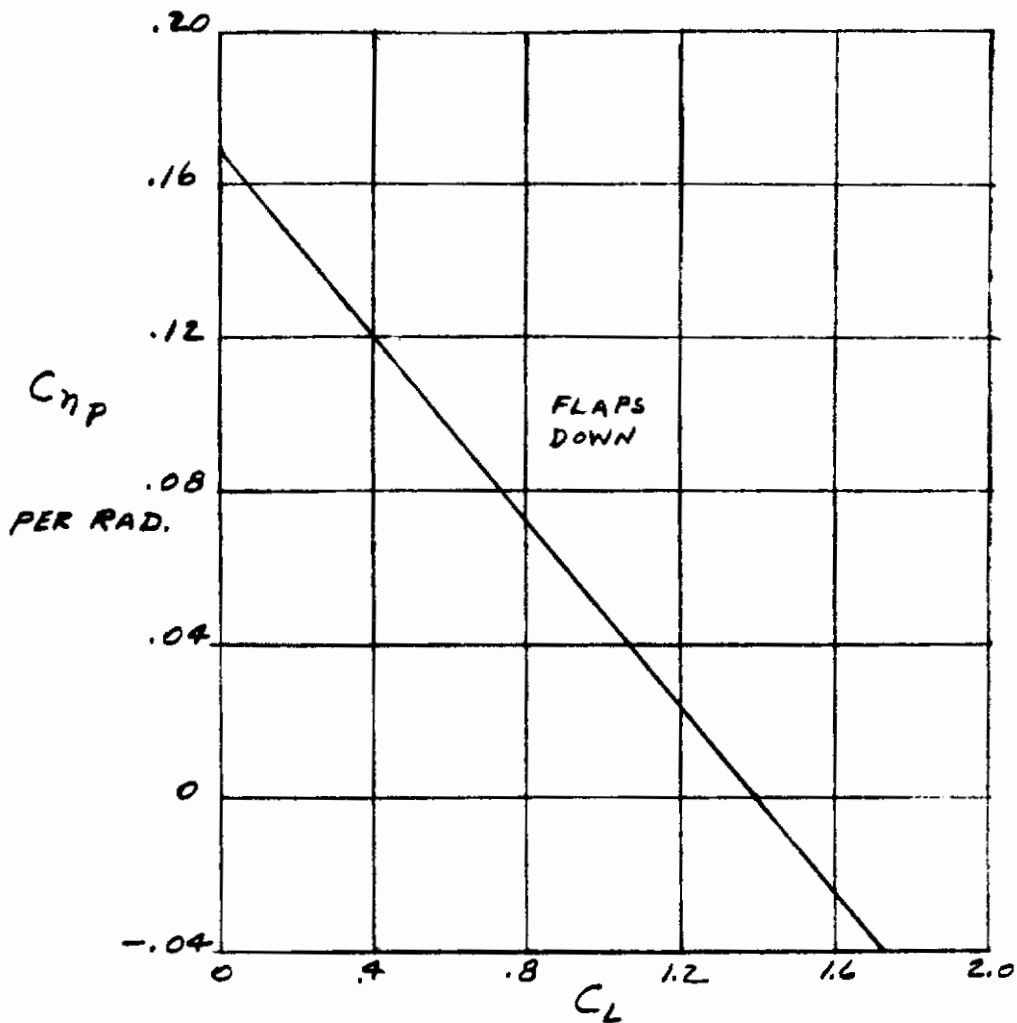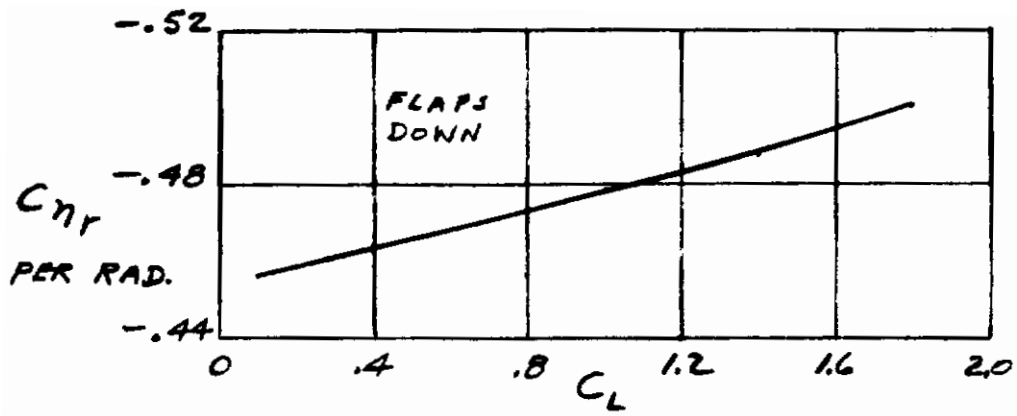
FIGURE 82. DAMPING IN YAW PARAMETER AND YAW DUE TO ROLL RATE PARAMETER (POWER-OFF)

$$\frac{Fc_{PE}}{T}$$

$$\frac{F_{N_{PE}}}{T}$$

$$\frac{M_{PE}}{T}$$

XV-4B SPEED-POWER PARAMETER , $\sqrt{\frac{1}{C_T}}$
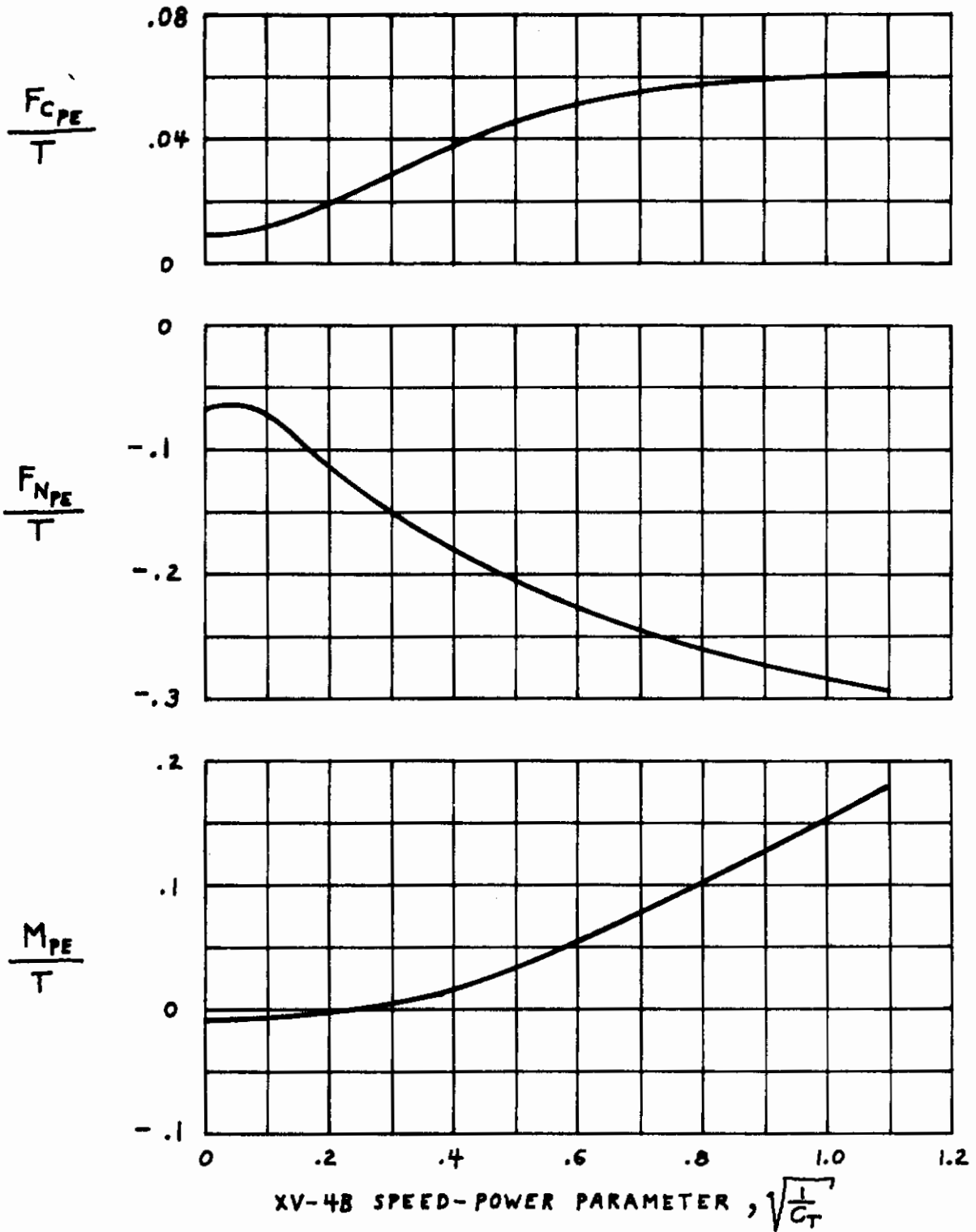
FIGURE 83. ESTIMATED LONGITUDINAL POWER EFFECTS
($\alpha = 0$; STRAKES OFF ; INLET EFFECTS REMOVED)

116

$$\frac{Fy_{PE}}{\beta T}$$
PER DEG.

$$\frac{N_{PE}}{\beta T b}$$
PER DEG.

$$\frac{\mathcal{L}_{PE}}{\beta T b}$$
PER DEG.

XV-4B SPEED-POWER PARAMETER, $\sqrt{\frac{1}{C_T}}$
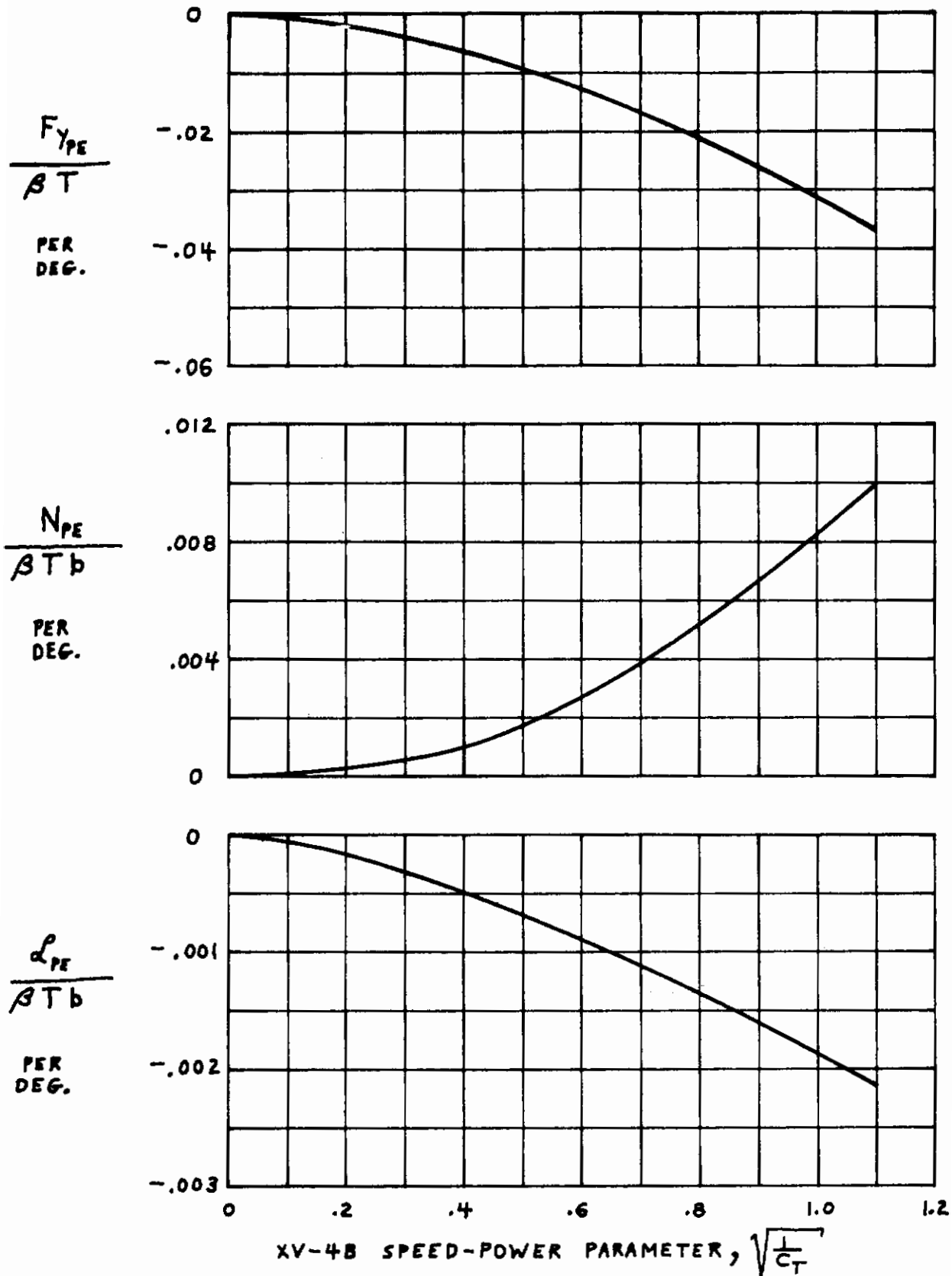
FIGURE 84. ESTIMATED LATERAL - DIRECTIONAL POWER EFFECTS
($\propto = 0$; STRAKES OFF ; INLET EFFECTS REMOVED)

117
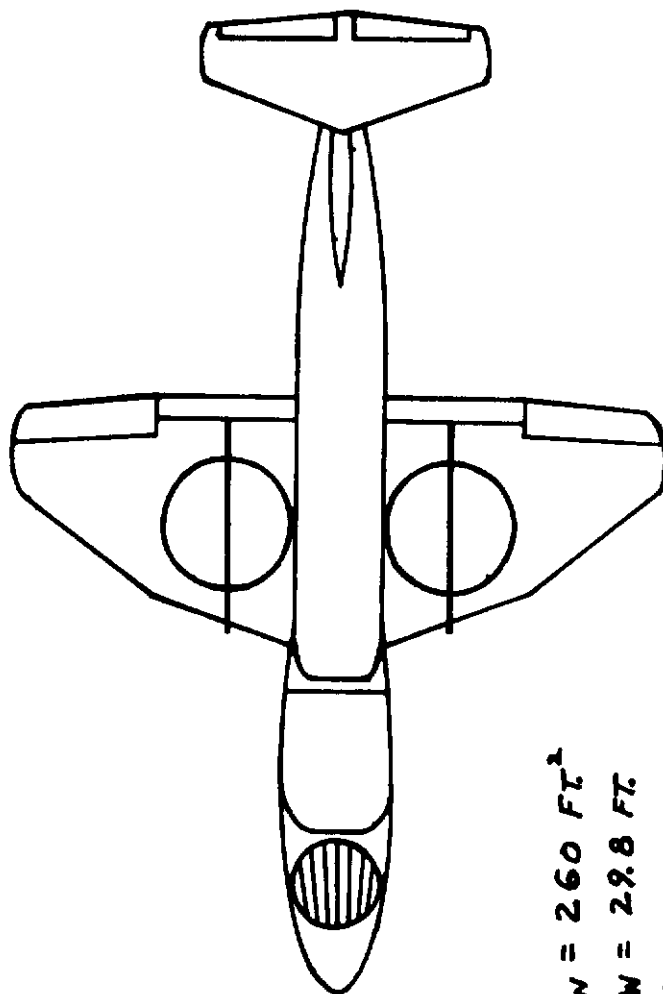
$$S_W = 260 \ FT^2$$
$$b_W = 29.8 \ FT.$$
$$\bar{c}_W = 11.3 \ FT$$
$$A_F = 42.6 \ FT^2$$
$$D_F = 5.2 \ FT.$$
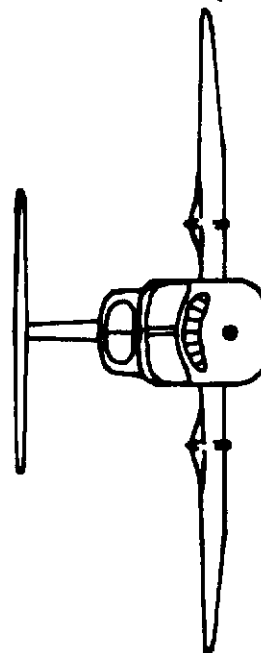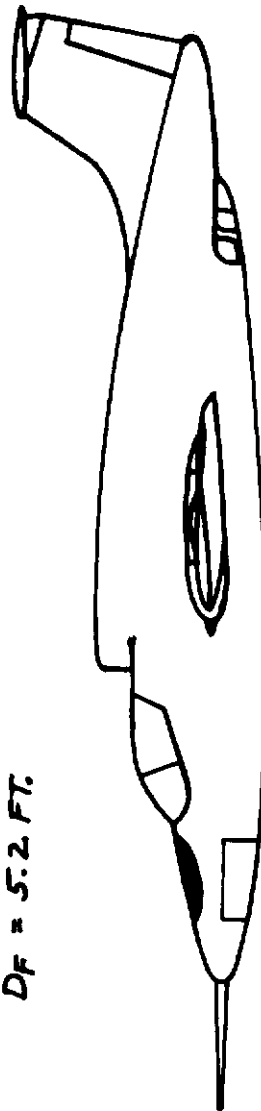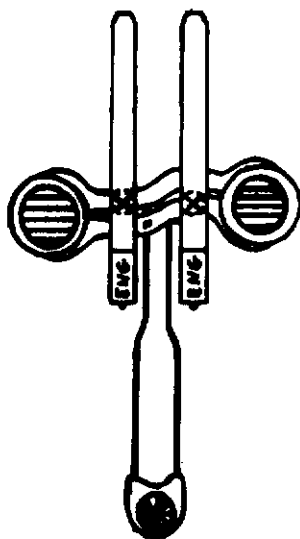
FIGURE 85. GENERAL ARRANGEMENT OF XV-5A AIRPLANE

118
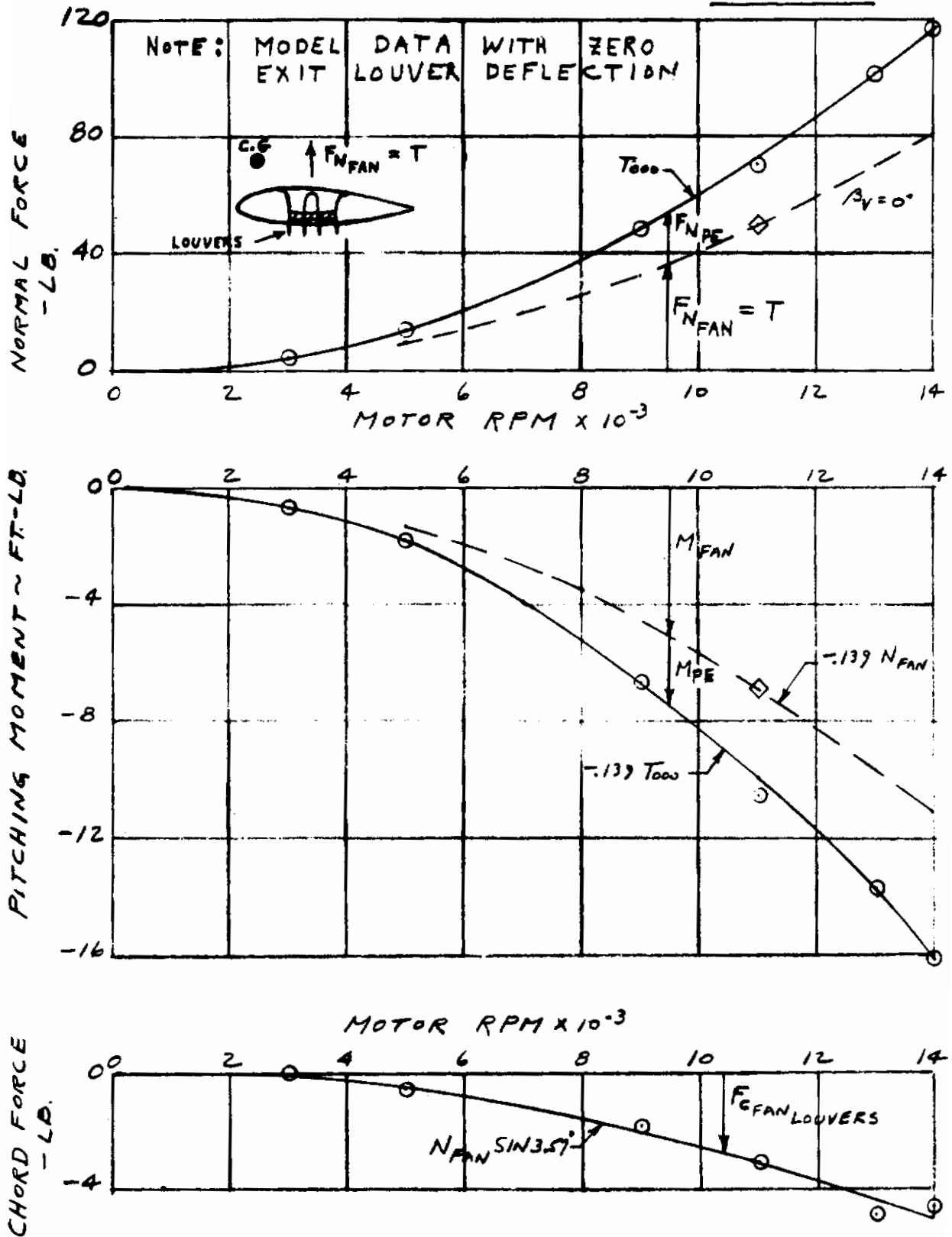
FIGURE 86. WING FAN STATIC NORMAL FORCE, CHORD FORCE AND
PITCHING MOMENT ($\alpha = 0$; $V = 0$; ALT. = S.L.)

FAN THRUST ~ LBS
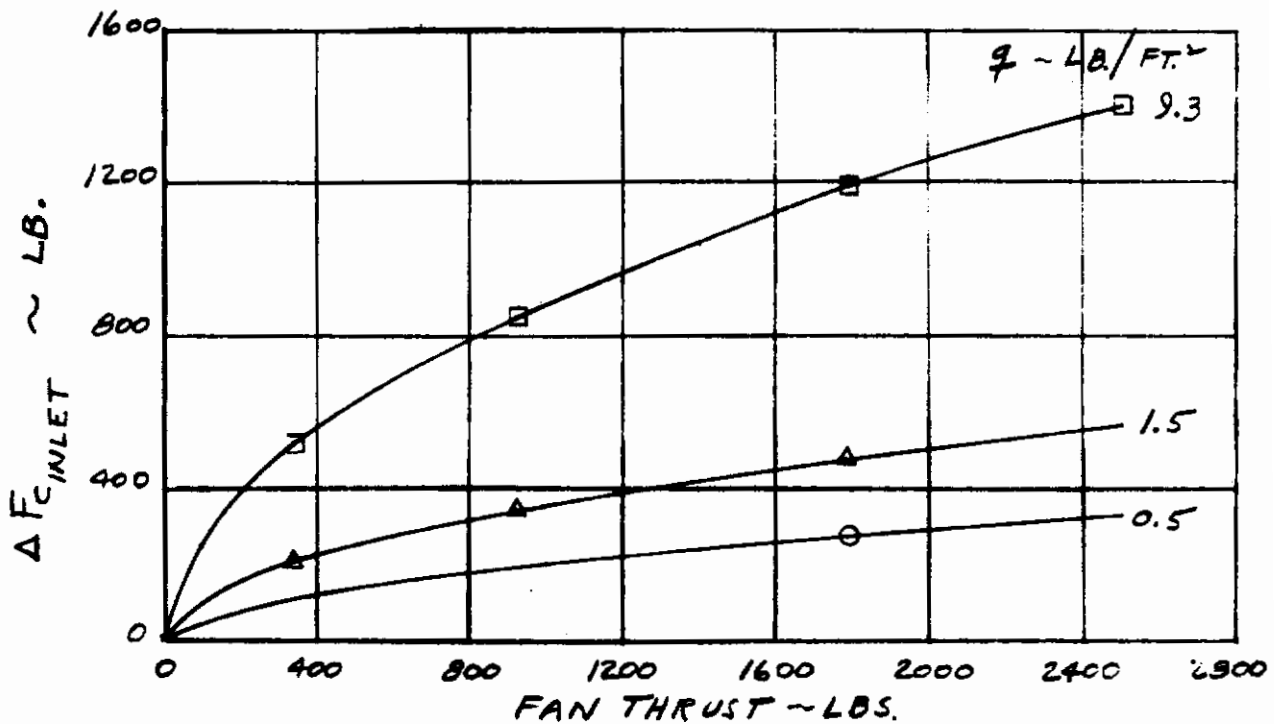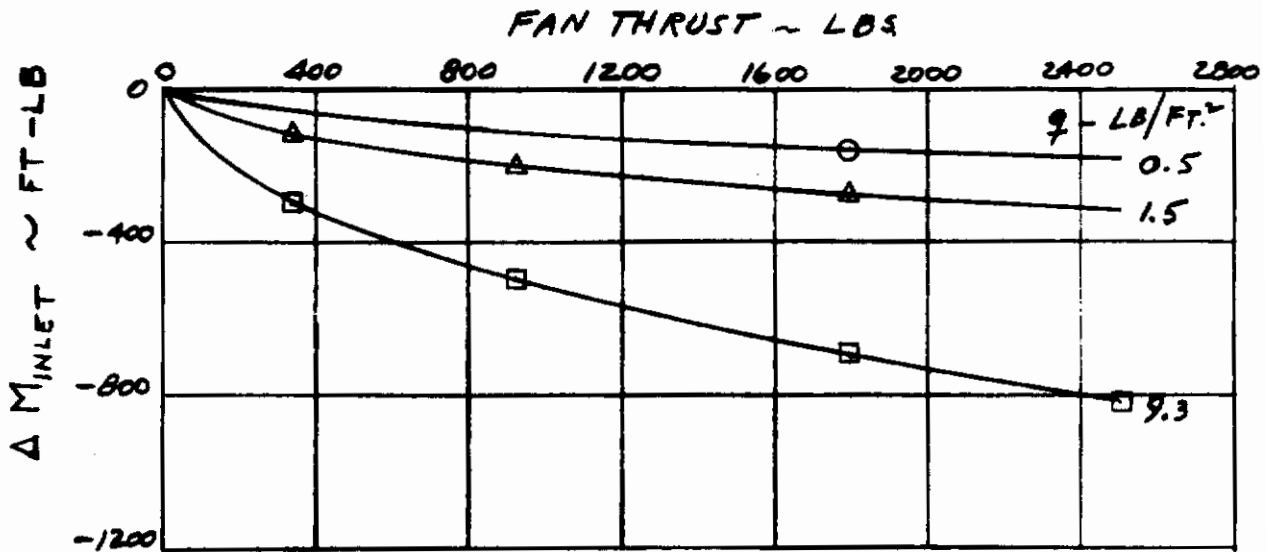
FIGURE 87. INLET RAM DRAG EFFECTS
FOR WING FANS

120

NORMAL
FORCE

F_N

POUNDS

$q = 0.5, \dfrac{LB}{FT.^2}$

$T = 1790\ LB.$

F_N

POUNDS

$q = 9.3, \dfrac{LB.}{FT.^2}$

$T = 2500\ LB.$

ANGLE OF ATTACK, α-DEG.
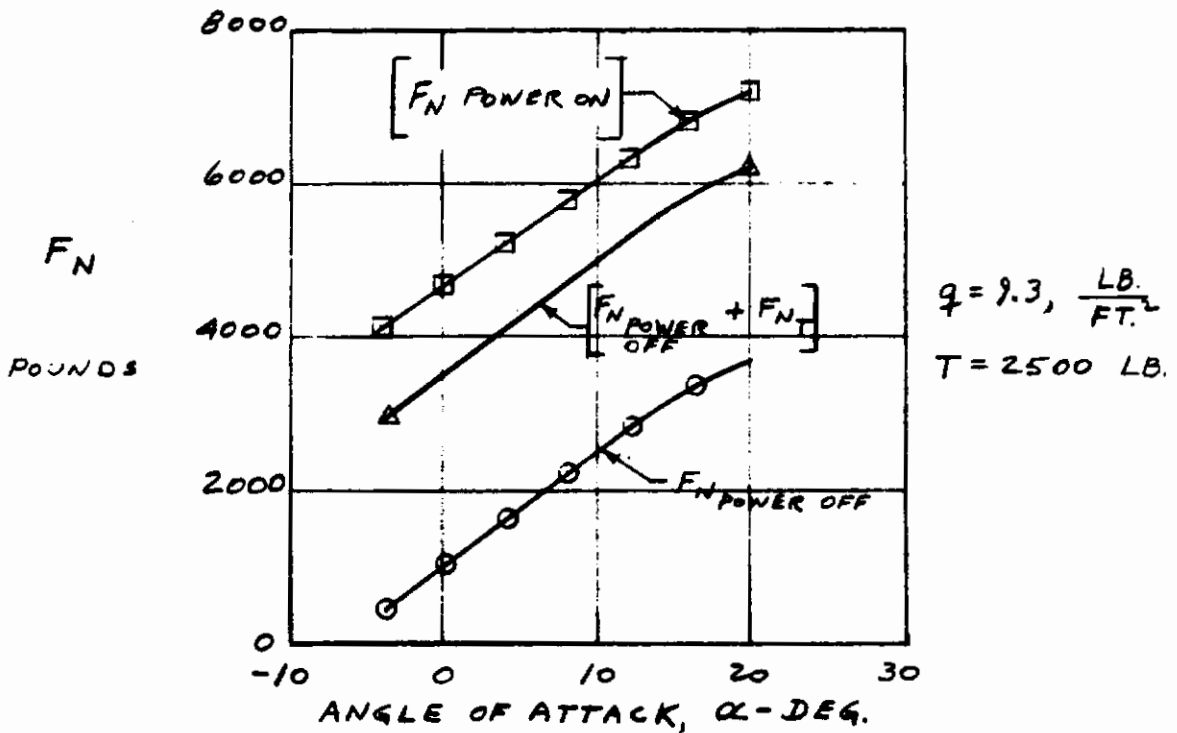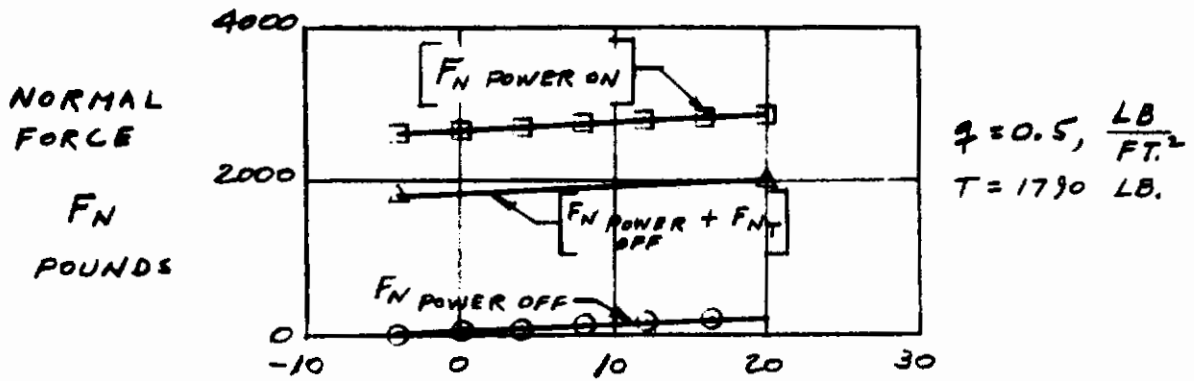
FIGURE 88. TYPICAL NORMAL FORCE VERSUS ANGLE OF ATTACK
DATA (TAIL-OFF; $\delta_f = 45°$; ZERO EXIT LOUVER DEFLECTION)

121
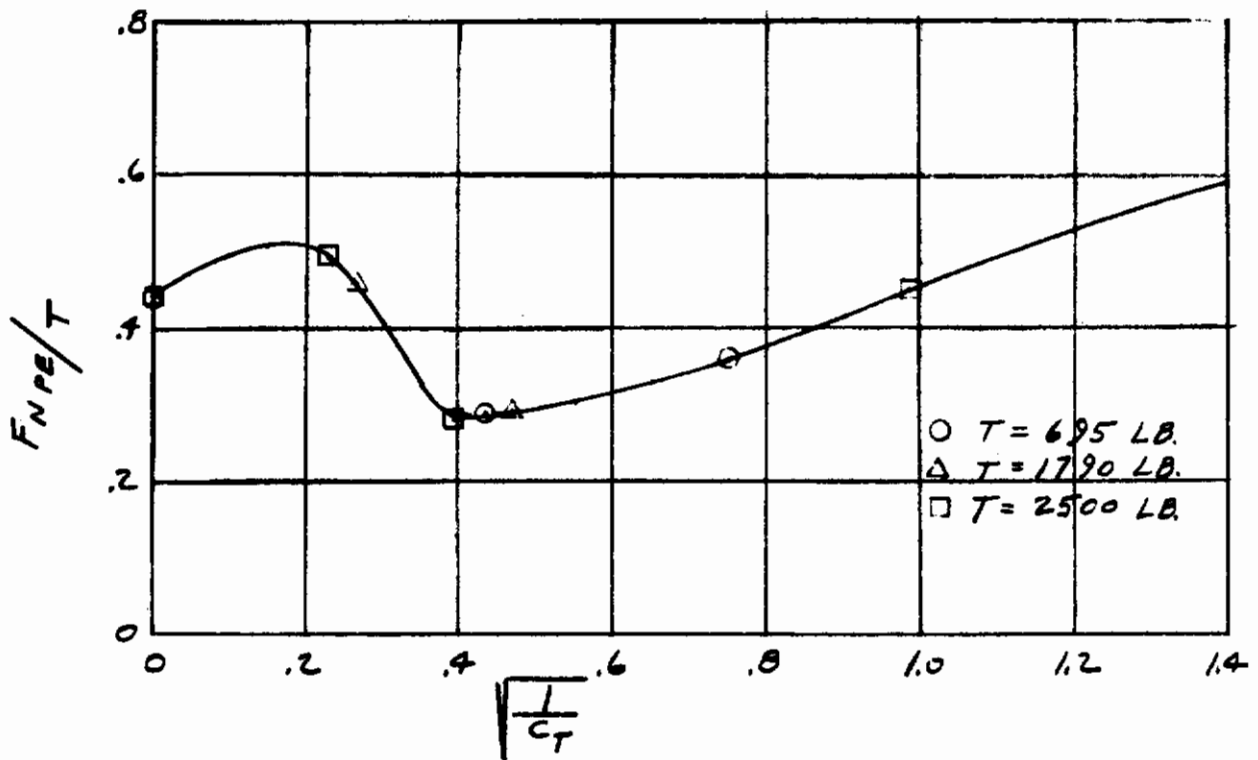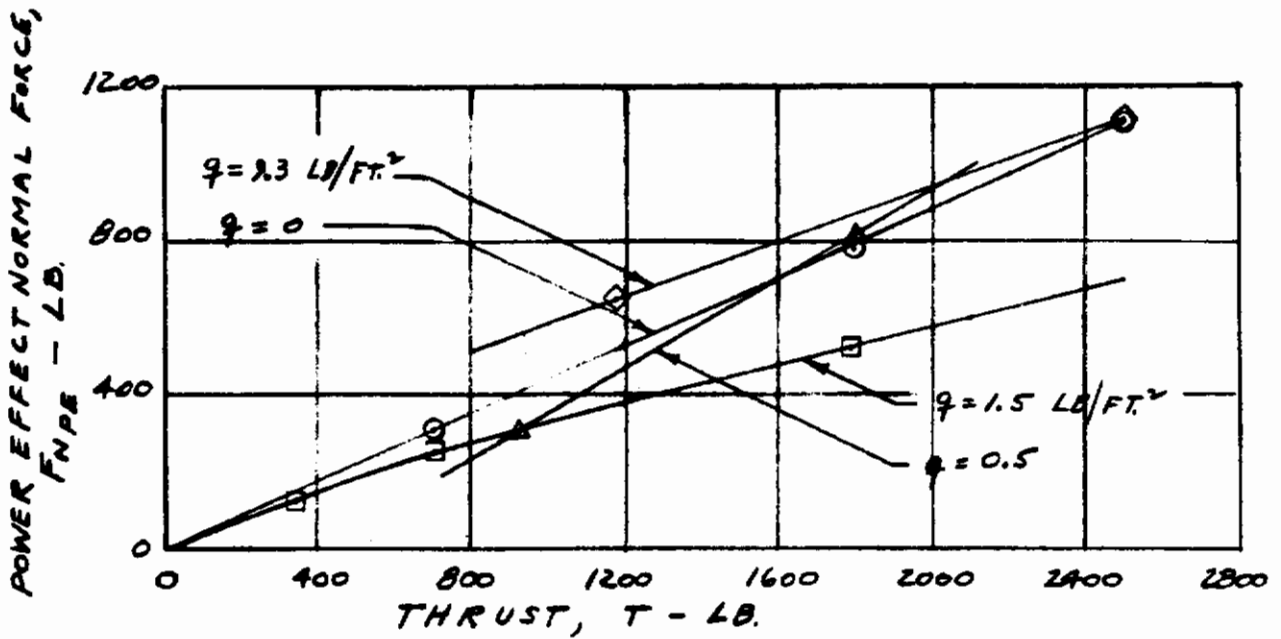
Fig. 89. Summary of power effect Normal Force Data at Zero Angle of Attack
(Tail-Off; δ_f=45°; Zero Exit Louver Deflection)

122

NOTE: FAN INLET RAM DRAG REMOVED

Fig. 90. Typical Chord Force Versus Angle of Attack Data
(Tail-Off; δ_f=45°; Zero Exit Louver Deflection)

123

NOTE: FAN INLET RAM
DRAG REMOVED.
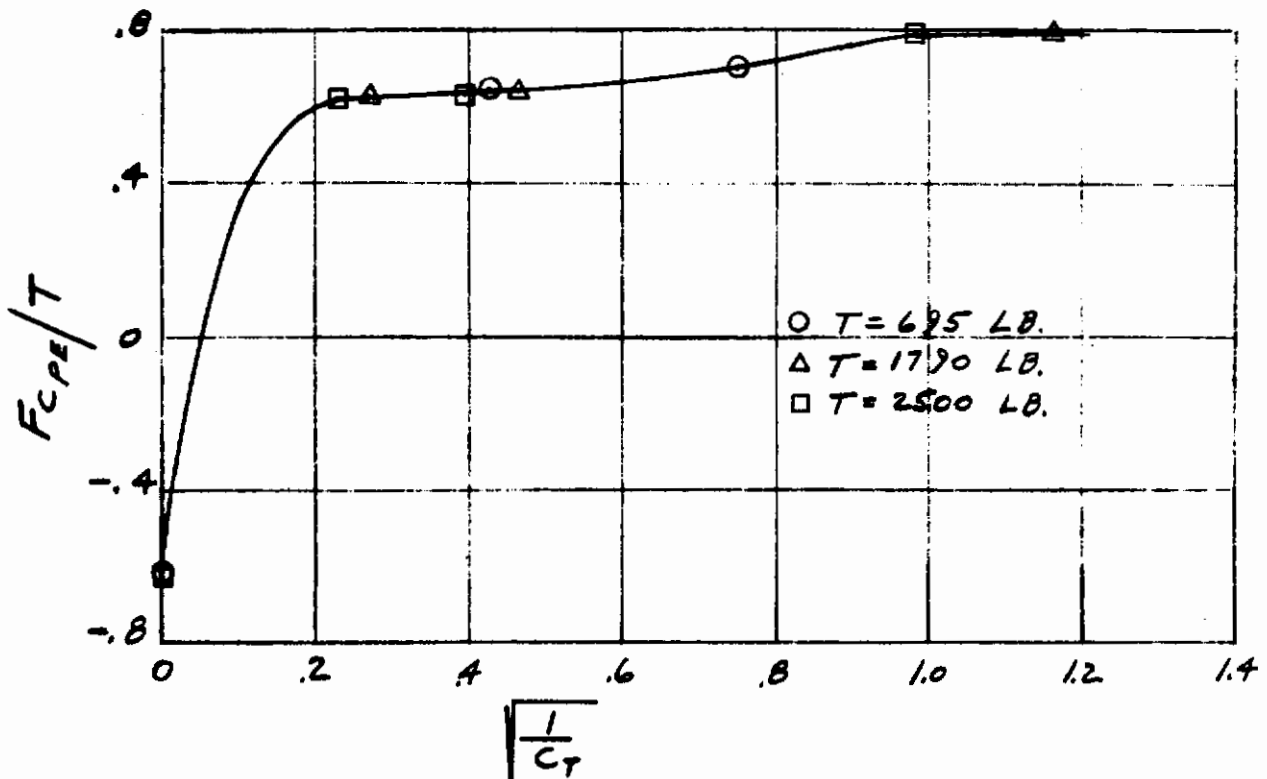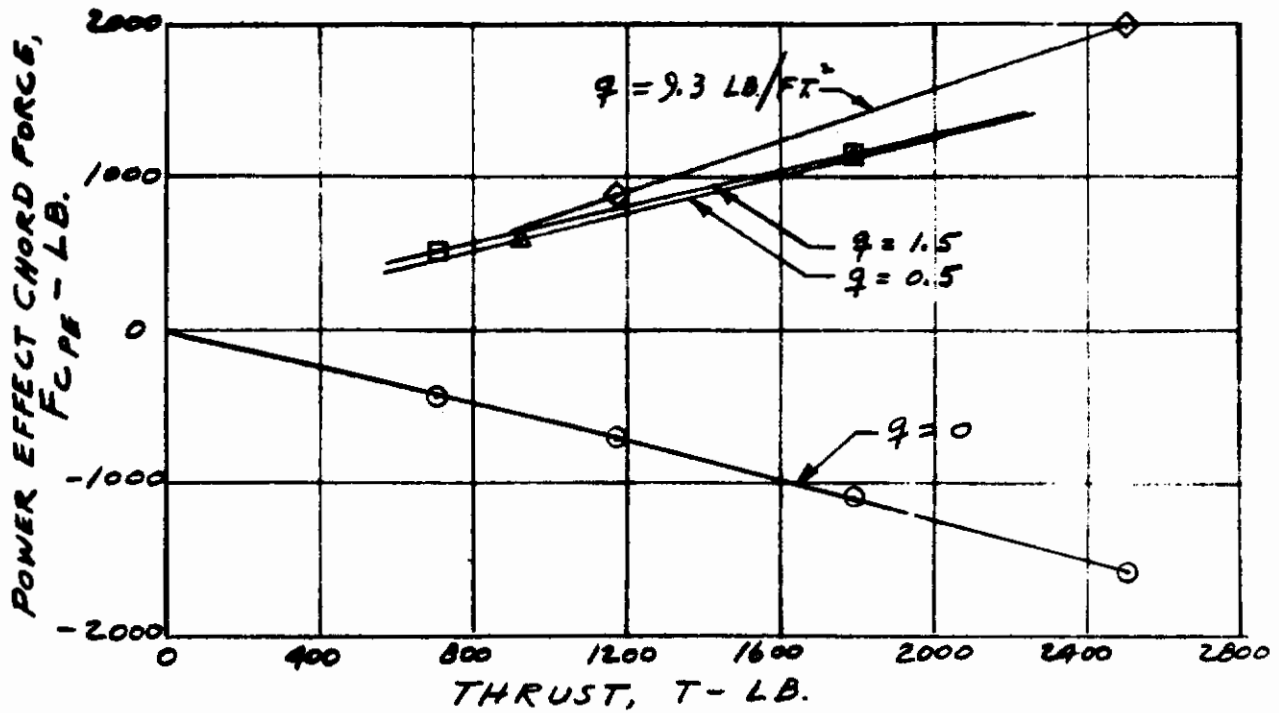
Fig. 91. Summary of Power Effect Chord Force Data at Zero Angle of Attack
(Tail-Off; δ_f=45°; Zero Exit Louver Deflection)

Fig. 92. Typical Pitching Moment versus Angle of Attack Data
(Rail-Off; δ_f=45°; Zero Exit Louver Deflection)

125

NOTE: FAN INLET RAM DRAG
MOMENT REMOVED
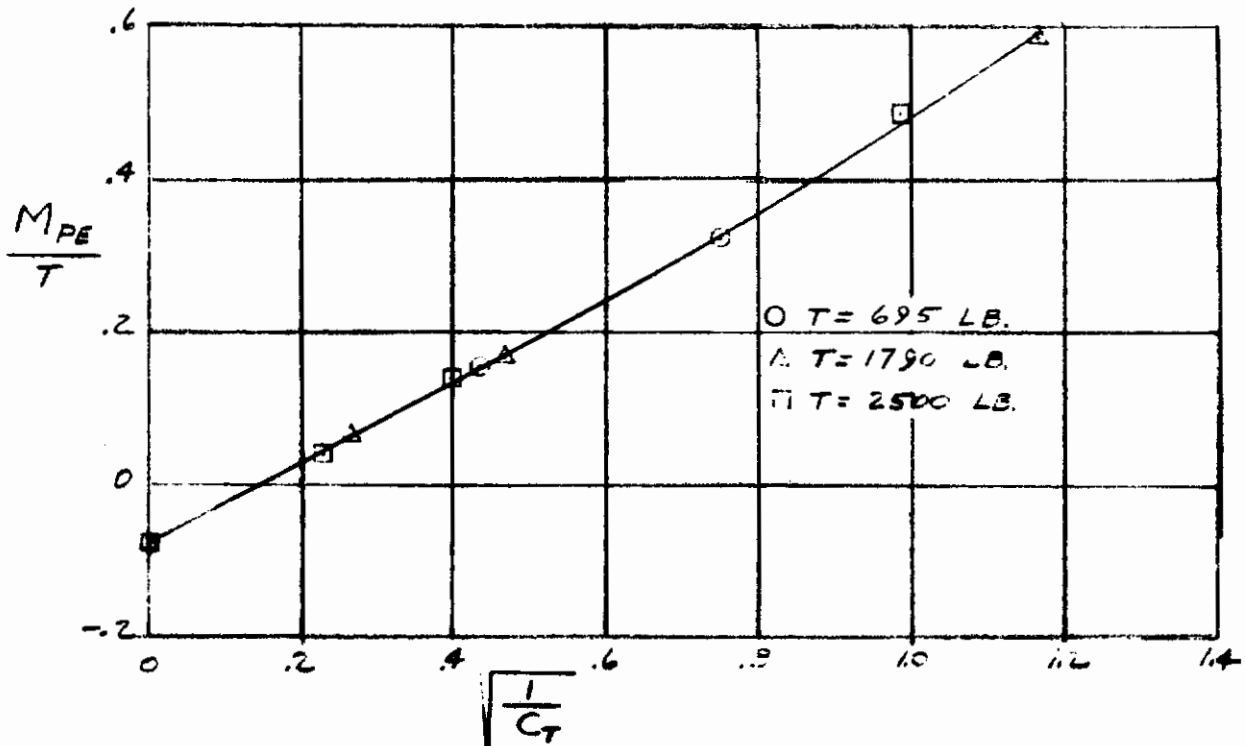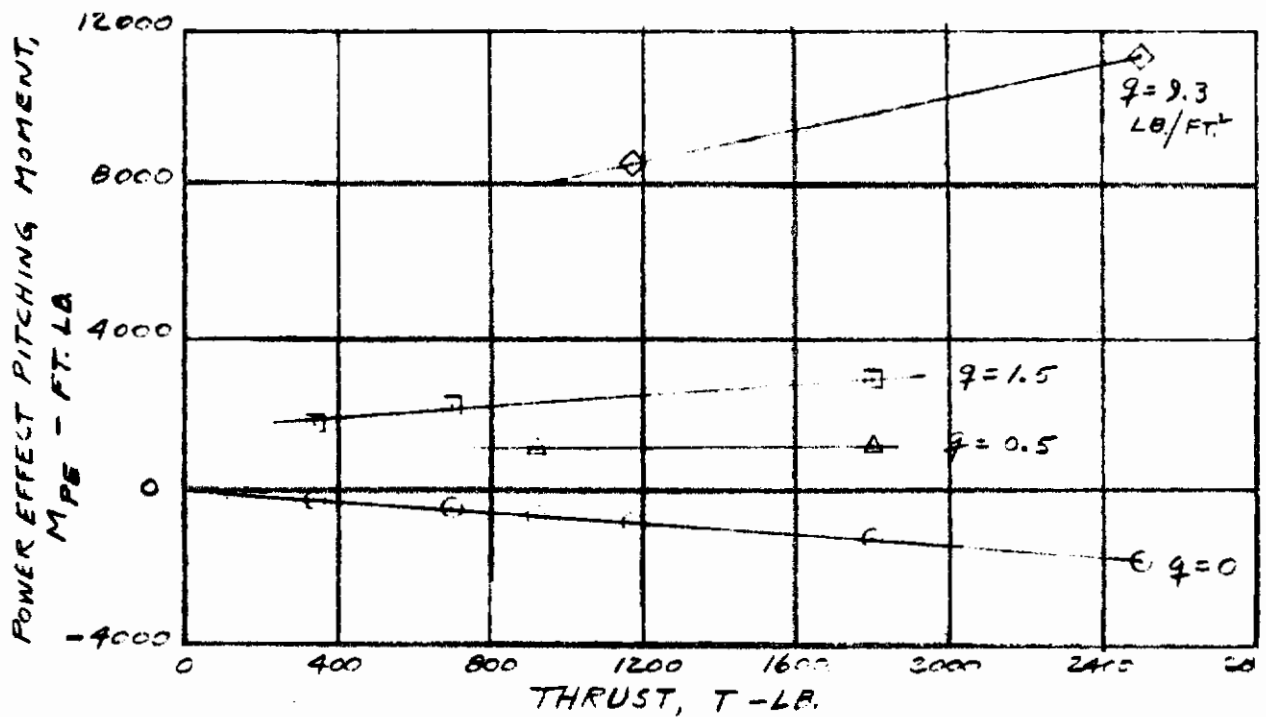
Fig. 93. Summary of Power Effect Pitching Moment Data at Zero Angle of Attack
(Tail-Off; $\delta_f = 45°$; Zero Exit Louver Deflection)

126
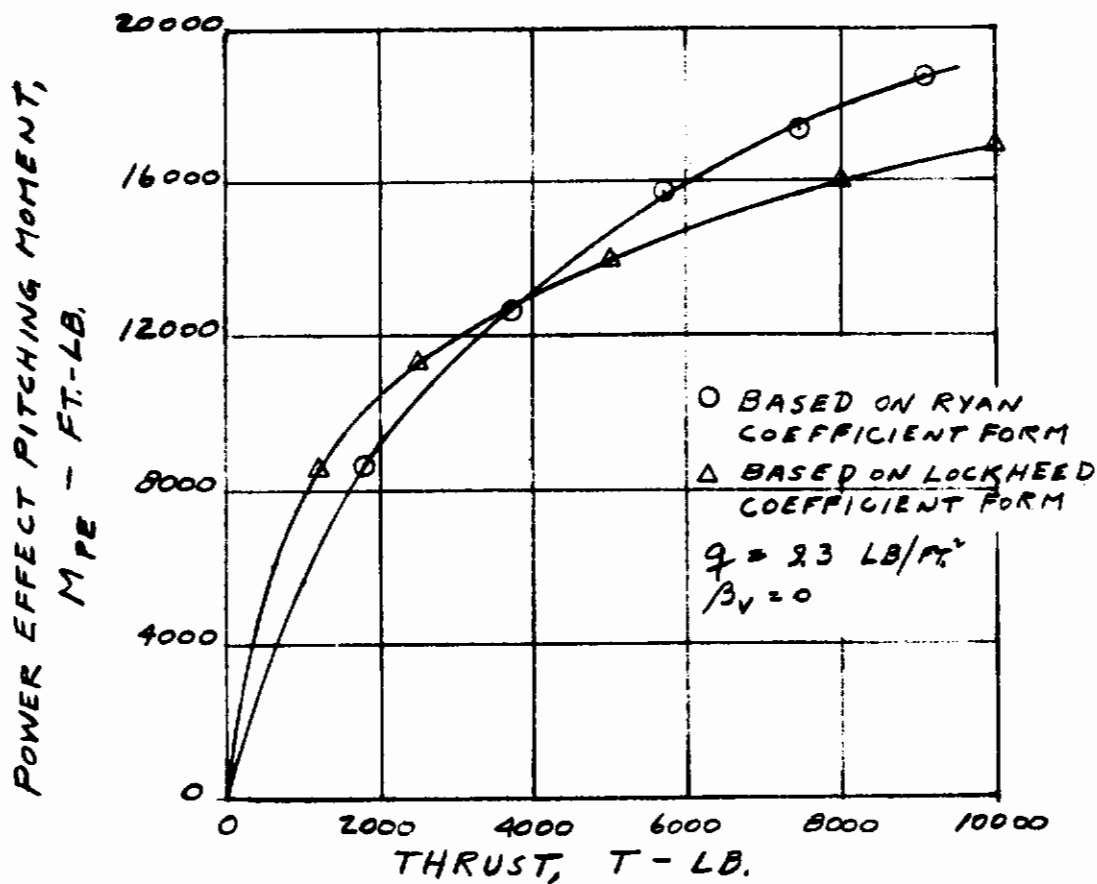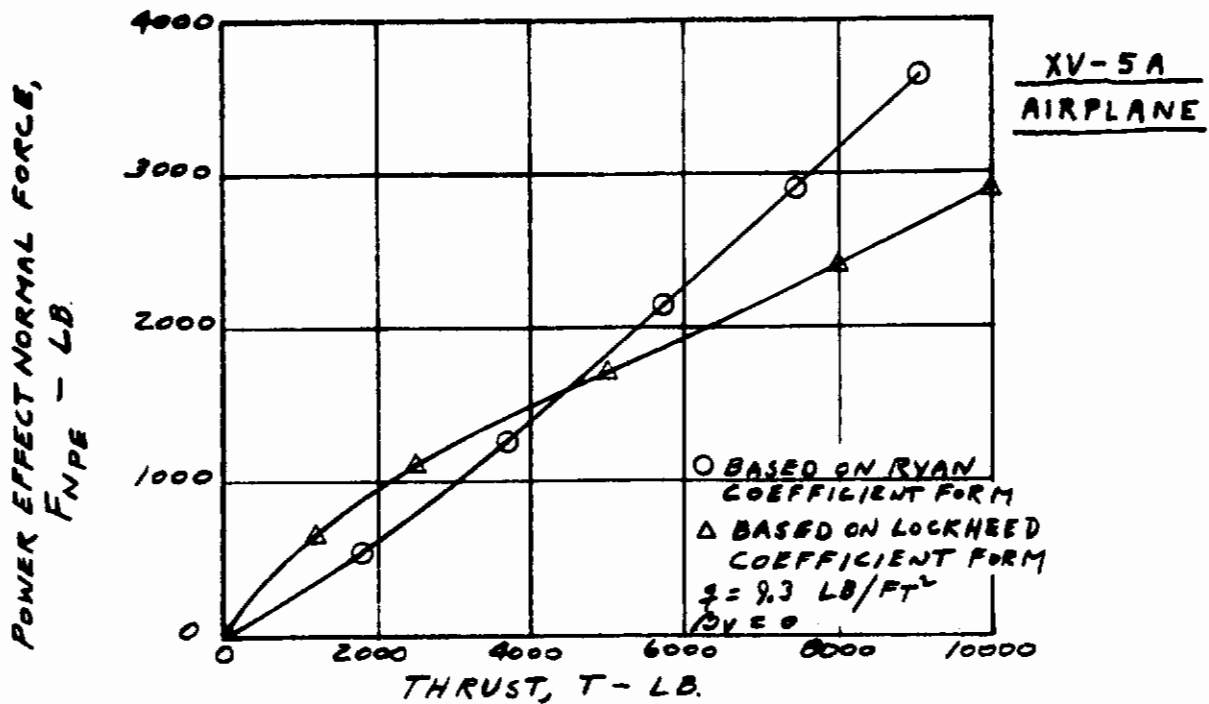
Fig. 94. Comparison of Power Effect Normal Force and Pitching Moment based on Lockheed and Ryan Parameters ($\alpha=0$; Tail-Off; $\delta_f=45°$; Zero Louver Deflection)
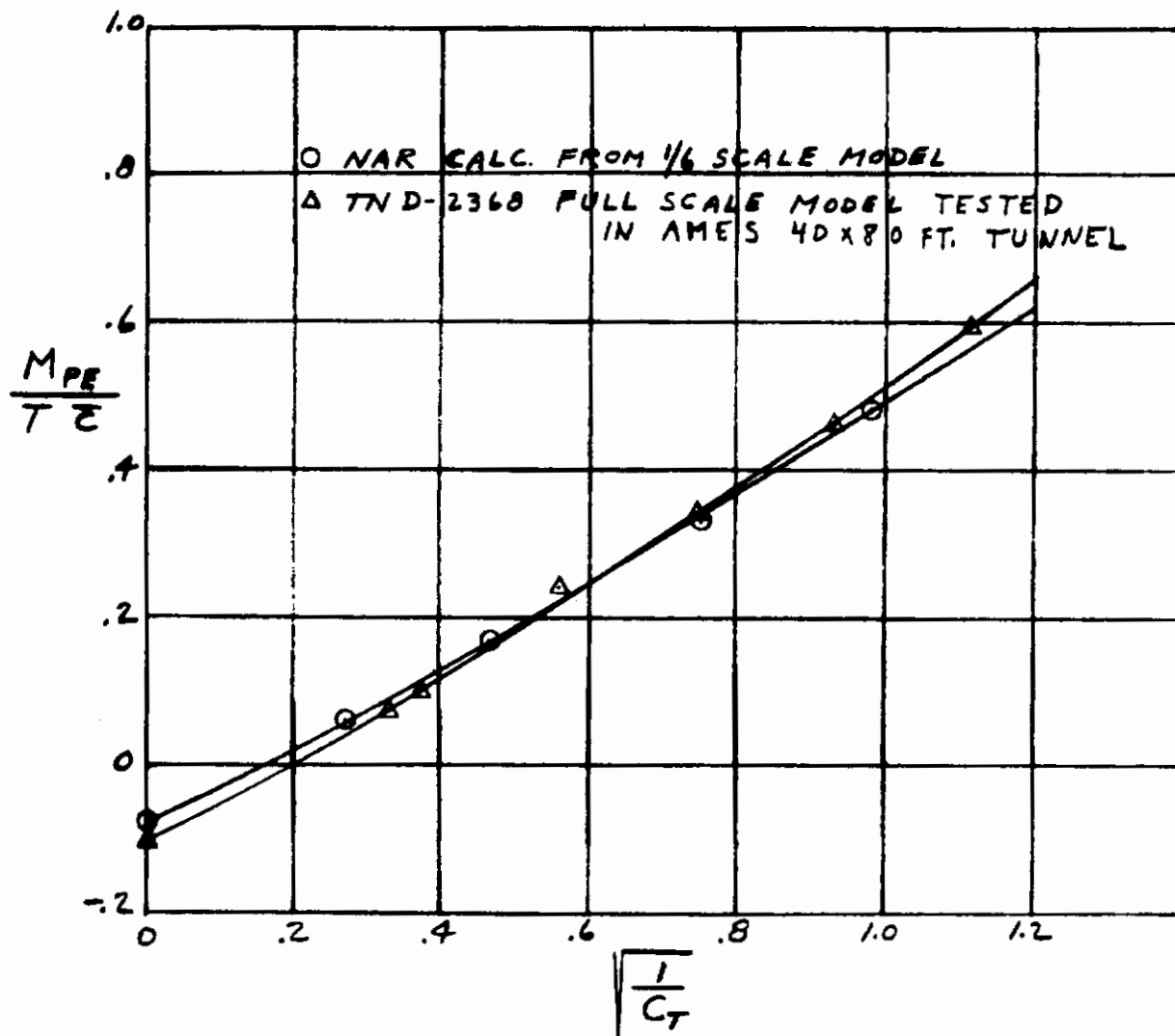
Fig. 95. Comparison of Full Scale and 1/6 Scale Model Data for
the Power Effect Pitching Moment

128
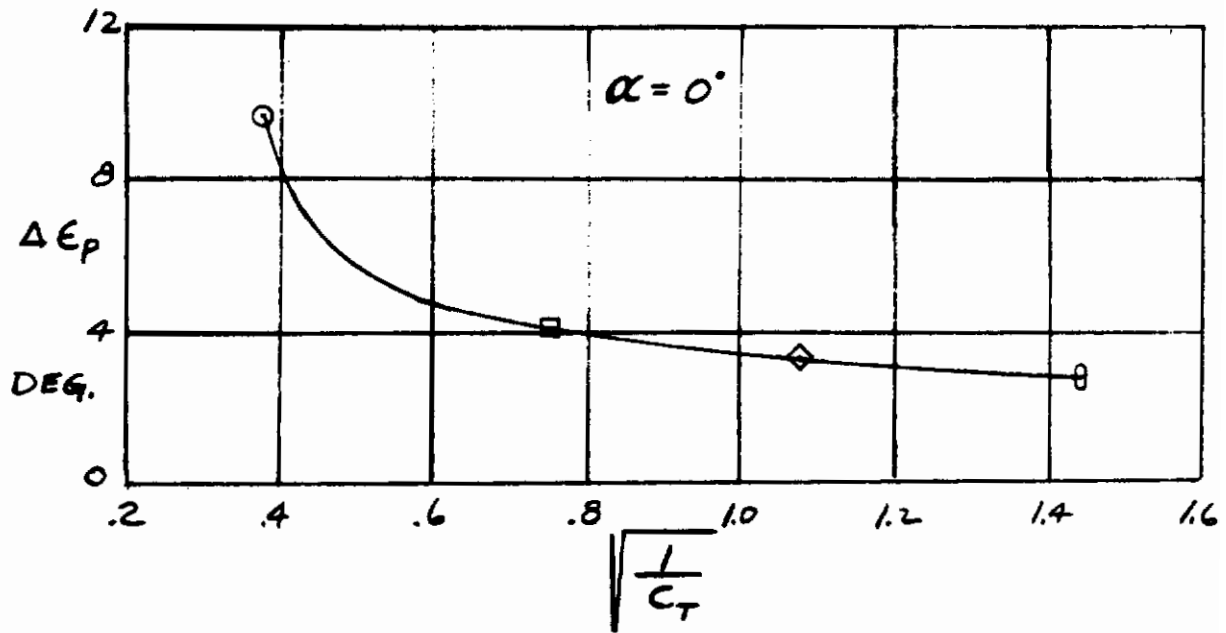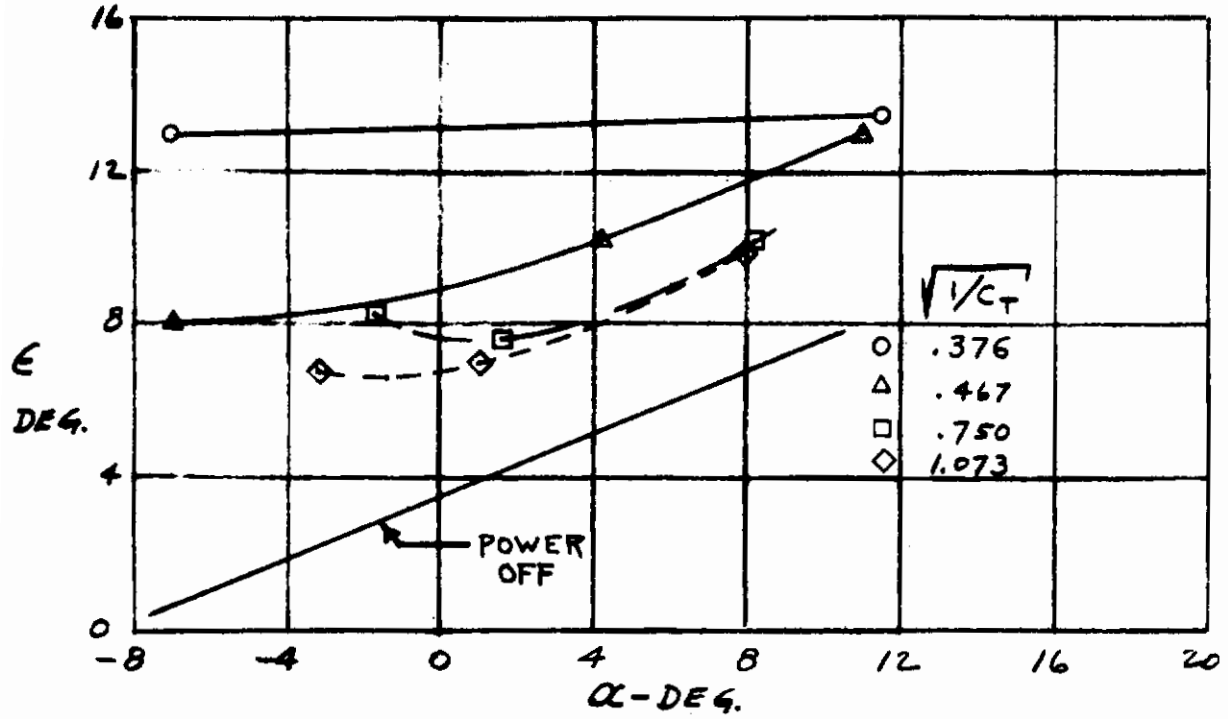
Fig. 96. Increment in downwash angle due to Fan Power

129
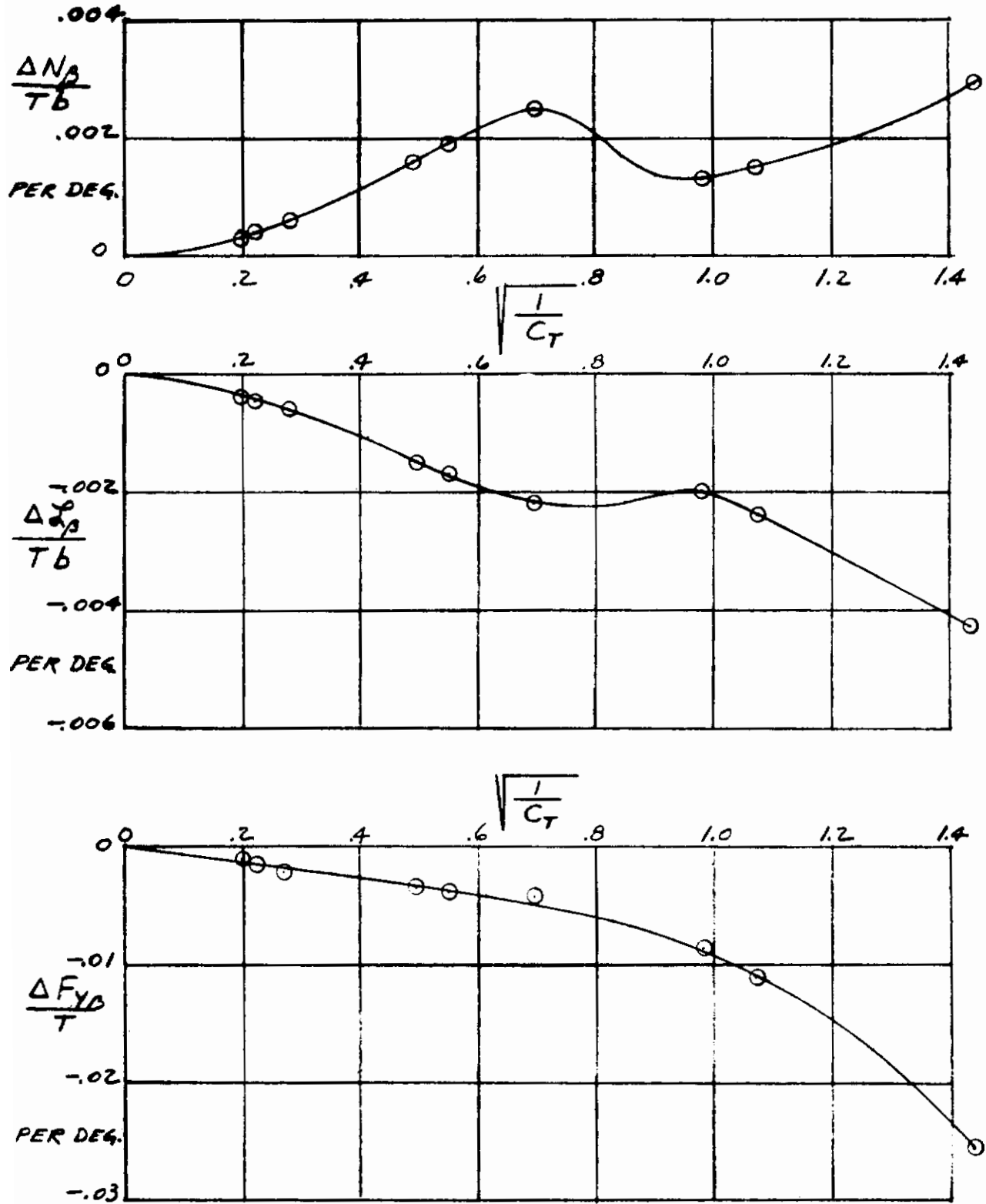
Fig. 97. Lateral-Directional Power Effects ($\alpha=0$; Tail-On; $\delta_f=45°$; Zero Exit Louver Deflection)

130

Section V

XV-4B WIND TUNNEL TESTS

A discussion of the wind tunnel tests conducted in support of the VIFCS program is presented in this section. The results of wind tunnel tests conducted by NR to investigate inlet and exit effects for an XV-4B type airplane are discussed, and a general review of all XV-4B model tests is presented.

XV-4B TYPE EXIT TEST

TEST PROGRAM AND OBJECTIVES

An XV-4B type exit jet model was tested in the NR 7.75 x 11 Foot Low Speed Tunnel during December 1968. The test, identified as NAAL Test 592, required 40 hours of tunnel occupancy time. The test objectives were to visualize and investigate the aerodynamic characteristics of a jet exiting into a freestream cross flow, estimate the magnitude of tunnel wall effects on the available XV-4B model data, and determine if the exit jets could influence the XV-4B flight test angle of attack vane readings. All recorded data for this test is contained in reference 5.

Some of the complex aerodynamic effects associated with jet VTOL models are illustrated in figure 98. In free flight the aerodynamic disturbances are believed to result from a local entrainment flow field surrounding the jet, a vortex system shed by the jet, and the freestream flowing around the jet volume. Also, the jet entrainment flow can have an indirect effect on the wing wake by altering the wing spanwise loading. When confined in a wind tunnel the walls will alter the streamlines for the jet entrainment flow, wing wake, and jet path relative to their free flight location. In addition, some effects not present in free flight may be present in a wind tunnel. For one thing, in small tunnels at very low speed the exhaust flow may have sufficient energy to climb the side walls and produce a vortex flow in the test section. For another thing, at low test velocities the jet upon contacting the tunnel floor may not move immediately downstream but rather form a standing splash which can obstruct the tunnel flow. To investigate these effects instrumentation was installed to visualize and measure the flow patterns in the test section with the jet operating. The jet path was made visible by injecting water vapor into the exhaust flow, and the jet entrainment flow and splash were investigated by means of oil flow studies. Local angle of attack measurements were obtained at numerous points surrounding the jet including locations relative to the jet where the XV-4B wing and tail surfaces are located. Tunnel speed and jet velocity were variables in the test.

As part of the VIFCS program two different XV-4B models were built and tested. An 0.16 scale model was tested in the 17 foot section of the Langley 7 x 10 foot Low Speed Tunnel, and a 0.18 scale model was tested in the Ling-Temco-Vought 7 x 10 foot Low Speed Tunnel. No attempt was made to correct

131

this test data for jet induced tunnel wall effects due to a lack of available methods. The two sets of data showed some differences when compared which might have been the result of wind tunnel wall effects. In order to provide some basis for verifying if the differences in model data was due to tunnel wall effects the following approach was adopted. The test section geometry for the two model tests were closely duplicated at a smaller scale, and an XV-4B type jet only model was tested in both sections. Angle of attack measurements at the wing and horizontal tail surfaces were obtained in both test sections. From this data the incremental angle of attack at these surfaces due to difference in wall size was measured. In turn, an increment in model data due to the wall effect was calculated using the incremental angle of attack values in combination with appropriate power-off lift-curve-slope values.

The question arose as to whether the exit flow can have any influence on the flight test angle of attack measurements. To resolve this question, angle of attack measurements at the XV-4B alpha vane location were obtained as part of this test for a variety of speed and power conditions. It was intended that the results would be applied to the analysis of the XV-4B flight test data.

MODEL AND TEST FACILITIES

The test was conducted using the ducting and air supply system originally built for an NR V/STOL fighter model. The original exit nozzles were replaced with new ones which represent the XV-4B nozzle geometry. The general arrangement of nozzles, ducting, and sting support are presented in figure 99, and a full scale drawing of one exit nozzle is shown in figure 100.

The XV-4B nozzles were sized to have the same ratio of exit area to tunnel area for the NR test as for Langley Test 178 and LTV Test 195. Using the NAAL tunnel area to represent the Langley tunnel, a model exit area of .035 square feet was required to represent the Langley model. In turn, using an .035 square foot model exit area to represent the LTV model, an 3.34 x 4.75 foot test section was required to represent the LTV tunnel. Thus, to simulate the LTV test, auxiliary walls of these dimensions were installed in the NAAL test section, see figure 101.

Jet flow visualization was accomplished by means of oil flow techniques and introducing water into the jet exhaust. Also, local angle of attack disturbances were recorded at positions representing the XV-4B nose boom, wing and horizontal tail locations, refer to figure 102.

RESULTS AND DISCUSSION

Jet Path

Jet paths were visualized for the basic six jet exit configuration and for a special two jet exit configuration, issuing into a cross stream direction to the freestream flow, in the large and small test sections. This combination provided model height variations of h'/D_{eff} = 9.5 and 27.5 for the six jet configuration and h'/D = 95, 47.5, 33 and 16.4. The velocity ratios studied varied from (V_o/V_j) = .036 to .145 which were sonic jet exit flows at varying freestream velocities from 42 fps to 159 fps. The visualized jet paths were compared with Ivanov's jet trajectory equation (reference 21) and plotted as a function of the geometric variables shown in figure 103.

Six Jets

Figures 104 through 108 show the visualized jet path of three of the six jets compared to the predicted trajectories computed for Ivanov's equation.

$$\frac{x'}{D} = \left(\frac{\rho_o}{\rho_j}\right)^{1.3} \left(\frac{V_o}{V_j}\right)^{2.6} \left(\frac{z'}{D}\right)^3 + \frac{z'}{D} \tan \theta_{j_o} \qquad \left[\begin{array}{c}\text{IVANOV}\\\text{EQUATION}\end{array}\right]$$

Each figure shows the model in the large and the small tunnel at model angles of attack of 0°, 10° and 20°, and the figures progress in test ratios from .036 to .145. The centerlines shown are computed for each individual jet and for an average single jet using the effective diameter (D_{eff}) and average jet inclination angle ($\theta_{j_{eff}}$) of the three exits on one side.

$$D_{eff} = \sqrt{3}\ D_{j_i} \qquad \text{where } D_{j_i} \text{ is individual jet diameter}$$

$$\theta_{j_{eff}} = \frac{1}{3}\left[\left(\theta_{j_o}\right)_{FWD} + \left(\theta_{j_o}\right)_{CENTER} + \left(\theta_{j_o}\right)_{AFT}\right]$$

The following is a tabulation of the inclination angle used in computing these trajectories.

α	$\theta_{j_{eff}}$	$\theta_{j_{FWD}}$	$\theta_{j_{CENTER}}$	$\theta_{j_{AFT}}$
0°	8.69°	1.35	9.27	15.45
10°	-1.31°	-8.65	- .733	5.45
20°	-11.31°	-18.65	-10.733	-4.55

It can be seen from these figures that when the wake is allowed to form (large tunnel data) the curvature of the wake follows the average computed trajectory, downstream of the intersection of the forward individual wake path and the average wake path. Also, the jet paths, studied without the centerboard in the tunnel, do not change appreciably from those shown herein. Consequently, it is felt that the Ivanov's suggested method of using the effective diameter for jets in tandem (rectangular exits) is adequate to define the overall multiple jet paths. So to define the path of an offset mounted side by side configuration such as that tested the average wake of each independent side is the same.

Single Jet

The Ivanov equation was superimposed on the visualized jet path of the two sets of single jet exit data, figures 109 and 110. From these visualizations it was observed that fair agreement between the path and Ivanov's equation was obtained. This result is supported by Margason's experiments (reference 22) and was suggested in the preliminary VIFCS work (reference 1). However, the jet impingement point on the tunnel floor, determined from oil flow studies such as those in figure 111, was not adequately predicted by the Ivanov equation. The impingement point was generally found to be considerably forward of the location predicted by Ivanov. As a consequence, the Ivanov equation would predict a smaller impingement angle and a smaller jet splash interference than indicated by the experimental results of this test.

To obtain a satisfactory expression of the jet trajectories, the observed leading edge paths were determined for all the single jet data in the $7\ 3/4 \times 11$ foot section and are plotted in figures 112 through 114. The observed leading edge paths were determined at $\alpha = 0$ only for the single jet in the small tunnel and are plotted in figure 115. The jet diameters of 1 inch and 1/2 inch in the two tunnel test section sizes provide a variation in h'/D (model height above floor) from 95 to 16.

The 1/2 inch diameter jet in the large tunnel was as close to free air as was tested ($h'/D \approx 95$ at $\alpha = 0$). Therefore, this condition was picked to define an expression of the jet trajectory. An increment in x'/D (at constant z'/D values) from observed values of the jet path (figures 112 through 114) to those computed by Ivanov's equation were obtained as:

$$\frac{\Delta X'}{D} = \left(\frac{X'}{D}\right)_{IVANOV} - \left(\frac{X'}{D}\right)_{OBSERVED}$$

These were expressed in the same terms as Ivanov's equation so that the result would yield a modified Ivanov equation.

134

The following expressions were determined:

$$\frac{\Delta X'}{D} = 1.98 \left(\frac{V_o}{V_j}\right)^{2.67} \left(\frac{z'}{D}\right)^{2.67} \qquad \theta_{j_o} = 1.35°$$

$$\frac{\Delta X'}{D} = 1.82 \left(\frac{V_o}{V_j}\right)^{2.67} \left(\frac{z'}{D}\right)^{2.67} \qquad \theta_{j_o} = -8.65°$$

$$\frac{\Delta X'}{D} = 1.54 \left(\frac{V_o}{V_j}\right)^{2.67} \left(\frac{z'}{D}\right)^{2.67} \qquad \theta_{j_o} = -18.65°$$

These equations were found to vary linearly as a function of the $\tan \theta_{j_o}$, and combining the increment to the Ivanov equation the resulting equation is:

$$\frac{X'}{D} = \left[\left(\frac{z'}{D}\right)^{\frac{1}{3}} - 1.985\right] \left(\frac{\rho_o}{\rho_j}\right)^{1.3} \left(\frac{V_o}{V_j}\right)^{2.6} \left(\frac{z'}{D}\right)^{2.67} + $$

$$\left[1 - 1.3167 \left(\frac{\rho_o}{\rho_j}\right)^{1.3} \left(\frac{V_o}{V_j}\right)^{2.6} \left(\frac{z'}{D}\right)^{1.67}\right] \frac{z'}{D} \tan \theta_{j_o} \qquad \begin{bmatrix} \text{MODIFIED} \\ \text{EQUATION} \end{bmatrix}$$

The same method was used to determine the equations for the 1.033 inch diameter jet in the large tunnel ($h'/D = 47.5$). These equations were not generalized for the variation of θ_{j_o}. The resulting equation at $\theta_{j_o} = 1.35$ is presented in figure 112, and the individual equation for the 1/2 inch jet is also presented. Figure 112 through 114 show the variation of jet trajectory for the one inch jet in the large (7 3/4 x 11 foot) tunnel as well as the measured impingement points of the jet wake.

The observed jet wake of the two exit sizes in the small tunnel are presented for $\alpha = 0$ in figure 115. It can be seen that these wakes will be influenced by the tunnel floor. For the small jet ($h'/D = 32.7$) with velocity ratios from .03 to .07 and for all cases for the large jet ($h'/D = 16.37$), the wake impinges on the floor. Equations to describe these observed paths were determined directly from the paths and are presented in figure 115. It should be noted here that the equations were written for the various investigated single jet trajectories with the object of expressing the wall effect on the jet wake as a function of the trajectory variables, but time did not permit further examination.

Tunnel Wall Effects

Jet Path Disturbance

The observed jet trajectories at $\alpha = 0$ for three of the tested jet exit conditions (i.e., 1/2 inch diameter in large tunnel and the 1 inch diameter jet in the large and small tunnel) is presented in figures 116 and 117. These figures show the effect of the proximity of the tunnel floor on the wake trajectory for $h'/D = 94.97$ (approximate for free air) to 16.3. For wake comparison purposes Ivanov's trajectory and measured impingement points are

135

also presented. It can be seen that at the lowest velocity ratio (V_0/V_j = .038) that the observed wakes show little variation within the range of observable data. As the velocity ratio increases and the jet trajectory turns to proceed downstream the observed wakes are affected more by the floor. The wake passes downstream in closer proximity of the model, and the wake downwash angle is less in the presence of the floor than the estimated free air wake.

The wake trajectory will affect estimates of interference caused by jet splash on the floor. Figure 118 presents the effect of the jet splash based on the Ivanov trajectory and the modified Ivanov trajectory developed in this study. The conditions for this comparison are: V_0/V_j = .038, h'/D = 22.2, and θ_{j_0} = 0. The comparison shows a change of maximum interference angle at the model location from 5.5 to 7.5 degrees and a change in dynamic pressure ratio along the model from 1.42 to 1.70.

Wake Properties

The properties of the jet wake and its influence on the surrounding flow field must be known to estimate interference to the model data caused by the proximity of the tunnel walls. It can be observed from the photographs, figures 104 through 110, that, as the jet wake trajectory turns to proceed downstream, the visual path widens. This would indicate, as is generally agreed to in reference 23, that the wake rolls up into a trailing counter rotating vortex system as it changes direction. The proximity of this vortex system to the model altered by the presence of the wind tunnel wall will change the flow field surrounding the model by its own presence and by the interference caused to the model wing wake.

Jet Entrainment

The properties of the initial jet wake issuing from the exit, prior to the change in direction, is felt to consist of highly energized viscous entrainment of the surrounding flow field. The presence of the wind tunnel walls would act as a restriction to this entrainment and thereby result in a reduction in local angle of attack in the proximity of the wing. This phenomenon, as previously stated in reference 1, is opposite in sign to the wall interference expressions derived for propeller theory.

Lateral Recirculation

Part of the purpose of the test, reported in reference 24, was to determine if at low speeds in small tunnels the exhaust flow would climb the wind tunnel walls and produce vortex flow in the test section and result in lateral recirculation. In figures 104, 105, 106 and 110, the water droplets visible on the window of the small tunnel define the extent to which the exhaust air proceed up the tunnel sidewall. It is evident that the exhaust flow on the sidewalls is quickly carried downstream by the free air and that complete lateral recirculation of the exhaust flow does not occur. However, this cross-tunnel flowing exhaust air is estimated to have an adverse effect on the local freestream flow and result in extreme interference in any resulting model data.

Jet Splash Interference

Jet flow issuing from a model in a subsonic stream and impinging on the wall of a wind tunnel causes disturbance to the flow field around the model. The physical obstruction in the channel created by a jet splash on the floor has been simulated mathematically in reference 24 by a distribution of sources whose strength is a function of jet size, velocity ratio, and impingement angle. The theory has been adjusted by empirical factors to fit observed small scale test data.

The XV-4B exit test (reference 5) provided an opportunity to apply the theory described above at a reasonably large scale. Furthermore, flow visualization studies by means of tufts, water droplets and oil flow in the subject tests confirmed the notion that splash shapes are well-defined regular contours that might lend themselves to theoretical treatment.

Theoretical flow interferences due to the jet splash were computed in the vertical plane of symmetry to illustrate the longitudinal variation of interference. Interferences were evaluated for a limited number of test variables, i.e., three angles of attack, two jet sizes, two tunnel sizes and two velocity ratios. Also, three specific field points were evaluated; nose, wing M.A.C. and tail. To simplify the investigation, a single source was used to represent the splash from multiple jets, an assumption whose validity is best when the source and model are remote from each other.

The theoretical splash effects are presented in three figures. Figure 119 shows the change in flow angularity due to turning two jets on and six jets on at a velocity ratio of .0392 in the large (7.75 x 11 ft.) tunnel. The stated velocity ratio corresponds to sonic jet speed and 41 ft./sec. airspeed. Figure 120 shows the effect of two jets on flow angularity in the small (3.34 x 4.75 ft.) tunnel, at the same velocity ratio. Figure 121 shows the effect of two jets on flow angularity and dynamic pressure ratio change in the small tunnel at a velocity ratio of .0619.

It should be noted that even in a large test section the jet splash can produce significant interference, refer to figure 119. In fact, the jet splash may be present in free flight if the aircraft is flown very close to the ground.

The incremental effect of the splash cannot be easily separated from the total tunnel wall interference, and no attempt was made to extract the splash effect from the XV-4B exit test data. However, the influence of the jet splash upon the test data is readily apparent. The splash results in a very rapid change in the wall interference data as the dynamic pressure drops below about 8 pounds per square foot.

Local Angle of Attack Measurements

Angle of attack measurements were obtained at geometric positions which would have been occupied by the nose boom, wing and horizontal tail components had the model been a complete model. Measurements were obtained in the large and small test sections as a function of jet velocity and tunnel dynamic

137

pressure. This data is presented in figures 122 through 125. The local angles of attack in these figures are presented in the form of an increment due to power and were determined by subtracting the power-off values from the power-on values. Also, the small and large test section data are shown plotted for constant test conditions to indicate the effect of tunnel size.

The nose probe data indicates a positive increment in angle of attack due to jet power is present at the flight test angle of attack vane location, figure 122. Values between .5 and 1.8 degrees were measured in the large test section which should be representative of free flight conditions.

The spanwise probes indicated negative increments in wing angle of attack due to jet power, figures 123 and 124. Values between zero and -15 degrees are present at the wing M.A.C. location with the model installed in the large test section. This data clearly shows the strong entrainment action of the jets. The wing angle of attack increment due to power becomes less negative with increasing speed and increased distance from the jet exits.

The tail probe data indicates a negative increment in angle of attack due to jet power, figure 125. The negative increment increases with thrust and decreases with increasing speed. Values between -0.2 and -8.0 degrees were recorded.

The effect of the wind tunnel walls upon the jet induced angle of attack increments is presented in figure 126 for the wing and in figure 127 for the horizontal tail. These test values are used to adjust the data for LTV Test 195 for correlation with the data for Langley Test 178. The actual correlation work has already been discussed in Section IV.

TEST CONCLUSIONS

The results of a wind tunnel investigation of the aerodynamic characteristics of an XV-4B type jet exiting normal to the tunnel flow indicate the following conclusions.

1.   Theoretical expressions for the jet path developed by Ivanov were compared with the observed jet paths. General agreement between the observed path and Ivanov's equation was obtained. However, the Ivanov equation did not adequately predict the tunnel floor impingement point.

2.   In the case of multiple jets the mean jet diameter and the average angle of inclination of the jets on one side can be used to approximate the jet wake path, downstream of the intersection of the forward most issuing jet path with the mean jet path.

3.   The wall effect on the jet trajectory is shown to place the downstream jet wake in closer proximity of a model and will cause a change in the resulting downwash angle of the wake. This will result in interference to the field surrounding the model.

4.   The properties of the jet wake are described as initially producing viscous entrainment action, which directly influences the local wing lift distribution, and subsequently breaking up into a trailing counter rotating vortex system. The wind tunnel wall effect on these properties would act opposite to the propeller derived theories in the immediate vicinity of the wing and depending on the local wake conditions would alter the downwash pattern of both the wing wake and the jet wake.

5.   Complete lateral recirculation of the exhaust flow in small test sections at low freestream velocities did not occur. Rather, the flow is quickly carried downstream. Still, at the test conditions where the exhaust flow was visible on the side wall, it is estimated that large interference to the model flow field occurs.

6.   The results of this test demonstrate that the jet splash effects can occur even in a large test section. However, in a large test section the splash effects can be easily avoided by not testing at very low tunnel velocities. For any given test a minimum test speed should be established. The minimum test speed could be the maximum velocity at which the exhaust flow could collect on the tunnel floor.

7.   The jet entrainment flow is the primary cause of the power effects measured in this test. The jet entrainment flow was suppressed by as much as 25 percent when the model was operated in the small test section.

8.   The flow disturbance caused by the exit flow is powerful and can significantly alter the local angles of attack over the entire airplane in free air.

XV-4B TYPE INLET TEST

TEST PROGRAM AND OBJECTIVES

The test described in this section was made to gain information on the nature of the XV-4B inlet air flow and its effect on the flow field near the airplane. The test was conducted in the NR low speed wind tunnel during February 1970, and 50 hours of tunnel occupancy time was used. All recorded data for this test, identified as NAAL 622, is contained in reference 6.

Langley wind tunnel data for the XV-4B with simulated inlet and exit flow indicated a large downwash due to power. Insufficient testing was done to determine if the downwash was primarily due to the inlet flow or the exit flow. Therefore, the NR inlet test was conducted to obtain direct measurement of the flow angle disturbances on the aircraft due to inlet flow. Five rates of inlet flow simulating zero to maximum lift-engine thrust were tested.

In addition to the horizontal tail location, flow angles were also measured in the NR test at two fuselage stations, at four vertical locations between the tail and the aft lift-engine inlets, and at the fuselage station of the airplane wing leading edge.

139

As a secondary objective, incremental sidewash angles at the location of the vertical tail were measured. Insufficient data were available from Lockheed wind tunnel tests to evaluate the effect of inlet flow on sidewash.

MODEL AND TEST FACILITIES

The inlet test was conducted in the NR 7.75 x 11 ft. atmospheric wind tunnel on a fuselage which had four inlets designed to be .10-scale duplication of the XV-4B inlets, figure 128. A total of eleven goniometers (angle-measuring total-pressure probes) were mounted in three rakes (A, B, and C, figure 129) to measure local flow angles in the pitch plane for the majority of the runs, the nose probe being moved to the wing rake after numerous runs established power effects for the nose location at all test conditions of inlet flow, tunnel speed, and angle of attack. For a few runs, local yaw angles were measured, and for the final seven runs all of the goniometer probes were mounted in a horizontal rake (D in figure 129) which extended from the model centerline to the location of the horizontal tail tip to determine the spanwise variation of incremental downwash due to inlet flow.

The goniometers fed total pressures to two Scanivalves which were connected to either a low-range or a high-range transducer, depending on the magnitude of the differential pressure being sensed by the goniometer.

Output data were printed as $\Delta\alpha$ or $\Delta\Psi$ (the local flow angle with inlet flow minus the local angle without inlet flow). By working with incremental angles, any errors in probe alignment were cancelled.

A more complete description of the model and test facilities is given in reference 6.

RESULTS AND DISCUSSION

As shown in figure 128, the .10 scale inlet model fuselage duplicated the XV-4B lift engine inlet arrangement and was a reasonable approximation to the fuselage adjacent to the inlets. The wind tunnel inlet airflow was scaled down from full-scale airflow by the model scale squared, assuming equal disk loadings.

To be consistent with thrust levels used in previous analyses (references 2 and 3), data from the inlet test were interpolated at the airflows corresponding to four-sixths of equivalent full-scale thrusts of 6,110 lb., 10,560 lb., and 14,920 lb. This was done because the four engines used only for lift were simulated, whereas the previous reports included the thrust from the two lift-cruise engines in addition to the four lift engines. Figure 130 presents the variation of full-scale airflow with thrust.

Data at zero airplane angle of attack only are analyzed herein, but reference 6 presents data taken at angles of attack between -8 degrees and +20 degrees.

Figures 131, 132 and 133 show the incremental downwash angles attributed to inlet airflow $(\Delta\epsilon)_{INLET}$ at the plane of symmetry at three vertical locations. Even at inlet airflows corresponding to maximum lift-engine thrust and at very low forward velocity, the increment in downwash was less than one degree at locations from zero to two horizontal tail $\overline{c}_H$ lengths ahead of $\overline{c}_H/4$. At the forward probe location (about $1.5\,\overline{c}_H$ lengths behind the aft inlet centerline), the maximum downwash increment was only 3-3/4 degrees. Increasing forward speed reduced these maximum effects much more than reducing inlet airflow to that corresponding to 40 percent of maximum engine thrust.

The low values of incremental downwash measured by the goniometers prompted a visual survey with a string wand using maximum inlet flow and low tunnel airspeed. This survey verified that the influence of the inlet flow was negligible a short distance away from the inlet and that there was noticeable turbulence aft of the inlets.

At the forward location, and to a lesser degree at the intermediate location of the centerline rake, the downwash increment was larger at the height of the horizontal tail than it was at 30 inches (full-scale) higher or lower. This decrease nearer the inlet may be the result of the probes being located in a system of vortices caused by the inlet flow. Insufficient data are available to map such a vortex pattern.

At the aft location of the centerline rake, incremental downwash generally did not decrease much with height above the fuselage for the region where local angles were measured (figure 134).

Figure 135 shows how the incremental downwash varied with height at the fuselage station and lateral location of the horizontal tail tip. Again, as at the fuselage centerline, there is some indication of vortices aft of the inlets.

Some evidence to support the theory of a vortex system is shown in figure 136, where the spanwise variation of incremental downwash at the location of the horizontal tail is presented. Although the magnitude of the incremental downwash due to inlet flow is quite small (less than one degree at the peaks), a definite spanwise variation is noticed, with one major negative peak occurring at the same lateral location as the inlet centerline, another peak halfway between the inlet centerline and side of the fuselage, and a lesser peak between the side of the fuselage and the horizontal tail. These peaks decrease in magnitude with increase in freestream velocity and increase with increasing inlet flow.

Local angles of attack measured at the fuselage station and buttock plane where the leading edge of the wing $\overline{c}$ would be located (but about 27 inches, full-scale, below the airplane wing) show a maximum of about $2\frac{1}{2}$ degrees of upflow caused by inlet airflow. The upflow changes to a maximum of 1-1/3 degrees of downflow at about 46 inches (full-scale) outboard of the wing location, figure 137.

141

The nose probe showed that power effects on local angles of attack at the fuselage nose were small, figure 138. They are plotted against the thrust parameter $(1/C_T)^{1/2}$ used in previous XV-4B analysis reports to reduce some of the scatter in the data.

Figure 139 presents incremental sidewash angles ($\Delta\sigma$) at the airplane vertical tail location resulting from inlet airflow with the fuselage yawed -5 degrees and -10 degrees. The $\Delta\sigma$ are plotted against the thrust parameter $(1/C_T)^{1/2}$. Increasing the yaw angle changes the incremental sidewash from about 1/2 degree unfavorable to a maximum of 2-3/4 degrees favorable, apparently the result of swinging the probes across the turbulent flow (or a vortex system) in the wake of the inlet flow. Additional sidewash data are given in tabular form in reference 6.

TEST CONCLUSIONS

Incremental downwash $(\Delta\epsilon)_{INLET}$ at the fuselage centerline due to inlet airflow is almost negligible at distances up to two $\overline{c}_H$ lengths forward of $\overline{c}_H/4$ except at freestream q = 2 psf. At 1.5 $\overline{c}_H$ lengths aft of the inlets, the $(\Delta\epsilon)_{INLET}$ is a maximum of 3-3/4 degrees at q = 2 psf and maximum inlet flow.

Variation of $(\Delta\epsilon)_{INLET}$ with height above the fuselage is small, over the range tested, at the fuselage centerline as well as at the lateral location of the horizontal tail tip.

The spanwise variation of $(\Delta\epsilon)_{INLET}$ at the horizontal tail location indicates a possible system of vortices in the wake of the inlet flow. Turbulent flow was seen in a visual probing of the flow angularities by means of a wand. The visual probing also verified the rapid decay of influence of the inlet flow with distance away from the inlets.

Incremental angles of attack (due to inlet flow) in the region just below the location of the airplane wing varied from a maximum upflow of $2\frac{1}{2}$ degrees at the inboard probe (at the $\overline{c}_w$) to about one-half as much downflow just outboard of $\overline{c}_w$, possibly indicating a vortex near the fuselage. Data from a probe just ahead of the fuselage showed only small power effects.

At the location of the airplane vertical tail, sidewash caused by inlet flow varied from 1/2 degree unfavorable at -5 degrees yaw angle to 2-3/4 degrees favorable at -10 degrees yaw angle, a result of swinging the probes across the inlet wake when the model was yawed.

REVIEW OF XV-4B MODEL TESTS

This subsection contains summary information concerning the models and test facilities used to obtain aerodynamic data for the XV-4B airplane. A total of seven small model tests were conducted.

LOCKHEED HOVER TEST

The purpose of this test was to investigate the nozzle exit interference effects in hover. The test was conducted by Lockheed at their Georgia Division during 1966. Information concerning this test was obtained from reference 25.

The model used was an 0.14 scale, approximate version of the XV-4B. The general arrangement of the model is shown in figure 140. The model had a wing area of 2.04 square feet, and a wing span of 3.50 feet. The model was designed such that the lift nozzle thrust system is supported free of the model fuselage. This isolates the thrust being produced at the nozzles from the model interference loads. Six component data due to the interference loads were recorded. Inlet flow was not simulated.

The test arrangement used required that the model be held in a fixed, inverted position near the ground. The jet exhaust was directed vertically, and an adjustable board was located over the model to provide an artificial ground plane relative to the model exhaust flow. Height and attitude changes were simulated by adjustments in the position of the board.

LING-TEMCO-VOUGHT TEST 195

The purpose of this test was to determine the aerodynamic forces and moments acting on the airplane during the transition from hover to horizontal flight. This test was identified by LTV facility number 195, and a total of 453 runs were obtained during 294 wind tunnel occupancy hours. The information presented here is from reference 26.

The test was conducted in the LTV 7 x 10 foot Low Speed Wind Tunnel located in Dallas, Texas, during July and August 1965. This tunnel is a horizontal, atmospheric pressure, single-return, closed throat system. The test section is operated at speeds up to 240 miles per hour.

An 0.18 scale model of a proposed modification to the XV-4A airplane was used for this test. The general arrangement of this model is shown in figure 141. The model had a wing area of 3.375 square feet, a mean aerodynamic chord of 0.798 feet, a wing span of 4.50 feet and a total jet exit area of 0.155 square feet. Vertical thrust was simulated by exhausting compressed air through six openings in the bottom of the model fuselage. The propulsion system was an integral part of the model, and inlet flow was not simulated.

The model was supported in the test section on the LTV conventional three support system, figure 142. A compressed air induction pipe was used as the rear support. The external balance system is of the pyramidal type. Six component data was recorded. Conventional corrections were made to the data for tunnel wall and support system tare effects. However, no correction was made to the data to allow for possible interference effects due to jet and tunnel wall interaction.

LANGLEY TEST 178

The purpose of this test was to define the aerodynamic characteristics of the XV-4B in the powered and non-powered phases of conventional, VTOL and hover modes of operation. The test, identified as Langley Test 178, consisted of 287 data runs obtained during 160 hours of tunnel occupancy time. Information presented here was obtained from reference 11.

The test was conducted in the 17 foot test section of the NASA-Langley 7 x 10 foot tunnel during February and March 1967. This facility is a rectangular, sing-return, closed throat, atmospheric type tunnel. The tunnel has two test sections: a 7 x 10 foot and a 17 x 15.5 foot. The large section which was used for this test has a dynamic pressure capability of 1 to 14 pounds per square foot.

An 0.16 scale model of the XV-4B airplane was used for this test. The general arrangement of the model can be seen in figure 143. The model had a wing area of 2.667 square feet, a mean aerodynamic chord of 0.71 feet, a wing span of 4.0 feet and a total jet exit area of 0.1205 square feet. The model was built with the capability of being mounted on the sting support facing forward or backward. An alternate nose mounting arrangement was used to obtain data for low speed rearward flight.

The direct lift jet engine system of the XV-4B was simulated by using externally supplied compressed air to power six ejector units, figure 143. These units, designated TD-350, were built by Tech Development Corporation in Dayton, Ohio. The compressed air is supplied to the model through a pipe which passes through but does not touch the hollow sting support. The air is distributed to the individual ejectors where it exhausts through numerous small nozzles. The entrainment action of the exhausting primary air flow produces a secondary flow which enters through the model inlet. The combined primary and secondary airflow is then exhausted to freestream through the model exit. Each nozzle exit was instrumented with eight total pressure probes manifolded together and one static pressure probe to determine thrust.

The model was mounted on a six component strain gage balance which measured the combined effect due to aerodynamic and propulsion forces. The sting was singularly supported by a telescoping strut which extended through the floor to a remotely controlled pitch and yaw mechanism. The telescoping strut allowed the model to be positioned at various heights above the tunnel floor for hover testing. Also, to simulate the conditions of a model in the proximity of the ground, a continuous-loop, moving belt was located under the model. In operation, the ground belt surface speed is maintained at the same speed as the tunnel section airflow. The general arrangement of the test installation is presented in figure 144.

144

UNIVERSITY OF MARYLAND TESTS 488 AND 493

The main purpose of these tests was to investigate the deep stall aero-
dynamic characteristics of the XV-4B configuration and improve its longitudinal
stability and control characteristics. Based on the results of these tests
an afterbody strake was added to the XV-4B configuration. Test 488 was
conducted during the period of 12-20 June 1967, and a total of 78 data runs
were obtained during 56 hours in the tunnel. Test 493 was conducted during
the period 21-26 August 1967, and a total of 71 data runs were obtained in
42 wind tunnel occupancy hours. The results of these two tests were obtained
from references 28 and 29.

The tests were conducted in the University of Maryland 7.75 x 11 foot
Low Speed Tunnel. The model was supported on a three-strut support system
connected to an external six-component balance. The model used in these tests
was the same 0.16 scale model used in the Langley tests, figure 143. Engine
power was not simulated during these tests.

LANGLEY TEST 221

The primary purpose of this test was to evaluate the interference effects
due to power with an afterbody strake added to the XV-4B configuration. A
secondary purpose was to define the airplane characteristics in low-speed
sideward flight. The test consisted of 129 runs in 145 hours of tunnel
occupancy time. The results of this test were published in reference 12.

The test was conducted in the 17 foot test section of the NASA-Langley
7 x 10 foot Tunnel during March 1968. The model and test installation were
previously described for Langley Test 178 with two modifications. An aero-
dynamic strake was added to the model afterbody, and a special sting arrange-
ment was required to support the model for the sideward flight runs. The
general arrangement of these modifications is indicated in figure 145.

LANGLEY TEST 226

The purpose of this test was to define the aerodynamic characteristics
in the conventional flight regime (unpowered). The test consisted of 47 runs
made during 29 hours of tunnel occupancy time. Information concerning this
test was obtained from reference 30.

The test was conducted in the Langley 7 x 10 foot Low Speed Wind Tunnel
from 23 April to 29 April 1968.   The model was the same 0.16 scale one
used for all the Langley tests, figure 143. The model was sting mounted,
and six component force and moment data were acquired.

(A) FLOW → WING WAKE

JET ENTRAINMENT FLOW

JET PATH

JET VORTEX

(B) FLOW →

JET PATH IN TUNNEL

FREE AIR JET PATH

(C)

(D) FLOW →

SPLASH BOUNDARY
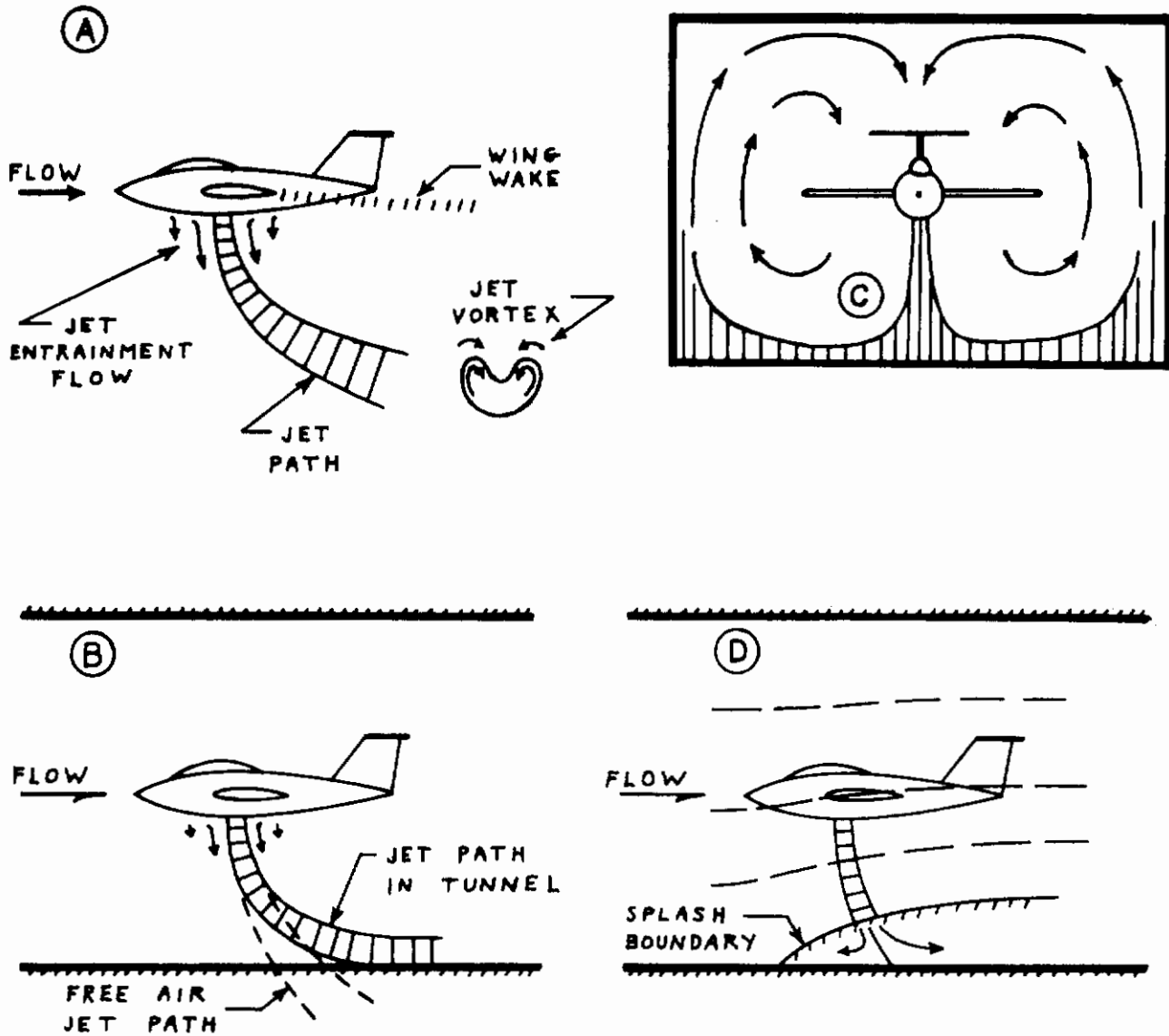
(A) FREE AIR EFFECTS: JET PATH, JET VORTEX, JET ENTRAINMENT FLOW, WING WAKE

(B) JET PATH IN FREE AIR AND IN WIND TUNNEL

(C) TUNNEL VORTEX FLOW RESULTING FROM JET CLIMBING WALL

(D) TUNNEL OBSTRUCTION CAUSED BY JET SPLASH ON TUNNEL FLOOR

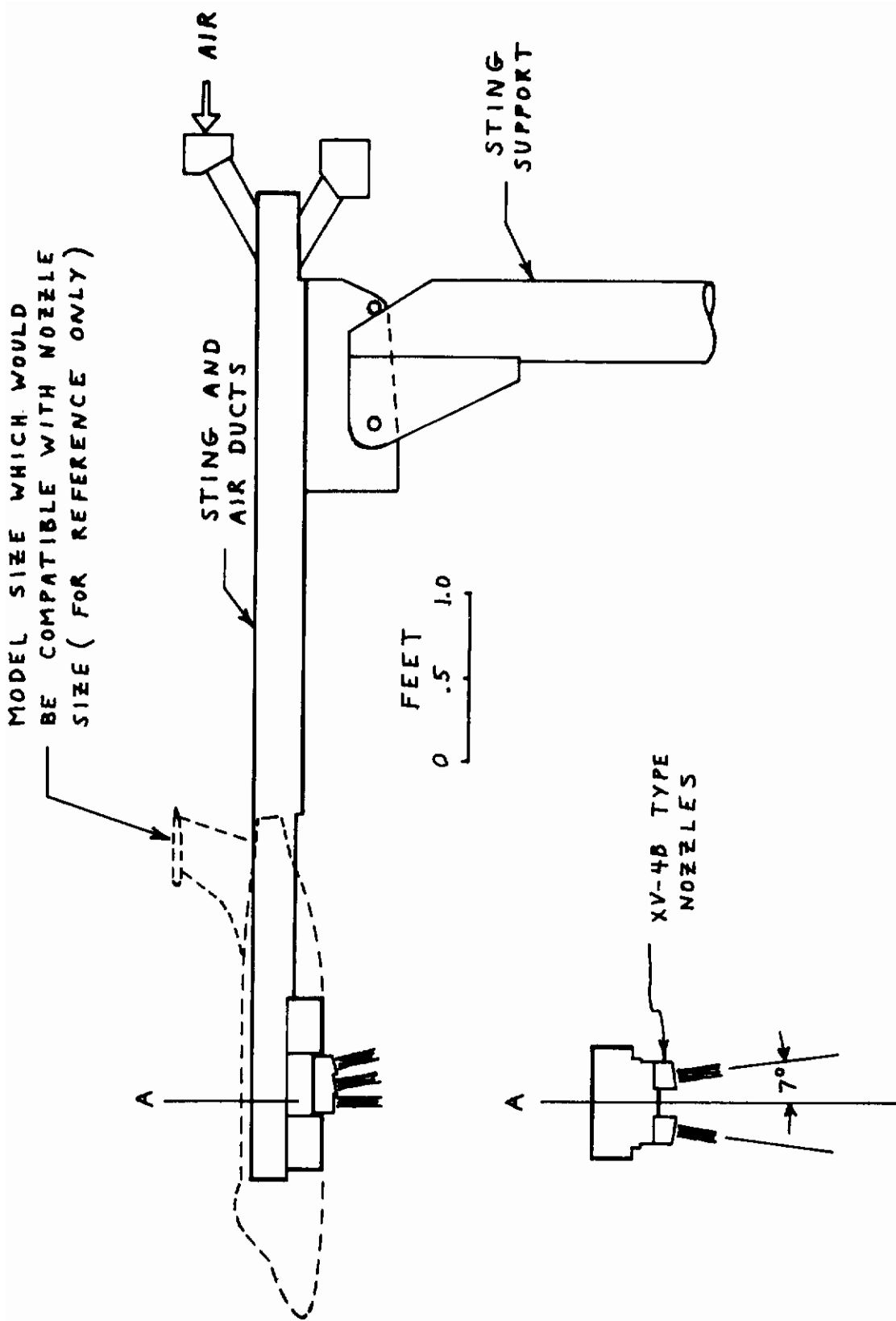Fig. 98. Sketches Illustrating Some Complex Aerodynamic Effects Associated with Jet VTOL Model Tests

146

MODEL SIZE WHICH WOULD BE COMPATIBLE WITH NOZZLE SIZE (FOR REFERENCE ONLY)

AIR

STING AND AIR DUCTS

STING SUPPORT

FEET
0 .5 1.0

XV-4B TYPE NOZZLES

A

7°

Fig. 99. Support System for XV-4B Type Exit Nozzle Model

147

NOTE: ALL DIMENSIONS IN INCHES

50 PERCENT POROUS PLATE
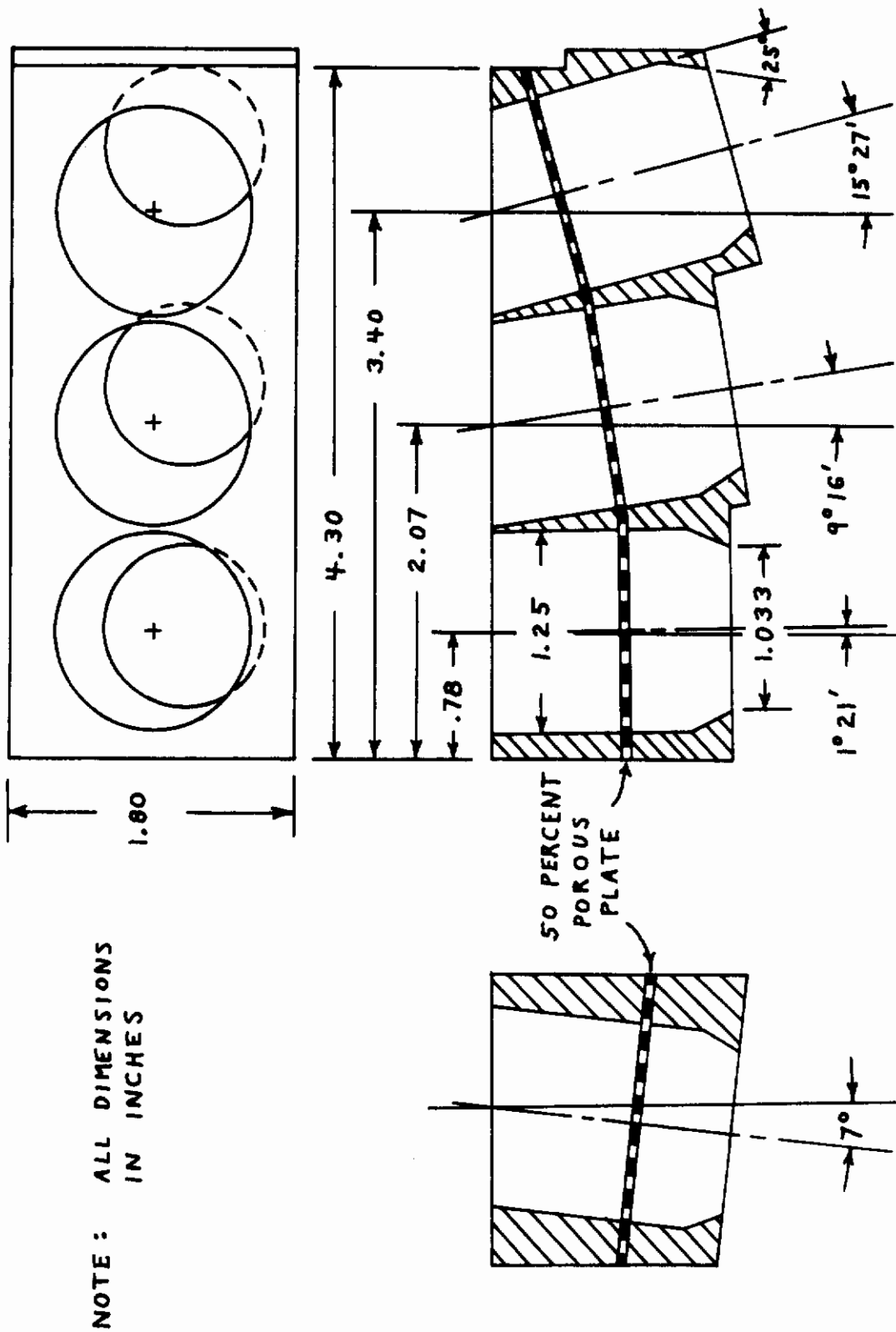
Fig. 100. XV-4B Type Exit Nozzle Geometry

EXISTING TUNNEL
WALLS 7.75 x 11 FT.

4.75 FT.

3.34 FT.

12 FT.

16 FT.

FLOW

WINDOW
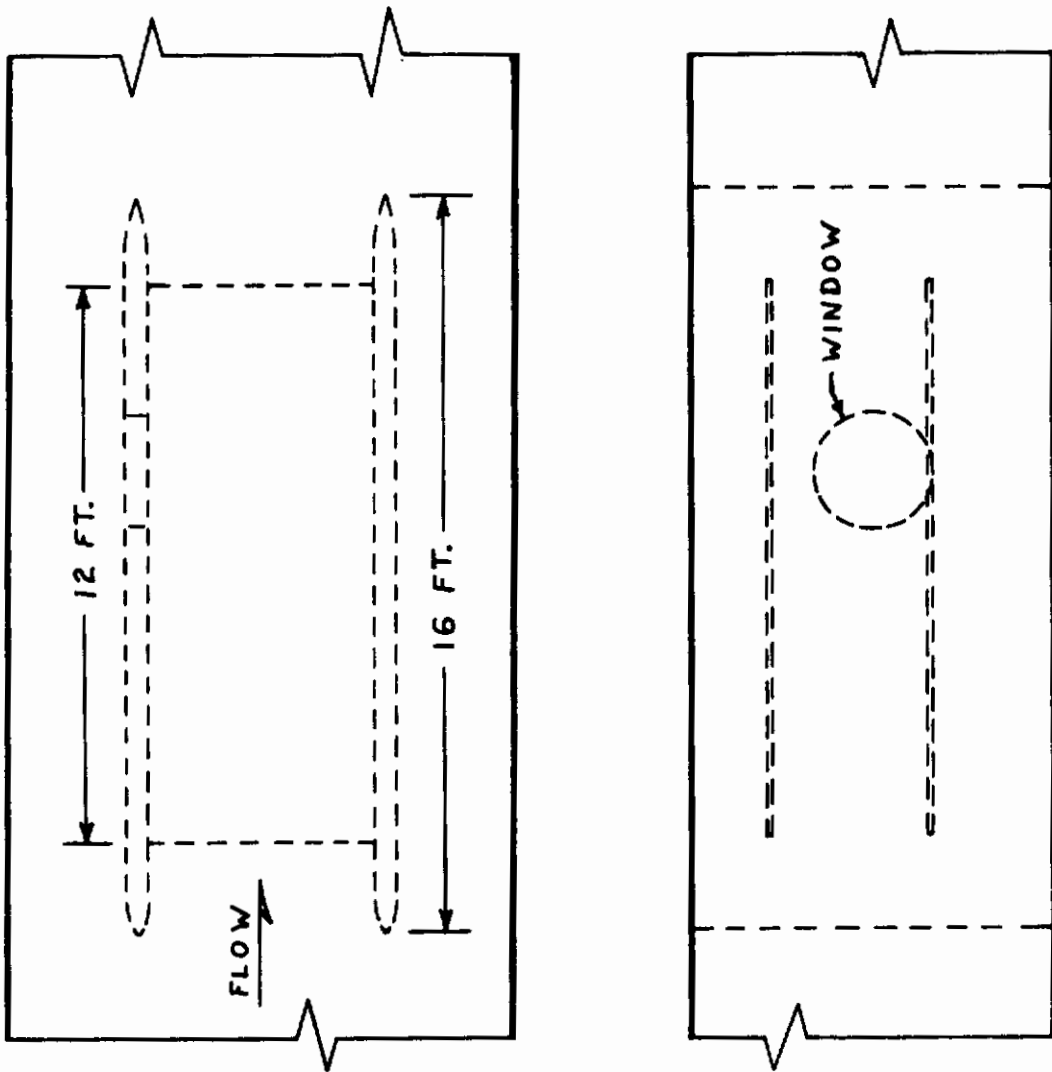
Fig. 101. Wind Tunnel Wall Geometry

149
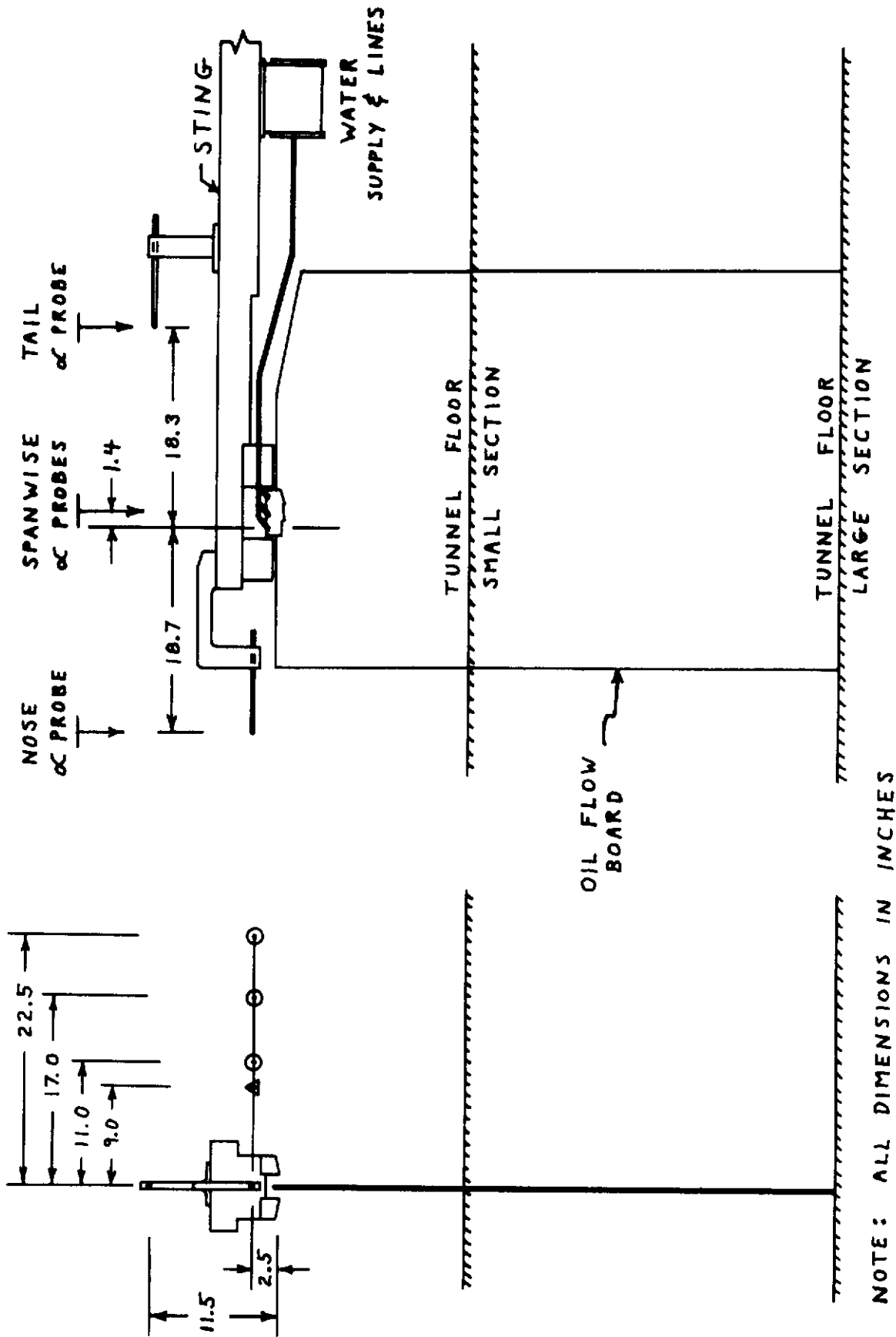
Fig. 102. Model Instrumentation

NOTE: ALL DIMENSIONS IN INCHES
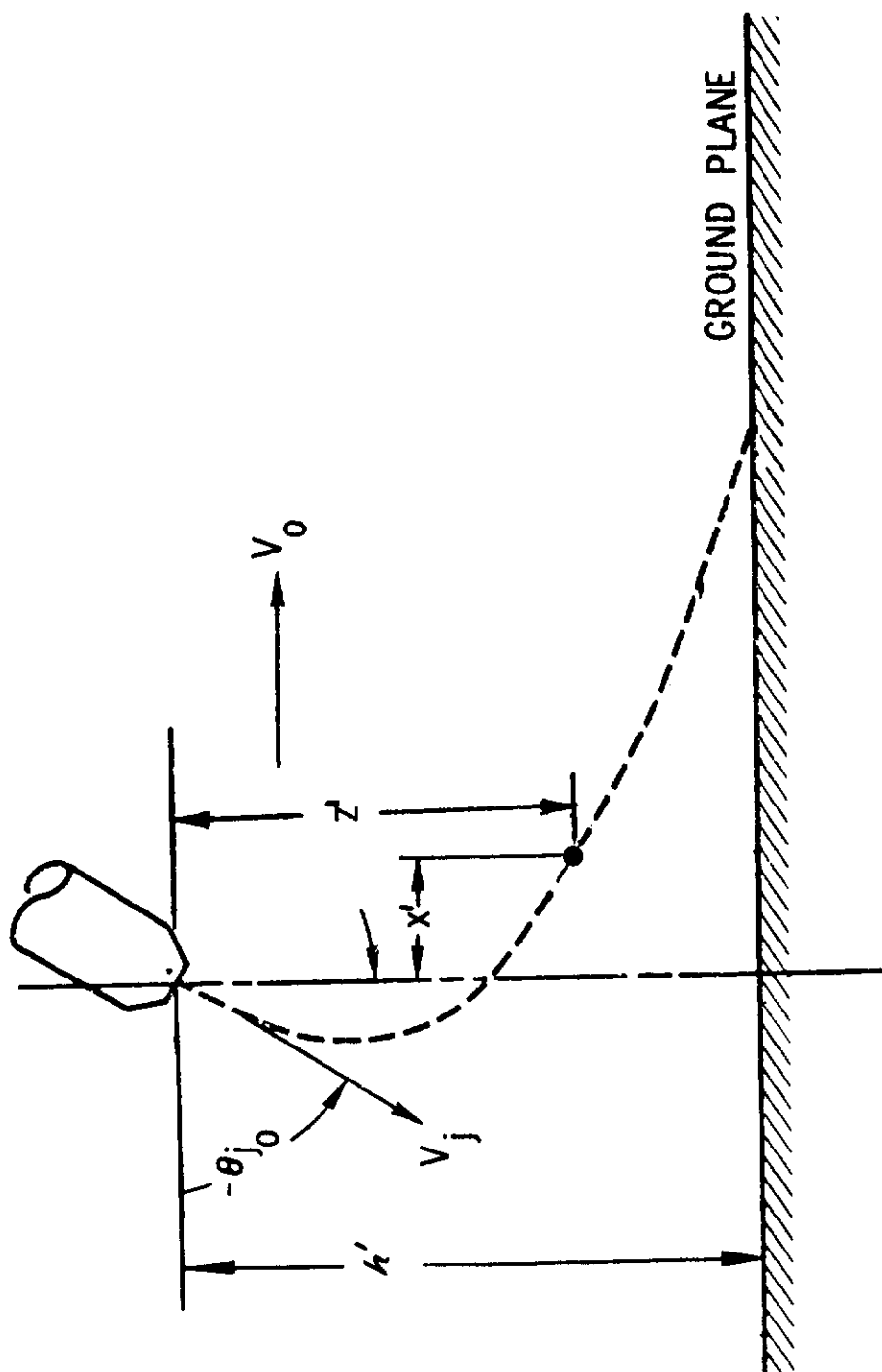
Fig. 103. Geometry of Jet Wake

151
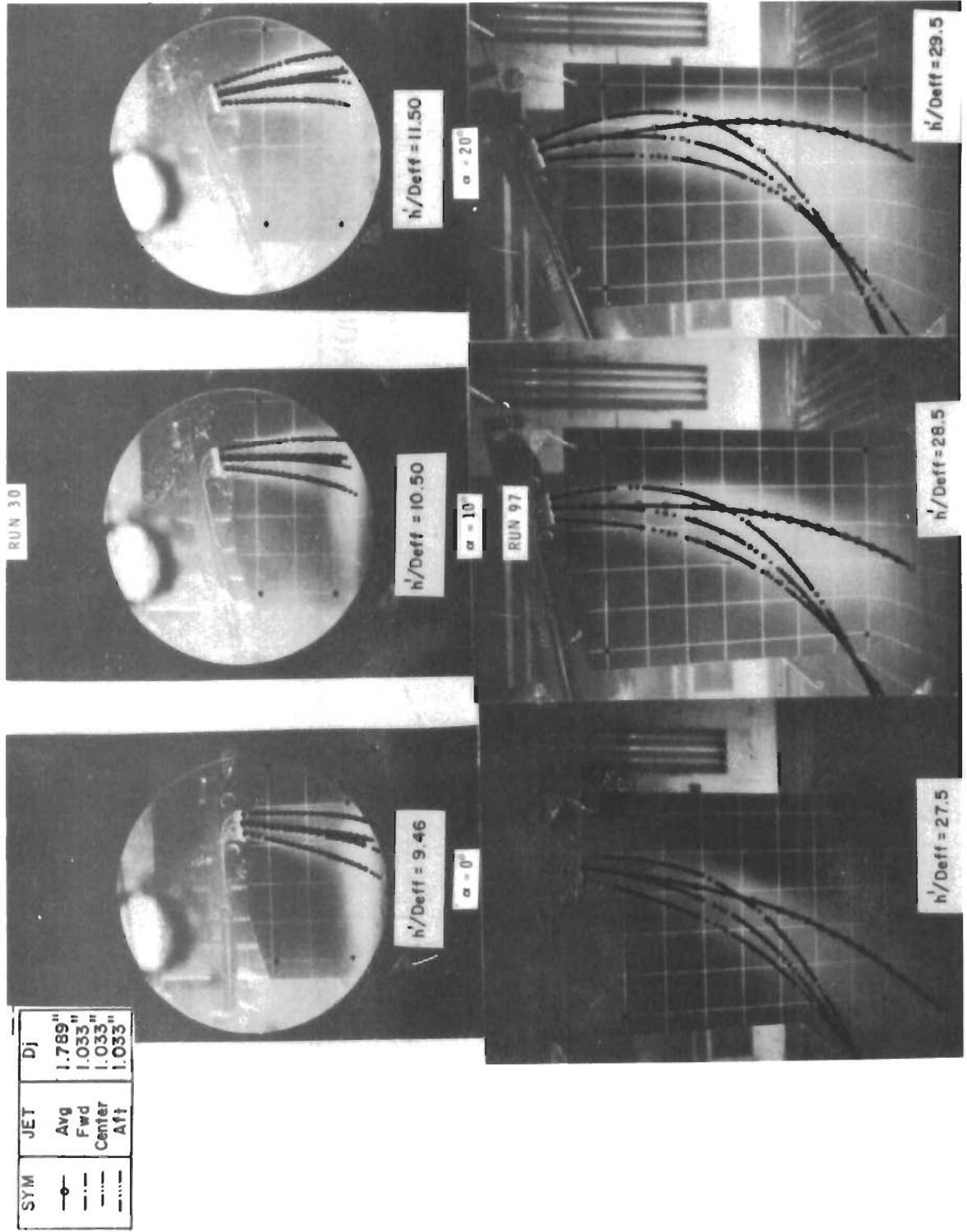
Figure 104. Comparison Ivanov's Trajectory and Observed Wake

152
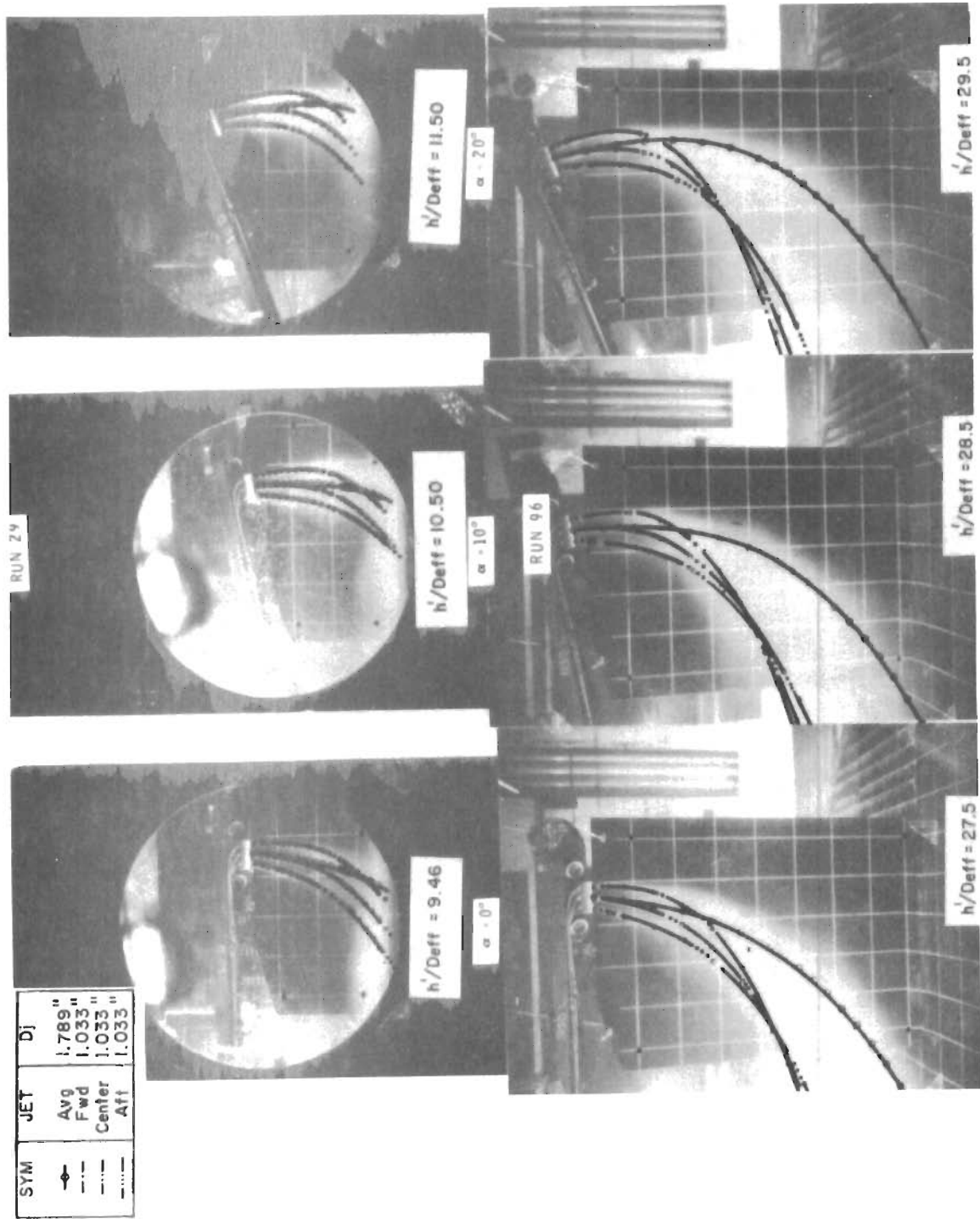
Figure 105. Comparison Ivanov's Trajectory and Observed Wake

153

Figure 106. Comparison Ivanov's Trajectory and Observed Wake

154

SYM	JET	Dj
—⬥—	Avg	1.789"
— —	Fwd	1.033"
— —	Center	1.033"
····	Aft	1.033"

RUN 27

h'/Deff = 11.50
α = 20°

h'/Deff = 10.50
α = 10°

h'/Deff = 9.46
α = 0°

RUN 94

h'/Deff = 29.5

h'/Deff = 28.5

h'/Deff = 27.5

6 JETS   Vo/Vj = .118   Vo = 130 fps   Dj = 1.033"
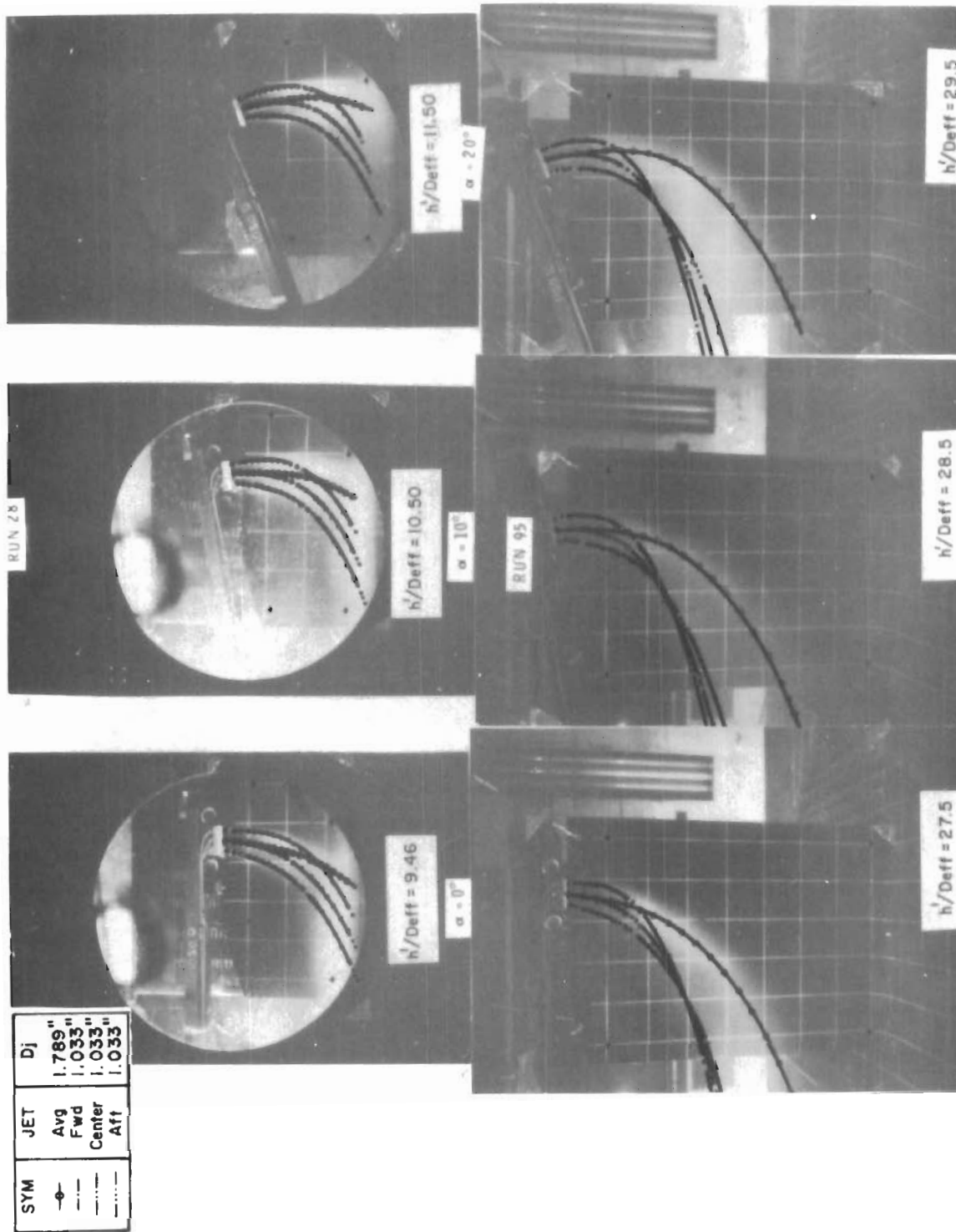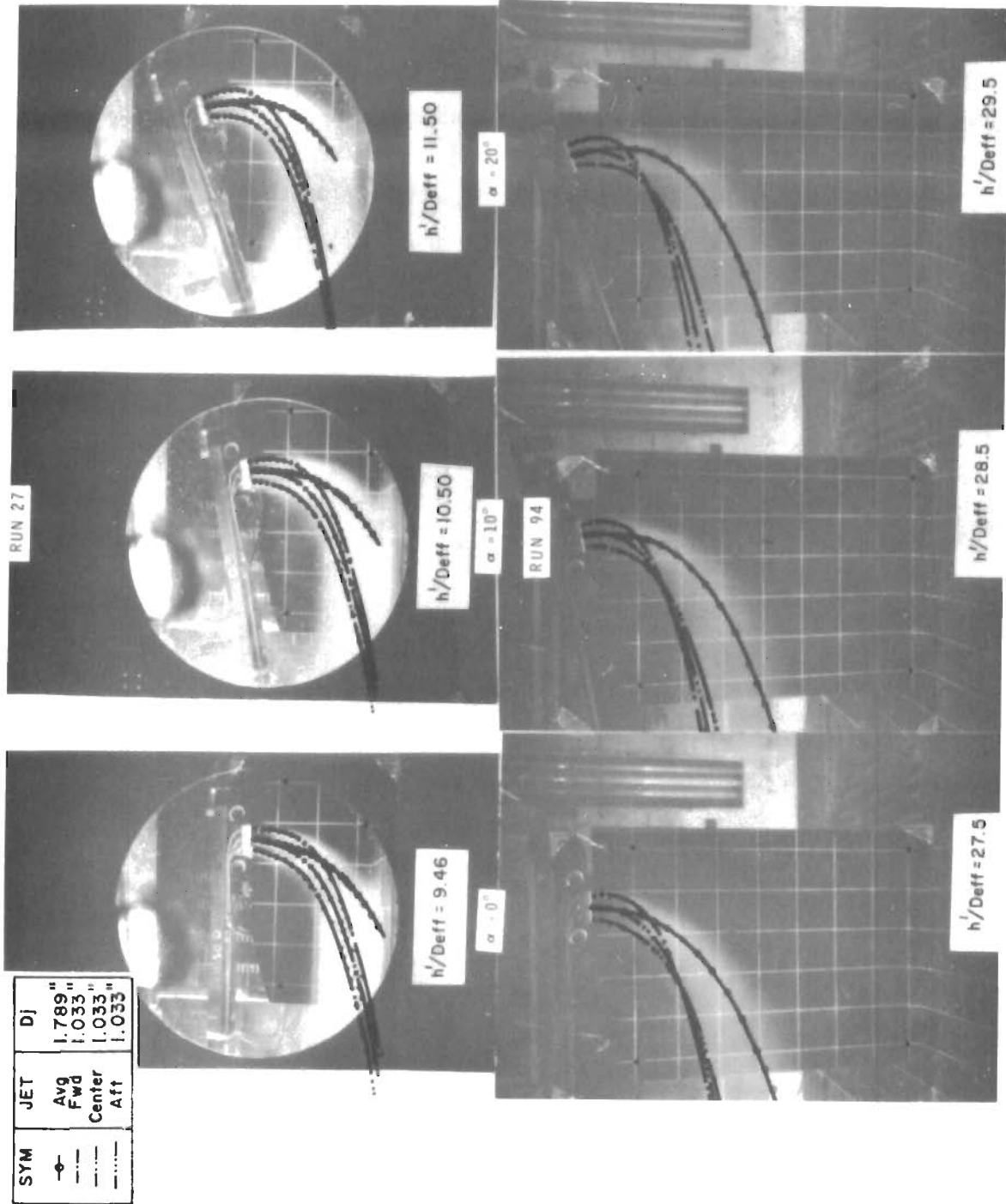
Figure 107. Comparison Ivanov's Trajectory and Observed Wake

155

Figure 106. Comparison Ivency's Trajectory and Observed Wake

6 JETS $V_o/V_j = .1450$ $V_o=159$ fps $D_j=1.033''$
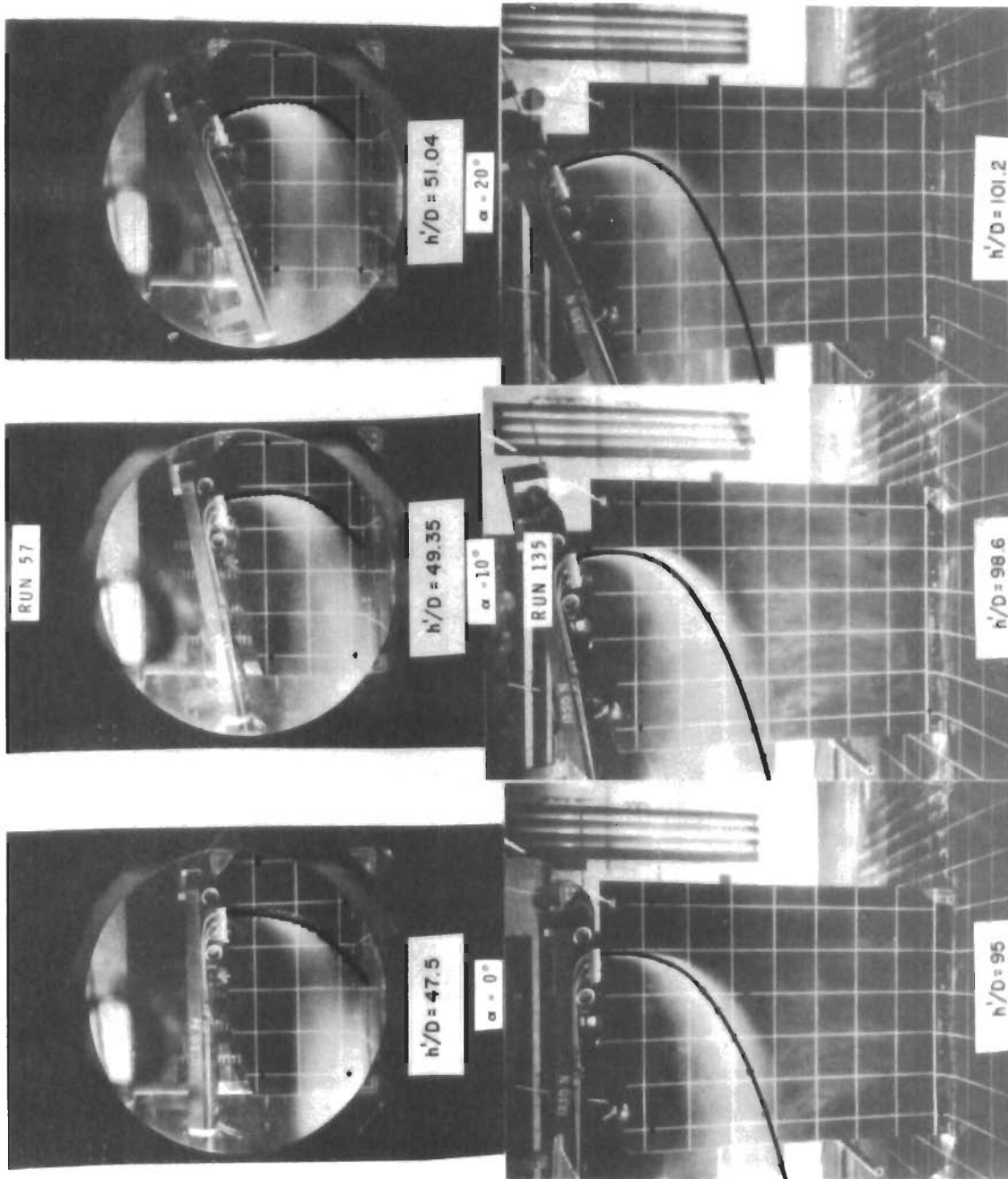
Figure 109. Comparison Ivanov's Trajectory and Observed Wake

2 JETS $V_o/V_j = .060$ $V_o = 65$ fps $D_j = 0.517"$

157
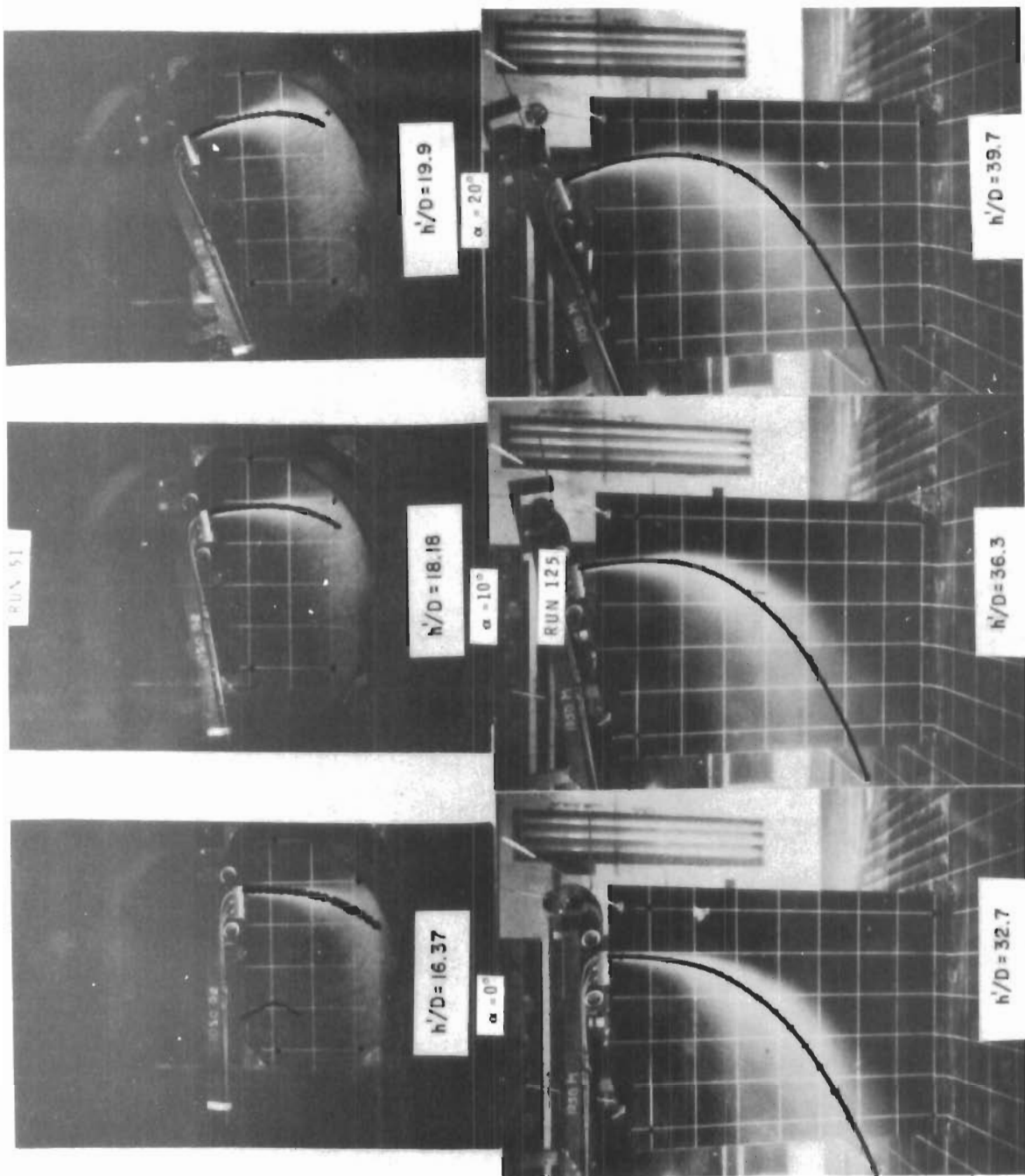
Figure 110. Comparison Ivanov's Trajectory and Observed Wake

158
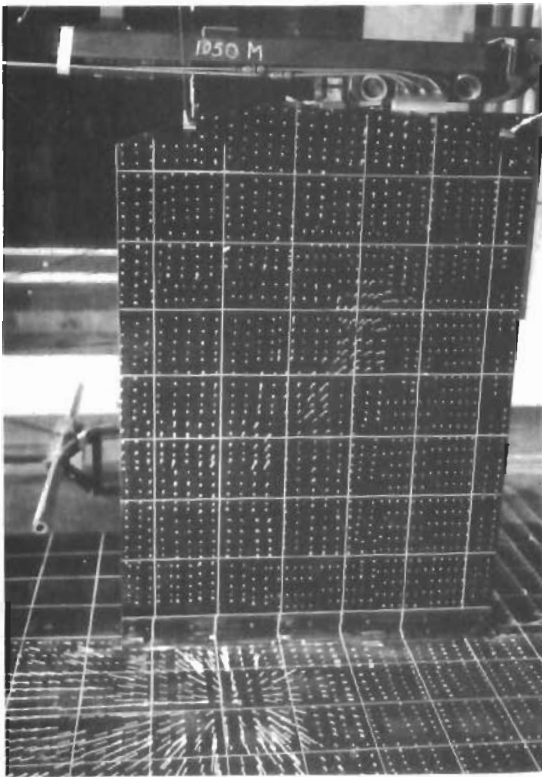
Run 128   Run 130
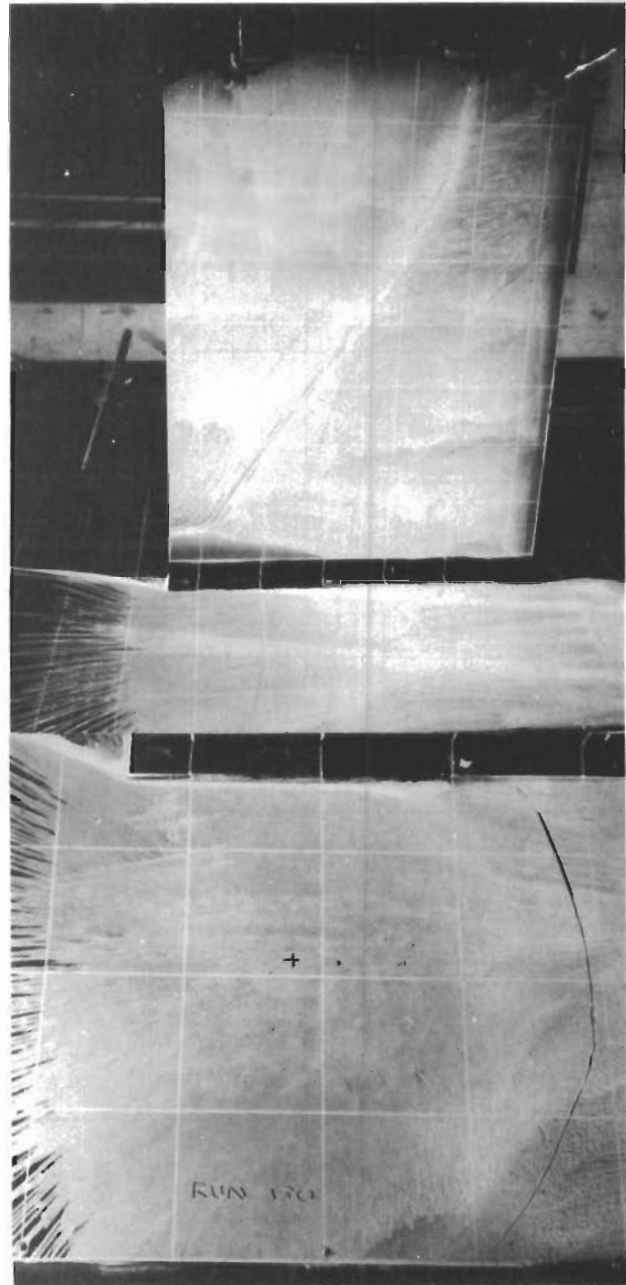
$$V_O/V_j = .038$$
$$h'/D = 47.5$$

Figure III.011 Photographs Locating Jet Impingement

159
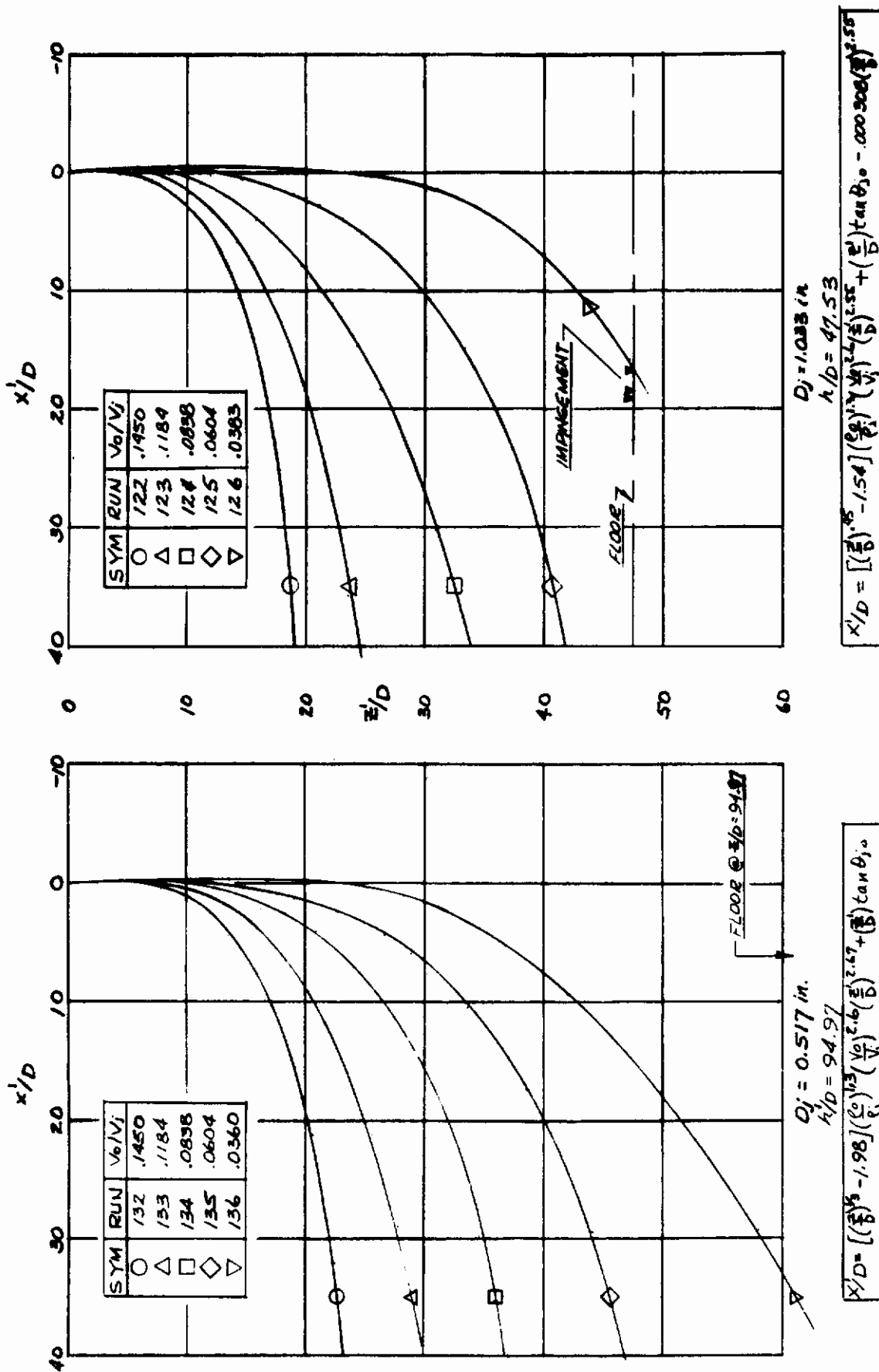
Fig. 112. Observed Jet Path
Large Tunnel, $\alpha = 0°$, $\theta_{jo} = 1.35°$
Single Jet
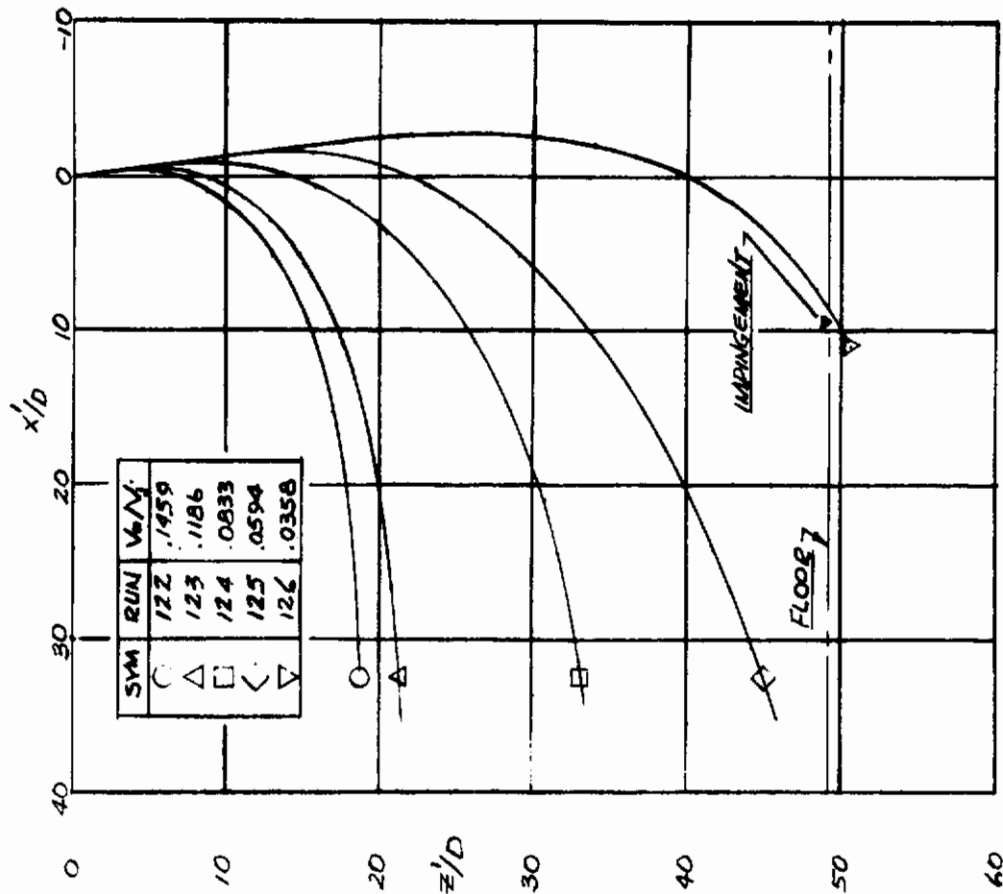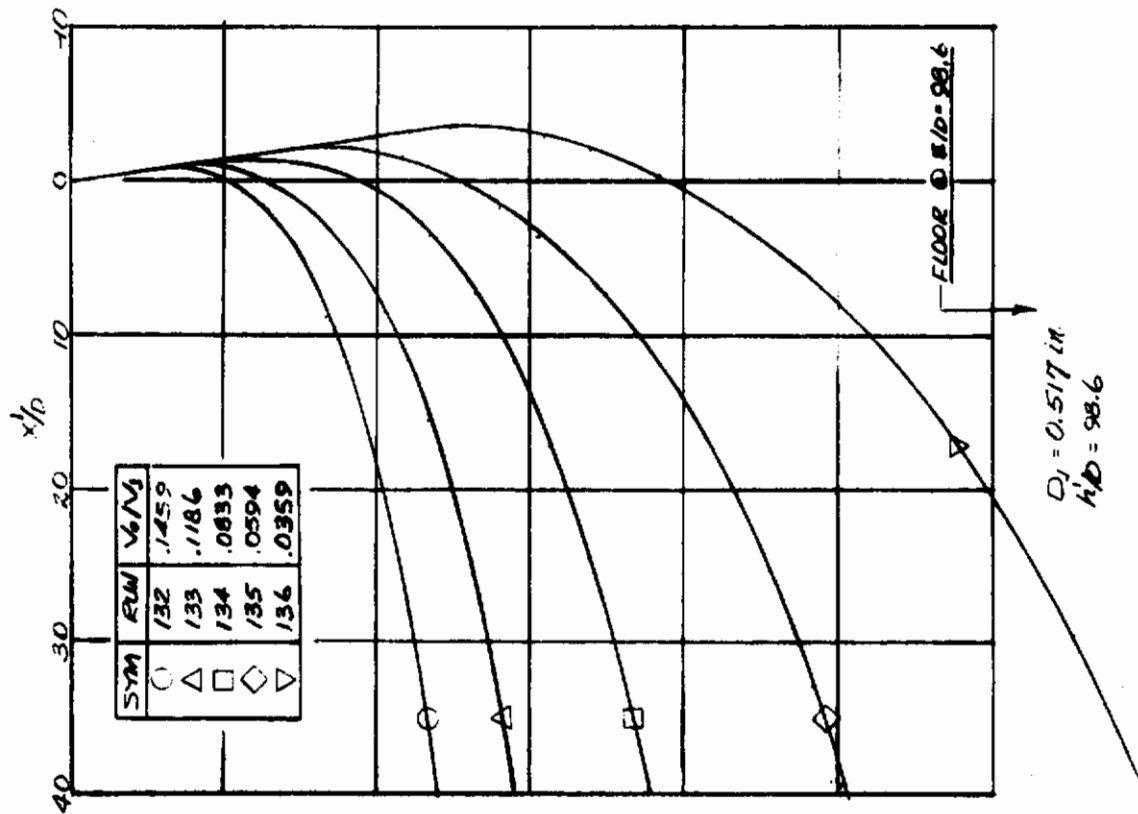
Fig. 113. Observed Jet Path
Large Tunnel, $\alpha = 10°$, $\theta_{jo} = -8.65°$
Single Jet

161
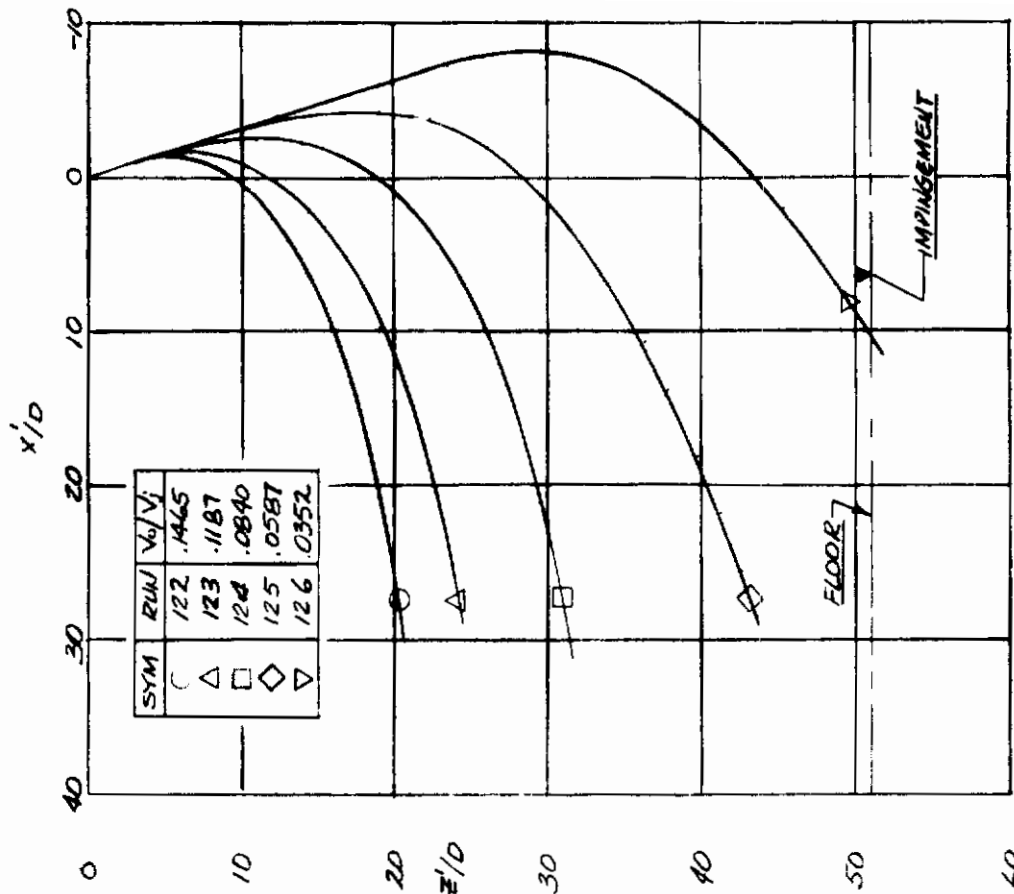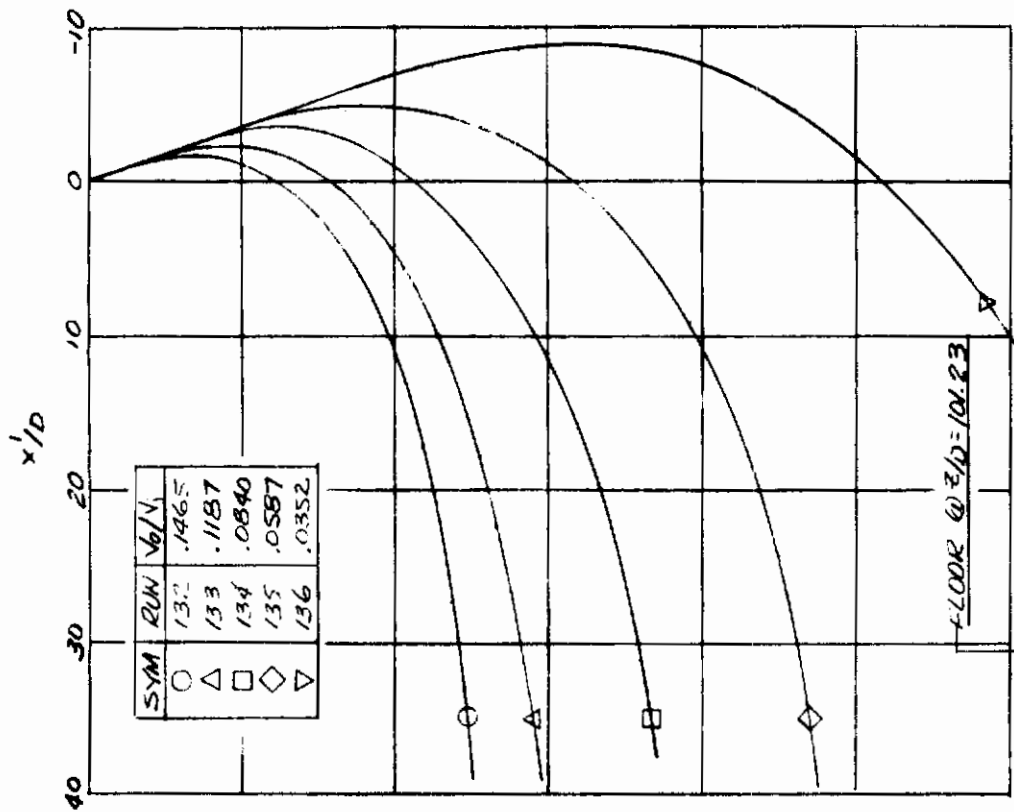
Fig. 114. Observed Jet Path
Large Tunnel, $\alpha = 10°$, $\theta_{jo} = -8.65°$
Single Jet
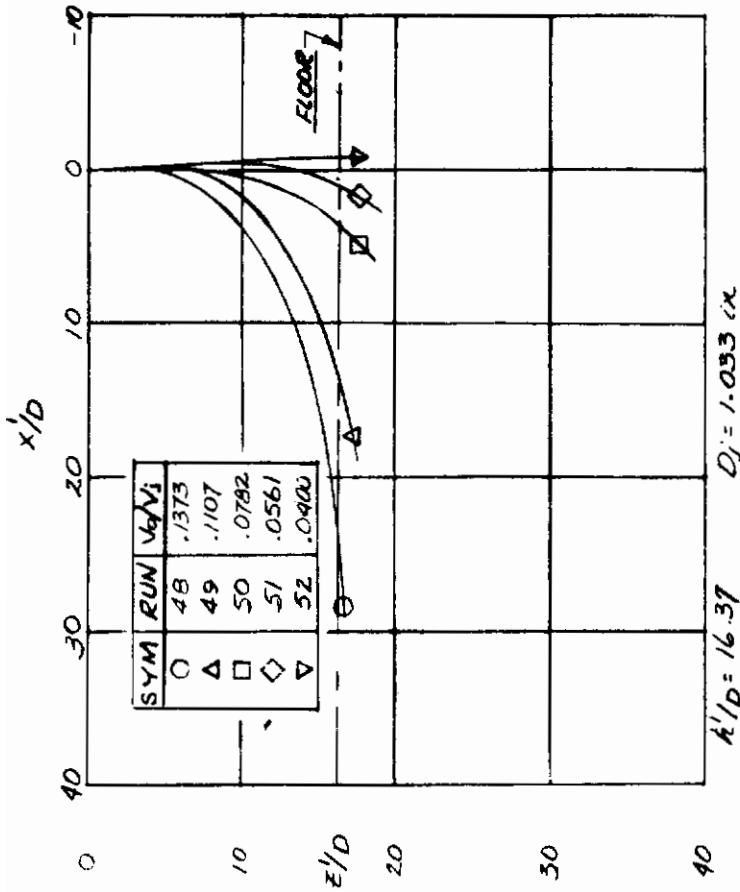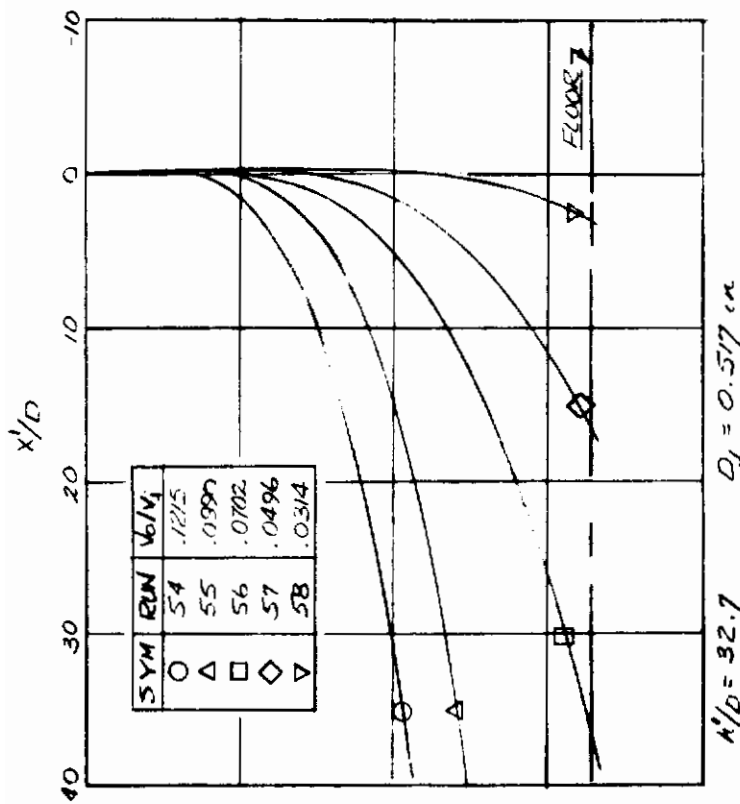
Fig. 115. Observed Jet Path
Small Tunnel, $\alpha = 0°$, $\theta_{jo} = 1.35°$

Single Jet

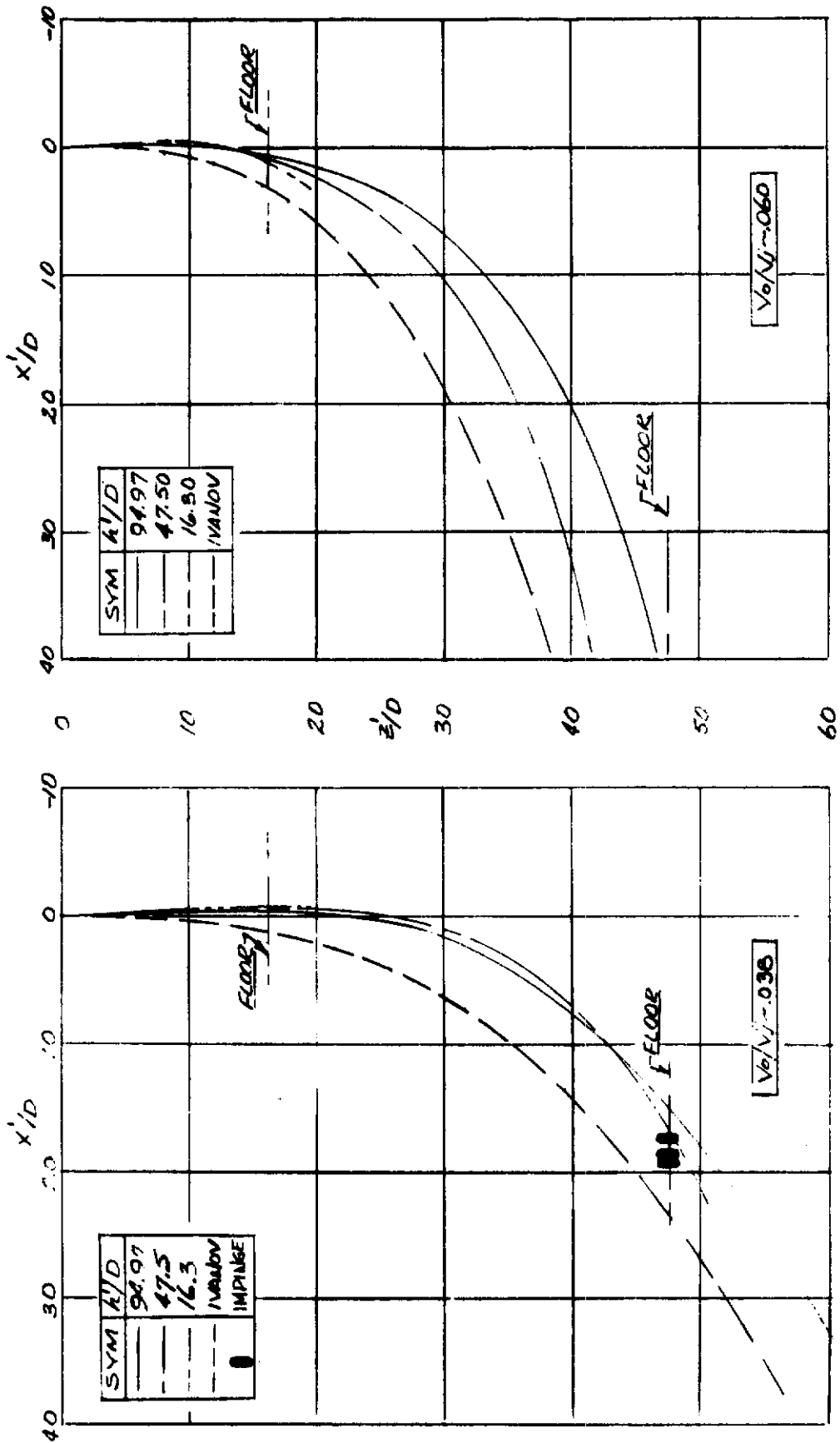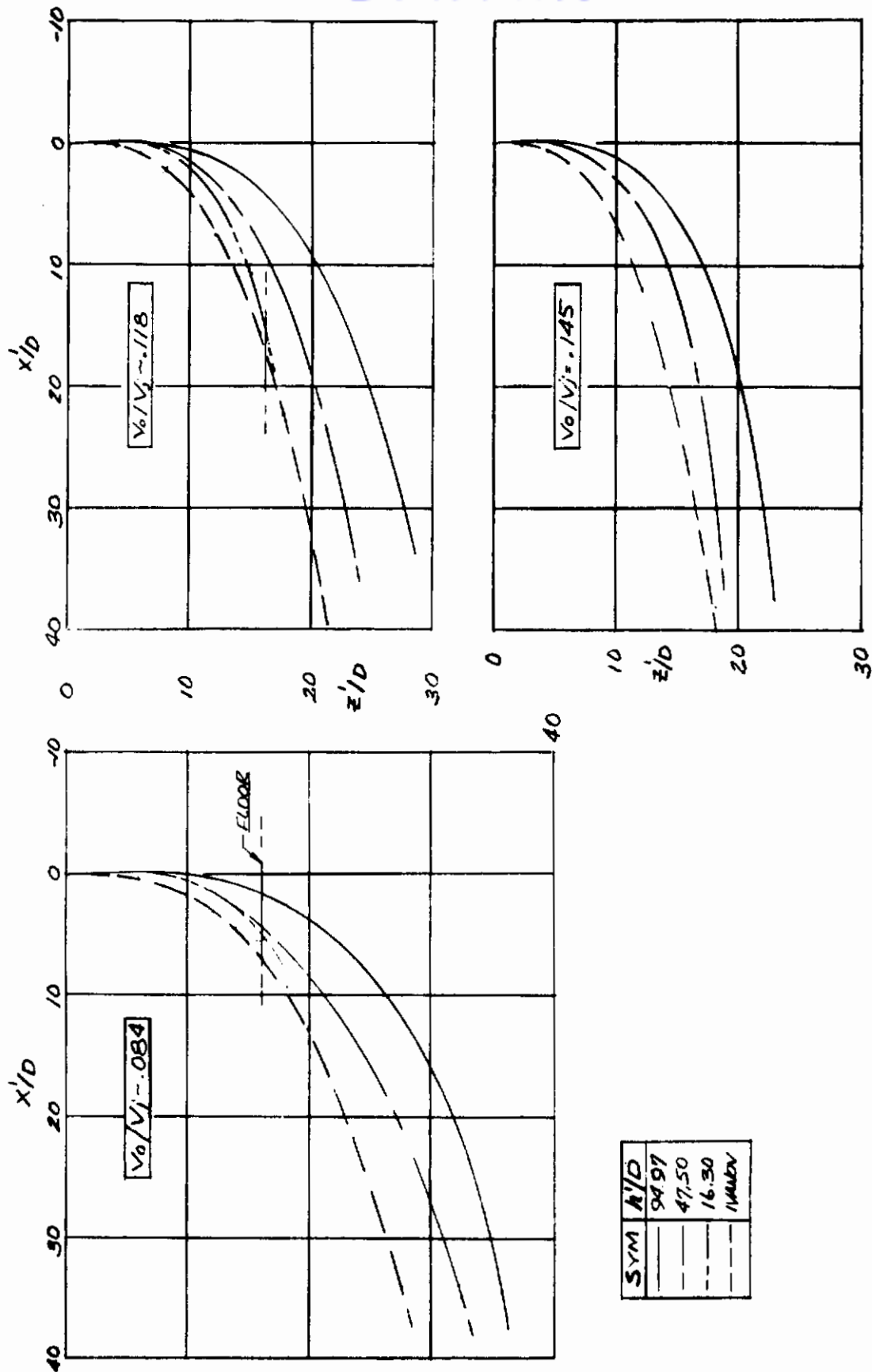Fig. 116. Effect of Floor Proximity
Observed Data, α = 0°

164

Fig. 117. Effect of Floor Proximity
Observed Data, $\alpha = 0°$
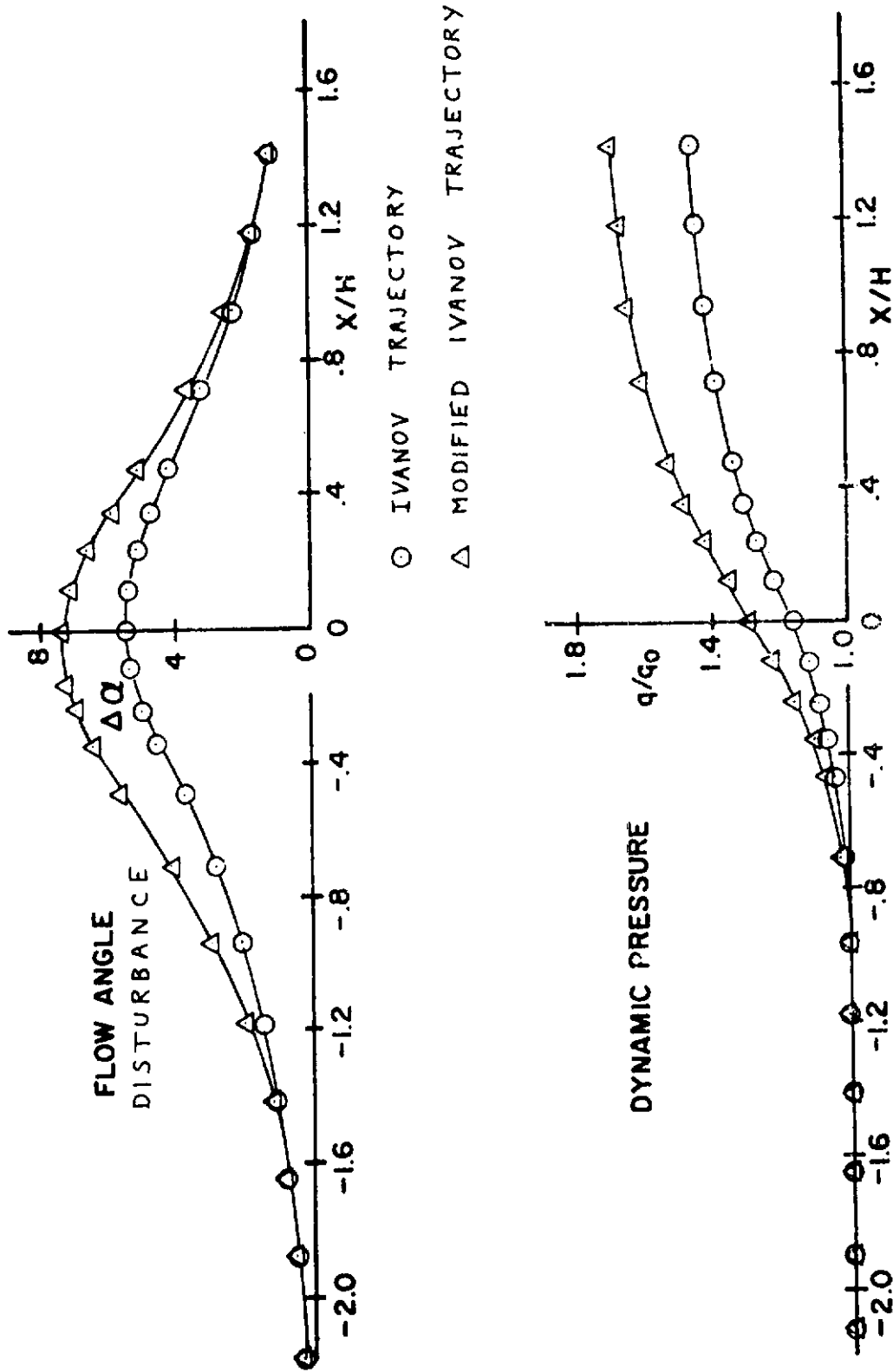
Fig. 118. Comparison of Tunnel & Flow Disturbances Computer Using
Ivanov and Modified Ivanov Trajectories

166

NOTE : SYMBOLS CORRESPOND TO LOCATION OF
INSTRUMENTATION AT NOSE, WING, AND TAIL

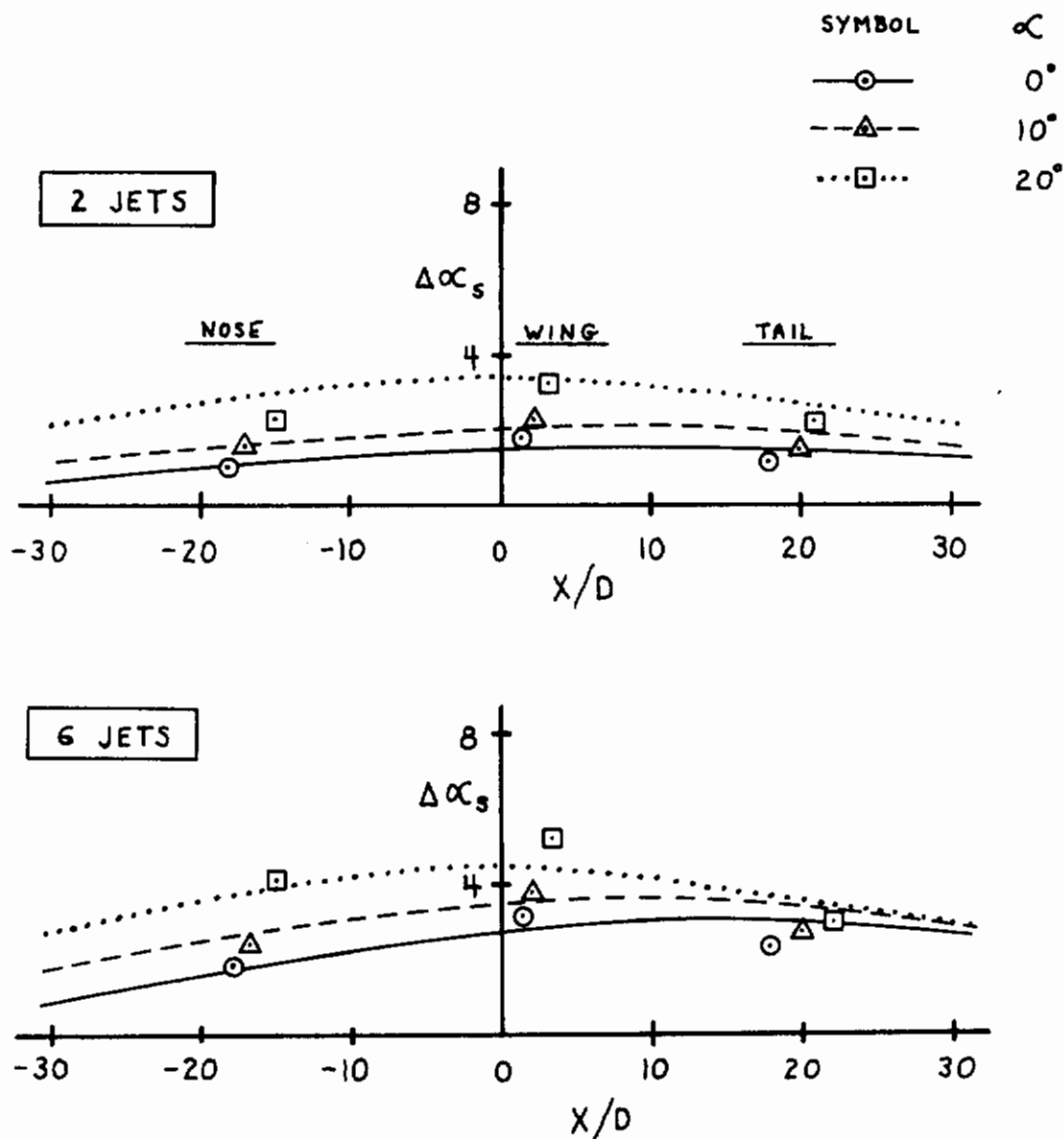|	z/D	y/D
NOSE	54	0
WING	50	10.6
TAIL	57	0

Fig. 119. Variation of Theoretical Jet Splash Flow Angle
Perturbations (7.75x11.0 Ft. Test Section; V_o/V_j=.0392)

167

NOTE : SYMBOLS CORRESPOND TO LOCATION OF
INSTRUMENTATION AT NOSE, WING, AND TAIL

	Z/D	Y/D
NOSE	23	0
WING	19	10.6
TAIL	26	0

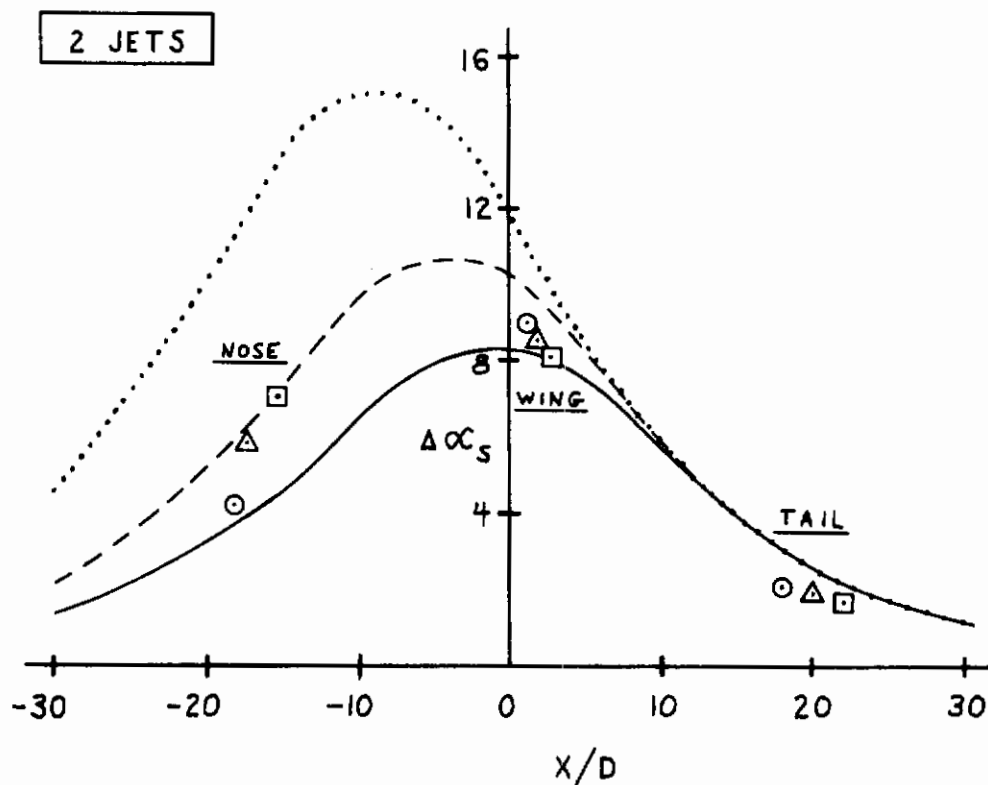| SYMBOL	α
—⊙—	$0°$
--△--	$10°$
···□···	$20°$

Fig. 120. Variation of Theoretical Jet Splash Flow Angle
Perturbations (3.34x4.75 Ft. Test Section; V_o/v_j=.0392)

168

NOTE: SYMBOLS CORRESPOND TO LOCATION OF
INSTRUMENTATION AT NOSE, WING & TAIL

	z/D	Y/D
NOSE	23	0
WING	19	10.6
TAIL	26	0

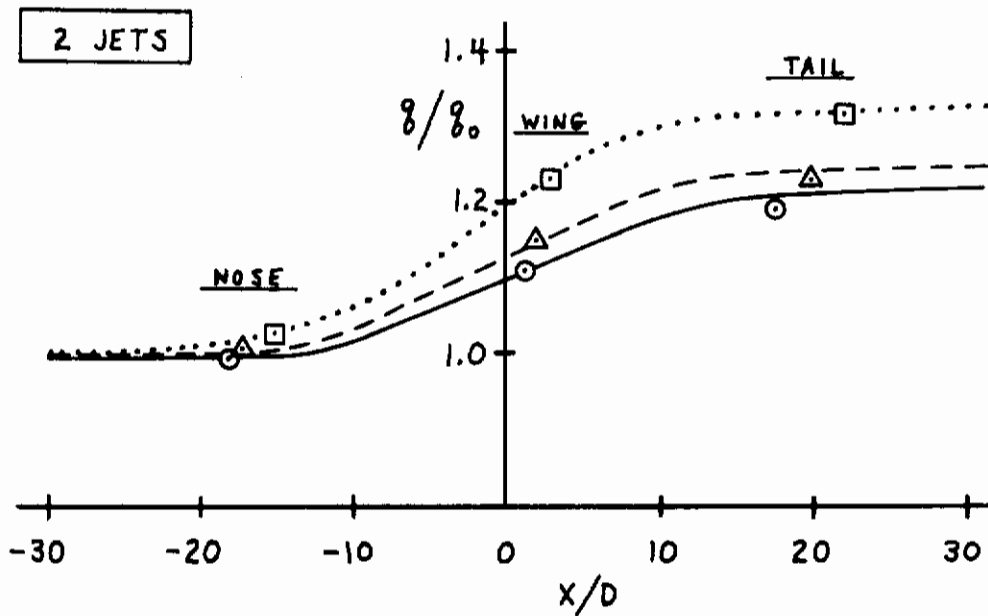| SYMBOL	α
—⊙—	0°
– –△– –	10°
···▢···	20°

2 JETS
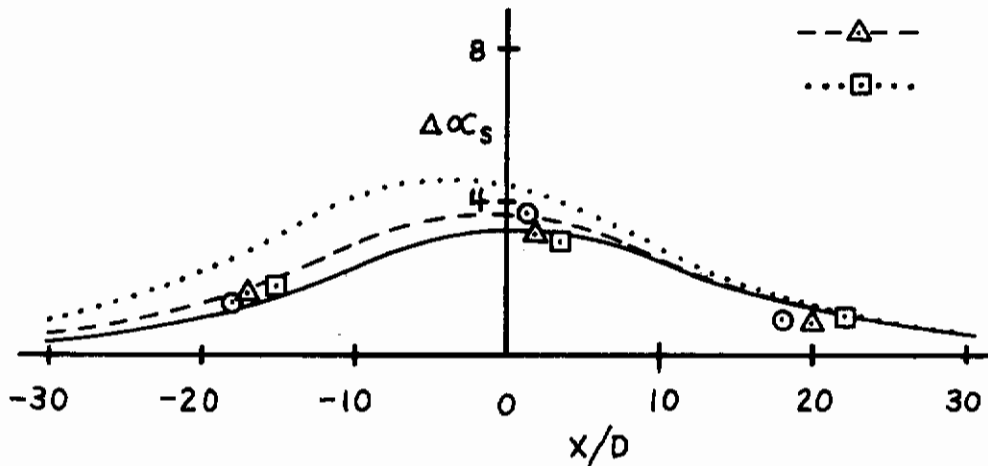
Fig. 121. Variation of theoretical Jet Splash Flow Angles
and Dynamic Pressures (3.34x4.75 Ft. Test Section; V_o/V_j=.0619

⊙ LARGE TEST SECTION (7.75 × 11 FT.)
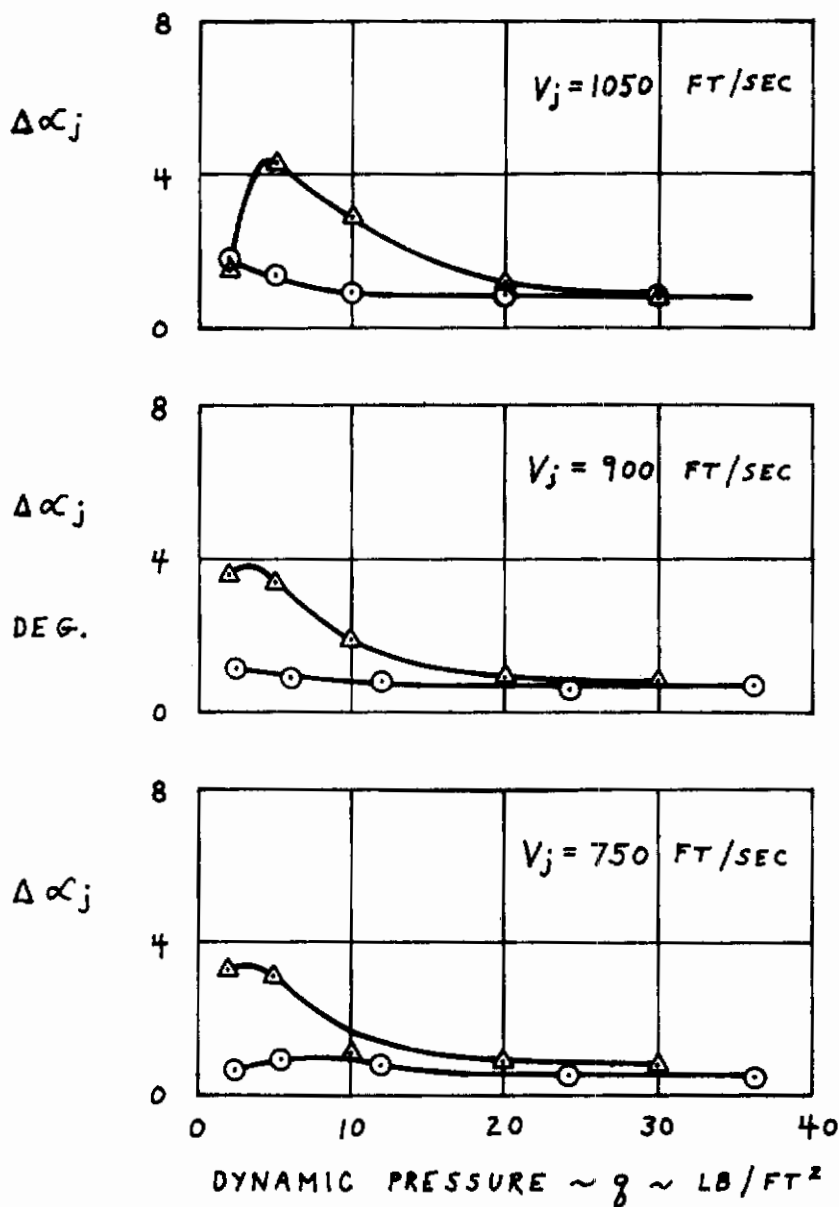△ SMALL TEST SECTION (3.34 × 4.75 FT.)

Fig. 122. Local Angle of Attack Increment due to Jet Flow
at the Nose Probe Location (α=0)

170
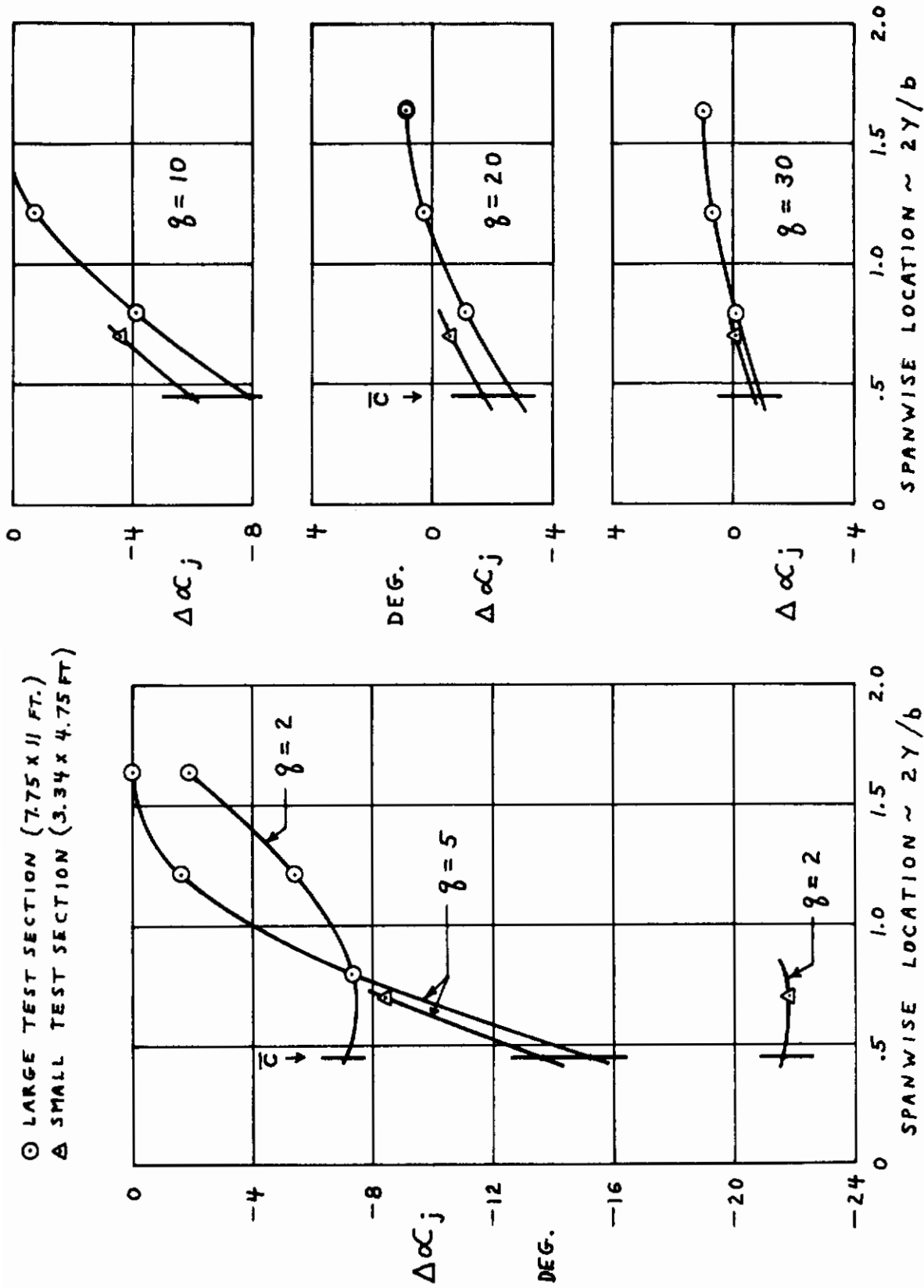
Fig. 123. Local Angle of Attack Increment due to Jet Flow at the Spanwise Probe Locations ($\alpha=0$; $V_j=1050$ Ft/Sec)

171
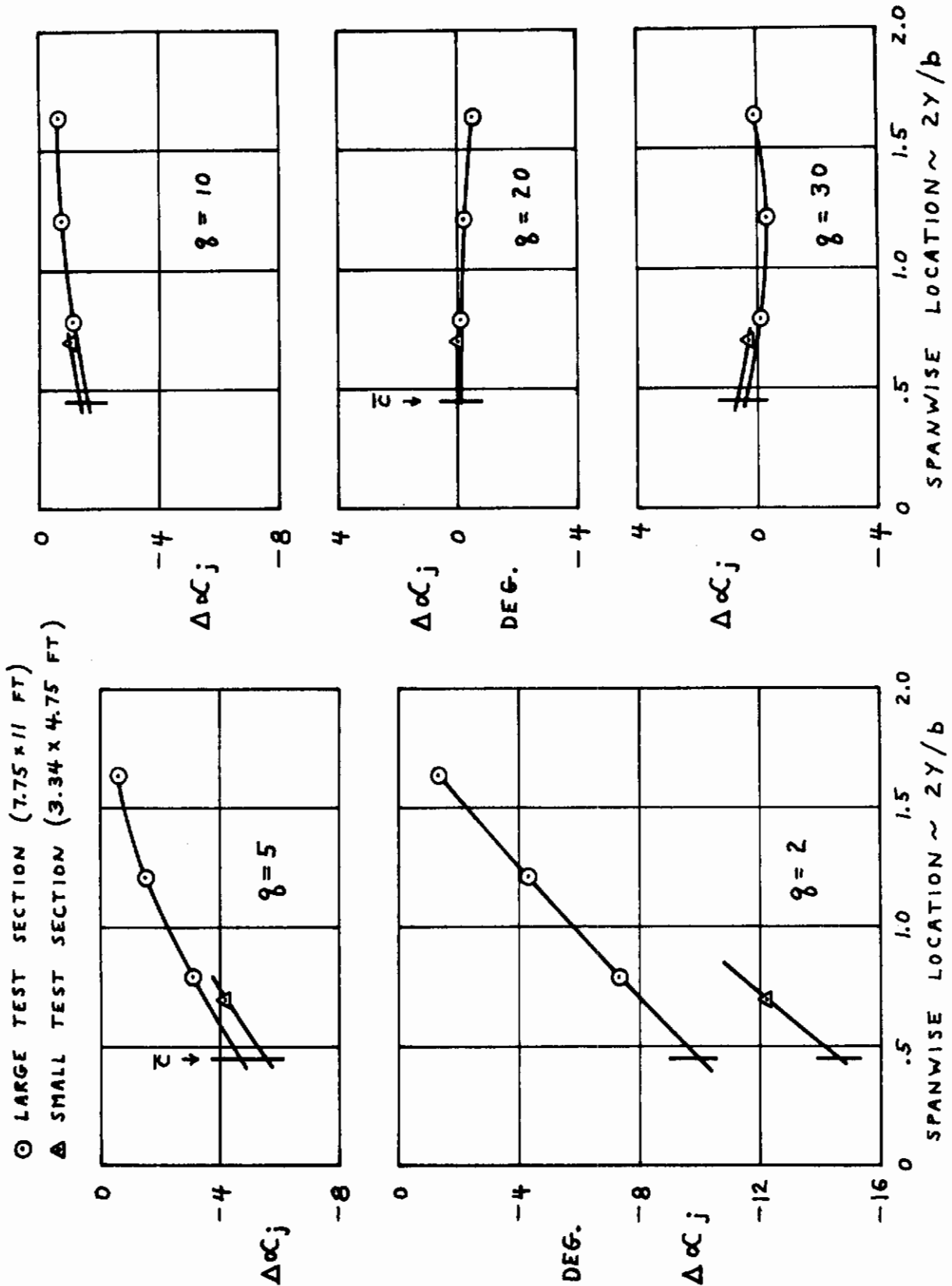
Fig. 124. Local Angle of Attack Increment due to Jet Flow at the Spanwise Probe Locations ($\alpha=0$; $V_j=750$ Ft/Sec)

172

⊙ LARGE TEST SECTION (7.75 × 11 FT.)
▲ SMALL TEST SECTION (3.34 × 4.75 FT.)

$\Delta \alpha_j$

DEG.

$V_j = 1050$ FT/SEC

$\Delta \alpha_j$

$V_j = 900$ FT/SEC

$\Delta \alpha_j$

DEG.

$V_j = 750$ FT/SEC

DYNAMIC PRESSURE ~ q ~ LB/FT²
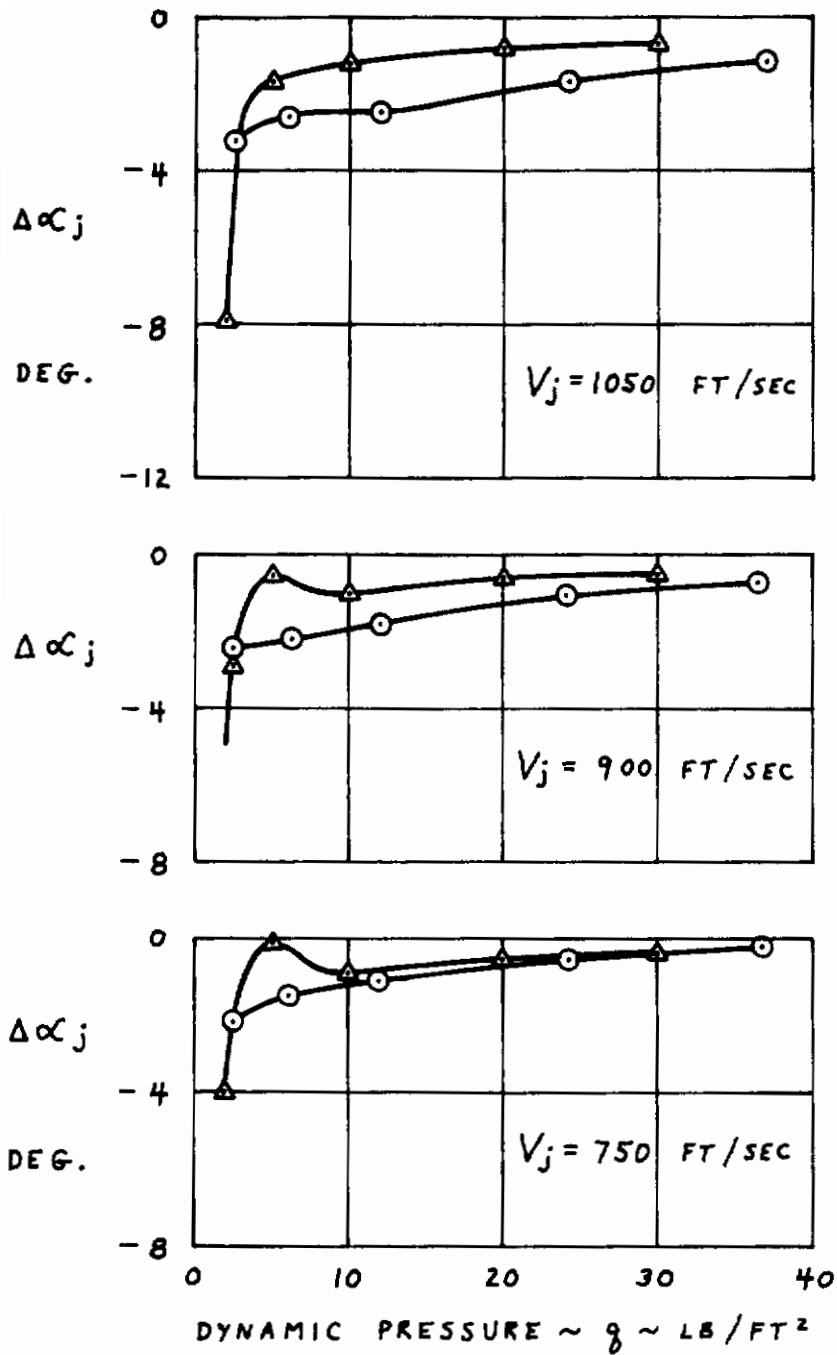
Fig. 125. Local Angle of Attack Increment due to Jet Flow
at the Tail Probe Location (α=0)

173
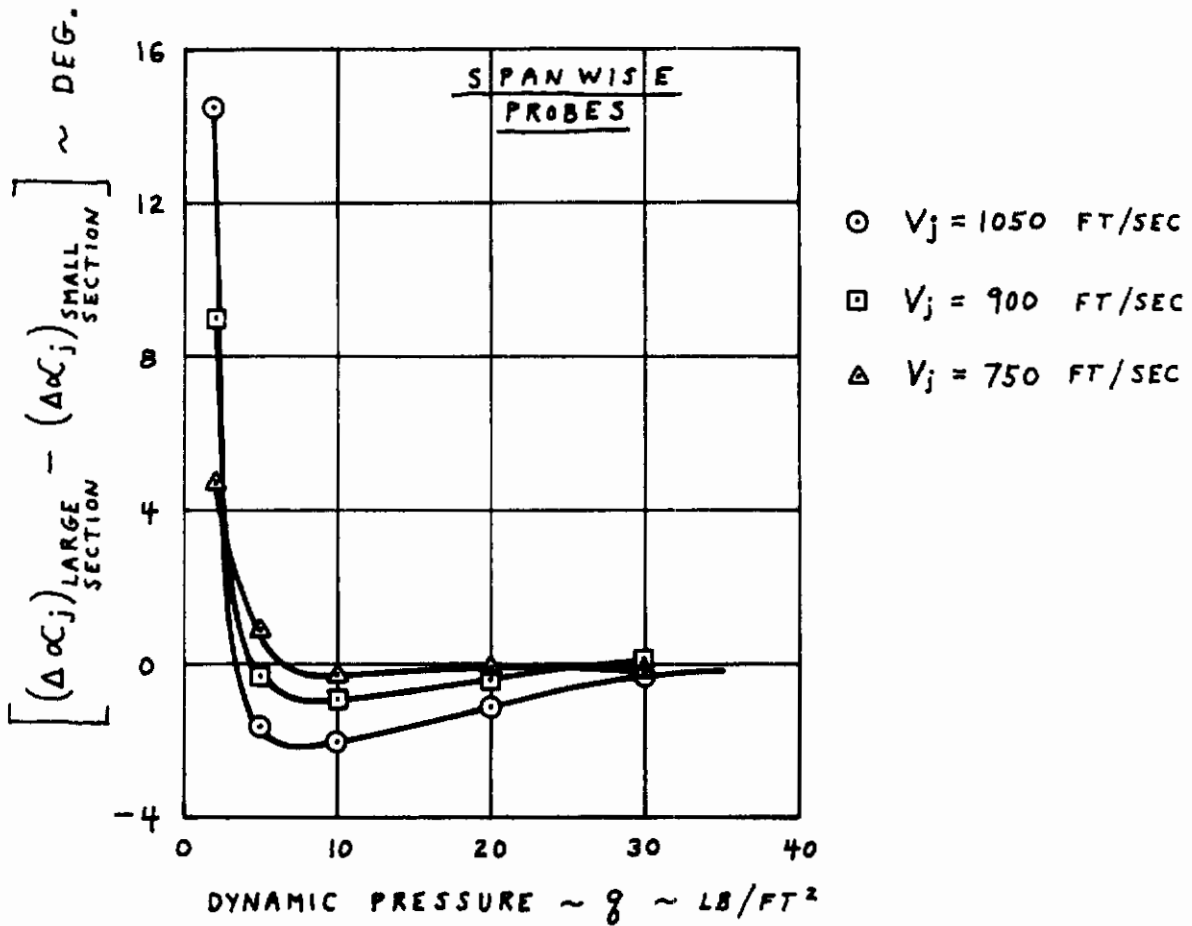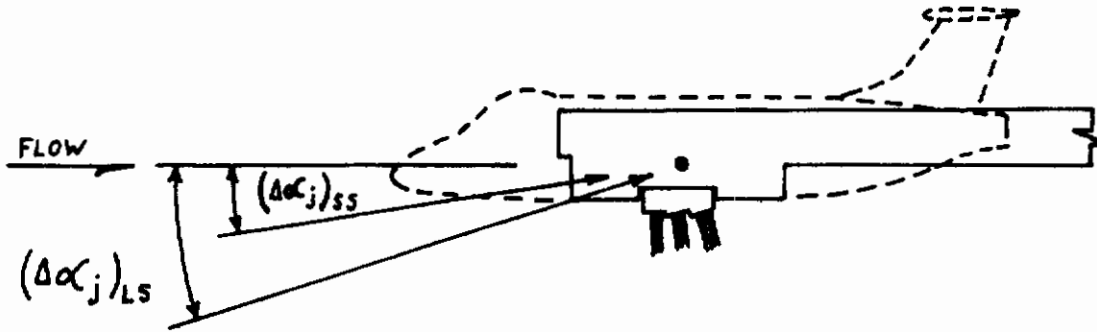
Fig. 126.   Increment in Local Angle of Attack at an Assumed Wing
m.a.c. Location due to Tunnel Walls ($\alpha=0$)

174
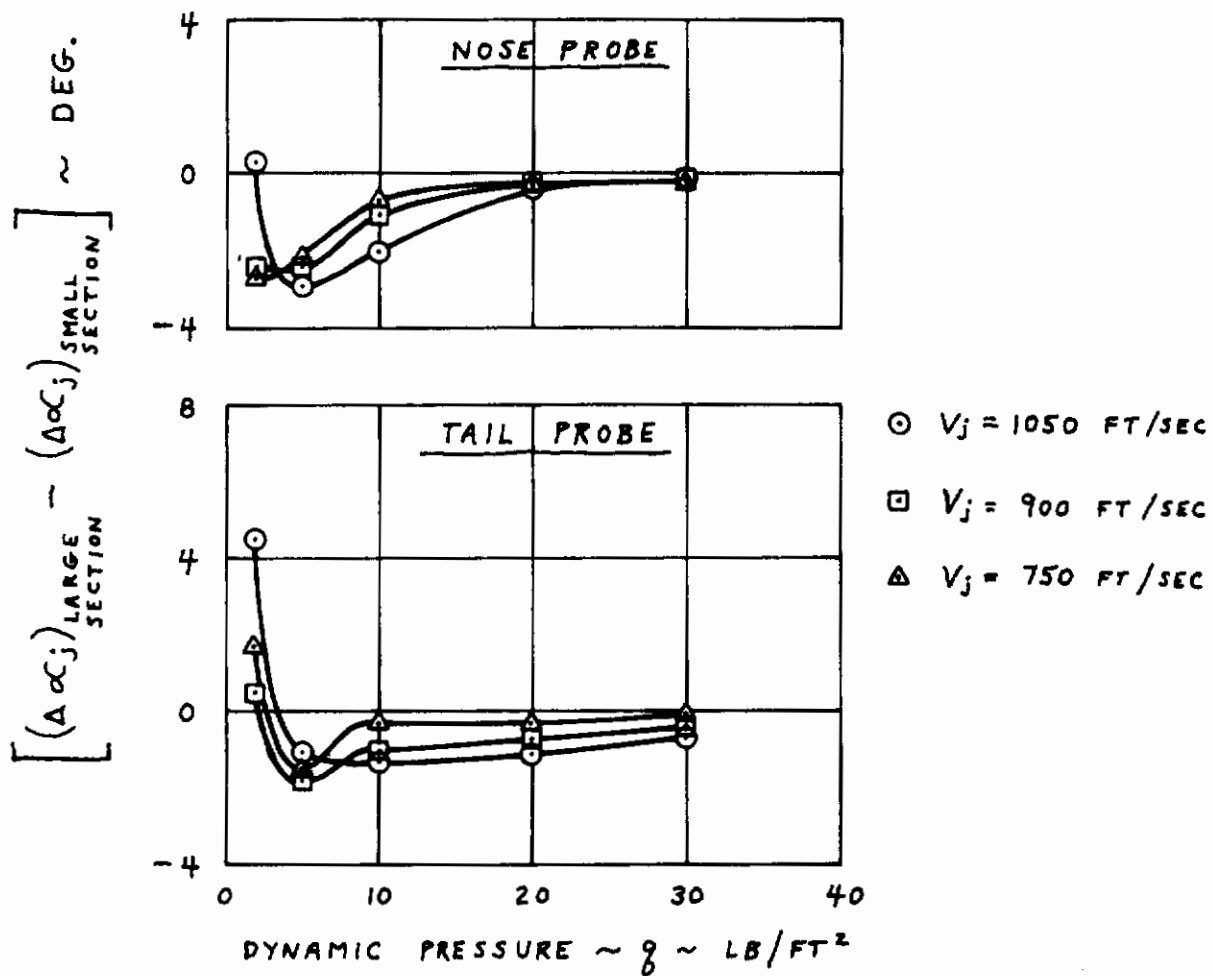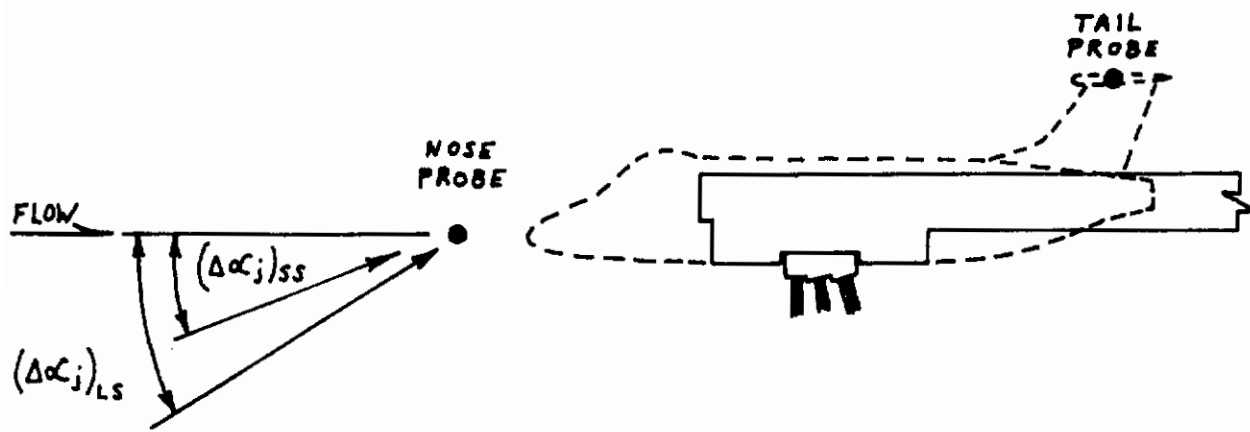
Fig. 127. Increment in Local Angle of Attack at an Assumed Nose
and Tail Location due to Tunnel Walls (α=0)

175

$\bar{c}_w$
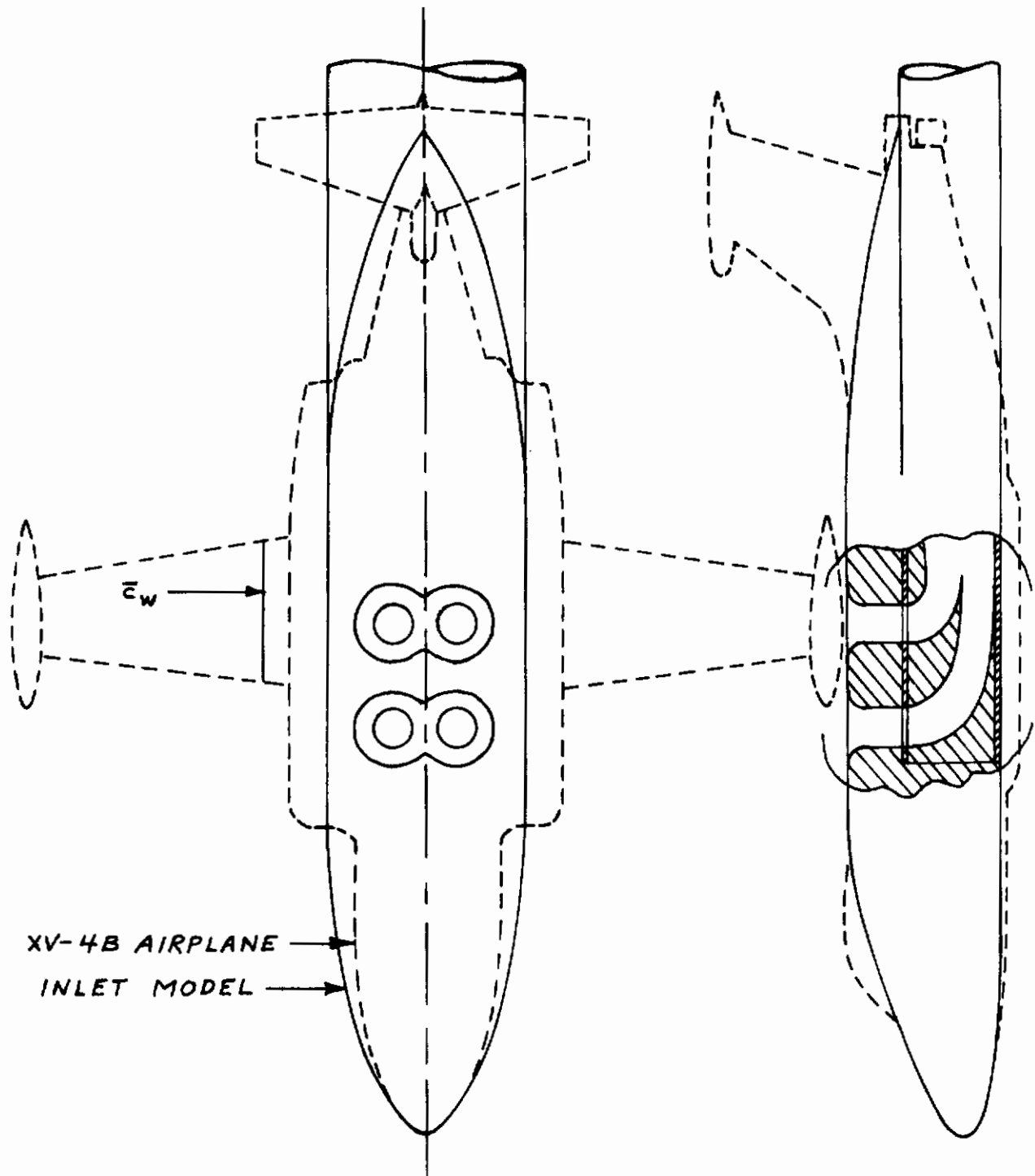
XV-4B AIRPLANE

INLET MODEL

Fig. 128.   Comparison of Model and Airplane Configurations

176
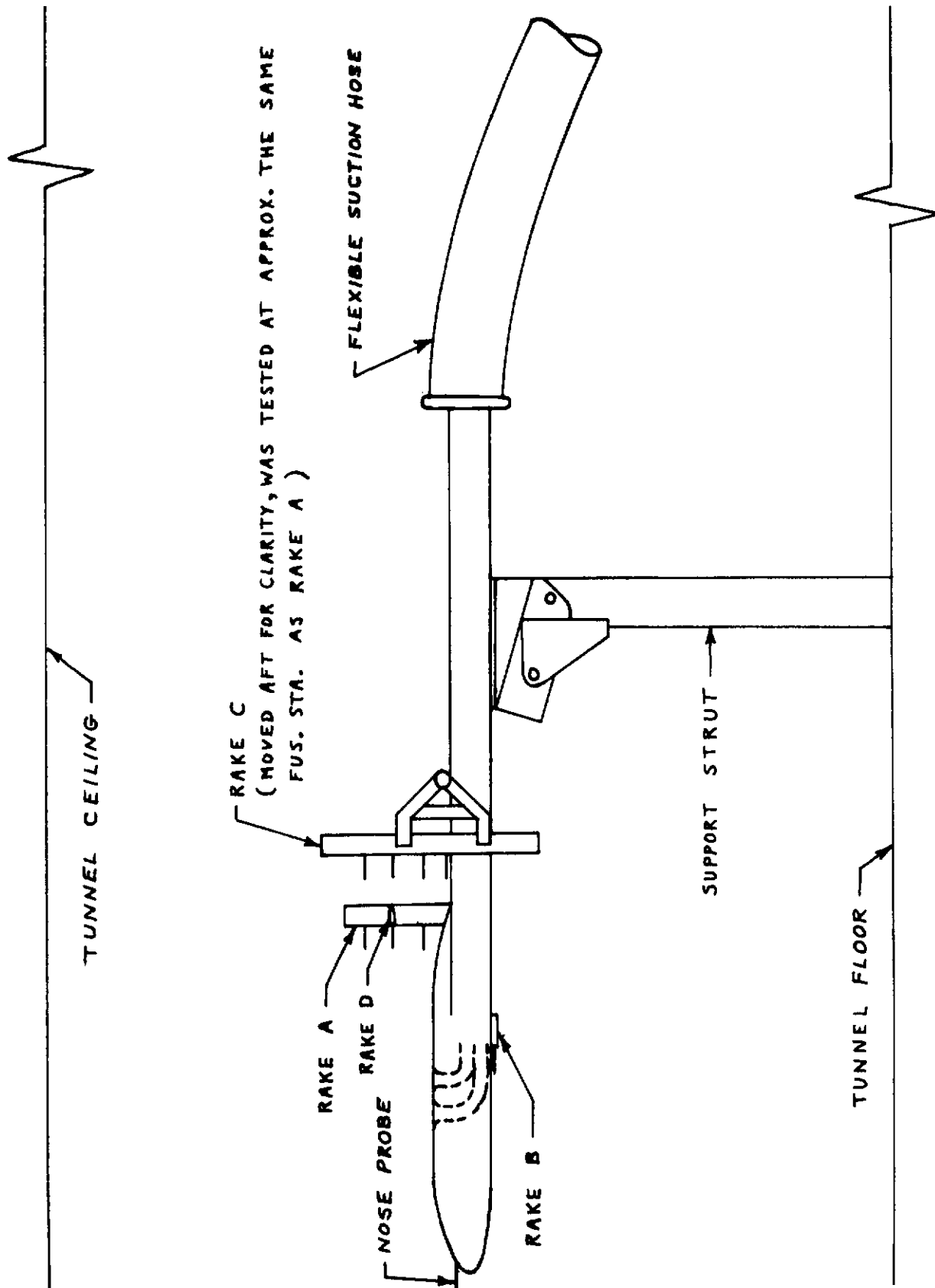
Fig. 129. 0.10 Scale Inlet Model Installation

TUNNEL CEILING

RAKE C
(MOVED AFT FOR CLARITY, WAS TESTED AT APPROX. THE SAME FUS. STA. AS RAKE A)

FLEXIBLE SUCTION HOSE

SUPPORT STRUT

TUNNEL FLOOR

RAKE A

NOSE PROBE

RAKE D

RAKE B

177
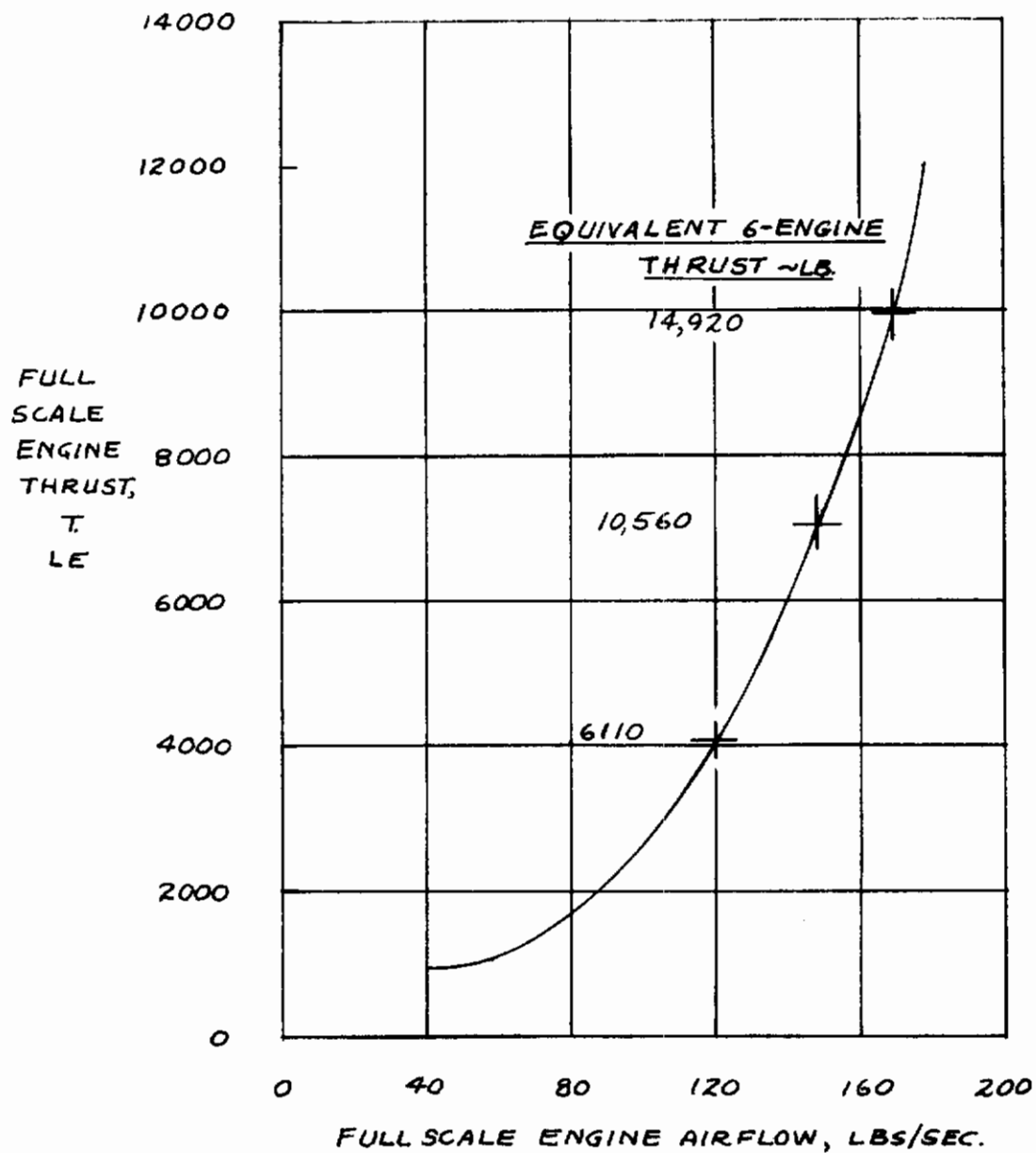
Fig. 130. Variation of XV-4B Lift-Engine Airflow with Engine Thrust
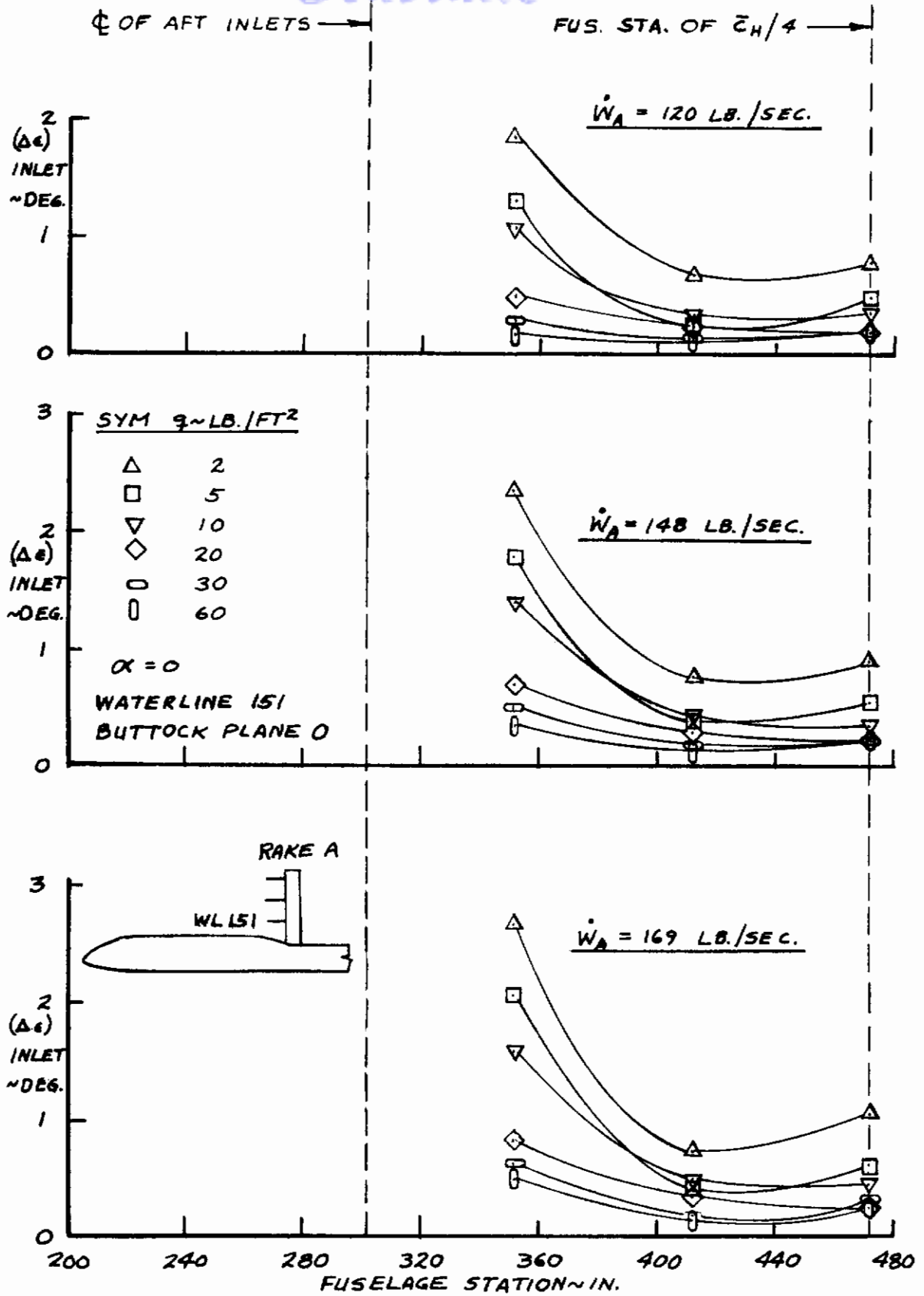
Fig. 131. Incremental Downwash Angle due to Inlet Flow versus
Fuselage Station at Waterline 151

179
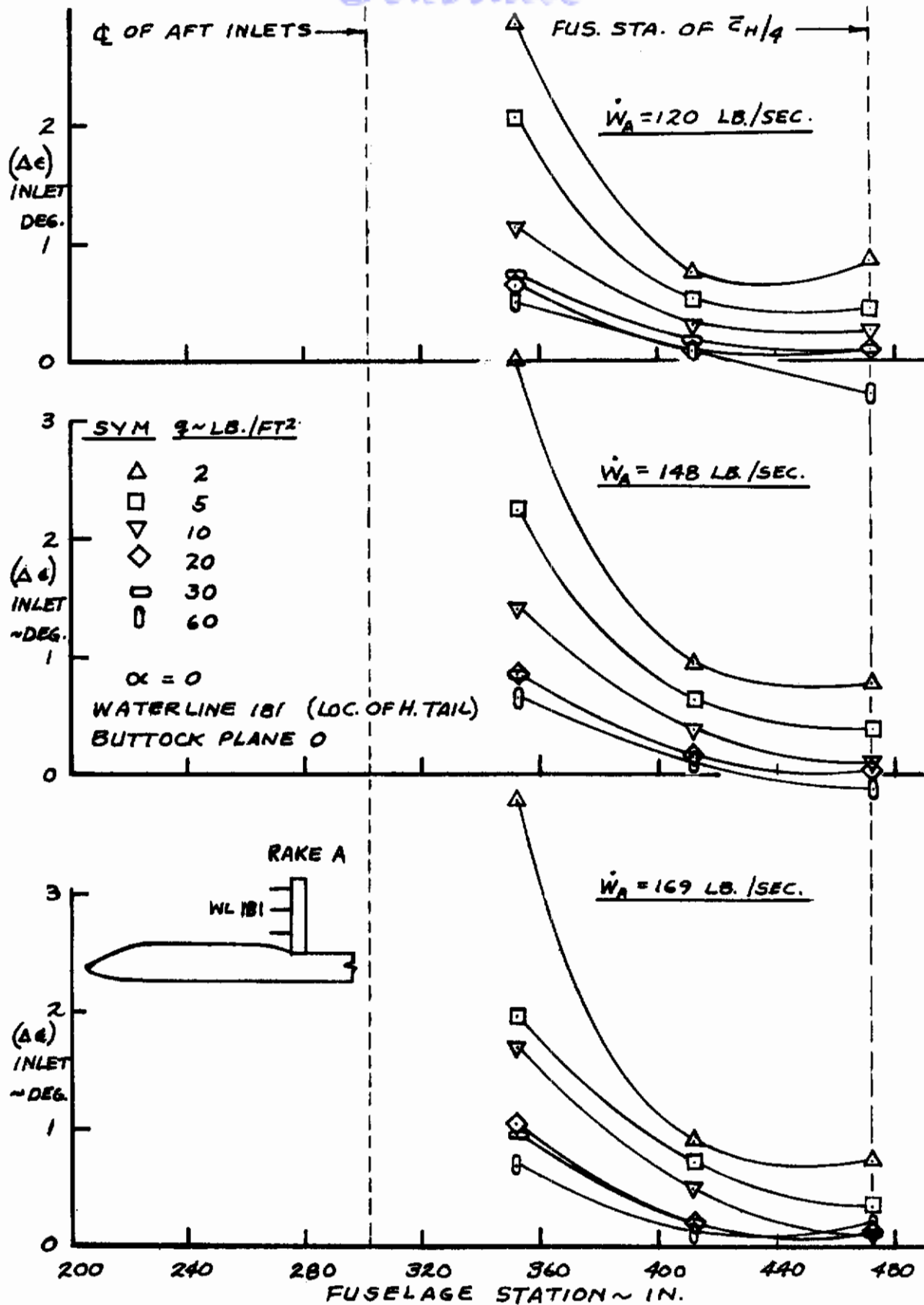
Fig. 132. Incremental Downwash Angle due to Inlet Flow versus Fuselage Station at Waterline 181

180

¢ OF AFT INLETS ——→

FUS. STA. OF $\bar{c}_H/4$ ——→

$\dot{W}_A = 120$ LB./SEC.

2

$(\Delta \epsilon)$ INLET ~DEG.

1

0

SYM	$q \sim LB/FT^2$
△	2
□	5
▽	10
◇	20
⊖	30
◧	60

$\alpha = 0$

WATERLINE 211

BUTTOCK PLANE 0

3

2

$(\Delta \epsilon)$ INLET ~DEG.

1

0

$\dot{W}_A = 148$ LB./SEC.

RAKE A

WL 211

$\dot{W}_A = 169$ LB./SEC.

3

2

$(\Delta \epsilon)$ INLET ~DEG.

1

0

200   240   280   320   360   400   440   480

FUSELAGE STATION ~IN.
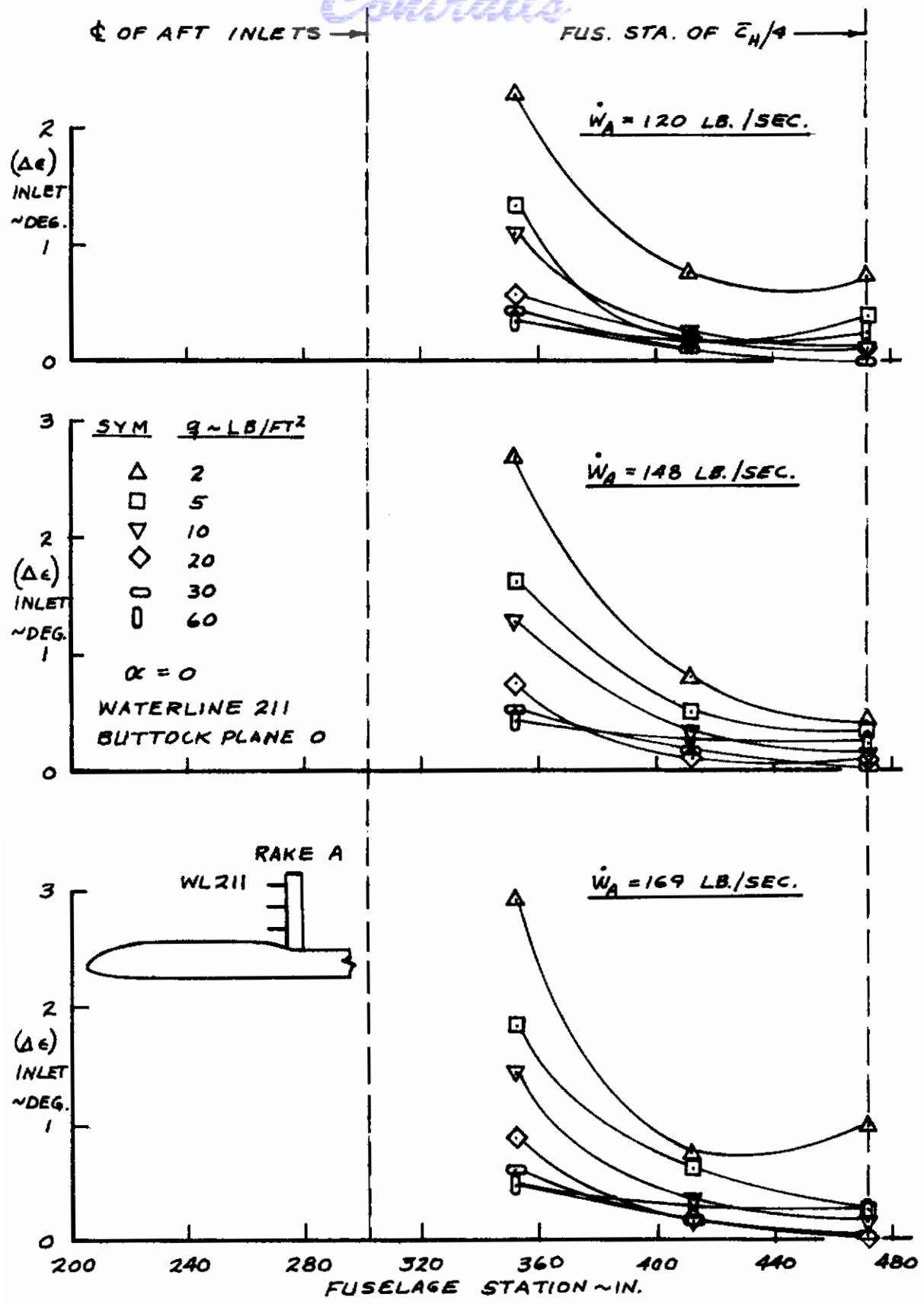
Fig. 133.   Incremental Downwash Angle due to Inlet Flow versus
Fuselage Station at Waterline 211

181
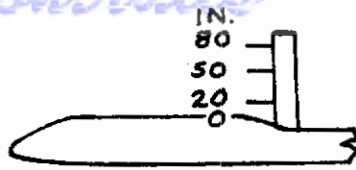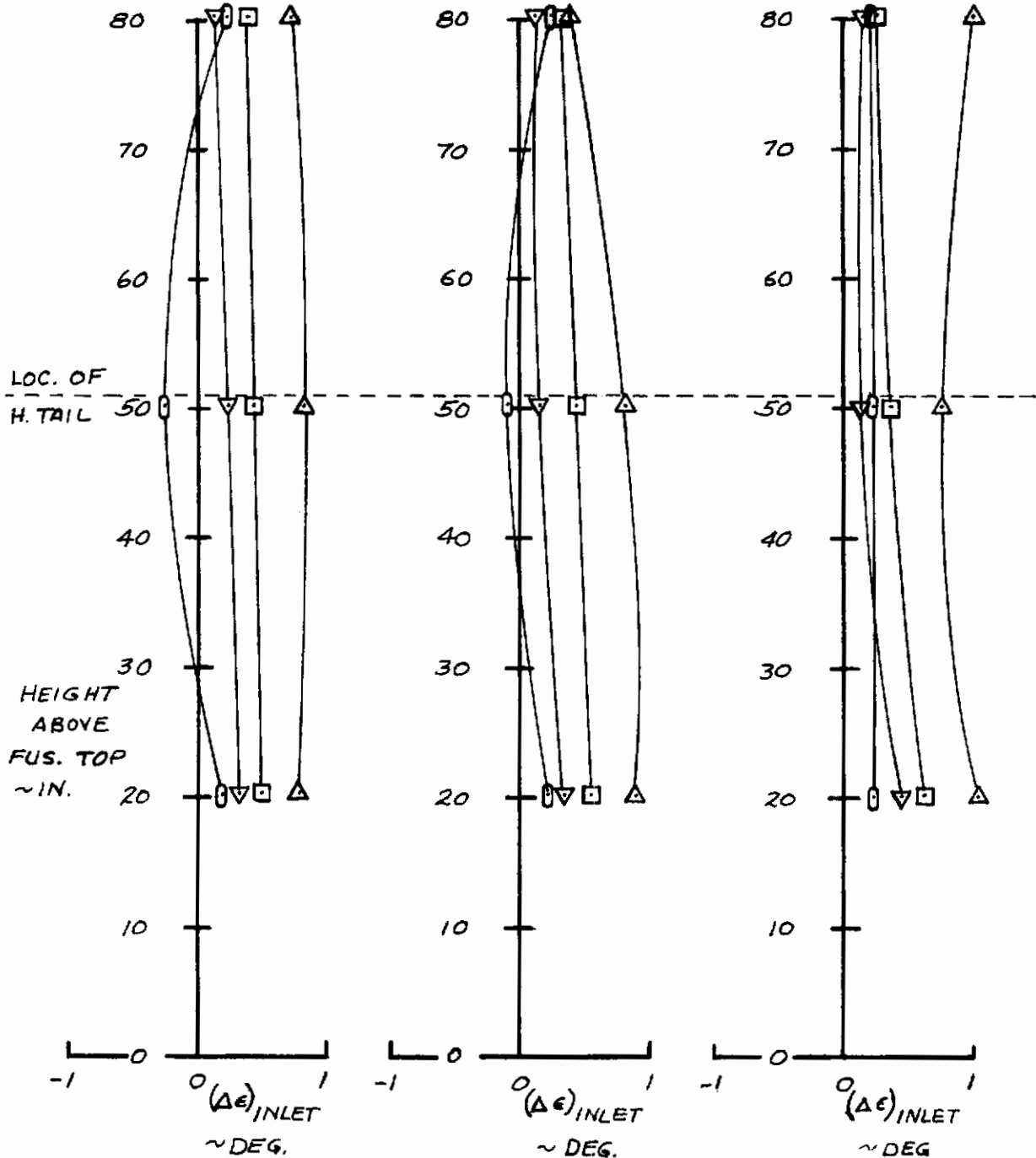
Fig. 134. Incremental Downwash Angle due to Inlet Flow versus Height above Fuselage at Fuselage Station of .25$\overline{C}_H$ in Plane of Symmetry

182
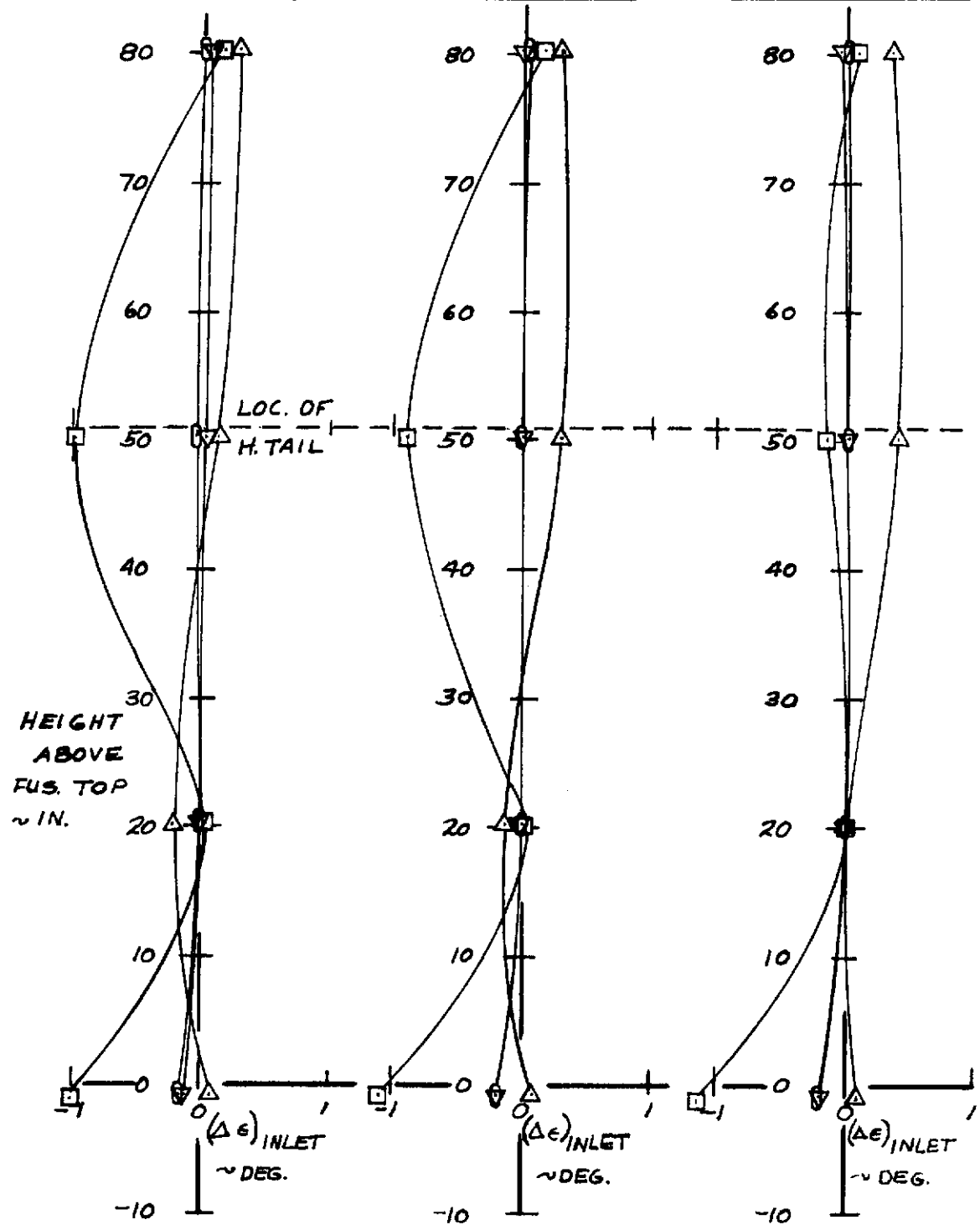
Fig. 135. Incremental Downwash Angle due to Inlet Flow versus Height above Fuselage at Fuselage Station of $.25C_H$ at Location of Horizontal Tail Tip
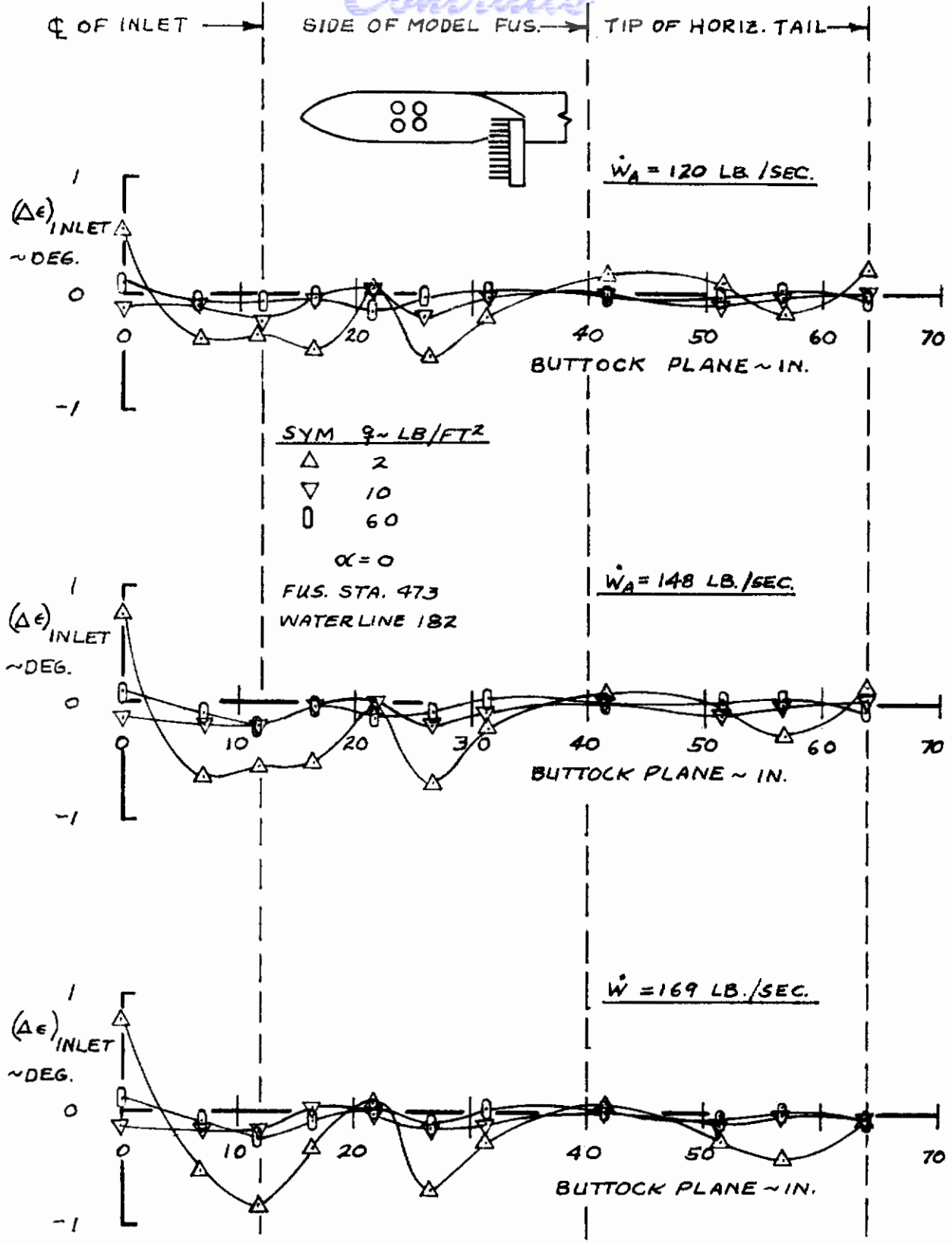
Fig. 136. Incremental Downwash Angle due to Inlet Flow versus Distance from Plane of Symmetry at Fuselage Station and Waterline of $.25\overline{C}_H$

184
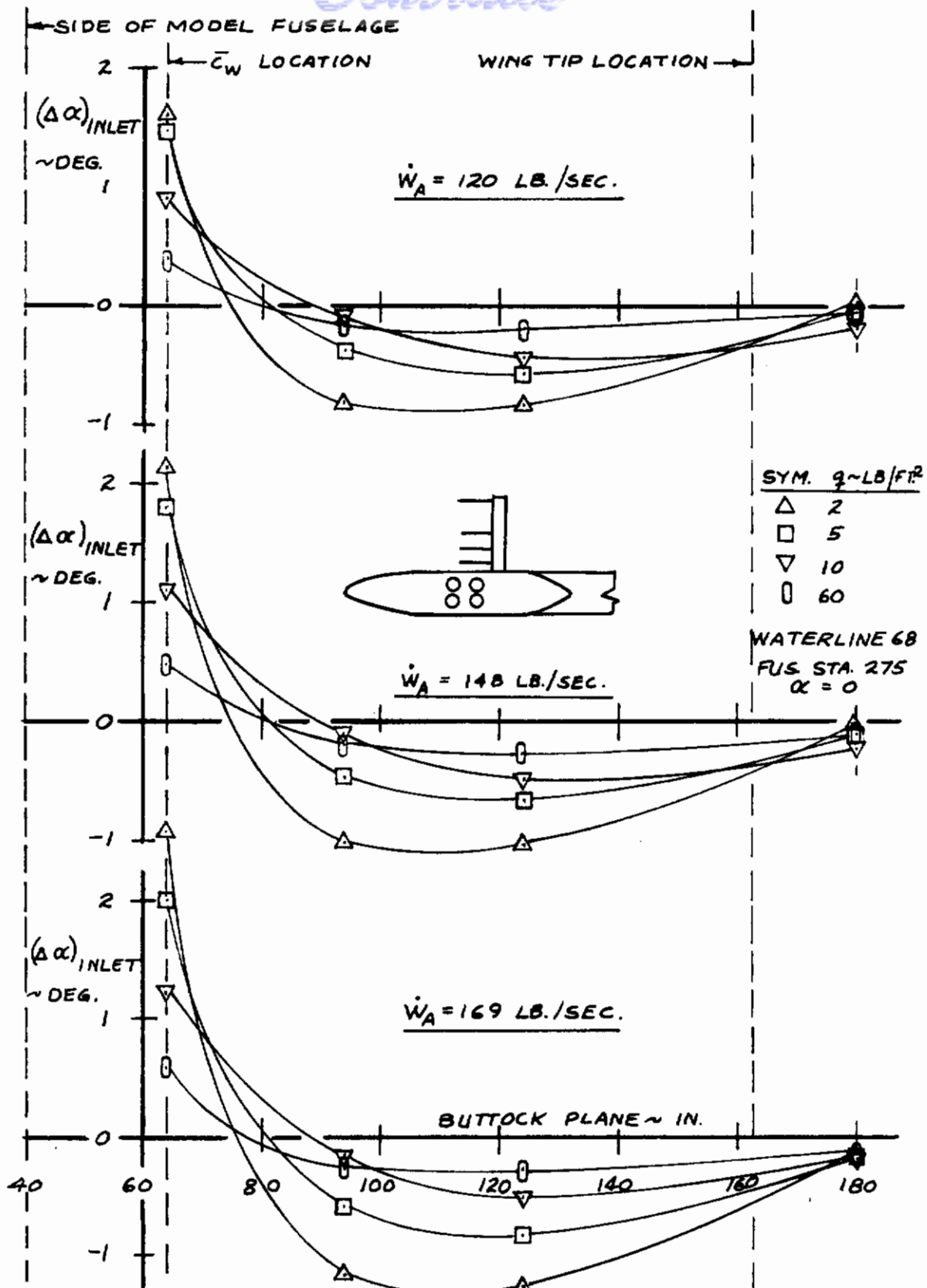
Fig. 137. Spanwise Variation of Incremental Local Angle of Attack due
to Inlet Flow at Fuselage Station of the Leading Edge of the Wing m.a.c.

185
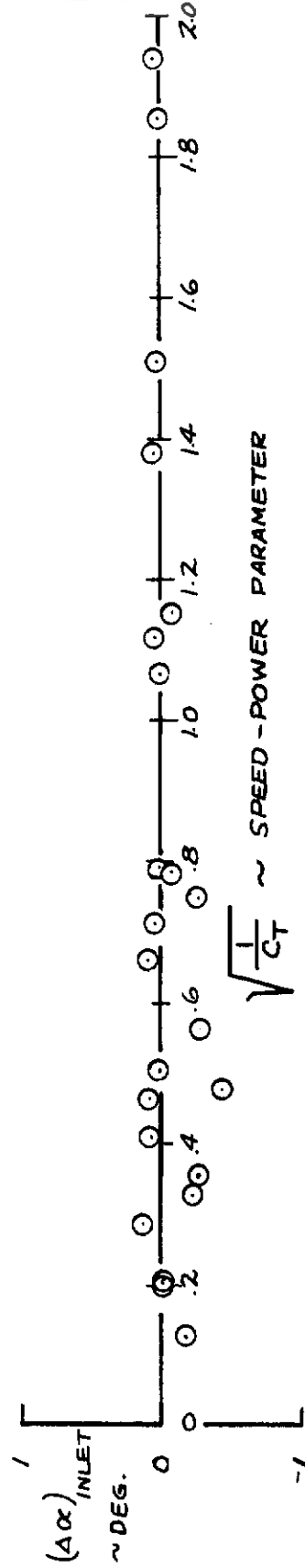
Fig. 138. Incremental Local Angle of Attack at Nose Probe versus Lockheed Speed-Power Parameter

186

BUTTOCK PLANE O, FUSELAGE STATION 472
O $\psi = -5°$ ▷ $\psi = -10°$
$\alpha = 0$

WATERLINE 181

RAKE A

WL 181
151

WATERLINE 151
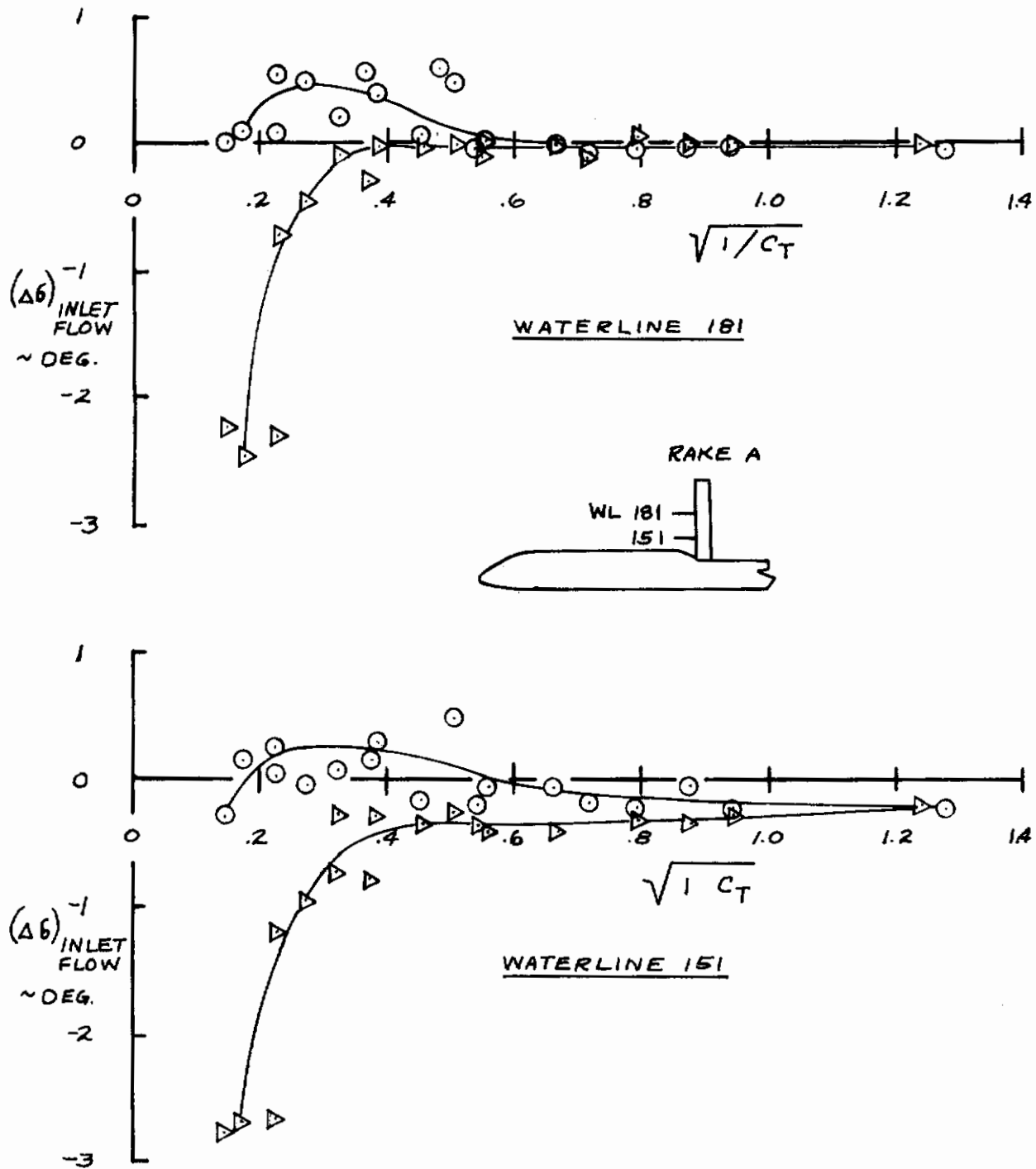
Fig. 139. Incremental Sidewash Angles at Vertical Tail
versus Lockheed Speed-Power Parameter

187

ADJUSTABLE BOARD TO SIMULATE GROUND PLANE

HEIGHT

HIGH PRESSURE AIR PIPE

FLOW

THRUST

PIPE SUPPORT

REAL GROUND PLANE
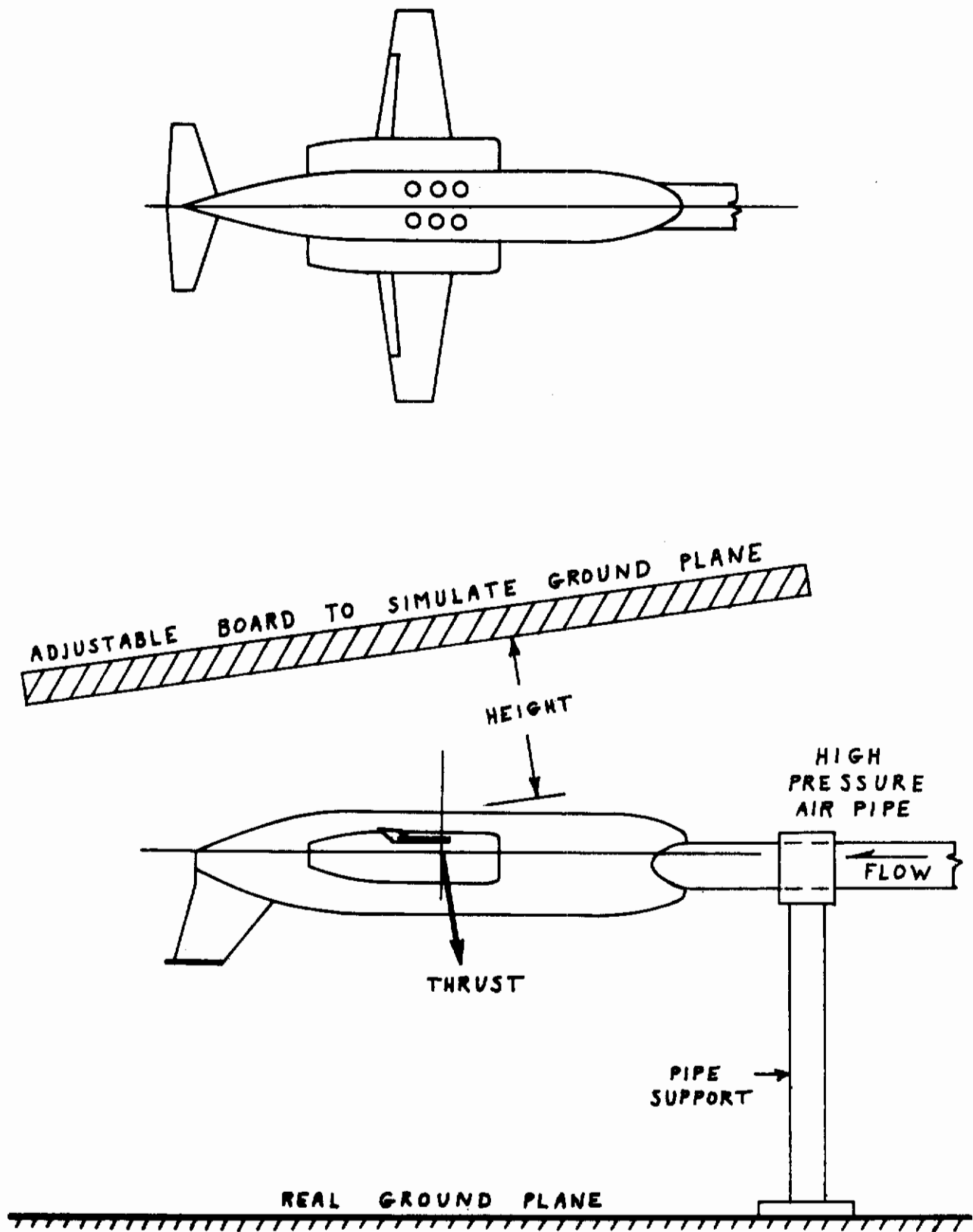
Fig. 140. XV-4B 0.14 Scale Hover Model and Test Installation

188

MODEL
DIMENSIONS

S_W = 3.375 FT^2
$\bar{c}$ = .798 FT
b = 4.500 FT
A_{JETS} = .155 FT^2
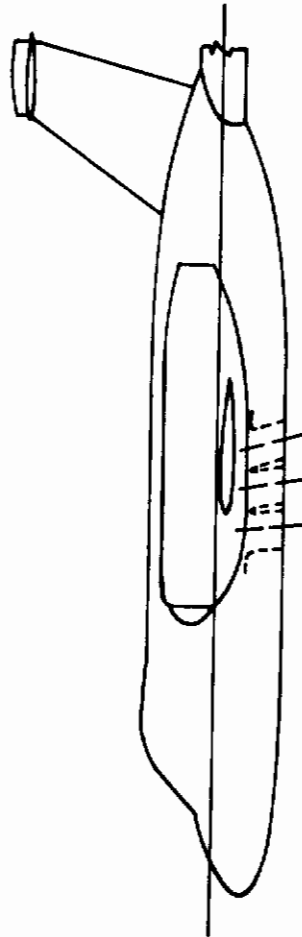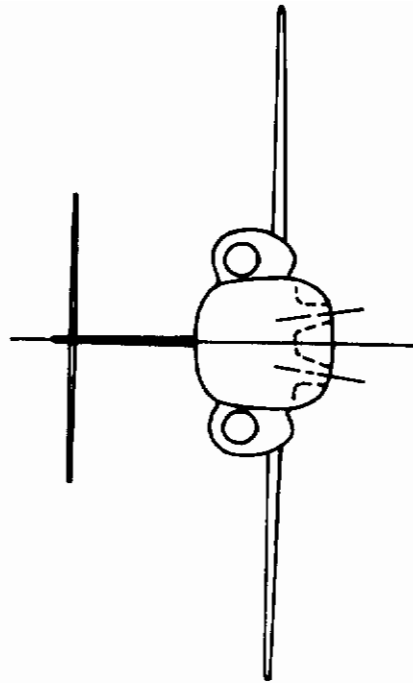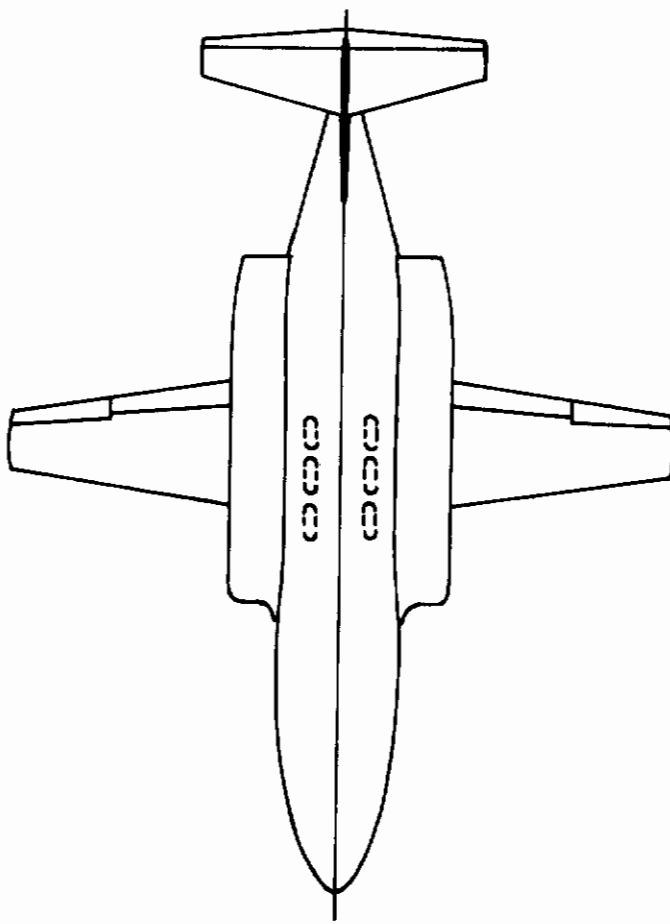
Fig. 141. General Arrangement of 0.18 Scale XV-4B Model

189

10 FT.

7 FT.

FLOW

HIGH
PRESSURE
AIR PIPE
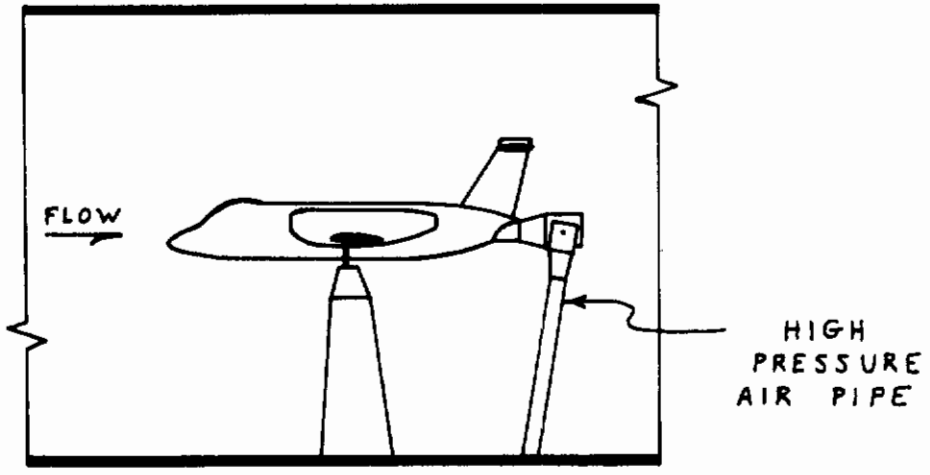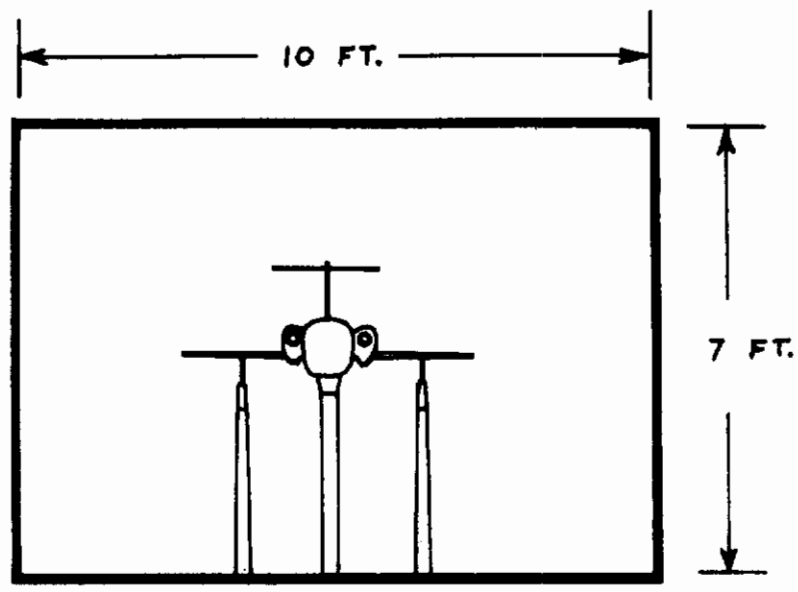
Fig. 142.   Model Installation for LTV Test 195

190

EJECTOR UNIT
ARRANGEMENT

SECONDARY
INLET FLOW

TOTAL EXIT
FLOW

HIGH
PRESSURE
PRIMARY AIR
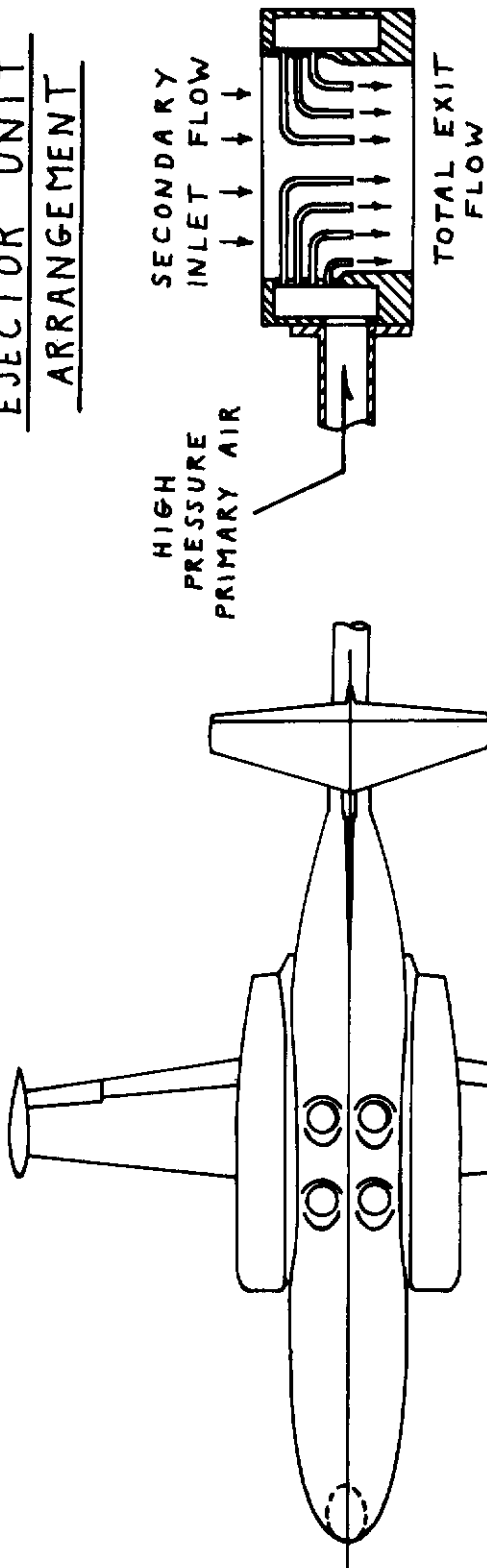
$S_W = 2.667 \ FT^2$

$\bar{c} = .71 \ FT$

$b = 4.00 \ FT$

$A_{JETS} = .1205 \ FT^2$

MODEL
EJECTOR UNIT

STING

ALTERNATE ACCESS
FOR STING ~ REARWARD
FLIGHT RUNS ONLY
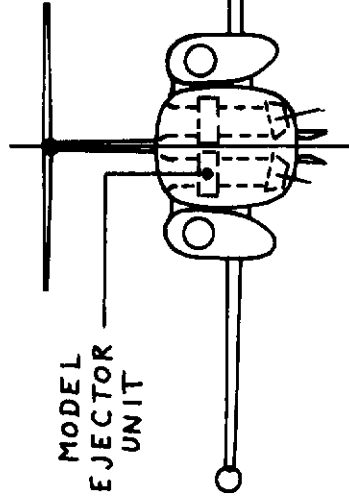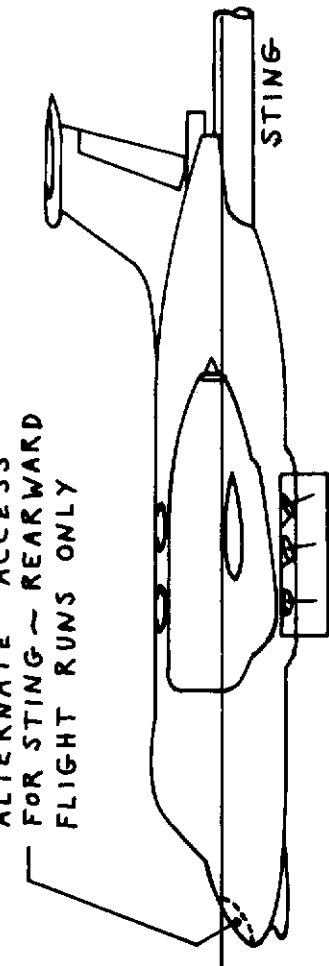
Fig. 143. General Arrangement of 0.16 Scale XV-4B Model

191
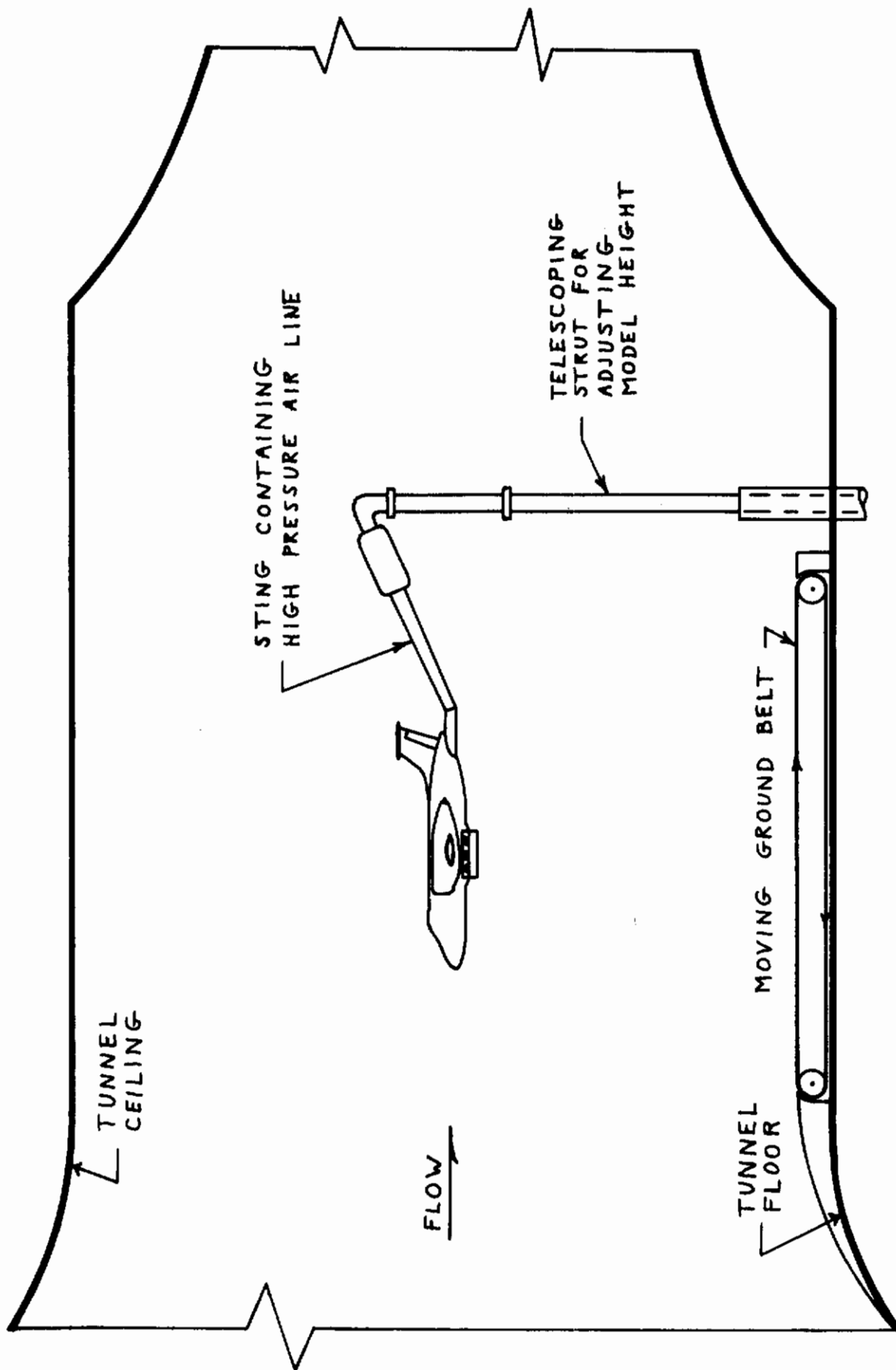
Fig. 144. General Arrangement of 0.16 Scale Model Installation in the Langley 17 Foot Test Section

192
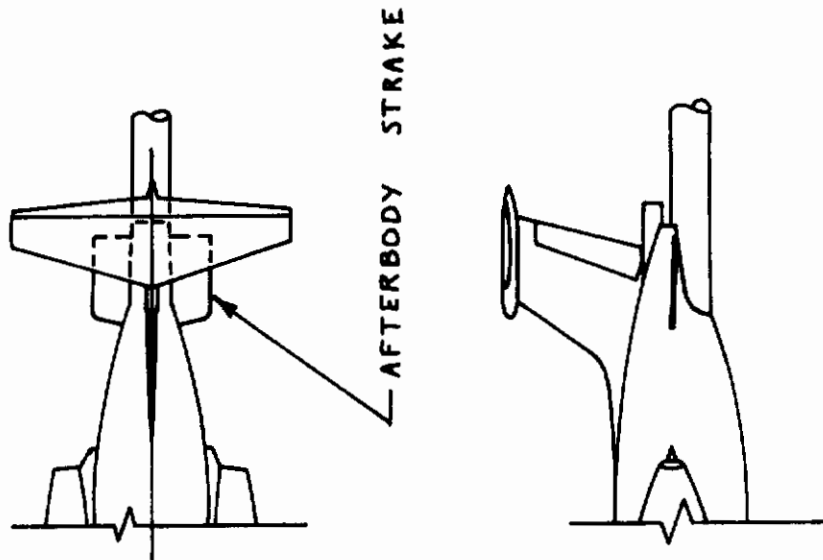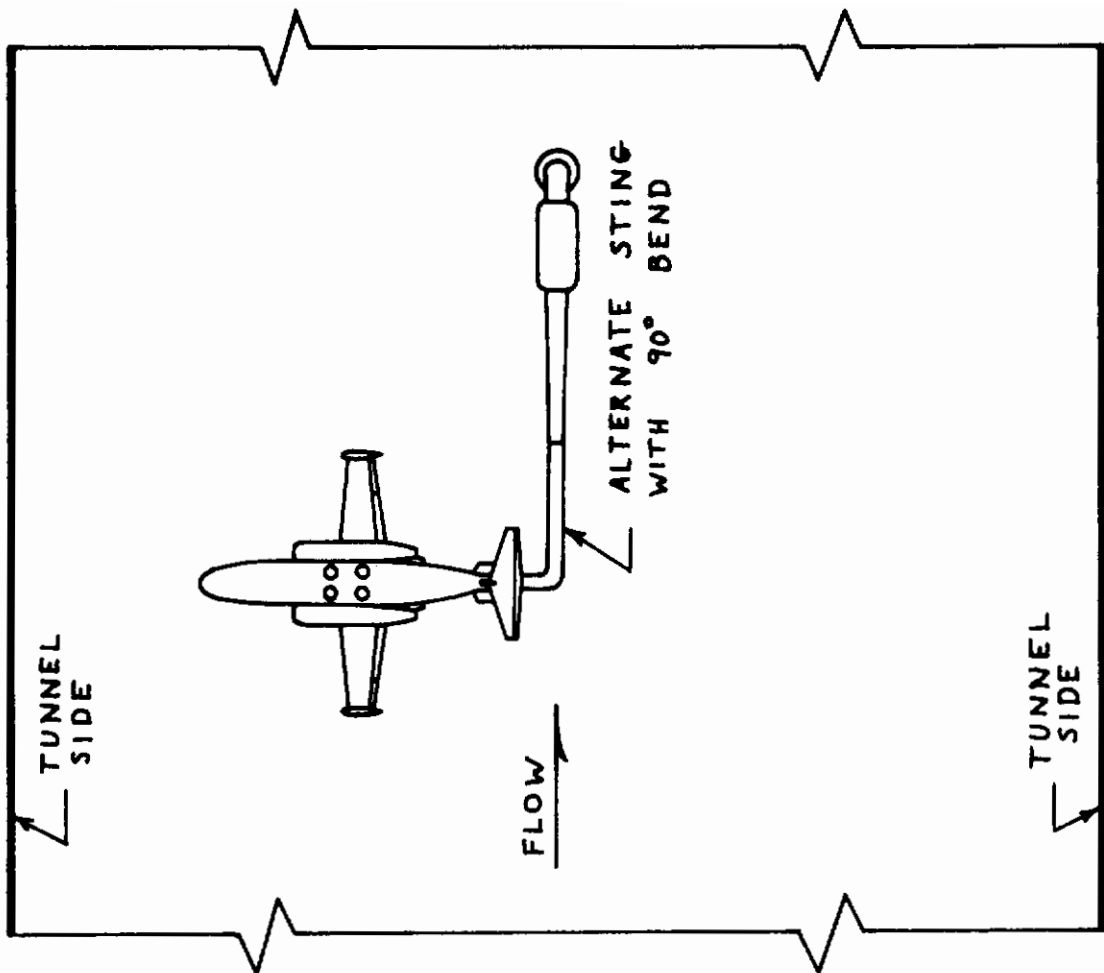
Fig. 145. General Arrangement of Afterbody Strake and Alternate Support System for Sideward Flight Runs

193

Section VI

GENERAL VTOL AERODYNAMICS

VTOL aerodynamic technology is in an evolutionary stage at the present time. Despite considerable government and industry effort, to date, reliable methods to estimate airplane data from model data have not emerged. This is due to the very complex nature of VTOL aerodynamic effects and the wide variety in propulsion variables. At the present time all aspects of VTOL aerodynamic testing and analysis techniques are suspect to some degree. In recognition of the need to improve aerodynamic technology for VTOL airplanes, the USAF has for many years sponsored research work in this area. The need for further technology development is clearly indicated.

This section contains an overview of VTOL aerodynamic problem areas and suggests some general approaches to solving these problems.

AERODYNAMIC PARAMETERS

A matter of concern to the VTOL designer is the manner in which the aerodynamic data should be formulated. Each agency has tended to present VTOL aerodynamic data in a form suitable for his own particular airplane-propulsion application. A variety of data presentations has come into use which has hindered attempts to compare the data for different VTOL aircraft on a common basis. This situation is likely to continue unless a satisfactory approach to representing VTOL forces and moments can be identified which will be valid for a wide variety of airframe-propulsion combinations.

Initial efforts to represent VTOL aerodynamic data were directed toward identifying simple nondimensional parameters which would be similar to the conventional power-off coefficients. To date, no simple overall parameters have been identified. At present, the total aerodynamic effect is regarded as a number of individual effects superimposed upon each other and functions of different variables. In the equations of motion the total aerodynamic contribution is best represented in two parts. The conventional power-off aerodynamic terms, and the aerodynamic power effect terms which result from propulsion-airframe interaction.

It is essential that a valid nondimensional parameter be used to represent the power effects. Data is normally available only for a limited number of speed and power conditions. The accuracy with which this limited data can be extrapolated or interpolated is related to the validity of the coefficient used. The speed-power ($\sqrt{1/C_T}$) adopted by Lockheed for the XV-4B airplane appears to be a valid correlating parameter. This parameter is proportional to one currently in use by NASA ($\sqrt{\rho V^2/\rho_j V^2 j}$). Also indications are that these parameters can be applied successfully to a fan-in-wing configuration. However, it is not known whether these parameters could be applied to a propeller configuration. These parameters appear to be very promising, but they need to be investigated further to determine any limits or restrictions on their use.

194

The following approach was adopted for the VIFCS program to investigate power-effect parameters. It was proposed that the available data for three VTOL airplanes with different propulsion systems be converted to dimensional force and moment values for standard sea level conditions. The dimensional data would then be nondimensionalized in a variety of ways. In this manner parameters developed for a particular configuration can be tried on several different configurations and the advantages and disadvantages noted. Some experimenting with new parameters could also be tried. It is felt that an exercise like this would help to verify whether or not any analysis technique or aerodynamic parameter which is developed in connection with a particular VTOL configuration has any general usefulness.

CORRELATION OF FLIGHT AND TUNNEL DATA

Continued effort to establish the degree of correlation between the wind tunnel test results and flight test results is needed. At the present time it would be difficult to determine if poor agreement between model and flight results was due to poor quality flight test information, errors in model test data or inaccurate correlation techniques. Poor quality flight test information could result from poorly defined thrust values, inaccurate angle of attack and sideslip values due to propulsion system interaction with vane instruments, inaccurate velocity measurements, etc. Bad model data could result from a series of factors such as wind tunnel wall effects, inaccurate propulsion system simulation, Reynolds number effects, etc. Correlation errors could also arise from the use of an inaccurate correlation parameters. It is felt that the greatest overall knowledge of VTOL correlation problems will result from a thorough examination of an individual VTOL aircraft rather than studying VTOL problems in general. It is not implied that general studies should stop, but rather that a thorough study of an individual aircraft should receive priority consideration. The advantage of researching problems on real aircraft is that the significance of new knowledge or techniques can be readily established.

MODEL TEST TECHNIQUES

Important problem areas in testing of small VTOL models are wall effects, propulsion simulation, and model support systems.

WALL EFFECTS

A workable method to correct wind tunnel data for an arbitrary VTOL configuration is not available at the present time. The general problem is a very complex one. What is needed at the present time is a more thorough knowledge of the flow fields in the test section. A better knowledge of the flow fields involved should lead to improved correction theories. While awaiting the emergence of a workable wall correction method much can be done to reduce the influence of sall effects by test techniques. Model size, tunnel test speeds, and model power settings are factors which can affect the magnitude of any tunnel wall error.

PROPULSION SIMULATION

To date, model propulsion systems have seldom provided the degree of versatility desired. Some models match the exit flow with compressed air units but do not provide an inlet flow. Other models provide an exit and inlet flow

195

but the flows often do not match the airplane values. It is often necessary to adjust the test data by some increment to compensate for the model propulsion system limits. Also, propulsion units requiring high pressure air to operate can introduce difficult plumbing and model support problems.

MODEL SUPPORT SYSTEMS

While hovering, a VTOL aircraft may move about slightly in a three dimensional manner or be subjected to winds from any direction. To study these effects in a wind tunnel requires that the model be capable of simulating unusual ranges of angle of attack (0 to 90 degrees) and angle of sideslip (0 to 180 degrees). No simple method of obtaining this type of test data is presently available. The limited amount of available data has been obtained by using a series of separate support methods, each having a limited test range, and then piercing the bits of data together.

VTOL AERODYNAMIC RECOMMENDATIONS

Development of techniques to allow accurate prediction of stability and control characteristics of VTOL aircraft, based on model wind tunnel tests, was one of the objectives of the VIFCS program that was only partially fulfilled due to the loss of the XV-4B. This is still an important objective.

A continued experimental program in conjunction with theoretical studies should be considered. A model of an existing VTOL airplane, such as the P-1127, should be built and used as a research model. A comprehensive wind tunnel test and analysis program should be conducted on the model, and the model results should be correlated with the flight test results. The influence of test and analysis techniques upon the model data and upon the estimated flight characteristics should be established.

The model should be built with the propulsion system independent of the airframe. Aerodynamic loads could then be measured instead of calculated. The propulsion system should consist of a compressed air powered exit flow and a suction powered inlet flow. Also, it should be possible to simulate any inlet or exit flow condition up to full scale values. A model built in this manner would allow investigation of a very large range of propulsion parameters. The model should be sized for testing in a conventional low speed tunnel section (7 x 10 feet). This would provide a very large range of tunnel speeds and keep the model power requirements within manageable limits. In addition, the model should be instrumented to obtain some wing and fuselage pressure data and reaction control units should be simulated.

The model support system should be capable of positioning the model to obtain very large angle of attack and angle of sideslip data. The same model should be capable of hover tests in the tunnel test section and on an outdoor test rig.

A series of wall inserts should be built to investigate the effect of test section size on model forces and moments. The test sections should

be instrumented to visualize and measure flow fields. This empirical data would then be used to formulate theoretical flow models for airplane and tunnel effects.

Once a final set of corrected model data defining the characteristics of the airplane was formulated, correlations between model data and flight data should be made to verify the results. The data should be formulated in a form suitable for simulation use.

A research program of this nature would exercise every variable affecting VTOL aerodynamics and should result in greater insight and improved test and analysis techniques. Though limited in scope to one aircraft configuration, the knowledge developed should apply in principle to other configurations.

REFERENCES

1. North American Rockwell Corporation, Los Angeles Division, "VIFCS Preliminary Wind Tunnel Test Techniques Study," NA-68-269, April 1968

2. North American Rockwell Corporation, Los Angeles Division, "Preliminary Analysis of XV-4B Longitudinal Interference Effects in Transition Flight," NA-68-287, April 1968

3. North American Rockwell Corporation, Los Angeles Division, "Preliminary Analysis of XV-4B Lateral-Directional Interference Effects in Transition Flight," NA-68-775, October 1968

4. North American Rockwell Corporation, Los Angeles Division, "Preliminary Analysis of XV-4B Interference Effects in Hover," NA-69-18, February 1969

5. North American Rockwell Corporation, Los Angeles Division, "Low Speed Wind Tunnel Tests of an 0.0863 Scale Simulated XV-4B Lift Jet Exit Configuration to Investigate the Effects of Cross Stream Directed Jet Exit Flow on the Flow Fields in Two Test Section Sizes (NAAL Test 592)," NA-70-160, Volumes I and II, February 1970

6. North American Rockwell Corporation, Los Angeles Division, "Low Speed Wind Tunnel Tests of a 0.10 Scale Simulation of the XV-4B V/STOL Aircraft to Investigate Inlet Airflow Effects (NAAL Test 622)," NA-70-251, 15 April 1970

7. NASA, TN D-3166, "Jet-Induced Lift Losses on VTOL Configurations Hovering In and Out of Ground Effect," Carl L. Gentry and Richard J. Margason, February 1966

8. NASA TN D-3435, "Jet-Induced Lift Loss of Jet VTOL Configurations In Hovering Condition," H. Clyde McLemore, June 1966

9. NASA TN D-4084, "Free-Stream Interference Effects on Effectiveness of Control Jets Near the Wing Tip of a VTOL Aircraft Model," August 1967

10. Lockheed-Georgia Company, "Full-Scale Tests of the XV-4A Hummingbird in the Ames 40 x 80 Foot Wind Tunnel," ER-7634, 12 January 1965

11. Lockheed-Georgia Company, Report ER 9092, "XV-4B Wind Tunnel Test of a 0.16-Scale Model in the 17-Foot Test Section of the NASA Langley 7 x 10 Foot Wind Tunnel," (Test 178), undated

12. Langley Research Center, "Tabulated Wind Tunnel Data for the 0.16-Scale XV-4B Model Tested in the 17-Foot Section of the 300 MPH 7 x 10 Foot Tunnel (Unpublished), Langley Test 221," February 1968

13. Lockheed-Georgia Company, Report ER-9052, "XV-4B Hummingbird Aerodynamic Analysis Report," 15 May 1968

14. Lockheed-Georgia Company, Rough Draft, "XV-4B Equations of Motion," 27 December 1967

15. Lockheed-Georgia Company, "XV-4B Hummingbird II VTOL Research Vehicle Engineering Flight Test Development and Evaluation Tests," ER-9635, 20 June 1969

16. Ryan Aeronautical Company, "Wind Tunnel Test Report One-Sixth Scale Powered Lift-Fan Model U.S. Army XV-5A Lift-Fan Research Aircraft," Report No. 63B092, 11 September 1963

17. Ryan Aeronautical Company, "Wind Tunnel Test Report Low Speed (M=.285) One-Eighth Scale Conventional Model U.S. Army XV-5A Lift Fan Research Aircraft," Report No. 63B128, Volumes I and II, 20 December 1963

18. Ryan Aeronautical Company, "Estimated Static Stability and Control Characteristics of the U.S. Army XV-5A Lift Fan Research Aircraft," Report No. 64B031, 6 March 1964

19. General Dynamics Convair, "Additional Low Speed Wind Tunnel Tests of a 1/6 Scale Powered Model of the Ryan Model 143 Airplane to Investigate Static Performance and Low Speed Aerodynamic Characteristics at a Variety of Model Attitude and Test Conditions," Report CVAL 344A, 15 July 1963

20. NASA TN D-2368, "Aerodynamic Characteristics of a Full-Scale Fan-in-Wing Model Including Results in Ground Effect With Nose-Fan Pitch Control," Jerry V. Kirk, David H. Hickey, and Leo P. Hall, July 1964

21. Abromovich, G.N., "Theory of Turbulent Jets," MIT Press, Cambridge, Massachusetts, 1963, pp 541-545

22. NASA TN D-4919, "The Path of a Jet Directed at Large Angle to a Subsonic Free Stream," Margason, R. J., November 1968

23. NASA SP-218, "Analysis of a Jet in a Subsonic Crosswind," Symposium held at Langley Research Center, Hampton, Virginia, 9-10 September 1969

24. North American Rockwell Corporation, "Flow Field Interference in a Low Speed Wind Tunnel Due to Splash of an Inclined Jet Against Tunnel Floor," Leef, C.R., Report NA-68-337 (Rev. 5-6-70)

25. Lockheed-Georgia Company informal data report, "XV-4B Scale Model Static Lift System Exit Interference Effects Data," 3 October 1966

26. Lockheed-Georgia Company, "Low Speed Wind Tunnel Tests Results of a 0.18 Scale Model of Lockheed's (Hummingbird) VTOL Airplane with a Direct and Diverted Thrust Lifting System," Ling-Temco-Vought Test 195, ER 8677, 30 September 1966, Revised May 1967

27. Langley Research Center, "Tabulated Wind Tunnel Data for the 0.16 Scale XV-4B Model Tested in the 17-Foot Section of the 300 MPH 7 x 10 Foot Tunnel (Unpublished)," Langley Test 178, Hampton, Virginia, March 1967

28. Lockheed-Georgia Company, "Test of a 0.16 Scale Model of the XV-4B Configuration in the University of Maryland Low Speed Tunnel," Maryland Test 488, unpublished data

29. Lockheed-Georgia Company, "Additional Tests of a 0.16 Scale Model of the XV-4B Configuration in the University of Maryland Low Speed Tunnel," Maryland Test 493, unpublished data

30. Langley Research Center, "Tabulated Wind Tunnel Data for the 0.16-Scale XV-4B Model Tested in the 7 x 10 Foot Section of the 300 MPH 7 x 10 Foot Wind Tunnel (Unpublished), Langley Test 226," May 1968

DOCUMENT CONTROL DATA - R & D

(Security classification of title, body of abstract and indexing annotation must be entered when the overall report is classified)

1. ORIGINATING ACTIVITY (Corporate author)	2a. REPORT SECURITY CLASSIFICATION
North American Rockwell	Unclassified
	2b. GROUP

3. REPORT TITLE

Aerodynamic Stability and Control/Wind Tunnel Data Correlation

4. DESCRIPTIVE NOTES *(Type of report and inclusive dates)*

Final Report

5. AUTHOR(S) *(First name, middle initial, last name)*

G. R. Casteel

6. REPORT DATE	7a. TOTAL NO. OF PAGES	7b. NO. OF REFS
May 1971	199	30

8a. CONTRACT OR GRANT NO.	9a. ORIGINATOR'S REPORT NUMBER(S)
AF33(615)-5323	NA-70-327-2
b. PROJECT NO. 698BT	
c.	9b. OTHER REPORT NO(S) *(Any other numbers that may be assigned this report)* AFFDL-TR-71-3
d.	

10. DISTRIBUTION STATEMENT

This document has been approved for public release and sale;
its distribution is unlimited

11. SUPPLEMENTARY NOTES	12. SPONSORING MILITARY ACTIVITY
	FV/V/STOL Division
	Flight Dynamics Laboratory, WPAFB, Ohio

13. ABSTRACT

This report presents the results of work performed under Task II (Aerodynamic Stability and Control) of the VTOL Integrated Flight Control System Program (VIFCS). The general objective of Task II was to collect and analyze aerodynamic stability and control data for the XV-4B, XV-5A, and P-1127 VTOL configurations. Correlation and analysis of existing model data were made to investigate hover and transition characteristics. Particular emphasis was placed on the aerodynamic power effects, sometimes referred to as interference effects. Other areas of investigation were nondimensional coefficients used to present VTOL data and wind tunnel test techniques. Wind tunnel tests were conducted using an inlet only model and a jet only model to investigate special test and analysis problems for these components.

The agreement between different sets of XV-4B model data was, in general, found to be poor. However, the nondimensional coefficients used by Lockheed to reduce to XV-4B model data appear to be valid parameters for this category of VTOL airplane. The jet entrainment flow was shown by experiment to be the primary cause of the XV-4B power effects, and the XV-4B jet path was experimentally and theoretically determined.

DD FORM 1 NOV 65 1473

14. KEY WORDS	LINK A		LINK B		LINK C	
	ROLE	WT	ROLE	WT	ROLE	WT
Effect of large sideslip						
Power effects						
Interference effects						
Stability and control						
XV-4B						
XV-5A						
VTOL						
Nondimensional VTOL coefficients						
VTOL wind tunnel tests						
Test techniques						
Aerodynamic parameters						
Correlation						
Transition						
Hover						
Engine inlet effects						
Engine wake efforts						
Jet Splash						
Jet path						
Local angle of attack						
Inlet momentum						
Flow visualization						